Aus dem Institut für Humanernährung und Lebensmittelkunde
der Christian-Albrechts-Universität zu Kiel

Site-directed spin labeling for the evaluation of amyloid and non-amyloid aggregation mechanisms of β-lactoglobulin using electron paramagnetic resonance spectroscopy and mass spectrometry

Dissertation
Zur Erlangung des Doktorgrades
der Agrar- und Ernährungswissenschaftlichen Fakultät
der Christian-Albrechts-Universität zu Kiel

vorgelegt von
M.Sc. Jacqueline Lux
aus Kiel

Kiel, 2020

Dekan: Prof. Dr. Dr. Christian Henning
1. Berichterstattung: Prof. Dr. Karin Schwarz
2. Berichterstattung: Prof. Dr. Stephan Drusch
Tag der mündlichen Prüfung: 13. Mai 2020

Acknowledgement

First of all, I would like to thank the German Research Foundation (DFG) for financial support. This work was part of the SPP DiSP Biotech (project number: 273937032).

Special thanks to Prof. Karin Schwarz, for giving me the opportunity to write my doctoral thesis in the department of food technology.

A very big thank you goes to Dr. Anja Steffen-Heins, who already supervised me during my master's thesis and continued to support me during my time as a PhD student. I thank her for her effort, her time, and her open ear.

I would like to thank Prof. Stephan Drusch (TU Berlin) and Prof. Gerhard Schembecker (Dortmund University), for letting me work in their laboratories as well as Helena Schestkowa and Jörg Koop for introducing me to their methods and supporting me in carrying out the experiments.

I would particularly like to thank Prof. Malte Drescher and Dr. Mykhailo Azarkh (University of Konstanz) for providing their expertise, their patience, and for answering my numerous questions about EPR and simulation of EPR spectra.

I am grateful to my working group, Eva, Jule, Timon, Fyn, Laura, Jonas, Jonas, Julia, Tobi, Therese, Meike and Anne for the support in every way.

I would like to extend my gratitude thank my colleague Timon Heyn, who went with me all the way.

I would like to thank my students Sarah, Judith, Rebecca, Davide and Desiree for supporting my work.

I am deeply indebted to my "children" who always managed to keep me distracted from my work and helped me to clear my head in stressful times.

I would like to express my heartfelt gratitude to my parents for enabling me to write this work, with all their encouragement and support.

Many thanks to Falko, who supported me in every situation and watched my back in difficult times.

Abstract

The approach of site-directed spin labeling can be implemented for the food protein β-lactoglobulin (β-lg), by adjusting the pH value and the spin label/β-lg ratio, although it contains five cysteine residues, and used to characterize the amyloid aggregation mechanism of β-lg. Further, the surface activity of the amyloid aggregate system is determined by the smaller aggregates, peptides, and monomeric sized protein of the non-amyloid fraction due to faster migration to the interface and a higher adsorption rate. The results of this work are mainly based on measurements using electron spin resonance spectroscopy and mass spectrometry.

MTSSL and IPSL bind covalently and reproducibly to all five cysteine residues with different preferences. The best labelling conditions for MTSSL are pH 7.5 and an equimolar MTSSL/β-lg ratio. Whereby MTSSL dimers are already formed at a pH value of 7.5. The bonding of the spin labels to β-lg is temperature (90°C) and acid (pH 2) resistant, whereas it is assumed the biradicals are reduced to monoradical dimers during heat incubation.

Spin labeling with IPSL reduces the intra- and intermolecular β-sheets at pH 3.5. However, SDSL does not change the morphology and building blocks of amyloid aggregates but interferes with the thioflavin-T measurement. Impact of the label on the secondary protein structure is lower for MTSSL compared to IPSL because of its flexible bond.

MTSSL is most sensitive to changes in the arrangement of β-sheets, whereas IPSL is most sensitive to changes in random coil at position Cys^{160}. The amyloid aggregates formed at pH 3.5 could be characterized using SDSL. The monomer-like β-lg aggregates had the form of a pearl chain. However, the spin labeled side chains were not incorporated into amyloid structures formed at pH 2.

Fibrils and non-amyloid material act synergistically at the air-water interface because non-amyloid material is embedded into fibrillar network. But the adsorption behavior of the amyloid aggregate system is dominated by the non-amyloid fraction. Only small amounts of amyloid aggregates were necessary to stabilize foams. The airflow used for foaming resulting in gas bubbles caused sufficient shearing to partly degrade fibrils.

Table of Content

List of Figures

List of Tables

List of Formulas

List of Abbreviations

AAS	Amyloid aggregate system
ALAS	Amyloid-like aggregate system
AF	Amyloid fraction
ALF	Amyloid-like fraction
AFM	Atomic force microscopy
AITC	Allyl isothiocyanate
ATR	Attenuated total reflection
cw	Continuous wave
Cys	Cystein
DEER	Double electron-electron resonance
EPR E	Electron paramagnetic resonance
ESI	Electrospray ionization
FQ	Fluorescence quenching
FT-ICR	Fourier-transform ion cyclotron resonance
FT-ICR-MS	Fourier-transform ion cyclotron resonance mass spectrometry
FT-IR	Fourier transform infrared spectroscopy
HPLC	High performance liquid chromatography
IEP	Isoelectric point
IFT	Interfacial tension
IPSL	Iodacetamido proxyl spin label
LC	Liquid chromatography
LLD	Lower limit of detection
m/z	Mass-to-charge ratio
MALDI	Matrix-assisted laser desorption/ionization
MS	Mass spectrometry

MTSSL	Methanthiosulfonate spin label
n-AF	Non-amyloid fraction
n-ALF	Non-amyloid-like fraction
QToF	Quadropole time of flight
RDM	Ratio dimer-monomer
RP-HPLC	Reversed-phase high performance liquid chromatography
RSH	Free thiol group measurement
SDSL	Aite-directed spin labelling, Site-directed spin labeling
SEC	Size exclusion chromatography
STH	Short-time heated
ThT	Thioflavin T
Trp	Tryptophan
UH	Unheated
WPI	Whey protein isolate
α-la	α-lactalbumin
β-lg	β-lactoglobulin

1 General introduction

1.1 Preface

Bovine whey protein isolate (WPI) is a byproduct of cheese manufacturing and widely used as food ingredient because of its techno-functional properties (Singh, 2009) and its nutritional values (Singh, 2009). It is used for gelation (Barbut & Foegeding, 1993; Puyol, Pérez, & Horne, 2001), films (Wang et al., 2008), coatings (Schmid et al., 2012), foaming (Davis & Foegeding, 2004), and emulsifying (Bernard, Regnault, Gendreau, Charbonneau, & Relkin, 2011). The main component of the WPI is β-lactoglobulin (β-lg). The rest consists, among other things, of α-lactalbumin and bovine serum albumin.

β-lg is a lipocaline and many hydrophobic molecules can be bound or carried in the hydrophobic cavity such as retinol, fatty acids, vitamin D, and cholesterol (Kontopidis, Holt, & Sawyer, 2002; Narayan & Berliner, 1997; Qin, Creamer, Baker, & Jameson, 1998; Sawyer & Kontopidis, 2000; Wu, Pérez, Puyol, & Sawyer, 1999). The primary structure contains five cysteine residues whereby four of them build disulphide bridges. Bioactive compounds such as allyl isothiocyanate (Keppler et al., 2014), dialyl-disulphide, and allicin (Wilde, Keppler, Palani, & Schwarz, 2016) can bind to the free cysteine residue.

Under extreme conditions, β-lg is able to form amyloid aggregates (Adamcik & Mezzenga, 2012; Akkermans, Venema et al., 2008; Bolder, Vasbinder, Sagis, & van der Linden, 2007; Cao & Mezzenga, 2019; Hettiarachchi, Melton, Gerrard, & Loveday, 2012; Schokker, Singh, Pinder, & Creamer, 2000), which are known to have techno-functional properties (Loveday, Anema, & Singh, 2017). Amyloid aggregates can adsorb to the air-water (Oboroceanu, Wang, Magner, & Auty, 2014; Peng, Yang, Li, Tang, & Li, 2017) and oil-water interface (Jordens et al., 2014; Serfert et al., 2014) to stabilize foams and emulsions. Furthermore, the amyloid aggregates are used as coating material (Wang et al., 2019) or for gelation (Bolisetty, Harnau, Jung, & Mezzenga, 2012; Veerman, Baptist, Sagis, & van der Linden, 2003), foaming (Oboroceanu et al., 2014; Peng et al., 2017), and emulsifying (Jung, Gunes, & Mezzenga, 2010), and they are able to reduce the lipid oxidation of spray dried emulsions (Serfert et al., 2014).

Varying the conditions during the formation of amyloid aggregates leads to changes in the morphology and the building blocks of the aggregates. The protein concentration, the ionic strength, the pH value, the temperature, and shearing have an influence on the amyloid aggregation. All these aggregates have in common that they consist of stacked β-sheets, which makes them amyloid or amyloid-like aggregates. Far below the isoelectric point (~pH 2), β-lg forms long semi-flexible aggregates (Krebs, Devlin, & Donald, 2009), which are often named fibrils. Close to the isoelectric point (~pH 5), spherical aggregates (Krebs et al.,

2009; Rühs, Scheuble, Windhab, Mezzenga, & Fischer, 2012) and at weak acid conditions (~pH 3.5) worm-like rods are formed (Heyn et al., 2019; Keppler, Heyn, Meissner, Schrader, & Schwarz, 2019). Depending on the pH value, the amyloid aggregates are built up of different building blocks. Amyloid aggregates formed at pH 2 and consist of peptides, which result from the acid hydrolysis (Akkermans, Venema et al., 2008; Heyn et al., 2019; Keppler et al., 2019), whereas the aggregates formed at pH 3.5 consist of monomeric protein (Heyn et al., 2019; Keppler et al., 2019).

The morphology, for example the length, of the amyloid aggregates is also affected by the conditions during food processing. Shearing (Hill, Krebs, Goodall, Howlett, & Dunstan, 2006) and high pressure (Oboroceanu et al., 2014; Serfert et al., 2014) break up the aggregates, changing the pH value after aggregates formation altered the morphology from long to spherical aggregates (Akkermans, van der Goot, Venema, van der Linden, & Boom, 2008; Veerman, Baptist et al., 2003), freeze-drying will reduce the zeta-potential and increase hydrophobicity (Heyn et al., 2019), and the drying and rehydration have a strong impact on the viscosity of the fibril solution (Mudgal, Daubert, & Foegeding, 2011).

While the structure of amyloid aggregates at pH 2 has been well researched, the formation and the exact structure of amyloid aggregates at pH 3.5 is still unknown and are therefore called amyloid-like aggregates. However, not all of the native protein is converted into amyloid aggregates. The amyloid aggregate system (AAS) contains two fractions: One fraction contains the amyloid aggregates (amyloid fraction, AF) and the other one contains the peptides, smaller aggregates and protein of monomeric size (non-amyloid fraction, n-AF). The surface activity of the pure aggregates (Jordens et al., 2014; Peng et al., 2017) and the complete system are already investigated (Oboroceanu et al., 2014). However, the role of the non-amyloid fraction as well as the combination of the two fractions during adsorption and their stabilizing mechanism is still unclear. Furthermore, it is not yet known how exactly the n-AF is composed. It is only known that no amyloid aggregates are present and that the components are <300 kDa (Heyn et al., 2019).

Amyloid aggregates can also be formed by many other proteins, like α-synuclein (Chen, Margittai, Chen, & Langen, 2007), amyloid β (Gu, Tran, Jiang, & Guo, 2016), lysozym (Mchaourab, Lietzow, Hideg, & Hubbell, 1996), and tau (Margittai & Langen, 2004). Site-directed spin labeling (SDSL) in combination with electron paramagnetic resonance (EPR) spectroscopy is a powerful tool for studying structure and dynamics of biological macromolecules and are already used to monitor amyloid aggregation (Drescher, 2012; Török et al., 2002). To characterize the aggregation of β-lg with EPR, the protein needs to be labeled with a stable radical. A free cysteine residue is necessary for spin labeling. Most proteins are genetically or chemically modified, so that the protein contains only one cysteine

residue at a targeted position. The spin labels provide information about their microenvironment. The structure and dynamic, as well as the location of the spin labeled side chain can be seen in the continuous wave (cw) EPR spectra. Furthermore, using pulsed EPR, the spatial distribution of the spin labels can be investigated and, therefore, the arrangement of the protein in the aggregates. However, the cw EPR spectra can be very complex and consist of many superimposed radical components. To get knowledge about the individual components, a spectra simulation can be conducted. Assumptions are made about the individual components, for example which motional regime they belong to in order to choose the right function for the fit. Furthermore, the number of components, the values for the rotation correlation times, and for the polarity of the microenvironment can be adapted to get the best fit.

SDSL has not yet been applied to food proteins. In order to maintain the integrity of the food, it is of great importance that the primary and secondary structure of protein is not altered. Even the replacement of a single amino acid can lead to a fundamental change in the behavior of the protein. Therefore the primary structure of the protein should not be altered. Since β-lg contains five cysteine residues, not only the binding conditions but also the binding position have to be investigated. Furthermore, the conditions, mainly the pH value, for spin labeling and for compounds to bind to β-lg were different. Thus, the influence of the binding conditions on the spin label and the stability of the bonding is of great importance.

1.2 Motivation and objectives

The aim of this work was to investigate the amyloid aggregation of β-lg using EPR to characterize the structure of the AAS and of its individual fractions after separation by ultrafiltration. The mechanism of aggregation from peptides and from the entire protein will be elucidated by simulation of the EPR spectra. Therefore, the best conditions to reach the highest labeling without influencing the protein structure and the spin label itself were investigated. In order to use SDSL for amyloid aggregation, it is of great importance that the label does not influence amyloid aggregation and that the spin labeled side chain can be assigned to the EPR spectrum using mass spectrometry. At pH 2 only ~ 20% of the WPI is converted into amyloid aggregares and therefore ~ 80% of AAS consits of smaller aggregates, monomeric sized proteins and peptides. Hence, it is of great importance to investigate the influence of the two fractions on the surface activity using pendant drop analysis and Langmuir-Blodgett measurements. Therefore, the following hypotheses will be discussed:

Hypothesis 1:

For labeling of β-lg with MTSSL, low spin label concentrations and slightly alkaline pH values can be used which did not affect the degree of polymerization. MTSSL is known to form biradicals at concentrations >200 µmol/l and at neutral to alkaline pH values. The spin-spin couplings within the biradical lead to an additional five-line EPR spectrum that superimposes the monomer spectra of bound and unbound MTSSL, which in turn impairs the evaluation of the EPR spectra. By means of high resolution mass spectrometry, various MTSSL monomer and dimer adducts can be identified by their mass-to-charge ratio and correlated with the MTSSL monomer and dimer components that will be obtained from the EPR measurement and by simulation of the EPR spectra using EasySpin software package.

Hypothesis 2:

Labeling conditions for binding of MTSSL and IPSL to β-lg can be optimized to reach the highest labeling rate and to ensure that the ability of the label to bind to the protein is not affected by the conditions selected. By varying the ratio of spin label/β-lg and the pH value, the optimal conditions can be determined, since an increasing pH raises the reactivity of the thiol group of the cysteine residue**.** The optimum conditions for the modification of β-lg with bioactive compounds and the spin labeling of other proteins differ mainly in their pH value and the ligand/protein ratio. The typical ligand binding methods, such as free thiol group measurements and determination of the bonding by changes of the hydrophobicity of the protein by reversed-phase high performance liquid chromatography, will be used to determine the highest labeling rate.

Hypothesis 3:

The application of SDSL to natural β-lg, which contains five cysteine residues, is possible without modification of protein primary structure, and the spin labeled side chains can be assigned to the different components of the superimposed EPR spectra by means of spectra simulation. SDSL is mostly used for proteins containing only one cysteine residue for labeling in a targeted position. Spin labels can bind to all five cysteine residues, because at the alkaline pH value bioactive compounds were able to shuffle to other cysteine residues. However, the five possible binding sites of β-lg are located in different regions of the protein. Therefore, the binding sides can be assigned to different spectral components in the EPR spectrum by spectral simulation. The assignment of the spectral components is validated by mass spectrometric analysis of labeled and unlabeled cysteine-containing peptides after tryptic digestion.

Hypothesis 4:

Spin labeling of β-lg with MTSSL or IPSL is possible without affecting the secondary and tertiary protein structure of the unheated protein or amyloid aggregates at pH 2 and pH 3.5 due to the small size and flexibility of the spin labels. Both spin labels have already been used to characterize amyloid aggregates from other proteins such as amyloid β and α-synuclein without affecting the structure of the aggregates. Conformational changes are determined by Fourier transformation infrared spectroscopy and intrinsic tryptophan fluorescence. Alterations in the conversion from labeled β-lg monomer to amyloid aggregates are measured by β-sheet specific fluorescent dye thioflavin-T. The conversion rate is determined by protein concentration measurements after ultrafiltration of amyloid aggregates from the non-amyloid material. The building blocks and morphologies of the amyloid aggregates are determined by size exclusion chromatography and atomic force microscopy.

Hypothesis 5:

The mechanism of aggregation at pH 2 and 3.5, which differ in their building blocks and morphology, can be described by the changes in the spectral components of the EPR spectra. EPR spectra provide information on the microenvironment of the spin labels, which is different in the native protein compared to amyloid aggregates. The separation of the amyloid and non-amyloid fraction result in different microenvironments, which are mainly reflected by the rotation correlation time. The ultrafiltration separates the amyloid aggregates from the non-amyloid peptides and proteins. Its recorded EPR spectra are simulated with the software package EasySpin that in turn provides information about the structural and dynamic properties of the two fractions. Pulsed EPR measurements provide information about the spatial distribution of the spin labels by determination of the distance between two labeled side chains.

Hypothesis 6:

The individual fractions of the WPI amyloid aggregate system formed at pH 2 has individual effects on the foaming properties caused by different diffusion and adsorption rates because of the different sizes of aggregates and peptides. The particle size dominates the migration of structures through a fluid, i.e., smaller structures migrate much faster to interfaces than long fibrils. The long fibrils form a two dimensional network at the interface. The adsorption behavior is investigated by drop tensiometery, while the film properties are measured with the Langmuir Blodgett trough. The contribution of each fraction to foam stability and foamability is determined with a glass jacket column, whereby the content of non-amyloid material is increased by lower initial protein concentrations.

2 Theoretical background

2.1 Whey protein isolate and its major compound β-lactoglobulin

Whey proteins are divided into two fractions: the albumin fraction (β-lg, α-lactalbumin (α-la), and serum albumin) and the globulin fraction (immunoglobulins and lactoferrin). All whey proteins have a globular structure, which is very compact due to disulfide bridges. The structure, the free thiol groups, the lysine residues, and the hydrophobic core enables to bound compounds to the protein and use them as a carrier for bioactive molecules (Keppler et al., 2014; Rade-Kukic, Schmitt, & Rawel, 2011; Wilde, Keppler et al., 2016). Whey is mostly used as WPI, it has the highest protein content compared to whey concentrate and whey isolate. Furthermore, it is almost free of lactose and fat. β-lg is the major whey protein and accounts for about 50-60% of the whey proteins in cow's milk. Since β-lg strongly contributes to the functional properties, it is often the focus of research. However, the function of β-lg in milk is still unclear, although it is assumed that β-lg serves as a transport protein (Kontopidis et al., 2002).

2.1.1 Structure of β-lactoglobulin

Bovine β-lg is a small globular protein consisting of 162 amino acids with a molecular weight of approximately 18.3 kDa and belongs to the lipocaline family. It occurs in a number a different genetic variants. In bovine milk, the most common variants are A and B (Aschaffenburg & Drewey, 1955). These two genetic variants differ in two amino acids: A: Asp^{64}, Val^{118} and B: Gly^{64}, Ala^{118}. These two amino acids influence the solubility and the thermal stability of the protein (Keppler, Sönnichsen, Lorenzen, & Schwarz, 2014; Qin, Bewley, Creamer, Baker, & Jameson, 1999).

The secondary structure of β-lg is stabilized by two disulfide bridges, which are formed by four of the five cysteine (Cys) residues (Cys^{66}-Cys^{160} and Cys^{106}-Cys^{119}/Cys^{121}). One disulfide bridge (Cys^{66}-Cys^{160}) is located close to the C-terminus on the surface of the protein and is, therefore, clearly accessible (McKenzie, Ralston, & Shaw, 1972). The other one (Cys^{106}-Cys^{119}/Cys^{121}) is located in the core between two β-sheets (Sakurai, Konuma, Yagi, & Goto, 2009). Because of thiol exchange reactions, Cys^{119} or Cys^{121} may be present as a free thiol group (Ferranti, Mamone, Picariello, & Addeo, 2011). The secondary structure consists of 50% β-sheets, 30% random coil, and 15% α-helix. Eight antiparallel β-strands, which form a β-barrel (β-strand A-H) are in the core (Papiz et al., 1986; Sawyer & Kontopidis, 2000). The ninth β-strand (β-I) connects the β-lg monomers to a dimer (Sakurai et al., 2009). Inside the β-barrel is a hydrophobic cavity, where small hydrophobic molecules can be deposited, like fatty acids, fat-soluble vitamins, as well as hydrophobic polyphenols, depending on the pH value. The loop from the β-strands E and F (residues 85-90) forms a lid to the β-barrel, which

is closed under pH 6.5 and open above 8.5, which is known as Tanford transition (Tanford, Bunville, & Nozaki, 1959).

The fluorescence of β-lg is dominated by the tryptophan (Trp) residues. The two tryptophan residues, Trp^{19} and Trp^{61}, are located in different environments. Trp^{19} is located in an apolar environment in the cavity of the protein, while Trp^{61} is involved in the antiparallel interaction of the dimer (Sakurai et al., 2009). The fluorescence of Trp^{61} is partially or completely suppressed by the disulfide bridge of Cys^{66}-Cys^{160} (Albani, Vogelaer, Bretesche, & Kmiecik, 2014; Croguennec, Mollé, Mehra, & Bouhallab, 2004). This can be determined over a broad pH range (pH 2-11) and is independent of the proportion of monomers and dimers in a solution (Albani et al., 2014).

The structure of β-lg also depends on the treatment of the protein. For example, heat and pH have an influence on the structure. Since the structure is decisive for the interfacial activity of the protein, it exhibits different interfacial activity at different pH values. At the natural pH value of milk (pH 6.7), β-lg is available as a dimer, which is held together by non-covalent bonds (Dickinson, 1998). In the acidic range (~pH 2), β-lg is increasingly present as a monomer (Shimizu, Saito, & Yamauchi, 1984; Uhrínová et al., 2000; Yan et al., 2013). Between pH 3 and pH 7.5, β-lg is mainly present as a dimer, but this is still dependent on protein concentration, ionic strength, and temperature and is also associated with an octamer in the range from pH 3.5 to isoelectric point (IEP) (pH 5.2) (Rade-Kukic et al., 2011; Shimizu et al., 1984).

By changing the conformation of the protein at different pH values, the hydrophobicity of the protein also changes (Fang & Dalgleish, 1997; Shimizu et al., 1984). Thus, the conformation at pH 3 is stronger and more resistant to denaturation than at pH 7. In acidic pH ranges, β-lg exhibits relatively low emulsifying and surface activity, with surface hydrophobicity higher than at neutral pH values. The cleavage of the intramolecular disulfide bridges increases the denaturability, as does the emulsifying activity of β-lg at pH 3 (Shimizu et al., 1984).

2.1.2 Binding properties of molecules to β-lactoglobulin

As the most lipocalins, β-lg also binds small hydrophobic molecules within its calyx. A variety of compounds bound to free cysteine residue which is buried between the β-barrel and the C-terminal major α-helix (Sakai, Sakurai, Sakai, Hoshino, & Goto, 2000). The bonding of many components to Cys^{121} is well described (Burova, Choiset, Tran, & Haertlé, 1998; Cupo & Pace, 1983; Keppler et al., 2014; Rade-Kukic et al., 2011; Sakai et al., 2000; Wilde, Keppler et al., 2016). The modification can affect the secondary, tertiary or quaternary structure of the protein. Furthermore, the conformational stability influences the denaturation, which becomes reversible due to the modification (Burova et al., 1998; Cupo & Pace, 1983).

After removing the label, β-lg can go back to its native folding state (Sakai et al., 2000). Furthermore, the dimer-monomer equilibrium is shifted towards the monomeric form (Burova et al., 1998). At neutral pH, the native protein is dimeric, whereas β-lg labeled with dithionitrobenzoic acid is monomeric. At pH 2, the modification of the buried thiol group destabilizes the rigid hydrophobic core and the dimer interface, producing a monomeric state that is native-like (Sakai et al., 2000). Because of the intermolecular disulfide exchange reaction, it is possible that the bound compound can shuffle to another thiol group. The enzymatic digestion of β-lg before mass spectrometry measurements enables the localization of the bound compound. Keppler et al. (2014) figured out, that the bioactive compound allyl isothiocyanate (AITC) can cleave the disulfide bridge Cys^{66}-Cys^{160} and bind to Cys^{66}, Cys^{160}, and Cys^{121}. Whereas the second disulfide bridge stays intact. It is also described, that both disulfide bridges Cys^{106}-Cys^{119} and Cys^{106}-Cys^{121} are simultaneously present (Ferranti et al., 2011) and Kehoe et al. (2007) figured out, that Cys^{160} seems to be always involved into the disulfide bridge and all four other cysteine residues can be modified by disulfide exchange. However, Cys^{119} and Cys^{121} seem to be the preferred side chains for modification (Wilde, Treitz et al., 2016).

2.1.3 Amyloid aggregation of β-lg

Amyloid aggregates are mostly associated with neurodegenerative diseases. In biomedical science, they are called amyloid fibrils and defined as ‘thermodynamically stable, structurally organized, highly insoluble, filamentous protein aggregates being composed of repeating units of β-sheets (Finder & Glockshuber, 2007). But not only the amyloid-β, which is associated with Alzheimer’s diseases, is able to form amyloid aggregates. Also various food proteins, like egg proteins (Veerman, Schiffart, Sagis, & van der Linden, 2003), soy proteins (Wan, Yang, & Sagis, 2016), and milk proteins (Adamcik & Mezzenga, 2012; Akkermans, Venema et al., 2008; Bolder, Hendrickx, Sagis, & van der Linden, 2006; Goers, Permyakov, Permyakov, Uversky, & Fink, 2002; Usov, Adamcik, & Mezzenga, 2013; Veerman, Sagis, Heck, & van der Linden, 2003) are able to form amyloid aggregates. In this case, all aggregates are sensitive to thioflavin-T (ThT), which means, aggregates with at least five strands of β-sheets (Krebs, Bromley, & Donald, 2005), are called amyloid aggregates. Fibrils are amyloid aggregates that have a long semi-flexible morphology. However, aggregates that are sensitive to ThT and whose structure is unclear are named amyloid-like aggregates.

At neutral pH, the denaturation temperature of β-lg is >70 °C. The β-lg dimer dissociates and begins to unfold and aggregates are formed by thiol disulfide exchange and thiol oxidation. The unfolding leads to the exposure of groups, which are buried in the core of the globular protein. Below pH 7 the reactivity of the disulfide bond is limited and other types of bonds (hydrogen bonds, hydrophobic associations) become more relevant. At acidic pH values

(<pH 3) β-lg is present as a monomer with a high net charge. The heat treatment at low pH values and low ionic strengths can cause structural changes of β-lg, which can lead to the formation of supramolecular aggregates. Two theories exist on how the amyloid aggregation is performed, while the theory of hydrolyzed peptides stuck together to form amyloid aggregates is predominant (Figure 2-1). Amyloid aggregates, which are formed by whey protein mixtures, seem to originate only from β-lg. Although some studies have shown that both α-lactalbumin (Goers et al., 2002) and serum albumin (Usov et al., 2013; Veerman, Sagis et al., 2003) can form amyloid aggregates, β-lg appears to be the only relevant whey protein that forms long amyloid structures during heating (Bolder et al., 2006). However, the amyloid aggregation can be influenced by many determinants such as pH value and other processing conditions.

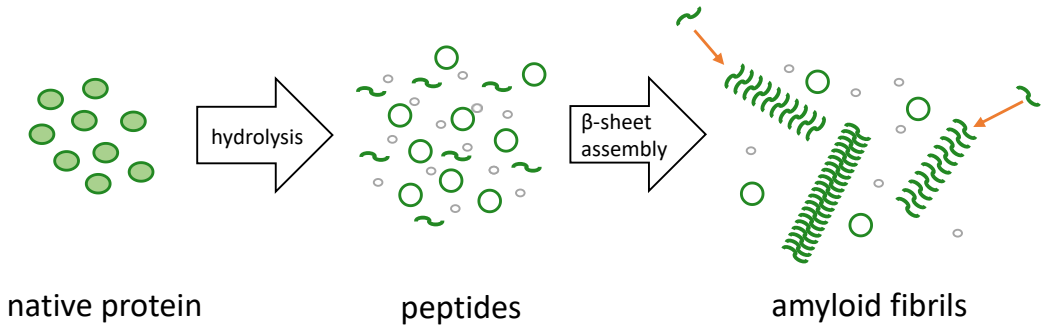

Figure 2-1: Schematic illustration of amyloid fibril formation of β-lg at pH 2. The native protein is hydrolyzed into peptides. The β-sheet rich peptides assemble into fibrils. Modified according to (Kroes-Nijboer, Venema, & van der Linden, 2012).

2.1.3.1 Influence of pH value on the formation of amyloid aggregates

The nearness to the isoelectric point (IEP) of β-lg determines the form of the aggregates. Fibrils are formed at pH values far from the IEPs, while spherical aggregates emerge at pH values near the IEP (Krebs et al., 2009). Furthermore, different pH values lead to amyloid aggregates with different morphologies and building blocks (Heyn et al., 2019; Keppler et al., 2019). At acidic pH values (<pH 3) long semi-flexible fibrils are formed. With increasing pH, the fibrils become shorter and worm-like. Also the mechanism of formation is changed. Hence, the building blocks are the main difference between the long semi-flexible fibrils and the worm-like aggregates (Heyn et al., 2019). At pH 2, acid hydrolysis cleaves the protein into peptides and the β-sheet rich peptides stuck together and form long semi-flexible aggregates, whereas at pH 3.5 the whole protein forms worm-like aggregates (Akkermans, Venema et al., 2008; Heyn et al., 2019; Keppler et al., 2019). However, not the entire protein is converted to amyloid aggregates. The amyloid aggregate system (AAS) consists of two fractions: the amyloid fraction (AF) and the non-amyloid fraction (n-AF). At pH 2 ~40% of the

initial protein is converted to long semi-flexible fibrils, whereby at pH 3.5 ~80% worm-like aggregates are formed (Keppler et al., 2019) (Figure 2-2). The n-AF represents the non-amyloid aggregated material and contains a mixture of peptides, smaller aggregates and monomeric sized protein (Akkermans, Venema et al., 2008). At pH 2, most of the monomeric β-lg is hydrolyzed during the fibril formation, preferred at peptide bonds involving aspartic acid residues (Akkermans, Venema et al., 2008; Hettiarachchi et al., 2012). The peptides in the AF are determined by their hydrophobicity, net charge, charge distribution, and capacity to form β-sheets (Akkermans, Venema et al., 2008). Both, Akkermans, Venema et al. (2008) and Hettiarachchi et al. (2012) found the region 1-53 in the amyloid aggregates, while Akkermans, Venema et al. (2008) also found the region 98-130 in the AF.

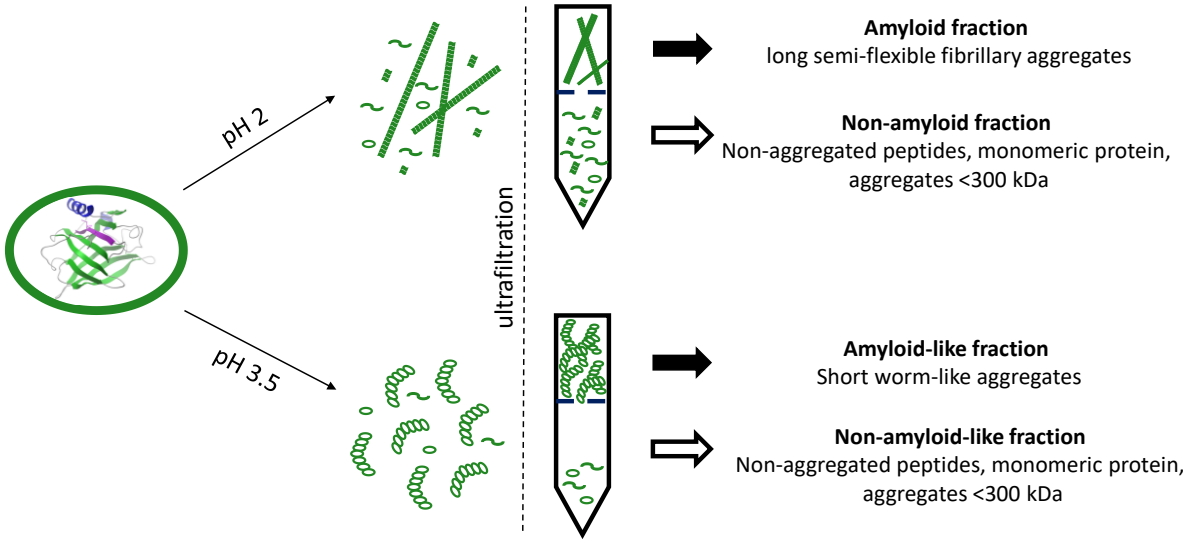

Figure 2-2: Amyloid aggregation of β-lactoglobulin at pH 2 and pH 3.5. Separation of the amyloid and non-amyloid fraction by ultrafiltration.

2.1.3.2 Influence of processing conditions on the structure of amyloid aggregates

Not only the pH value influences the fibril formation. Also other parameters like stirring, heating time, and the initial protein concentration influence either the morphology and/or the conversion rate of the amyloid aggregates. Without stirring, it is possible to form spherulites using WPI (Sagis et al., 2002). Stirring during heating the protein solution enhances the fibril formation significantly (Bolder, Sagis, Venema, & van der Linden, 2007). The conversion of the monomeric protein into amyloid aggregates (Aymard, Nicolai, Durand, & Clark, 1999; Bolder, Vasbinder et al., 2007) and the aggregate size (Schokker et al., 2000) is increased with increasing heating time.

Shearing induces aggregation of spheroidal seed-like species. These seeds enhance the fibril formation of native β-lg (Hill et al., 2006). Shear flow produces an amyloidogenic precursor and a higher shear rate increases the rate and extent of precursor formation. The shear flow is an onset of sufficient magnitude to initiate amyloid aggregation. Without shear flow, the initiation of the fibril formation is much slower (Akkermans et al., 2006). However, extended shear treatment does not have any effect and preformed amyloid fibrils degrade in continuous high shear (Akkermans et al., 2006; Hill et al., 2006). Because β-lg amyloid fibrils are much weaker compared to covalently bound polymers, even relatively low strain rates cause fibril fracture (Kroes-Nijboer, Venema, Baptist, & van der Linden, 2010). The morphology is not influenced by the temperature during the fibril formation. Only the ThT-fluorescence indicated the maximal formation rate at temperatures above 100°C, but the overall conversion rate is not affected (Loveday, Wang, Rao, Anema, & Singh, 2012).

In addition, the initial protein concentration can influence amyloid aggregation. An increasing initial WPI concentration leads to a higher amount of amyloid aggregates in solution (Bolder, Vasbinder et al., 2007; Schokker et al., 2000). However, an increasing concentration of the egg protein ovalbumin leads to the formation of longer aggregates (Veerman, Schiffart et al., 2003).

2.1.3.3 Surface activity of amyloid aggregates

The interfacial properties of β-lg fibrils have drawn wide attention in the food industry to serve as food ingredients. Therefore, the reduction of interfacial tension (IFT) of the air-water and oil-water interface in the presence of β-lg fibrils was investigated. β-lg fibrils formed at pH 2 built a highly elastic interface resulting in a 2-dimensional liquid crystalline domain (Jordens et al., 2014; Jung et al., 2010). The aggregates form networks of interdependence, which are responsible, among other things, for their viscosity-increasing effect (Loveday et al., 2017). As more fibrils adsorb at the interface, a multilayer is created and fibril fracture in the topmost layer can be observed, resulting in a decrease in interfacial elasticity (Jordens et al., 2014). The fibrillary structure reduces the IFT more rapidly than the native monomer system (Jung et al., 2010) and a fibrillated WPI solution has a higher foam stability compared to untreated WPI (Mohammadian & Madadlou, 2016). This is attributed to a higher viscosity and a gel-like network in the solution. However, the foam stability is dependent on the pH value of the fibril solution. Fibrils at pH 2 had the lowest foam stability due to the strong electrostatic repulsion and the slower adsorption to the interface compared to fibrils at pH 5 (Peng et al., 2017). The slower adsorption was accompanied by slower diffusion to the interface, which is due to the bigger size of the fibrils. At pH 5, the fibrils are much shorter than at pH 2 (Peng et al., 2017). Whereas Oboroceanu et al. (2014) demonstrated that the foam stability and foamability seemed to be independent of the fibril length. Also at the oil-water interface, fibrillated WPI

exerted a significantly higher elasticity and a better emulsifying activity compared to native WPI (Serfert et al., 2014).

The adsorption kinetic of the amyloid aggregate system of soy protein is mainly dominated by the high proportion of smaller peptide material (80%). The initially faster adsorption can be explained by the faster adsorption of the small peptides at the interface. The pure fibrils adsorb slower due to the larger size of fibril clusters. At pH 5 and 7, the fibrils and peptide clusters contribute to the foam stability (Wan et al., 2016).

2.2 Foams

Foams are polydisperse systems with a gas-liquid interface. The interface is the area between two phases. The cohesion forces are responsible for the interfacial tension (IFT) (Equation 1) and act on the molecules inside the phase and are the same in all directions, resulting in a net force of zero. The molecules on the surface are surrounded by the same molecular species. Therefore, the cohesion forces are directed into the inner phase. This leads to a higher energy level and forces the liquid to minimize the surface area. To increase the surface area (A), work must be done (W).

Equation 1: Interfacial tension

$$\gamma = \Delta W/\Delta A \qquad (1)$$

The gas bubbles are separated with thin films of liquid. To create a foam three conditions are needed: 1. Energy is necessary to increase the interfacial area. This energy is proportional to the interfacial tension. 2. Surface-active compounds are needed to reduce the interfacial tension and thus the free energy of the system to achieve a kinetically stable foam. 3. The formation needs to be faster than its breakdown. The gas bubble in a foam is stabilized by a bilayer of surface-active compounds and thus the thin film determines the stability of the foam.

Surface-active compounds reduce the surface tension which can be measured with different methods. For example, with the pendant drop tensiometry (2.4.4.2) and the Langmuir Blodgett trough (2.4.4.1). In the case of proteins, adsorption to the interface does not only influence the IFT but also the proteins itself. The adsorption leads to the exposure of hydrophobic residues during structural rearrangements at the interface (Zare, McGrath, & Allison, 2015).

Foamability is an overall capacity of surfactant solution to produce foams, whereas foam stability refers to the lifetime of foam column. The foamability of a solution is a measure of its

capacity to produce a foam. During the foam formation, the surface energy (E) increases with the creation of gas-liquid interfaces with the surface tension (σ) and the interfacial area (A) (Equation 2).

Equation 2: Surface energy

$$E = \sigma A \qquad (2)$$

The increase in surface energy means, the foam formation is not a spontaneous process, and the input of energy is indispensable to generate a column of foam (Wang, Nguyen, & Farrokhpay, 2016). The foam surface area is inversely proportional to the surface tension, which means that a lower surface tension will increase the foamability from the perspective of surface energy.

On the macroscopic scale, physical properties, like stability, structural or rheological properties, are important. On the contrary, at the microscopic scale it is important to consider the interaction of surface-active compounds with the interface and with each other. The main goal is improving the macroscopic characteristics by controlling the microscopic scale.

2.3 SDSL for structural characterization of proteins

2.3.1 Site-directed spin labeling (SDSL)

Site-directed spin labeling (SDSL) in combination with electron paramagnetic resonance (EPR) spectroscopy (2.4.1) is a powerful tool for studying structure and dynamics of biological macromolecules and is already used to monitor amyloid aggregation (Drescher, 2012; Török et al., 2002). In SDSL, unpaired electrons are attached as spin labels to the system under investigation. The labeling allows EPR measurements of an otherwise diamagnetic molecule. The consideration of the EPR spectrum allows to draw conclusions about the microenvironment of the spin label. SDSL can provide detailed information about the binding site and provide insights into kinetic and structural aspects of the protein under investigation. Beyond that, advanced applications of this approach enable the measurement of intramolecular distance between two spin labels within proteins (Berliner, Grunwald, Hankovszky, & Hideg, 1982; Schmidt et al., 2015). However, SDSL has not been applied so far in food chemistry and food biophysics to evaluate the dynamics of non-covalent protein aggregation.

SDSL can also be used for distance measurements due to dipole-dipole coupling between electron spins. If two labeled molecules are in a stable macromolecule complex or two-spin

label side chains are introduced into a biomolecule, the distance between these two labels can be determined (Klare, 2012). This coupling can be measured and the distance determined. With cw-EPR distances up 2 nm can be measured, whereas with pulsed EPR technique of double electron-electron resonance (DEER) the frequency of dipolar interaction between paramagnetic centers can be measured and distances up to 8 nm can be accessed (Borbat, Davis, Butcher, & Freed, 2004; Godt, Schulte, Zimmermann, & Jeschke, 2006; Jeschke, Bender, Paulsen, Zimmermann, & Godt, 2004). For such experiments, the microwave is not continuous but pulsed (2.4.1). The spin label distribution and, therefore, the 3D-structure of aggregated proteins can also be measured with pulsed EPR (Milov et al., 2004).

2.3.1.1 Spin labels

For successful use of spin labels, it is of particular importance that the labeling does not significantly alter the structure of the protein. Nitroxide spin labels are often used for this approach. They carry a thiol-reactive group, such as a maleimido group, a methanethiosulfonate group, or an iodoacetamido group. The most widely used cysteine-specific spin label is the (1-oxyl-2,2,5,5-tetramethylpyrroline-3-methyl) methanthiosulfonate spin label (MTSSL) (Berliner et al., 1982), mainly because of its high selectivity towards thiol groups and its high flexibility due to the five rotatable bonds and the resulting low influence on the protein structure (Bordignon, 2007). MTSSL is bound to the protein by the formation of a disulfide bridge (S-S) with the cysteine. The linker between the nitroxide ring and the protein backbone leads to flexibility of the spin labels side chain and thus minimizes interference with the folding and function of the labeled protein. The unique dynamics of MTSSL are able to provide detailed structural information from the shape of the EPR spectrum. It's main disadvantage is the unstable character of the disulfide bridge under reducing conditions. Malmeidio or iodoacetamido labels are preferable. Iodoacetamide and maleimide reactive groups result in a C-S bond, an irreversible bond to cysteines that is not influenced by reducing conditions (Klare, 2012) (Figure 2-3). One example for an iodoacetamido spin label is the 3-(2-*Iodoacetamido)-proxyl* (IPSL), which is also used in structural biology. The disadvantage of this spin label is its lower selectivity for cysteines compared to MTSSL. Furthermore, the iodoacetamide group can interact with lysine, histidine, methionine, and carboxylates especially at high pH-values (>8) (Goldfarb & Stoll, 2018). Compared to MTSSL, IPSL is bigger (MW_{MTSSL} = 264.38 Da; MW_{IPSL} = 325.17 Da) and has a lower flexibility which may destabilize the protein or alter its conformation, but the bonding is more stable.

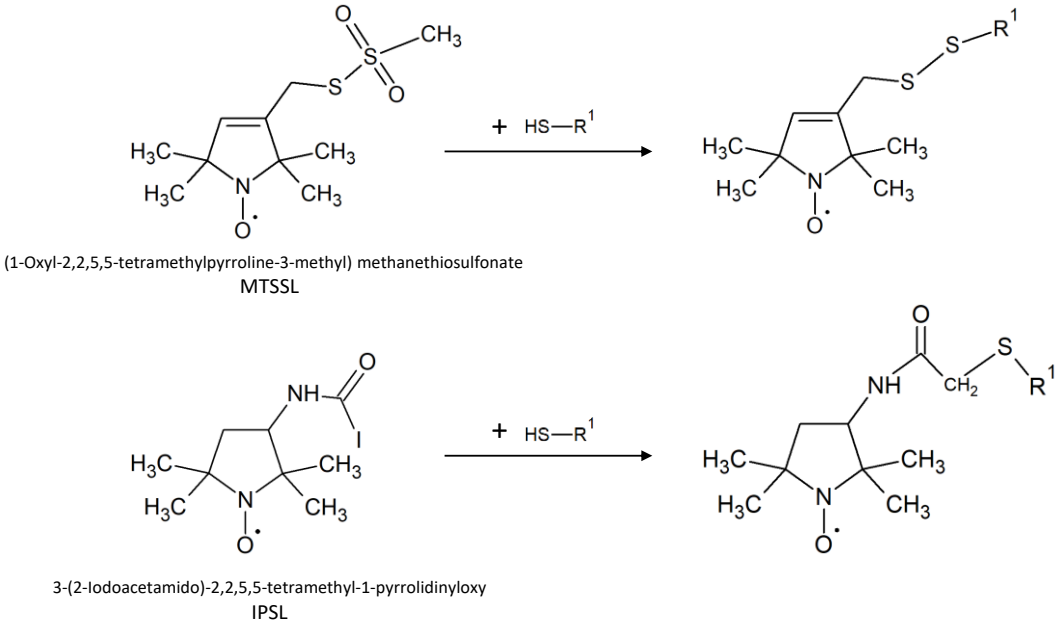

Figure 2-3: Bonding of the spin labels MTSSL and IPSL to a free thiol group.

Complications with spin labels can be for example due to internal dynamics and conformational distributions of spin labels. It would be conceivable that those complications with spin labels can be prevented by selecting a rigid, conformational unambiguous label, as a short linker, which has no bonds that can undergo rotations. However, such labels also have the highest propensity for distorting structure and function of the researched substance. A shortening of the linker can lead to less selectivity or reactivity of the thiol group, which makes such labels less versatile than MTSSL. At alkaline pH values, MTSSL monomers are able to dimerize via a disulfide bridge and form biradicals (Bordignon, 2007) (Figure 2-4). In EPR spectra, those biradicals exhibit a five-line spectrum as the two electrons interact by spin exchange (Luckhurst, 1966). However, the majority of SDSL studies are still performed with MTSSL.

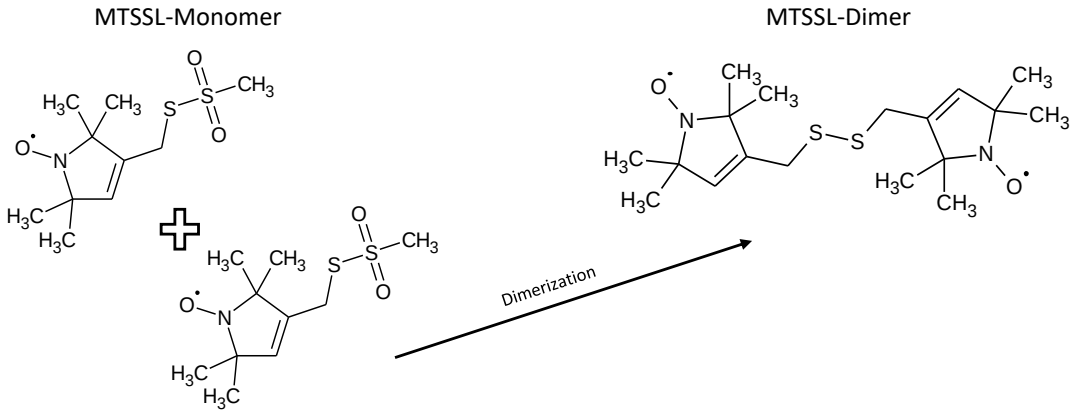

Figure 2-4: Dimerization of MTSSL-monomers at basic pH values

2.3.1.2 Binding conditions of spin labels to various proteins

A cysteine residue is required for the covalent binding of a spin label to a protein. If the protein does not naturally contain cysteine residues, it has to be engineered into the distinct positions (Chen et al., 2007; Gu et al., 2016; Sepkhanova et al., 2009; Török et al., 2002). The amyloid β, which forms pathogenic amyloid aggregates, and its mutants, contain cysteine residues at different positions and can be expressed in *Escheria coli* (Gu et al., 2016; Mchaourab et al., 1996). If the protein contains more than one free cysteine it is recommended to remove the disruptive cysteine residues (Kirby, Karim, & Thomas, 2004; Margittai & Langen, 2004) to avoid spin-spin interactions. Spin labeling is mostly performed at pH values of 7.4 to 7.6 and with a 4- to 10-fold molar excess compared to protein concentration with a subsequent removal of the unbound spin label (Chen et al., 2007; Kirby et al., 2004; Mchaourab et al., 1996; Török et al., 2002). The removal of the excess is mostly conducted by gel filtration (Chen et al., 2007; Gu et al., 2016; Margittai & Langen, 2004; Török et al., 2002) or (semi-)preparative high performance liquid chromatography (HPLC) (Kirby et al., 2004; Sepkhanova et al., 2009).

2.3.2 Spectra simulation and interpretation

EPR spectra contain different information about the microenvironment of the radical. Out of a single spectrum, information such as micropolarity, mobility, or concentration can be extracted. The micropolarity of a radical, such as a nitroxide spin probe or spin label, can be seen in hyperfine splitting (a_N), the distance between the peaks, and the hyperfine component A_{zz}. The A_{zz} value shifts to a higher value with increasing polarity, whereas the g-tensor decreases. However, the A_{zz} component can only be obtained in frozen samples (Klare, 2012). The nitroxide spin probe Tempol has an a_N value ~17.1 G in the high polar solvent water, whereas an unpolar solvent (carbon tetrachloride) leads to lower a_N values (~15.4 G) (Windle, 1981). However, the exact values are also dependent on the chemical

structure of the nitroxide radical (Janzen, Coulter, Oehler, & Bergsma, 1982). The mobility is given as rotation correlation time (τ_C) and is seen within the line shape (Figure 2-5). A free rotating electron undergoes isotropic motions, which result in sharp peaks. A fast motion, on a time scale of $\tau_C < 10^{-9}$ s, the spectra display g-values (g) and hyperfine splitting (a_N) that are the average of the principal components of the corresponding tensor (Schreier, Polnaszek, & Smith, 1978). A slower radical results in peaks broadening and the outer peaks become smaller. The concentration of the free electrons can be seen within the peak height and the integral. As the peak height is also influenced by the mobility, only concentrations with the same mobility can be determined by the peak height. The integral includes also the peak broadening and is therefore also applicable for different mobilities. But as the integral is sensitive to noise, it is not useful for low concentrations. These values always reflect an average of all free electrons, but do not take into account that electrons may have different microenvironments. In order to obtain information about the individual components, a simulation of the spectrum is necessary. In a simulation, assumptions are made about the number and microenvironment of the individual components and thus approximate the original spectrum. EasySpin, a tool running on Matlab, is the most common program to simulate EPR spectra (Stoll & Schweiger, 2006). Different simulations for different motional regimes are available for the spectra simulation with EasySpin (Figure 2-5).

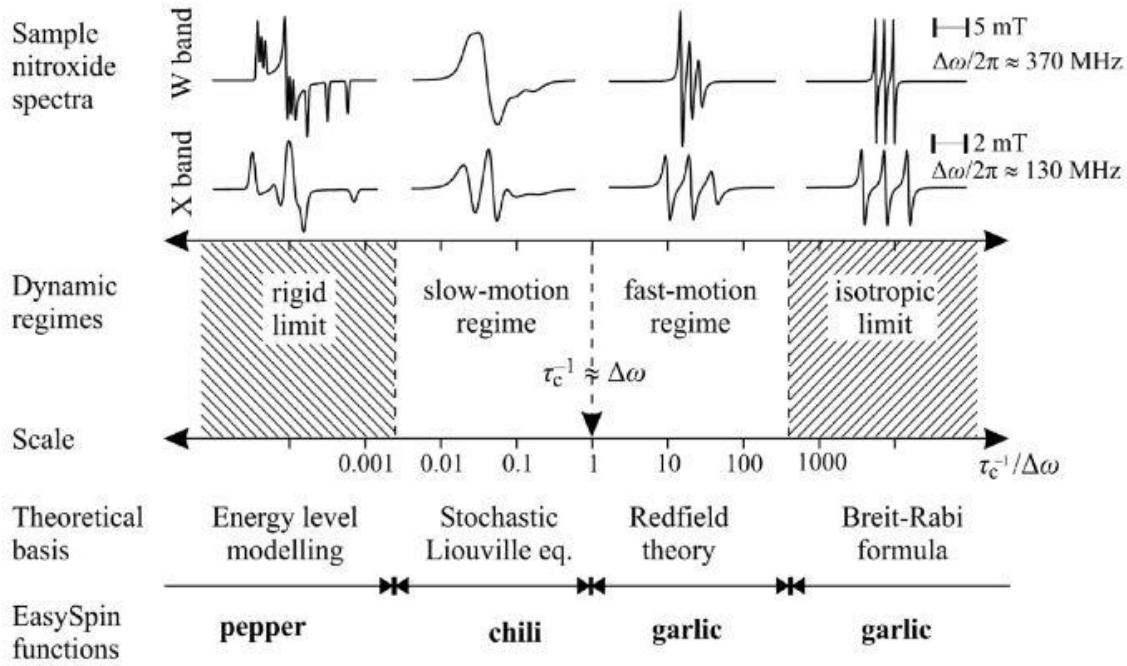

Figure 2-5: Motional regimes of EPR spectra and EasySpin simulation functions (Stoll & Schweiger, 2006).

2.4 Analytical methods

2.4.1 Electron paramagnet resonance spectroscopy

EPR spectroscopy can be used to measure unpaired electrons, such as radicals or transition metals. Because of their intrinsic angular momentum, also known as spin, unpaired electrons have a magnetic moment, a magnetic dipole. The spin is an inner quantum mechanical property of an electron and can only assume two values m_S = -½ or m_S = +½. For a free electron, there are two possibilities to orientate in an external magnetic field: the parallel state, which is the ground state and only corresponds to the attraction of the external magnetic field, and the antiparallel state, an active or excited state (Figure 2-6). The repulsion in the external magnetic field dominates here. This is called Zeeman splitting. The difference of the potential energy ΔE between the two energy levels is linearly dependent on the external magnetic field strength and ΔE is proportional to B_0 (Figure 2-6). In continuous wave (cw) EPR, the microwave frequency is constant and the magnetic field is swept until the resonance condition is fulfilled. During resonance, additional absorption by the sample leads to a detuning of the resonator and microwave power is reflected. The EPR spectrum is obtained by recording this reflected microwave power as a function of the magnetic field. The first derivation of the signal reflects the typical EPR spectrum (Figure 2-6).

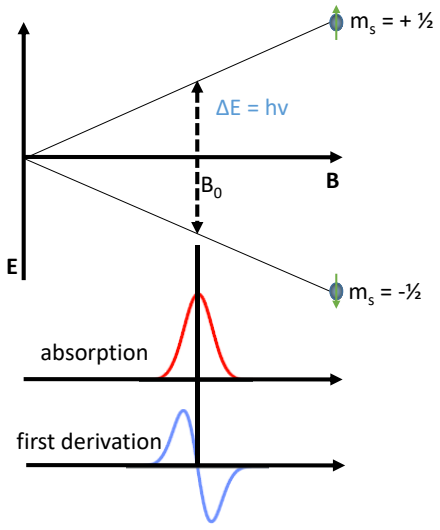

Figure 2-6: Schematic illustration of the Zeeman splitting and the absorption of the EPR signal.

Most biological systems consist of diamagnetic molecules. To gain knowledge about these molecules or systems, spin probes and spin labels can be used. Spin probes are stable radicals that provide information about their microenvironment. Two conditions are required

for the successful use of spin probes and spin labels: Firstly, the spectrum of the probe must be significantly influenced by the properties of the system to be investigated. Secondly, the probe itself must not significantly influence the system. However, these two conditions are conflictive. As an example for food applications, spin probes provide information on the interface of micellar solutions, liposomes or emulsions (Frenzel & Steffen-Heins, 2015; Krudopp, Sönnichsen, & Steffen-Heins, 2015) or can be used as model components for the monitoring of drug release (Jores, Mehnert, & Mäder, 2003). Spin labels are used in the approach of site-directed spin labeling, which was already described in detail (2.3).

2.4.2 Mass spectrometry measurements

Mass spectrometry is a useful approach for the identification of proteins and the characterization of protein modifications. For the analysis, all molecules need to be charged, as the measurement is based on the separation of ions according to their mass-to-charge (m/z) ratio. At each m/z value, the number of ions is detected (Dunn et al., 2013). For the ionization of the molecules, there are different possibilities, such as electrospray ionization (ESI) and matrix-assisted laser desorption/ionization (MALDI).

In case of ESI, the sample is sprayed into an electric field and the needle charges the surface of the droplet. The droplets can be positively or negatively charged, depending on the electric field. High temperatures are used to assist the nebulization of the solution and the evaporation of the solvent. The evaporation results in quasimolecular ions (Fenn, Mann, Meng, Wong, & Whitehouse, 1989). A positive voltage produces positively charged ions $[M+H]^+$ and a negative voltage produces negatively charged ions $[M-H]^-$. Also, other cations such as sodium ions ($[M+Na]^+$) or potassium ions ([M+K]+) can be added during ionization. Multiply charged ions such as $[M+nH]^{n+}$, are often observed especially for larger molecules. Proteins can have many charge states, resulting in a characteristic charge state envelope (Heck & van den Heuvel, 2004).

The mass spectrometer consists of four parts:

- Separation of neutral molecules from the ion beam
- Selection of the m/z range with quadrupoles
- Focusing of the ion beam with hexa- or octapole
- Detection of the masses with FT-ICR, QToF or Orbitrap

2.4.2.1 LC Quadrupole Time-of-Flight mass spectrometry

The combination of liquid chromatography (LC) and Quadrupole Time-of-Flight (QToF) mass spectrometry can be used for protein analysis. The liquid chromatography is used for purification of the proteins or to separate individual peptides for better evaluation. The mass-to-charge (m/z) ratio of the measuring molecule is determined by the time required for the ion

to reach the detector at a known distance. Labeling can be verified and binding sides determined by LC-QToF. For binding verification, intact protein is measured and the modification is seen by the mass shift in the mass spectrum. For binding site evaluation, the protein has to be digested prior to mass spectrometry measurements. The digestion results in a typical peptide pattern which can be measured by mass spectrometry. The modification of the peptides can be identified by the mass shift.

2.4.2.2 Fourier transform ion cyclotron resonance mass spectrometry

The Fourier transform ion cyclotron resonance (FT-ICR) mass spectrometry is a technique with very high sensitivity, which allows the measurements of very low concentrations, down to a femtomolar range, and with a high mass accuracy. The m/z ratio is determined by the cyclotron frequency of the ions in a homogeneous magnetic field. The FT-ICR-MS can be used to distinguish between the monomeric spin label and the monoradical dimer, which were not distinguishable by EPR. Furthermore, monoradical spin labels and biradicals can be measured at very low concentration, which are under the resolution of the EPR.

2.4.3 Fourier transform infrared spectroscopy

With Fourier transform infrared (FT-IR) spectroscopy, it is possible to measure the secondary structure of the protein backbone, or in general, to characterize materials. In contrast to the UV-Vis spectroscopy (10.1.2.1), the FT-IR spectroscopy works with a beam containing many frequencies of light instead of monochromatic light. The wavelength-dependent adsorption of liquid or solid samples is measured. The beam is spliced into two beams. One beam is reflected from a fixed mirror and the other from a movable mirror (Figure 2-7). When the IR radiation penetrates a sample, part of the radiation is absorbed by the sample because their energies stimulate the oscillation of particular groups of the molecules. The interferogram is converted by Fourier transformation to a spectrum. The infrared spectrum is a fingerprint that is characteristic of the molecule under investigation and can be used, for example, to identify substances.

The attenuated total reflection (ATR) unit allows the direct measurement of liquid and solid samples without any preparation. The total internal reflection results in an evanescent wave and pass the ATR crystal and is at least once in contact and is reflected by the sample. Therefore the crystal needs a higher reflective index than the sample. The number of reflections is dependent on the angle of incidence and determines, amongst others, the signal to noise ratio. After exiting the crystal, the beam is collected and detected (Mirabella, 1993). With this technique, the secondary structure of the protein can be monitored, for example, during amyloid aggregation. An increase and a shift in the β-sheet region is typical for amyloid aggregation. Furthermore, the change in secondary structure because of ligand binding can be measured.

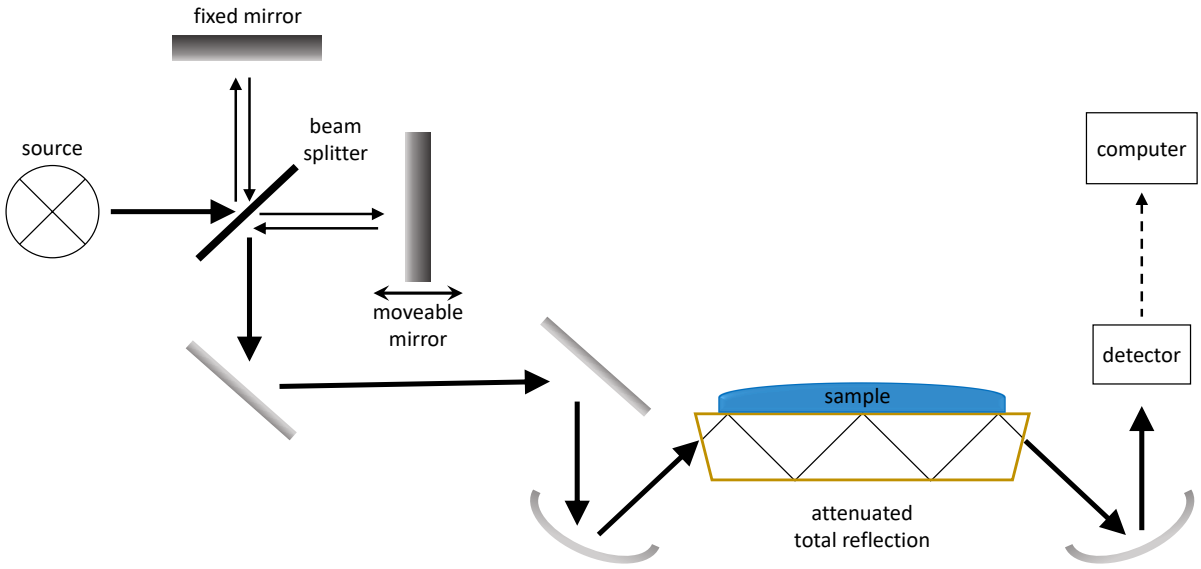

Figure 2-7: Schematic illustration of attenuated total reflection Fourier transformation infrared (ATR-FTIR) spectrometer.

2.4.4 Measuring the interfacial tension

2.4.4.1 Langmuir-Blodgett trough

A Langmuir-Blodgett trough is used to measure the surface pressure of two-dimensional monolayers of amphiphilic molecules. The trough consists of a highly hydrophobic chemical inert material, mostly polytetrafluoroethylene. One or two barriers vary the surface area to compress and expand the sample film. The surface pressure is measured with a Wilhelmy plate which consists of platinum, glass, or filter paper. The Wilhelmy plate weight the liquid lamella formed during the wetting of the plate (Schwuger & Rostek, 1971). The form of the lamella is determined by the IFT (Equation 3). The force (F) on the plate is measured with a tensiometer or a microbalance and determines the surface tension (γ):

Equation 3: Interfacial tension by Langmuir-Blodgett trough

$$\gamma = \frac{F}{L * \cos\theta} \qquad (3)$$

L : perimeter of plate

Θ : contact angle of plate and liquid

For characterization of monolayer film with the Langmuir-Blodgett trough, a phase diagram can be expressed by the pressure – area (π–A) isotherm. The monolayer undergoes four phases during compression. In the gas-like phase, the molecules are widely spread out at the interface. The area per molecule is big and the surface pressure low. By compressing the

film, a phase transition to the liquid-phase can be seen. The film is packed denser and the repulsive interactions between the molecules lead to an increase in pressure. Through further compression of the monolayer, a solid-phase is created and a compression beyond the solid-phase leads to a collapse of the film (Oliveira, 1992) (Figure 2-8).

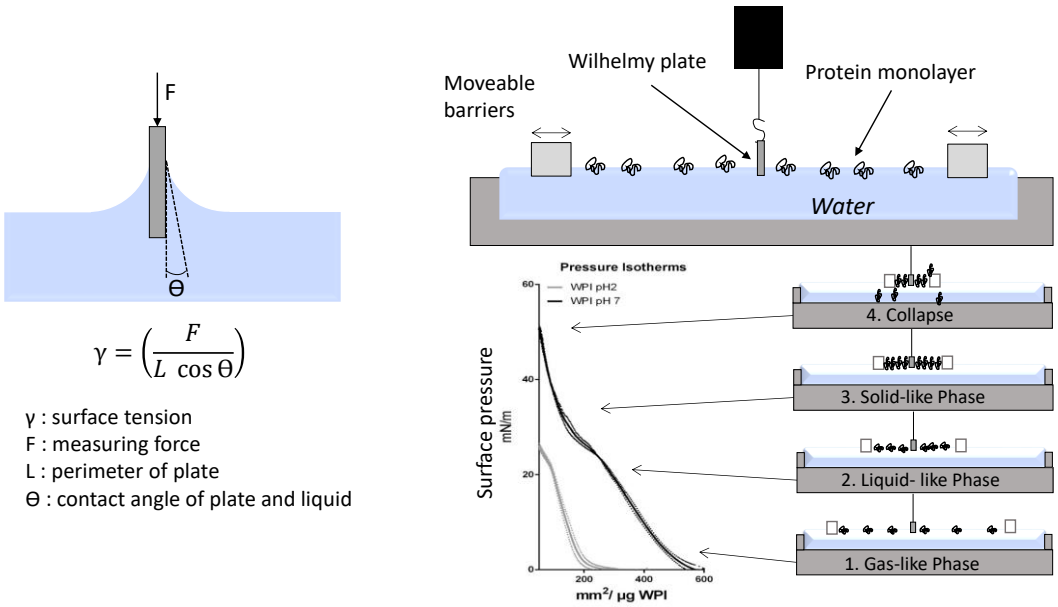

Figure 2-8: Schematic illustration of Langmuir-Blodgett trough measurements. Interfacial tension is measured using the Wilhelmy plate method. The decreasing lead to increasing surface pressure and different phases can be seen in the line shape.

2.4.4.2 Pendant drop analysis

With the pendant drop tensiometer, the surface tension can be determined by the shape of a droplet due to Laplace's law. In absence of any other forces like gravity or other molecules, the water droplet would be almost spherical as this is the geometric shape with the smallest surface area in relation to volume. For the pendant drop measurement, a sample droplet is generated with a syringe in front of a light source. From the other side, a camera takes pictures of the droplet shape. The droplet shape depends on the interfacial tension, which is calculated through the Young-Laplace equation (Young, 1805). The Young-Laplace equation (Equation 4) states that the difference between the hydrostatic pressure of a spherical surface is proportional to the surface tension and the mean curvature (Figure 2-9):

Equation 4: Young-Laplace equation

$$\Delta p = \gamma \left(\frac{1}{R_1} + \frac{1}{R_2}\right) \qquad (4)$$

Δp : Laplace pressure

γ: surface tension

R_1 and R_2: principal radii of curvature

To measure the adsorption rate of the amyloid aggregates system and the individual fractions, a water droplet of pH adjusted water is generated manually with a syringe. Using a second syringe, with a smaller needle, the sample solution can be injected into the previously generated droplet with an automatic dosing system (Drusch, Hamann, Berger, Serfert, & Schwarz, 2012) (Figure 2-9). The changes of the interfacial tension are followed as described above. From the reduction of the IFT, the lag time, the adsorption rate, and the overall reduction of the IFT can be determined. The lag time represents the time between the sample injection and the beginning change of the interfacial tension. This is a measure of the diffusion time required by the sample to reach the interface. The adsorption rate is the slope of the reduction. The faster the sample reduces the IFT, the higher is the adsorption rate. The difference between the initial IFT and the tension reached at the saturation is the overall reduction of the IFT.

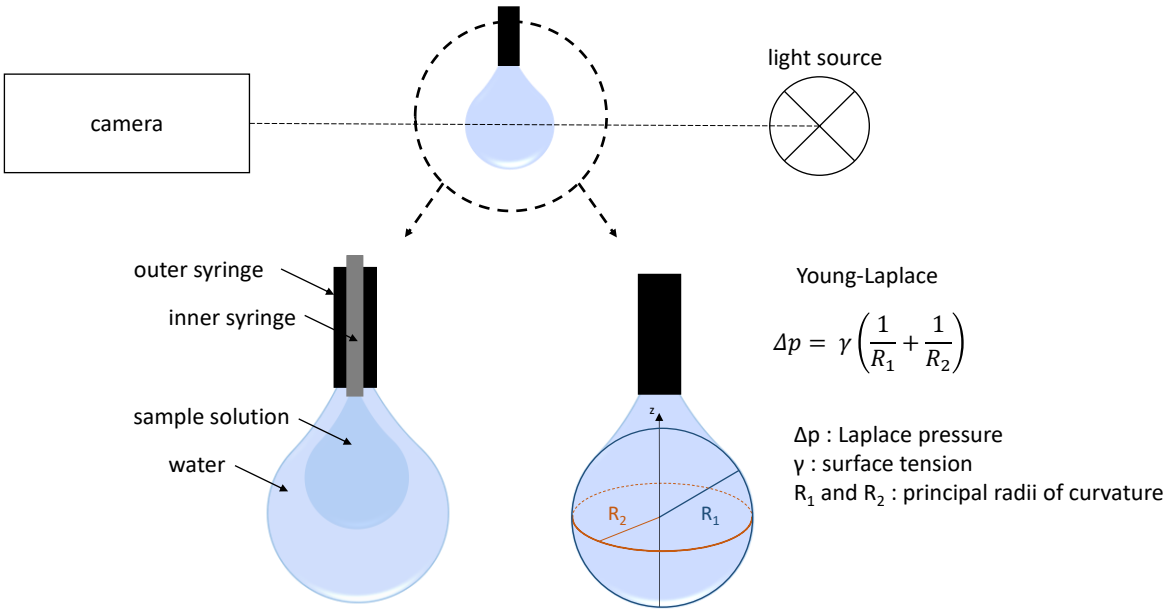

Figure 2-9: Schematic illustration of the pendant drop measurements. The interfacial tension of the air-water interface is calculated using the Young-Laplace equation. For the measurement, the sample solution is injected in a previously generated droplet of water.

2.5 References

Adamcik, J., & Mezzenga, R. (2012). Study of amyloid fibrils via atomic force microscopy. *Current Opinion in Colloid & Interface Science*, *17*(6), 369–376. https://doi.org/10.1016/j.cocis.2012.08.001

Akkermans, C., van der Goot, A. J., Venema, P., van der Linden, E., & Boom, R. M. (2008). Properties of protein fibrils in whey protein isolate solutions: Microstructure, flow behaviour and gelation. *International Dairy Journal*, *18*(10-11), 1034–1042. https://doi.org/10.1016/j.idairyj.2008.05.006

Akkermans, C., Venema, P., Rogers, S. S., van der Goot, A. J., Boom, R. M., & van der Linden, E. (2006). Shear Pulses Nucleate Fibril Aggregation. *Food Biophysics*, *1*(3), 144–150. https://doi.org/10.1007/s11483-006-9012-5

Akkermans, C., Venema, P., van der Goot, A. J., Gruppen, H., Bakx, E. J., Boom, R. M., & van der Linden, E. (2008). Peptides are building blocks of heat-induced fibrillar protein aggregates of beta-lactoglobulin formed at pH 2. *Biomacromolecules*, *9*(5), 1474–1479. https://doi.org/10.1021/bm7014224

Albani, J. R., Vogelaer, J., Bretesche, L., & Kmiecik, D. (2014). Tryptophan 19 residue is the origin of bovine β-lactoglobulin fluorescence. *Journal of Pharmaceutical and Biomedical Analysis*, *91*, 144–150. https://doi.org/10.1016/j.jpba.2013.12.015.

Aschaffenburg, R., & Drewey, J. (1955). Occurrence of different beta-lactoglobulins in cow's milk. *Nature*, *176*(4474), 218–219. https://doi.org/10.1038/176218b0

Aschaffenburg, R., & Drewery, J. (1957). Improved method for the preparation of crystalline beta-lactoglobulin and alpha-lactalbumin from cow's milk. *The Biochemical Journal*, *65*(2), 273–277. https://doi.org/10.1042/bj0650273

Atkinson, P. J., Dickinson, E., Horne, D. S., & Richardson, R. M. (1995). Neutron reflectivity of adsorbed β-casein and β-lactoglobulin at the air/water interface. *Journal of the Chemical Society, Faraday Trans.*, *91*(17), 2847–2854. https://doi.org/10.1039/FT9959102847

Aymard, P., Nicolai, T., Durand, D., & Clark, A. (1999). Static and Dynamic Scattering of β-Lactoglobulin Aggregates Formed after Heat-Induced Denaturation at pH 2. *Macromolecules*, *32*(8), 2542–2552. https://doi.org/10.1021/ma981689j

Baldassarre, M., Bennett, M., & Barth, A. (2016). Simultaneous acquisition of infrared, fluorescence and light scattering spectra of proteins: Direct evidence for pre-fibrillar species in amyloid fibril formation. *The Analyst*, *141*(3), 963–973. https://doi.org/10.1039/c5an02283e.

Barackov, I., Mause, A., Kapoor, S., Winter, R., Schembecker, G., & Burghoff, B. (2012). Investigation of structural changes of β-casein and lysozyme at the gas-liquid interface during foam fractionation. *Journal of Biotechnology*, *161*(2), 138–146. https://doi.org/10.1016/j.jbiotec.2012.01.030

Barut, S., & Foegeding, E. A. (1993). Ca 2+ -Induced Gelation of Pre-heated Whey Protein Isolate. *Journal of Food Science*, *58*(4), 867–871. https://doi.org/10.1111/j.1365-2621.1993.tb09379.x

Belloque, J., & Smith, G. M. (1998). Thermal Denaturation of β-Lactoglobulin. A 1 H NMR Study. *Journal of agricultural and food chemistry*, *46*(5), 1805–1813. https://doi.org/10.1021/jf9709313

Berliner, L. J., Grunwald, J., Hankovszky, H.O., & Hideg, K. (1982). A novel reversible thiol-specific spin label: Papain active site labeling and inhibition. *Analytical Biochemistry*, *119*(2), 450–455. https://doi.org/10.1016/0003-2697(82)90612-1

Berliner, L. J., & Reuben, J. (1989). *Spin Labeling: Theory and Applications* (N). Boston: Springer US.

Bernard, C., Regnault, S., Gendreau, S., Charbonneau, S., & Relkin, P. (2011). Enhancement of emulsifying properties of whey proteins by controlling spray-drying

parameters. *Food Hydrocolloids*, *25*(4), 758–763. https://doi.org/10.1016/j.foodhyd.2010.08.011

Bolder, S. G., Hendrickx, H., Sagis, L. M. C., & van der Linden, E. (2006). Fibril assemblies in aqueous whey protein mixtures. *Journal of Agricultural and Food Chemistry*, *54*(12), 4229–4234. https://doi.org/10.1021/jf060606s

Bolder, S. G., Sagis, L. M. C., Venema, P., & van der Linden, E. (2007). Effect of stirring and seeding on whey protein fibril formation. *Journal of Agricultural and Food Chemistry*, *55*(14), 5661–5669. https://doi.org/10.1021/jf063351r

Bolder, S. G., Vasbinder, A. J., Sagis, L. M.C., & van der Linden, E. (2007). Heat-induced whey protein isolate fibrils: Conversion, hydrolysis, and disulphide bond formation. *International Dairy Journal*, *17*(7), 846–853. https://doi.org/10.1016/j.idairyj.2006.10.002

Bolisetty, S., Harnau, L., Jung, J.-M., & Mezzenga, R. (2012). Gelation, phase behavior, and dynamics of β-lactoglobulin amyloid fibrils at varying concentrations and ionic strengths. *Biomacromolecules*, *13*(10), 3241–3252. https://doi.org/10.1021/bm301005w

Borbat, P. P., Davis, J. H., Butcher, S. E., & Freed, J. H. (2004). Measurement of large distances in biomolecules using double-quantum filtered refocused electron spin-echoes. *Journal of the American Chemical Society*, *126*(25), 7746–7747. https://doi.org/10.1021/ja049372o

Bordignon, E. (2007). EPR Spectroscopy of Nitroxide Spin Probes. *EMagRes*. (6), 235–254. https://doi.org/10.1002/9780470034590.emrstm1513

Bordignon, E., & Polyhach, Y. (2013). EPR techniques to probe insertion and conformation of spin-labeled proteins in lipid bilayers. *Methods in Molecular Biology (Clifton, N.J.)*, *974*, 329–355. https://doi.org/10.1007/978-1-62703-275-9_15

Bordignon, E. (2018). EPR Spectroscopy of Nitroxide Spin Probes. In D. Goldfarb & S. Stoll (Eds.), *EMagRes Bks. EPR Spectroscopy: Fundamentals and Methods* (pp. 277–301). Newark: John Wiley & Sons Incorporated.

Burova, T. V., Choiset, Y., Tran, V., & Haertlé, T. (1998). Role of free Cys121 in stabilization of bovine beta-lactoglobulin B. *Protein Engineering*, *11*(11), 1065–1073. https://doi.org/10.1093/protein/11.11.1065

Cao, Y., & Mezzenga, R. (2019). Food protein amyloid fibrils: Origin, structure, formation, characterization, applications and health implications. *Advances in Colloid and Interface Science*, *269*, 334–356. https://doi.org/10.1016/j.cis.2019.05.002

Chen, M., Margittai, M., Chen, J., & Langen, R. (2007). Investigation of alpha-synuclein fibril structure by site-directed spin labeling. *The Journal of Biological Chemistry*, *282*(34), 24970–24979. https://doi.org/10.1074/jbc.M700368200

Considine, T., Patel, H. A., Anema, S. G., Singh, H., & Creamer, L. K. (2007). Interactions of milk proteins during heat and high hydrostatic pressure treatments — A Review. *Innovative Food Science & Emerging Technologies*, *8*(1), 1–23. https://doi.org/10.1016/j.ifset.2006.08.003

Creighton, T. E. (1980). Kinetic study of protein unfolding and refolding using urea gradient electrophoresis. *Journal of Molecular Biology*, *137*(1), 61–80. https://doi.org/10.1016/0022-2836(80)90157-6

Croguennec, T., Mollé, D., Mehra, R., & Bouhallab, S. (2004). Spectroscopic characterization of heat-induced nonnative beta-lactoglobulin monomers. *Protein Science*, *13*(5), 1340–1346. https://doi.org/10.1110/ps.03513204.

Cupo, J. F., & Pace, C. N. (1983). Conformational stability of mixed disulfide derivatives of beta-lactoglobulin B. *Biochemistry*, *22*(11), 2654–2658. https://doi.org/10.1021/bi00280a010

Damodaran, S. (2005). Protein Stabilization of Emulsions and Foams. *Journal of Food Science*, *70*(3), R54-R66. https://doi.org/10.1111/j.1365-2621.2005.tb07150.x

Davis, J. P., & Foegeding, E. A. (2004). Foaming and Interfacial Properties of Polymerized Whey Protein Isolate. *Journal of Food Science*, *69*(5), C404-C410. https://doi.org/10.1111/j.1365-2621.2004.tb10706.x

Dickinson, E. (1998). Proteins at interfaces and in emulsions Stability, rheology and interactions. *Journal of the Chemical Society, Faraday Transactions*, *94*(12), 1657–1669. https://doi.org/10.1039/A801167B

Dickinson, E., & Matsumura, Y. (1994). Proteins at liquid interfaces: Role of the molten globule state. *Colloids and Surfaces B: Biointerfaces*, *3*(1-2), 1–17. https://doi.org/10.1016/0927-7765(93)01116-9

Drescher, M. (2012). Elektronenspinresonanz-Spektroskopie: Struktur und Dynamik intrinsisch ungeordneter Proteine. *Chemie in unserer Zeit*. (46), 150–157.

Drescher, M., Godschalk, F., Veldhuis, G., van Rooijen, B. D., Subramaniam, V., & Huber, M. (2008). Spin-label EPR on alpha-synuclein reveals differences in the membrane binding affinity of the two antiparallel helices. *Chembiochem: a European Journal of Chemical Biology*, *9*(15), 2411–2416. https://doi.org/10.1002/cbic.200800238

Drusch, S., Hamann, S., Berger, A., Serfert, Y., & Schwarz, K. (2012). Surface accumulation of milk proteins and milk protein hydrolysates at the air–water interface on a time-scale relevant for spray-drying. *Food Research International*, *47*(2), 140–145. https://doi.org/10.1016/j.foodres.2011.04.037

Dunn, W. B., Erban, A., Weber, R. J. M., Creek, D. J., Brown, M., Breitling, R., Viant, M. R. (2013). Mass appeal: Metabolite identification in mass spectrometry-focused untargeted metabolomics. *Metabolomics*, *9*(S1), 44–66. https://doi.org/10.1007/s11306-012-0434-4

Dunnill, P., & Green, D. W. (1966). Sulphydryl groups and the N⇄R conformational change in β-lactoglobulin. *Journal of Molecular Biology*, *15*(1), 147–151. https://doi.org/10.1016/S0022-2836(66)80216-4

Ellman, G. L. (1959). Tissue Sulfhydryl Groups. *Archnieves of Biochemistry and Biophysics*, *82*, 70–77.

Fang, Y. & Dalgleish, D.G.(1997). Conformation of beta-Lactoglobulin Studied by FTIR: Effect of pH, Temperature, and Adsorption to the Oil-Water Interface. *Journal of Colloid and Interface Science*, *196*(2), 292–298. https://doi.org/10.1006/jcis.1997.5191

Fenn, J. B., Mann, M., Meng, C. K., Wong, S. F., & Whitehouse, C. M. (1989). Electrospray ionization for mass spectrometry of large biomolecules. *Science (New York, N.Y.)*, *246*(4926), 64–71. https://doi.org/10.1126/science.2675315

Fernández, A., & Riera, F. (2013). β-Lactoglobulin tryptic digestion: A model approach for peptide release. *Biochemical Engineering Journal*, *70*, 88–96. https://doi.org/10.1016/j.bej.2012.10.001

Ferranti, P., Mamone, G., Picariello, G., & Addeo, F. (2011). The “dark side” of β-lactoglobulin: Unedited structural features suggest unexpected functions. *Journal of Chromatography. a*, *1218*(22), 3423–3431. https://doi.org/10.1016/j.chroma.2011.03.059

Finder, V. H., & Glockshuber, R. (2007). Amyloid-beta aggregation. *Neuro-Degenerative Diseases*, *4*(1), 13–27. https://doi.org/10.1159/000100355

Fogliano, V., Monti, S. M., Visconti, A., Randazzo, G., Facchiano, A. M., Colonna, G., & Ritieni, A. (1998). Identification of a β-lactoglobulin lactosylation site. *Biochimica et Biophysica Acta (BBA) - Protein Structure and Molecular Enzymology*, *1388*(2), 295–304. https://doi.org/10.1016/S0167-4838(98)00177-0

Frenzel, M., & Steffen-Heins, A. (2015). Whey protein coating increases bilayer rigidity and stability of liposomes in food-like matrices. *Food Chemistry*, *173*, 1090–1099. https://doi.org/10.1016/j.foodchem.2014.10.076

Gilbert, H. F. (1995). [2] Thiol/disulfide exchange equilibria and disulfidebond stability. In H. F. Gilbert (Ed.), *Methods in Enzymology. Thiol/disulfide exchange quilibria and disulphidebond stability* (Vol. 251, pp. 8–28). Elsevier. https://doi.org/10.1016/0076-6879(95)51107-5

Glomm, W. R., Volden, S., Halskau, Ø., & Ese, M.-H. G. (2009). Same system-different results: The importance of protein-introduction protocols in Langmuir-monolayer studies of lipid-protein interactions. *Analytical Chemistry*, *81*(8), 3042–3050. https://doi.org/10.1021/ac8027257

Godt, A., Schulte, M., Zimmermann, H., & Jeschke, G. (2006). How flexible are poly(para-phenyleneethynylene)s? *Angewandte Chemie (International Ed. in English)*, *45*(45), 7560–7564. https://doi.org/10.1002/anie.200602807

Goers, J., Permyakov, S. E., Permyakov, E. A., Uversky, V. N., & Fink, A. L. (2002). Conformational prerequisites for alpha-lactalbumin fibrillation. *Biochemistry*, *41*(41), 12546–12551. https://doi.org/10.1021/bi0262698

Goldfarb, D., & Stoll, S. (Eds.) (2018). *EPR Spectroscopy: Fundamentals and Methods*. *EMagRes Bks*. Newark: John Wiley & Sons Incorporated.

Gu, L., Tran, J., Jiang, L., & Guo, Z. (2016). A new structural model of Alzheimer's Aβ42 fibrils based on electron paramagnetic resonance data and Rosetta modeling. *Journal of Structural Biology*, *194*(1), 61–67. https://doi.org/10.1016/j.jsb.2016.01.013

Halling, P. J. (1981). Protein-stabilized foams and emulsions. *Critical Reviews in Food Science and Nutrition*, *15*(2), 155–203. https://doi.org/10.1080/10408398109527315

Hammarström, P., Owenius, R., Mårtensson, L.-G., Carlsson, U., & Lindgren, M. (2001). High-Resolution Probing of Local Conformational Changes in Proteins by the Use of Multiple Labeling: Unfolding and Self-Assembly of Human Carbonic Anhydrase II Monitored by Spin, Fluorescent, and Chemical Reactivity Probes. *Biophysical journal*, *80*(6), 2867–2885. https://doi.org/10.1016/S0006-3495(01)76253-4

Heck, A. J. R., & van den Heuvel, R. H. H. (2004). Investigation of intact protein complexes by mass spectrometry. *Mass Spectrometry Reviews*, *23*(5), 368–389. https://doi.org/10.1002/mas.10081

Hettiarachchi, C. A., Melton, L. D., Gerrard, J. A., & Loveday, S. M. (2012). Formation of β-lactoglobulin nanofibrils by microwave heating gives a peptide composition different from conventional heating. *Biomacromolecules*, *13*(9), 2868–2880. https://doi.org/10.1021/bm300896r

Heyn, T. R., Garamus, V. M., Neumann, H. R., Uttinger, M. J., Guckeisen, T., Heuer, M., Keppler, J. K. (2019). Influence of the polydispersity of pH 2 and pH 3.5 beta-lactoglobulin amyloid fibril solutions on analytical methods. *European Polymer Journal.* Advance online publication. https://doi.org/10.1016/j.eurpolymj.2019.08.038

Hill, E. K., Krebs, B., Goodall, D. G., Howlett, G. J., & Dunstan, D. E. (2006). Shear flow induces amyloid fibril formation. *Biomacromolecules*, *7*(1), 10–13. https://doi.org/10.1021/bm0505078

Hoffmann, M. A. M., & van Mil, P. J. J. M. (1997). Heat-Induced Aggregation of β-Lactoglobulin: Role of the Free Thiol Group and Disulfide Bonds. *Journal of agricultural and food chemistry*, *45*(8), 2942–2948. https://doi.org/10.1021/jf960789q

Hofmann, A., Schembecker, G., & Merz, J. (2015). Role of bubble size for the performance of continuous foam fractionation in stripping mode. *Colloids and Surfaces A: Physicochemical and Engineering Aspects*, *473*, 85–94. https://doi.org/10.1016/j.colsurfa.2014.12.042

Hubbell, W. L., & Altenbach, C. (1994). Investigation of structure and dynamics in membrane proteins using site-directed spin labeling. *Current Opinion in Structural Biology*, *4*(4), 566–573. https://doi.org/10.1016/S0959-440X(94)90219-4

Hunt, J. A., & Dalgleish, D. G. (1994). Effect of pH on the stability and surface composition of emulsions made with whey protein isolate. *Journal of agricultural and food chemistry*, *42*(10), 2131–2135. https://doi.org/10.1021/jf00046a011

Ionuţ, I. M., Cozma, C., Tomczyk, N., Rontree, J., Desor, M., Drescher, M., & Przybylski, M. (2009). Structural characterization of beta-amyloid oligomer-aggregates by ion mobility

mass spectrometry and electron spin resonance spectroscopy. *Analytical and Bioanalytical Chemistry*, *395*(8), 2509–2519. https://doi.org/10.1007/s00216-009-3164-3.

Iuraşcu, I. M., Cozma, C., Tomczyk, N., Rontree, J., Desor, M., Drescher, M., & Przybylski, M. (2009). Structural characterization of beta-amyloid oligomer-aggregates by ion mobility mass spectrometry and electron spin resonance spectroscopy. *Analytical and Bioanalytical Chemistry*, *395*(8), 2509–2519. https://doi.org/10.1007/s00216-009-3164-3

Janzen, E. G., Coulter, G. A., Oehler, U. M., & Bergsma, J. P. (1982). Solvent effects on the nitrogen and β-hydrogen hyperfine splitting constants of aminoxyl radicals obtained in spin trapping experiments. *Canadian Journal of Chemistry*, *60*(21), 2725–2733. https://doi.org/10.1139/v82-392

Jayasinghe, S. A., & Langen, R. (2004). Identifying structural features of fibrillar islet amyloid polypeptide using site-directed spin labeling. *The Journal of Biological Chemistry*, *279*(46), 48420–48425. https://doi.org/10.1074/jbc.M406853200

Jeschke, G., Bender, A., Paulsen, H., Zimmermann, H., & Godt, A. (2004). Sensitivity enhancement in pulse EPR distance measurements. *Journal of Magnetic Resonance (San Diego, Calif. : 1997)*, *169*(1), 1–12. https://doi.org/10.1016/j.jmr.2004.03.024

Jeschke, G., Chechik, V., Ionita, P., Godt, A., Zimmermann, H., Banham, J.,Jung, H. (2006). DeerAnalysis2006—a comprehensive software package for analyzing pulsed ELDOR data. *Applied magnetic resonance*, *30*(3-4), 473–498. https://doi.org/10.1007/BF03166213

Jordens, S., Isa, L., Usov, I., & Mezzenga, R. (2013). Non-equilibrium nature of two-dimensional isotropic and nematic coexistence in amyloid fibrils at liquid interfaces. *Nature Communications*, *4*, 1917. https://doi.org/10.1038/ncomms2911

Jordens, S., Rühs, P. A., Sieber, C., Isa, L., Fischer, P., & Mezzenga, R. (2014). Bridging the gap between the nanostructural organization and macroscopic interfacial rheology of amyloid fibrils at liquid interfaces. *Langmuir: the ACS Journal of Surfaces and Colloids*, *30*(33), 10090–10097. https://doi.org/10.1021/la5020658

Jores, K., Mehnert, W., & Mäder, K. (2003). Physicochemical investigations on solid lipid nanoparticles and on oil-loaded solid lipid nanoparticles: A nuclear magnetic resonance and electron spin resonance study. *Pharmaceutical Research*, *20*(8), 1274–1283. https://doi.org/10.1023/A:1025065418309

Jung, J.-M., Gunes, D. Z., & Mezzenga, R. (2010). Interfacial activity and interfacial shear rheology of native β-lactoglobulin monomers and their heat-induced fibers. *Langmuir: the ACS Journal of Surfaces and Colloids*, *26*(19), 15366–15375. https://doi.org/10.1021/la102721m

Kayser, J. J., Arnold, P., Steffen-Heins, A., Schwarz, K., & Keppler, J. K. (2020). Functional ethanol-induced fibrils: Influence of solvents and temperature on amyloid-like aggregation of beta-lactoglobulin. *Journal of Food Engineering*, *270*, 109764. https://doi.org/10.1016/j.jfoodeng.2019.109764

Kehoe, J. J., Brodkorb, A., Mollé, D., Yokoyama, E., Famelart, M.-H., Bouhallab, S., Croguennec, T. (2007). Determination of exposed sulfhydryl groups in heated beta-lactoglobulin A using IAEDANS and mass spectrometry. *Journal of Agricultural and Food Chemistry*, *55*(17), 7107–7113. https://doi.org/10.1021/jf070397r

Keppler, J. K., Heyn, T. R., Meissner, P. M., Schrader, K., & Schwarz, K. (2019a. Protein oxidation during temperature-induced amyloid aggregation of beta-lactoglobulin. *Food Chemistry*, *289*, 223–231. https://doi.org/10.1016/j.foodchem.2019.02.114

Keppler, J. K., Sönnichsen, F. D., Lorenzen, P.-C., & Schwarz, K. (2014). Differences in heat stability and ligand binding among β-lactoglobulin genetic variants A, B and C using (1)H NMR and fluorescence quenching. *Biochimica Et Biophysica Acta*, *1844*(6), 1083–1093. https://doi.org/10.1016/j.bbapap.2014.02.007

Keppler, J. K., Steffen-Heins, A., Berton-Carabin, C. C., Ropers, M.-H., & Schwarz, K. (2018). Functionality of whey proteins covalently modified by allyl isothiocyanate. Part 2:

Influence of the protein modification on the surface activity in an O/W system. *Food Hydrocolloids*, *81*, 286–299. https://doi.org/10.1016/j.foodhyd.2018.03.003

Keppler, J. K., Koudelka, T., Palani, K., Stuhldreier, M. C., Temps, F., Tholey, A., & Schwarz, K. (2014). Characterization of the covalent binding of allyl isothiocyanate to β-lactoglobulin by fluorescence quenching, equilibrium measurement, and mass spectrometry. *Journal of Biomolecular Structure & Dynamics*, *32*(7), 1103–1117. https://doi.org/10.1080/07391102.2013.809605

Keppler, J. K., Martin, D., Garamus, V. M., Berton-Carabin, C., Nipoti, E., Coenye, T., & Schwarz, K. (2017). Functionality of whey proteins covalently modified by allyl isothiocyanate. Part 1 physicochemical and antibacterial properties of native and modified whey proteins at pH 2 to 7. *Food Hydrocolloids*, *65*, 130–143. https://doi.org/10.1016/j.foodhyd.2016.11.016

Kirby, T. L., Karim, C. B., & Thomas, D. D. (2004). Electron paramagnetic resonance reveals a large-scale conformational change in the cytoplasmic domain of phospholamban upon binding to the sarcoplasmic reticulum Ca-ATPase. *Biochemistry*, *43*(19), 5842–5852. https://doi.org/10.1021/bi035749b

Klare, J. P. (2012). *Site-Directed Spin Labeling and Electron Paramagnetic Resonance (EPR) Spectroscopy: A Versatile Tool to Study Protein-Protein Interactions*. Rijeka: InTech.

Kontopidis, G., Holt, C., & Sawyer, L. (2002). The Ligand-binding Site of Bovine β-Lactoglobulin: Evidence for a Function? *Journal of Molecular Biology*, *318*(4), 1043–1055. https://doi.org/10.1016/S0022-2836(02)00017-7

Krebs, M. R. H., Bromley, E. H. C., & Donald, A. M. (2005). The binding of thioflavin-T to amyloid fibrils: Localisation and implications. *Journal of Structural Biology*, *149*(1), 30–37. https://doi.org/10.1016/j.jsb.2004.08.002.

Krebs, M. R. H., Devlin, G. L., & Donald, A. M. (2009). Amyloid fibril-like structure underlies the aggregate structure across the pH range for beta-lactoglobulin. *Biophysical Journal*, *96*(12), 5013–5019. https://doi.org/10.1016/j.bpj.2009.03.028

Kroes-Nijboer, A., Venema, P., Baptist, H., & van der Linden, E. (2010). Fracture of protein fibrils as induced by elongational flow. *Langmuir : the ACS Journal of Surfaces and Colloids*, *26*(16), 13097–13101. https://doi.org/10.1021/la1025262

Kroes-Nijboer, A., Venema, P., & van der Linden, E. (2012). Fibrillar structures in food. *Food & Function*, *3*(3), 221–227. https://doi.org/10.1039/c1fo10163c

Krudopp, H., Sönnichsen, F. D., & Steffen-Heins, A. (2015). Partitioning of nitroxides in dispersed systems investigated by ultrafiltration, EPR and NMR spectroscopy. *Journal of Colloid and Interface Science*, *452*, 15–23. https://doi.org/10.1016/j.jcis.2015.03.001

Kuwata, K., Shastry, R., Cheng, H., Hoshino, M., Batt, C. A., Goto, Y., & Roder, H. (2001). Structural and kinetic characterization of early folding events in beta-lactoglobulin. *Nature Structural Biology*, *8*(2), 151–155. https://doi.org/10.1038/84145

Levin, R. L. (1977). Fluorescence-Quenching Studies of the Binding of Bilirubin to Albumin. *Clinical Chemistry*. (23), 2292–2301.

Liang, L., & Subirade, M. (2010). Beta-lactoglobulin/folic acid complexes: Formation, characterization, and biological implication. *The Journal of Physical Chemistry. B*, *114*(19), 6707–6712. https://doi.org/10.1021/jp101096r

Likhtenshtein, G., Yamauchi, J., Nakatsuji, S.'i., Smirnov, A. I., & Tamura, R. (2008). *Nitroxides: Applications in Chemistry, Biomedicine, and Materials Science*. Hoboken: Wiley-VCH.

Loveday, S. M., Wang, X. L., Rao, M. A., Anema, S. G., & Singh, H. (2012). β-Lactoglobulin nanofibrils: Effect of temperature on fibril formation kinetics, fibril morphology and the rheological properties of fibril dispersions. *Food Hydrocolloids*, *27*(1), 242–249. https://doi.org/10.1016/j.foodhyd.2011.07.001

Loveday, S. M., Anema, S. G., & Singh, H. (2017). β-Lactoglobulin nanofibrils: The long and the short of it. *International Dairy Journal*, *67*, 35–45. https://doi.org/10.1016/j.idairyj.2016.09.011

Luckhurst, G. R. (1966). Alternating linewidths. A novel relaxation process in the electron resonance of biradicals. *Molecular Physics*, *10*(6), 543–550. https://doi.org/10.1080/00268976600101481

Margittai, M., & Langen, R. (2004). Template-assisted filament growth by parallel stacking of tau. *Proceedings of the National Academy of Sciences of the United States of America*, *101*(28), 10278–10283. https://doi.org/10.1073/pnas.0401911101

Margittai, M., & Langen, R. (2006). Spin Labeling Analysis of Amyloids and Other Protein Aggregates. In M. Margittai & R. Langen (Eds.), *Methods in Enzymology. Spin labeling Analysis of Amyloids and Other Protein Aggregates* (Vol. 413, pp. 122–139). Elsevier. https://doi.org/10.1016/s0076-6879(06)13007-4

Mchaourab, H. S., Lietzow, M. A., Hideg, K., & Hubbell, W. L. (1996). Motion of spin-labeled side chains in T4 lysozyme. Correlation with protein structure and dynamics. *Biochemistry*, *35*(24), 7692–7704. https://doi.org/10.1021/bi960482k

McKenzie, H. A., Ralston, G. B., & Shaw, D. C. (1972). Location of sulfhydryl and disulfide groups in bovine -lactoglobulins and effects of urea. *Biochemistry*, *11*(24), 4539–4547. https://doi.org/10.1021/bi00774a017

Medrano, A., Abirached, C., Araujo, A. C., Panizzolo, L. A., Moyna, P., & Añón, M. C. (2012). Correlation of average hydrophobicity, water/air interface surface rheological properties and foaming properties of proteins. *Food Science and Technology International = Ciencia Y Tecnologia De Los Alimentos Internacional*, *18*(2), 187–193. https://doi.org/10.1177/1082013211415137

Milov, A. D., Ponomarev, A. B., & Tsvetkov, Y.D. (1984). Electron-electron double resonance in electron spin echo: Model biradical systems and the sensitized photolysis of decalin. *Chemical Physics Letters*, *110*(1), 67–72. https://doi.org/10.1016/0009-2614(84)80148-7

Milov, A. D., Tsvetkov, Y. D., Formaggio, F., Oancea, S., Toniolo, C., & Raap, J. (2004). Solvent effect on the distance distribution between spin labels in aggregated spin labeled trichogin GA IV dimer peptides as studied by pulsed electron–electron double resonance. *Phys. Chem. Chem. Phys.*, *6*(13), 3596–3603. https://doi.org/10.1039/B313701E

Mirabella, F. M. (Ed.) (1993). *Internal reflection spectroscopy: Theory and applications*. *Practical spectroscopy: Vol. 15*. New York: Dekker. Retrieved from http://www.loc.gov/catdir/enhancements/fy0647/92026050-d.html

Mohammadian, M., & Madadlou, A. (2016). Characterization of fibrillated antioxidant whey protein hydrolysate and comparison with fibrillated protein solution. *Food Hydrocolloids*, *52*, 221–230. https://doi.org/10.1016/j.foodhyd.2015.06.022

Moreland, J. L., Gramada, A., Buzko, O. V., Zhang, Q., & Bourne, P. E. (2005). The Molecular Biology Toolkit (MBT): A modular platform for developing molecular visualization applications. *BMC Bioinformatics*, *6*, 21. https://doi.org/10.1186/1471-2105-6-21

Mousavi, S. H.-A., Bordbar, A.-K., & Haertlé, T. (2008). Changes in structure and in interactions of heat-treated bovine beta-lactoglobulin. *Protein and Peptide Letters*, *15*(8), 818–825. https://doi.org/10.2174/092986608785203700

Mudgal, P., Daubert, C. R., & Foegeding, E. A. (2011). Effects of protein concentration and CaCl2 on cold-set thickening mechanism of β-lactoglobulin at low pH. *International Dairy Journal*, *21*(5), 319–326. https://doi.org/10.1016/j.idairyj.2010.11.014

Narayan, M., & Berliner, L. J. (1997). Fatty acids and retinoids bind independently and simultaneously to beta-lactoglobulin. *Biochemistry*, *36*(7), 1906–1911. https://doi.org/10.1021/bi9621526

Oboroceanu, D., Wang, L., Magner, E., & Auty, M. A.E. (2014). Fibrillization of whey proteins improves foaming capacity and foam stability at low protein concentrations. *Journal of Food Engineering*, *121*, 102–111. https://doi.org/10.1016/j.jfoodeng.2013.08.023

Oliveira, O. N. (1992). Langmuir-Blodgett films - Properties and Possible Applications. *Brazilian Journal of Physics*, *22*(2), 60–69.

Owenius, R., Engström, M., Lindgren, M., & Huber, M. (2001). Influence of Solvent Polarity and Hydrogen Bonding on the EPR Parameters of a Nitroxide Spin Label Studied by 9-GHz and 95-GHz EPR Spectroscopy and DFT Calculations. *The Journal of Physical Chemistry A*, *105*(49), 10967–10977. https://doi.org/10.1021/jp0116914

Owenius, R., Österlund, M., Lindgren, M., Svensson, M., Olsen, O. H., Persson, E., Carlsson, U. (1999). Properties of Spin and Fluorescent Labels at a Receptor-Ligand Interface. *Biophysical journal*, *77*(4), 2237–2250. https://doi.org/10.1016/S0006-3495(99)77064-5

Pannier, M., Veit, S., Godt, A., Jeschke, G., & Spiess, H. W. (2000). Dead-time free measurement of dipole-dipole interactions between electron spins. *Journal of Magnetic Resonance (San Diego, Calif.: 1997)*, *142*(2), 331–340. https://doi.org/10.1006/jmre.1999.1944

Papiz, M. Z., Sawyer, L., Eliopoulos, E. E., North, A. C., Findlay, J. B., Sivaprasadarao, R., . . . Kraulis, P. J. (1986). The structure of beta-lactoglobulin and its similarity to plasma retinol-binding protein. *Nature*, *324*(6095), 383–385. https://doi.org/10.1038/324383a0

Peng, D., Yang, J., Li, J., Tang, C., & Li, B. (2017). Foams Stabilized by β-Lactoglobulin Amyloid Fibrils: Effect of pH. *Journal of Agricultural and Food Chemistry*, *65*(48), 10658–10665. https://doi.org/10.1021/acs.jafc.7b03669

Phelan, P., & Malthouse, J. P. (1994). 13C-n.m.r. of the cyanylated beta-lactoglobulins: Evidence that Cys-121 provides the thiol group of beta-lactoglobulins A and B. *The Biochemical Journal*, *302 (Pt 2)*, 511–516. https://doi.org/10.1042/bj3020511

Puyol, P., Pérez, M.D., & Horne, D.S. (2001). Heat-induced gelation of whey protein isolates (WPI): Effect of NaCl and protein concentration. *Food Hydrocolloids*, *15*(3), 233–237. https://doi.org/10.1016/S0268-005X(01)00018-2

Qin, B. Y., Bewley, M. C., Creamer, L. K., Baker, H. M., Baker, E. N., & Jameson, G. B. (1998). Structural basis of the Tanford transition of bovine beta-lactoglobulin. *Biochemistry*, *37*(40), 14014–14023. https://doi.org/10.1021/bi981016t

Qin, B. Y., Bewley, M. C., Creamer, L. K., Baker, E. N., & Jameson, G. B. (1999). Functional implications of structural differences between variants A and B of bovine beta-lactoglobulin. *Protein Science*, *8*(1), 75–83. https://doi.org/10.1110/ps.8.1.75

Qin, B. Y., Creamer, L. K., Baker, E. N., & Jameson, G. B. (1998). 12-Bromododecanoic acid binds inside the calyx of bovine β-lactoglobulin. *FEBS Letters*, *438*(3), 272–278. https://doi.org/10.1016/S0014-5793(98)01199-5

Rade-Kukic, K., Schmitt, C., & Rawel, H. M. (2011). Formation of conjugates between β-lactoglobulin and allyl isothiocyanate: Effect on protein heat aggregation, foaming and emulsifying properties. *Food Hydrocolloids*, *25*(4), 694–706. https://doi.org/10.1016/j.foodhyd.2010.08.018

Rühs, P. A., Scheuble, N., Windhab, E. J., Mezzenga, R., & Fischer, P. (2012). Simultaneous control of pH and ionic strength during interfacial rheology of β-lactoglobulin fibrils adsorbed at liquid/liquid Interfaces. *Langmuir : the ACS Journal of Surfaces and Colloids*, *28*(34), 12536–12543. https://doi.org/10.1021/la3026705

Rullier, B., Novales, B., & Axelos, M. A.V. (2008). Effect of protein aggregates on foaming properties of β-lactoglobulin. *Colloids and Surfaces A: Physicochemical and Engineering Aspects*, *330*(2-3), 96–102. https://doi.org/10.1016/j.colsurfa.2008.07.040

Sagis, L. M.C., Veerman, C., Ganzevles, R., Ramaekers, M., Bolder, S. G., & van der Linden, E. (2002). Mesoscopic structure and viscoelastic properties of β-lactoglobulin gels

at low pH and low ionic strength. *Food Hydrocolloids*, *16*(3), 207–213. https://doi.org/10.1016/S0268-005X(01)00084-4

Sakai, K., Sakurai, K., Sakai, M., Hoshino, M., & Goto, Y. (2000). Conformation and stability of thiol-modified bovine beta-lactoglobulin. *Protein Science*. (9), 1719–1729.

Sakurai, K., Konuma, T., Yagi, M., & Goto, Y. (2009). Structural dynamics and folding of beta-lactoglobulin probed by heteronuclear NMR. *Biochimica Et Biophysica Acta*, *1790*(6), 527–537. https://doi.org/10.1016/j.bbagen.2009.04.003

Salemme, F. R. (1983). Structural properties of protein β-sheets. *Progress in Biophysics and Molecular Biology*, *42*, 95–133. https://doi.org/10.1016/0079-6107(83)90005-6

Sarkar, A., Goh, K. K.T., Singh, R. P., & Singh, H. (2009). Behaviour of an oil-in-water emulsion stabilized by β-lactoglobulin in an in vitro gastric model. *Food Hydrocolloids*, *23*(6), 1563–1569. https://doi.org/10.1016/j.foodhyd.2008.10.014

Savitsky, A., Kühn, M., Duché, D., Möbius, K., & Steinhoff, H.-J. (2004). Spontaneous Refolding of the Pore-Forming Colicin A Toxin upon Membrane Association As Studied by X-Band and W-Band High-Field Electron Paramagnetic Resonance Spectroscopy †. *The Journal of Physical Chemistry B*, *108*(27), 9541–9548. https://doi.org/10.1021/jp036397l

Sawyer, L., & Kontopidis, G. (2000). The core lipocalin, bovine β-lactoglobulin. *Biochimica et Biophysica Acta (BBA) - Protein Structure and Molecular Enzymology*, *1482*(1-2), 136–148. https://doi.org/10.1016/S0167-4838(00)00160-6

Schestkowa, H., Wollborn, T., Westphal, A., Maria Wagemans, A., Fritsching, U., & Drusch, S. (2019). Conformational state and charge determine the interfacial stabilization process of beta-lactoglobulin at preoccupied interfaces. *Journal of Colloid and Interface Science*, *536*, 300–309. https://doi.org/10.1016/j.jcis.2018.10.043

Schmid, M., Dallmann, K., Bugnicourt, E., Cordoni, D., Wild, F., Lazzeri, A., & Noller, K. (2012). Properties of Whey-Protein-Coated Films and Laminates as Novel Recyclable Food Packaging Materials with Excellent Barrier Properties. *International Journal of Polymer Science*, *2012*(5), 1–7. https://doi.org/10.1155/2012/562381

Schmidt, M. J., Fedoseev, A., Bücker, D., Borbas, J., Peter, C., Drescher, M., & Summerer, D. (2015). EPR Distance Measurements in Native Proteins with Genetically Encoded Spin Labels. *ACS Chemical Biology*, *10*(12), 2764–2771. https://doi.org/10.1021/acschembio.5b00512

Schokker, E.P., Singh, H., Pinder, D.N., & Creamer, L.K. (2000). Heat-induced aggregation of β-lactoglobulin AB at pH 2.5 as influenced by ionic strength and protein concentration. *International Dairy Journal*, *10*(4), 233–240. https://doi.org/10.1016/S0958-6946(00)00047-9

Schreier, S., Polnaszek, C. F., & Smith, I. C.P. (1978). Spin labels in membranes problems in practice. *Biochimica et Biophysica Acta (BBA) - Reviews on Biomembranes*, *515*(4), 395–436. https://doi.org/10.1016/0304-4157(78)90011-4

Schwuger, M. J., & Rostek, H. M. (1971). Automatische Apparatur zur Messung der Oberflächenspannung nach der Wilhelmy-Methode. *Chemie Ingenieur Technik - CIT*, *43*(19), 1075–1078. https://doi.org/10.1002/cite.330431906

Sepkhanova, I., Drescher, M., Meeuwenoord, N. J., Limpens, R. W. A. L., Koning, R. I., Filippov, D. V., & Huber, M. (2009). Monitoring Alzheimer Amyloid Peptide Aggregation by EPR. *Applied Magnetic Resonance*, *36*(2-4), 209–222. https://doi.org/10.1007/s00723-009-0019-1

Serfert, Y., Lamprecht, C., Tan, C.-P., Keppler, J. K., Appel, E., Rossier-Miranda, F. J. Schwarz, K. (2014). Characterisation and use of β-lactoglobulin fibrils for microencapsulation of lipophilic ingredients and oxidative stability thereof. *Journal of Food Engineering*, *143*, 53–61. https://doi.org/10.1016/j.jfoodeng.2014.06.026

Shimizu, M., Saito, M., & Yamauchi, K. (1984). Emulsifying and Structural Properties of β-Lactoglobulin at Different pHs. *Agricultural and Biological Chemistry*, *49*(1), 189–194. https://doi.org/10.1080/00021369.1985.10866680

Singh, H. (2009). Protein interactions and functionality of milk protein products. In H. Singh (Ed.), *Dairy-Derived Ingredients* (pp. 644–674). Elsevier. https://doi.org/10.1533/9781845697198.3.644

Slichter, C. P. (1955). Spin Resonance of Impurity Atoms in Silicon. *Physical Review*, *99*(2), 479–480. https://doi.org/10.1103/PhysRev.99.479

Song, C. Y., Chen, W. L., Yang, M. C., Huang, J. P., & Mao, S. J. T. (2005). Epitope mapping of a monoclonal antibody specific to bovine dry milk: Involvement of residues 66-76 of strand D in thermal denatured beta-lactoglobulin. *The Journal of Biological Chemistry*, *280*(5), 3574–3582. https://doi.org/10.1074/jbc.M407031200

Steinhoff, H.-J., Pfeiffer, M., Rink, T., Burlon, O., Kurz, M., Riesle, J., Oesterhelt, D. (1999). Azide Reduces the Hydrophobic Barrier of the Bacteriorhodopsin Proton Channel. *Biophysical journal*, *76*(5), 2702–2710. https://doi.org/10.1016/S0006-3495(99)77422-9

Stoll, S., & Schweiger, A. (2006). EasySpin, a comprehensive software package for spectral simulation and analysis in EPR. *Journal of Magnetic Resonance*, *178*(1), 42–55. https://doi.org/10.1016/j.jmr.2005.08.013

Tamm, F., Sauer, G., Scampicchio, M., & Drusch, S. (2012). Pendant drop tensiometry for the evaluation of the foaming properties of milk-derived proteins. *Food Hydrocolloids*, *27*(2), 371–377. https://doi.org/10.1016/j.foodhyd.2011.10.013

Tanford, C., Bunville, L. G., & Nozaki, Y. (1959). The Reversible Transformation of β-Lactoglobulin at pH 7.5 1. *Journal of the American Chemical Society*, *81*(15), 4032–4036. https://doi.org/10.1021/ja01524a054

Tayeh, N., Rungassamy, T., & Albani, J. R. (2009). Fluorescence spectral resolution of tryptophan residues in bovine and human serum albumins. *Journal of Pharmaceutical and Biomedical Analysis*, *50*(2), 107–116. https://doi.org/10.1016/j.jpba.2009.03.015

Török, M., Milton, S., Kayed, R., Wu, P., McIntire, T., Glabe, C. G., & Langen, R. (2002). Structural and dynamic features of Alzheimer's Abeta peptide in amyloid fibrils studied by site-directed spin labeling. *The Journal of Biological Chemistry*, *277*(43), 40810–40815. https://doi.org/10.1074/jbc.M205659200

Uhrínová, S., Smith, M. H., Jameson, G. B., Uhrín, D., Sawyer, L., & Barlow, P. N. (2000). Structural changes accompanying pH-induced dissociation of the beta-lactoglobulin dimer. *Biochemistry*, *39*(13), 3565–3574. https://doi.org/10.1021/bi992629o.

UniProt: A worldwide hub of protein knowledge (2019). *Nucleic Acids Research*, *47*(D1), D506-D515. https://doi.org/10.1093/nar/gky1049

Unterhaslberger, G., Schmitt, C., Sanchez, C., Appolonia-Nouzille, C., & Raemy, A. (2006). Heat denaturation and aggregation of β-lactoglobulin enriched WPI in the presence of arginine HCl, NaCl and guanidinium HCl at pH 4.0 and 7.0. *Food Hydrocolloids*, *20*(7), 1006–1019. https://doi.org/10.1016/j.foodhyd.2005.10.017

Usov, I., Adamcik, J., & Mezzenga, R. (2013). Polymorphism in bovine serum albumin fibrils: Morphology and statistical analysis. *Faraday Discussions*, *166*, 151–162. https://doi.org/10.1039/C3FD00083D

Uttinger, M. J., Heyn, T. R., Jandt, U., Wawra, S. E., Winzer, B., Keppler, J. K., & Peukert, W. (2020). Measurement of length distribution of beta-lactoglobulin fibrils by multiwavelength analytical ultracentrifugation. *European Biophysics Journal: EBJ.* Advance online publication. https://doi.org/10.1007/s00249-020-01421-4

Van Duuren, B. L. (1961). Solvent Effects in the Fluorescence of Indole and Substituted Indoles 1. *The Journal of Organic Chemistry*, *26*(8), 2954–2960. https://doi.org/10.1021/jo01066a079

Veerman, C., Ruis, H., Sagis, L.M.C., & van der Linden, E. (2002). Effect of Electrostatic Interactions on the Percolation Concentration of Fibrillar β-Lactoglobulin Gels. *Biomacromolecules*. (3), 869–873.

Veerman, C., Baptist, H., Sagis, L. M. C., & van der Linden, E. (2003). A new multistep Ca2+-induced cold gelation process for beta-lactoglobulin. *Journal of Agricultural and Food Chemistry*, *51*(13), 3880–3885. https://doi.org/10.1021/jf0261396

Veerman, C., Sagis, L. M.C., Heck, J., & van der Linden, E. (2003). Mesostructure of fibrillar bovine serum albumin gels. *International Journal of Biological Macromolecules*, *31*(4-5), 139–146. https://doi.org/10.1016/S0141-8130(02)00074-0

Veerman, C., Schiffart, G. de, Sagis, L. M.C., & van der Linden, E. (2003). Irreversible self-assembly of ovalbumin into fibrils and the resulting network rheology. *International Journal of Biological Macromolecules*, *33*(1-3), 121–127. https://doi.org/10.1016/S0141-8130(03)00076-X

Wan, Z., Yang, X., & Sagis, L. M. C. (2016). Contribution of Long Fibrils and Peptides to Surface and Foaming Behavior of Soy Protein Fibril System. *Langmuir: the ACS Journal of Surfaces and Colloids*, *32*(32), 8092–8101. https://doi.org/10.1021/acs.langmuir.6b01511

Wang, J., Nguyen, A. V., & Farrokhpay, S. (2016). A critical review of the growth, drainage and collapse of foams. *Advances in Colloid and Interface Science*, *228*, 55–70. https://doi.org/10.1016/j.cis.2015.11.009

Wang, L., Liu, L., Holmes, J., Huang, J., Kerry, J. F., & Kerry, J. P. (2008). Effect of pH and addition of corn oil on the properties of whey protein isolate-based films using response surface methodology. *International Journal of Food Science & Technology*, *43*(5), 787–796. https://doi.org/10.1111/j.1365-2621.2007.01517.x

Wang, Q., Yu, H., Tian, B., Jiang, B., Xu, J., Li, D., Liu, C. (2019). Novel Edible Coating with Antioxidant and Antimicrobial Activities Based on Whey Protein Isolate Nanofibrils and Carvacrol and Its Application on Fresh-Cut Cheese. *Coatings*, *9*(9), 583. https://doi.org/10.3390/coatings9090583

Wang, Z., & Narsimhan, G. (2005). Interfacial dilatational elasticity and viscosity of beta-lactoglobulin at air-water interface using pulsating bubble tensiometry. *Langmuir: the ACS Journal of Surfaces and Colloids*, *21*(10), 4482–4489. https://doi.org/10.1021/la047374g

Ward, A. F. H., & Tordai, L. (1946). Time-Dependence of Boundary Tensions of Solutions I. The Role of Diffusion in Time-Effects. *The Journal of Chemical Physics*, *14*(7), 453–461. https://doi.org/10.1063/1.1724167

Weiner, L. (2012). Quantitative Determination of Thiol Status of Proteins and Cells by Nitroxyl Biradical RS-SR. In A. Kokorin (Ed.), *Nitroxides - Theory, Experiment and Applications* (pp. 369–384). InTech. https://doi.org/10.5772/45620

Wilde, S. C., Keppler, J. K., Palani, K., & Schwarz, K. (2016). β-Lactoglobulin as nanotransporter—Part I: Binding of organosulfur compounds. *Food Chemistry*, *197*(Pt A), 1015–1021. https://doi.org/10.1016/j.foodchem.2015.11.010

Wilde, S. C., Treitz, C., Keppler, J. K., Koudelka, T., Palani, K., Tholey, A., Schwarz, K. (2016). β-Lactoglobulin as nanotransporter—Part II: Characterization of the covalent protein modification by allicin and diallyl disulfide. *Food Chemistry*, *197*(Pt A), 1022–1029. https://doi.org/10.1016/j.foodchem.2015.11.011

Windle, J.J. (1981). Hyperfine coupling constants for nitroxide spin probes in water and carbon tetrachloride. *Journal of Magnetic Resonance (1969)*, *45*(3), 432–439. https://doi.org/10.1016/0022-2364(81)90150-5

Wu, S. Y., Pérez, M. D., Puyol, P., & Sawyer, L. (1999). beta-lactoglobulin binds palmitate within its central cavity. *The Journal of Biological Chemistry*, *274*(1), 170–174. https://doi.org/10.1074/jbc.274.1.170

Yan, Y., Seeman, D., Zheng, B., Kizilay, E., Xu, Y., & Dubin, P. L. (2013). pH-Dependent aggregation and disaggregation of native β-lactoglobulin in low salt. *Langmuir : the ACS Journal of Surfaces and Colloids*, *29*(14), 4584–4593. https://doi.org/10.1021/la400258r.

Yang, J., Thielen, I., Berton-Carabin, C. C., van der Linden, E., & Sagis, L. M.C. (2020). Nonlinear interfacial rheology and atomic force microscopy of air-water interfaces

stabilized by whey protein beads and their constituents. *Food Hydrocolloids*, *101*, 105466. https://doi.org/10.1016/j.foodhyd.2019.105466

Young, T. (1805). III. An essay on the cohesion of fluids. *Philosophical Transactions of the Royal Society of London*, *95*, 65–87. https://doi.org/10.1098/rstl.1805.0005

Zare, D., McGrath, K. M., & Allison, J. R. (2015). Deciphering β-Lactoglobulin Interactions at an Oil-Water Interface: A Molecular Dynamics Study. *Biomacromolecules*, *16*(6), 1855–1861. https://doi.org/10.1021/acs.biomac.5b00467

Zimmerman, J. K., Barlow, G. H., & Klotz, I. M. (1970). Dissociation of β-lactoglobulin near neutral pH. *Archives of Biochemistry and Biophysics*, *138*(1), 101–109. https://doi.org/10.1016/0003-9861(70)90289-4

3 Manuscript 1: Changes in protein and label properties during site-directed spin labeling

of MTSSL to β-lactoglobulin

Effect of pH-values, concentration rations, and temperatures

Jacqueline Lux[a], Tobias Demetrowitsch[a], Karin Schwarz[a], Julia Keppler[a], Anja Steffen-Heins[a]

[a]Institute of Human Nutrition and Food Science, Division of Food Technology, Kiel University, 24118 Kiel, Germany.

3.1 Abstract

Site-directed spin labeling (SDSL) of β-lactoglobulin (β-lg) with the label MTSSL was established to use EPR spectroscopy for investigating non-covalent protein aggregation in food for the first time. Labeling was verified by RP-HPLC, fluorescence quenching, and ATR-FTIR. Because of the high affinity of MTSSL (K_α = 2.1), an equimolar ratio of MTSSL and β-lg was sufficient for SDSL at pH 7.5 resulting in a high labeling rate without significant change in protein structure and with low dimerization of MTSSL. FT-ICR-MS results indicated that MTSSL biradicals formed during incubation were further reduced to monoradical dimers $[MH_2]^+$, which cannot be distinguished in the EPR spectra from the monoradical monomers [M]. This should be addressed in the spectral analysis. MTSSL and β-lg remained stably bound at high temperature (90°C) and acidic (pH 2) condition which is the prerequisite for the investigation of conformational changes of the protein backbone during amyloid protein aggregation.

3.2 Introduction

Electron paramagnetic resonance spectroscopy (EPR) combined with site-directed spin labeling (SDSL) is a common method to characterize the structure and dynamics of proteins particularly during amyloid aggregation (Drescher, 2012; Török et al., 2002). The mobility of the spin label provides structural information about amyloid aggregates at the level of the protein backbone, without influencing the protein aggregation (Chen, Margittai, Chen, & Langen, 2007; Hubbell, Gross, Langen, & Lietzow, 1998; Margittai & Langen, 2004). The vast majority of protocols uses small paramagnetic labels that are thiol-specific such as methanethiosulfonates (e.g. S-[(1-Hydroxy-2,2,5,5-tetramethyl-2,5-dihydro-1H-pyrrol-3-yl)methyl] methanesulfonothioate, often abbreviated as MTSSL, MTSL or MMTS) which are covalently linked via disulfide bridges to free cysteine residues (Figure 3-1B and C). Prior to the labeling of the protein, cysteine residues are mostly engineered at distinct positions of the proteins (Chen et al., 2007; Gu, Tran, Jiang, & Guo, 2016; Margittai & Langen, 2004; Sepkhanova et al., 2009; Török et al., 2002) or disruptive cysteine residues need to be removed (Kirby, Karim, & Thomas, 2004; Margittai & Langen, 2004). Spin labeling with MTSSL is usually performed at pH values of 7.4 to 7.6 and in 4 to 10 times molar excess compared to protein concentration (Chen et al., 2007; Kirby et al., 2004; Schmidt et al., 2015; Török et al., 2002). In particular at alkaline pH values, unbound labels tend to dimerize via thiol groups and form biradicals (Figure 3-1D) (Bordignon, 2007), which are therefore chromatographically removed in most protocols (Chen et al., 2007; Kirby et al., 2004; Margittai & Langen, 2004; Török et al., 2002). In EPR spectra, those biradicals exhibit a five line spectrum as the two electrons interact by spin exchange (Luckhurst, 1966). In addition,

advanced applications of this approach enable the measurement of intramolecular distance between two spin labels within proteins (Berliner, Grunwald, Hankovszky, & Hideg, 1982; Schmidt et al., 2015). SDSL has therefore been used for some time in various areas of structural biology and the investigation of neurodegenerative diseases (Margittai & Langen, 2004) such as Alzheimer's disease (Chen et al., 2007; Gu et al., 2016; Sepkhanova et al., 2009; Török et al., 2002). However, SDSL has not been applied so far in food chemistry and food biophysics to evaluate the dynamics of non-covalent protein aggregation.

Bovine β-lactoglobulin (β-lg) is the major whey protein and widely used in the food industry. β-lg consists of 162 amino acids with five cysteine residues, of which two intramolecular disulfide bridges (Cys^{66}-Cys^{160} and Cys^{106}-Cys^{119}) are formed and a free thiol group (Cys^{121}) remains (Figure 3-1A). Compared to other proteins already analyzed by SDSL, β-lg is larger and more compact. Various studies show that different ligands can be covalently bound to β-lg via the free thiol group, whereby the concentration ratios depend on the reactivity of the ligand. The optimum thiol modification conditions are at pH values above the pk_a value of the targeted amino acid. For β-lg, often pH values as high as pH 8.5 are chosen due to its high pH value tolerance. A 2- to 40-fold molar excess of ligands can be observed in the literature in order to achieve saturation of the binding sites, for example for covalent modification with allicin from garlic or allyl isothiocyanate from cabbage. However, these thiol-group modifications frequently alter the proteins functionality or thermal stability of the proteins by inducing conformational changes (Keppler et al., 2017; Wilde, Keppler, Palani, & Schwarz, 2016), which should be avoided as far as possible in SDSL. Apart from labeling, β-lg undergoes changes in conformation and aggregation as a function of the pH value (Casal, Köhler, & Mantsch, 1988; Fang & Dalgleish, 1997; McKenzie & Sawyer, 1967). Particularly between pH 7 and 8, which is the commonly used pH value range for SDSL, the local secondary and tertiary structure of the EF loop is changed, which is called Tanford transition (Tanford, Bunville, & Nozaki, 1959). The protein modification depends elementarily on the type of amino acids neighboring the amino acid to be labeled, so that for each protein best labeling conditions must be re-examined.

The aim of this work is therefore to establish a method for spin-labeling β-lg for the first time. Sites buried in the core, as it is in β-lg, are not preferential targets for SDSL, because of the high probability of conformational changes (Bordignon, 2007). Hence, it is mandatory to verify biochemically, that labeling and the labeling conditions (pH value) do not affect the protein structure and functionality or the spin label for further investigation of the protein. The minimization of changes in the secondary and tertiary protein structure by the labeling process is necessary in order to investigate influences on the aggregation behavior of the labeled β-lg such as solvents, high temperature, pH values or interactions with interfaces,

systematically. For this reason, it is also essential that the protein-label disulfide bridge is stable against acidic pH values and temperatures above 60°C. Previous protocols for SDSL with MTSSL and the modification of the β-lg are in contrast, since a sufficiently high labeling rate of β-lg can probably only be achieved at pH values >8.5 and at high excess of MTSSL, while under these conditions an increased biradical formation of the MTSSL is to be expected.

Thus, the challenge of the study lies in finding the optimal conditions also for the label to inhibit or reduce its dimerization propensity by varying the pH value and the ligand concentration. Consequently, aqueous solutions differing in terms of label/protein ratios and pH values and being not exempt from unbound labels are investigated according to the number of binding sites and hydrophobicity of β-lg by HPLC and fluorescence quenching. In addition, alterations in the protein structure were monitored using infrared spectroscopy (ATR-FTIR). Special attention was paid to the dimerization of MTSSL, which was monitored by using Fourier transformation – ion cyclotron resonance – mass spectrometer system (FT-ICR-MS).

3.3 Materials and methods

3.3.1 Materials

β-lactoglobulin (β-lg) was purchased from Davisco Foods International (Eden Prairie, Minnesota, USA) with a purity of ≥ 88.6%, 97% protein and 96% β-lg in dry matter. Calculated NaCl content was 0.29%. MTSSL (S-[(1-Hydroxy-2,2,5,5-tetramethyl-2,5-dihydro-1H-pyrrol-3-yl)methyl] methanesulfonothioate) was purchased from Enzo life science Inc. (Farmingdale, NY, USA) with a purity of ≥ 98%. DTNB (5,5'-dithiobis(2-nitrobezoic acid)) was purchased from Sigma-Aldrich (St. Louis, USA) with a purity of ≥ 98%.

3.3.2 Sample preparation

All measurements were conducted with native β-lg. For labeling, β-lg was dissolved in MilliQ water, stirred until complete hydration and the pH-value adjusted to 6, 7, 7.5, 8 or 9 with ammonium hydroxide (NH_4OH) and formic acid (FA, CH_2O_2). The final concentration of β-lg was 100 µmol/l. The ligand stock solution was prepared and diluted with DMSO to obtain different concentrations of MTSSL (20–250 µmol/l final concentration). Each MTSSL/β-lg ratio was prepared separately, 1.38 ml/100 ml ligand-solution was added to one volume of β-lg. The molar ratio of ligand/protein ranges from 0.2–2.5. As controls 1.38 ml/100 ml DMSO were added to β-lg solution instead of MTSSL solution. All samples were incubated over night at 4°C in the dark and prepared in triplicate. To confirm the protein concentration, the

absorption at 278 nm was measured using a UV-Vis spectrometer (Helios Gamma, UV-Vis, Thermo Spectronic, Cambridge, UK) and calculated by using the molar absorption coefficient of 17600 $M^{-1}cm^{-1}$.

3.3.3 Determination of free thiol groups (RSH)

Free thiol groups were determined by using the Ellman's assay (Ellman, 1959) using a UV-Vis spectrometer (Helios Gamma, UV-Vis, Thermo Spectronic, Cambridge, UK) and a quartz cell. Each MTSSL/β-lg ratios were investigated in triplicate.

The binding constant was calculated by nonlinear regression of the saturation binding curve using the software Graphpad Prism version 6 (Graphpad Software, La Jolla, USA) according to (Keppler et al., 2014; Wilde et al., 2016). To obtain the binding curves the molar ratio of MTSSL to β-lactoglobulin (B, µM/µM) were plotted against the ligand concentration (µM). B was calculated in the assumption that each thiol group can bind one molecule of MTSSL.

3.3.4 RP-HPLC analysis

Prolonged retention times of proteins in the RP-HPLC spectra were assumed to indicate a stronger protein hydrophobicity. The amount of bound ligand can be calculated by means of RP-HPLC measurements which were performed using Agilent 1100 Series HPLC with a diode-array detector and PLRP-S column (300 Å, 8 µm, 150 x 4.6 mm, Agilent Technologies, Santa Clara, USA) as described previously (Keppler et al. 2017). The binding parameters were calculated according to (Wilde et al., 2016) using the software Graphpad Prism version 6 (Graphpad Software, La Jolla, USA). The area of the unmodified β-lg was used to determine the binding sites using the fractional quench method of Levine (1977) according to Keppler et al. (2014).

3.3.5 Fluorescence quenching (FQ)

The fluorescence measurements were carried out according to Keppler et al. (2014) and Wilde et al. (2016). Measurements were conducted on Varian Cary Eclipse right angle fluorescence spectrometer (Varian Australia PTY Ldt.) at room temperature using a 1 x 1 cm quartz cell with four polished sides.

3.3.6 EPR measurements

EPR spectra of the spin label MTSSL were recorded on a Bruker Elexsys E 500 EPR spectrometer (Bruker, Rheinstetten, Germany) using a X-band microwave frequency of 9.85 GHz and modulation frequency of 100 kHz. The center field was optimized to 351.185 mT with a sweep width of 6 mT, a time constant of 81.93 ms, a conversion time of 40.96 ms, a microwave power of 20 mW and a modulation amplitude of 0.13 mT. At a pH value of 7.5, a

calibration curve was performed for the concentration range of MTSSL between 5 and 350 µM with a calculated lower limit of detection of 6.6 µmol/l.

Xepr software from Bruker was used to analyze first derivative EPR spectra. The double integral of the entire spectrum was calculated indicating the concentration of the spin probe. An increase of the width of the spectrum (A_{ZZ}), and of the middle field peak (ΔH_0) indicates the binding to β-lg. The rotational correlation time τ_c [ns] was calculated by Equation 5 for isotropic high mobility regime measurements,

Equation 5: Rotation correlation time τ_c [ns]

$$\tau_c = 6{,}51 \cdot 10^{-10} \cdot \Delta H_0 \left(\sqrt{\frac{h_0}{h_{+1}}} + \sqrt{\frac{h_0}{h_{-1}}} - 2 \right) \qquad (5)$$

where ΔH_0 is the peak width of the central line of the EPR spectrum and the peak amplitudes are given by h_{+1}, (low-field peak), h_0 (central peak), and h_{-1} (high-field peak). The factor is customarily used for X-band experiments taken into account the magnetic field, the anisotropic g value and the hyperfine coupling a_N (Keith, Bulfield, & Snipes, 1970). Equation 5 is valid for isotropic motions ($\tau_c < 3 \cdot 10^{-9}$ ns) where the spectra display g and A tensors as an average of the principle components (Schreier, Polnaszek, & Smith, 1978). The increase in the value of τ_c means a decrease of the rotational motion of the nitroxides due to higher spin concentrations or increased microviscosity. The calculated rotational correlation time is a mean of all MTSSL molecules including bound and free MTSSL monomers. Simulation of EPR spectrum was done using the EasySpin package with the *garlic function* for fast-motion dynamics ($\tau_c^{-1} > \Delta\omega$, unbound MTSSL) and *chili function* for slow-motion dynamics ($\tau_c^{-1} < \Delta\omega$, bound MTSSL) (Stoll & Schweiger, 2006) for Matlab software (The MathWorks Inc., Natick, Massachusetts, United States) to extract multiple fractions of different bound MTSSL components. For the three monoradicals, the following simulation parameters were kept constant: g-tensor g = [2.0082 2.0056 2.0025], hyperfine tensor A = [18 18 100] MHz, and intrinsic linewidth 0.15 mT. The parameters for the simulation of the biradical used were: g-tensor g = [2.0055 2.0055], hyperfine tensor A = [45 45 45 0 0 0; 0 0 0 45 45 45] MHz, coupling constant J = 840, and intrinsic linewidth 0.36 mT.

3.3.7 ATR-FTIR measurements

ATR-FTIR measurements were carried out at a constant temperature (25 °C) on a Confocheck Tensor 2 spectrometer (Bruker Optics, Ettlingen, Germany), specialized to protein analysis in aqueous solution and equipped with a temperature controlled Attenuated Total Reflection (BioATRII) crystal. 20 µl of each sample (10 mg/ml protein) were prepared on the crystal. After a few minutes of equilibrating for the given temperature (20°C), the measurements were started. For the analysis of the FTIR spectra the range from 1600 to 1700 cm^{-1} (Amide I) was considered. All spectra were first standardized to Amide region

(1550-1700 cm^{-1}), a mean spectra consisting of 6 to 12 measurements was calculated, and the second derivation was interpreted. The software OPUS 7.5 (Bruker Optik GmbH, Ettlingen, Germany) was used.

3.3.8 FT-ICR-MS measurements

The samples were analyzed with a seven Tesla Fourier transformation – ion cyclotron resonance – mass spectrometer (FT-ICR-MS, solariXR) from Bruker (Bremen, Germany). The system was equipped with an electro spray ionization source (ESI). The samples were measured with flow injection analysis method (FIA, flow rate of 15 µl/min and methanol/water + 0.1% acetic acid as solvent) by means of a 1260 HPLC from Agilent (Waldbronn, Germany) but without any chromatographic separations. A small molecule method were used for identifying different unbound MTSSL compounds with a mass range of 85–1000 m/z; a so called wide method were used for β-lg and spin labeled β-lg with a mass range between 400-3000 m/z. The calibration was conducted using sodium format with a precision of <0.2 ppm. All samples were measured in the positive and negative ionization mode. The source temperature was set to 200°C with nitrogen as drying gas with a flow of 4 L/min and a nebulizer pressure of 4 bar. The sweep excitation power was set to 18%. 32 scans were averaged and stored with 4 M. A complete list of measurement parameters is provided in the supplementary information (Table 3-2).The data analysis were conducted with Data Analysis 5.0 from Bruker (Bremen, Germany) and recalibrated with a tailored mass list, containing different charge states of β-lg and the different isoforms of MTSSL (precision <2 ppm). The check of the sum formula was performed with SmartFormula (a program part of DataAnalysis 5.0, Bruker, Bremen, Germany), using the following parameters: mSigma limit of 200, a tolerance of 5 ppm, adducts: M+H, M+Na, M+K in even and odd electron configuration. All considered adducts are listed in the supplementary information (Table 3-3). To level the dependence of the ionization on the pH value, all monomer and dimer adducts were summed up and presented as a ratio of monomers to dimers (RDM). The typical working range of the FT-ICR-MS reaches into the pico- and femtomol range.

3.3.9 Statistical analysis

All results were presented as means and standard deviations of the replicated analyses. The data were analyzed by two-way ANOVA with Tukey's multiple comparison test at a significance level of $\alpha=0.05$. The maximum number of binding sites and the affinity constant were calculated by nonlinear fit. All statistics and figures were created using GraphPad Prism (version 6.07, GraphPad Software, San Diego, CA, USA).

3.4 Results

3.4.1 Covalent bonding, maximum binding sites, and binding affinity

The binding behavior of MTSSL to β-lg was analyzed as a function of pH value and ligand concentration by means of mass spectrometry (MS), retention time in RP-HPLC, free thiol group (RSH) measurements, and fluorescence quenching (FQ). The unlabeled β-lg showed two peaks which demonstrate the two genetic variants of the protein with a MW of 18278 Da (β-lg B) and 18362 Da (β-lg A) (Figure 3-2A, *blue*). By labeling β-lg with an equimolar ratio of MTSSL at pH 7.5, there were two additional peaks with a MW of 18463 Da (B') and 18547 Da (A'), one for each genetic variant (Figure 3-2A, *red*). This mass shift of 185 Da corresponds to the mass of the protein-bound MTSSL with elimination of methane sulfinic acid from MTSSL monomer (Figure 3-1C), i.e., one MTSSL monomer is bound to one β-lg molecule. The specific binding of MTSSL to β-lg at pH 7.5 was determined both by RP-HPLC measurements and the number of unmodified free thiol groups (RSH): maximum number of binding sites (n) of n_{RSH} = 0.866 and $n_{RP\text{-}HPLC}$ = 0.8138 (Figure 3-2B) was observed for an equimolar ratio of MTSSL and β-lg. The affinity constant (K_α) and n at different pH values are based only on the RP-HPLC measurements (Figure 3-2C see Figure 3-6). With increasing pH value, n increased and reached a maximum of 1.1 ± 0.03 mol/mol at pH 8 which was found to be significantly different from all lower pH values. With further increasing pH value, n decreased to 0.9 ± 0.014 mol/mol, but was not significantly different to the values at pH 7, 7.5 and 8. The affinity constants were significantly lower at pH 7.5, 8 and 9 ($K_\alpha \approx 2.1$ mol^{-1}) compared to pH 7 ($K_\alpha = 5.5$ mol^{-1}) and not measurable at pH 6. To measure the free thiol groups of the hidden Cys^{121}, the unfolding of β-lg in the presence of urea was crucial concentration of 8 mol/l. Although urea is a weak base (pk_B = 13.8), the used concentration increased the pH value of the sample. This influenced the protein-ligand–binding kinetics. The interpretation of the RSH results are misleading and thus not suitable to compare the influence of pH value. This effect was already described by Wilde et al. (2016).

The FQ provides insight in the region of Trp^{19}, a covalent or non-covalent bonding in its vicinity is able to quench the fluorescence of this amino acid. This amino acid is also sensitive to changes in its microenvironment, such as increasing solvent accessibility by protein unfolding, which would shift the fluorescence intensity (Hettiarachchi, Melton, Gerrard, & Loveday, 2012). There was no alteration in the fluorescence over the whole range of MTSSL:β-lg ratios (Figure 3-2B, *dotted line*).

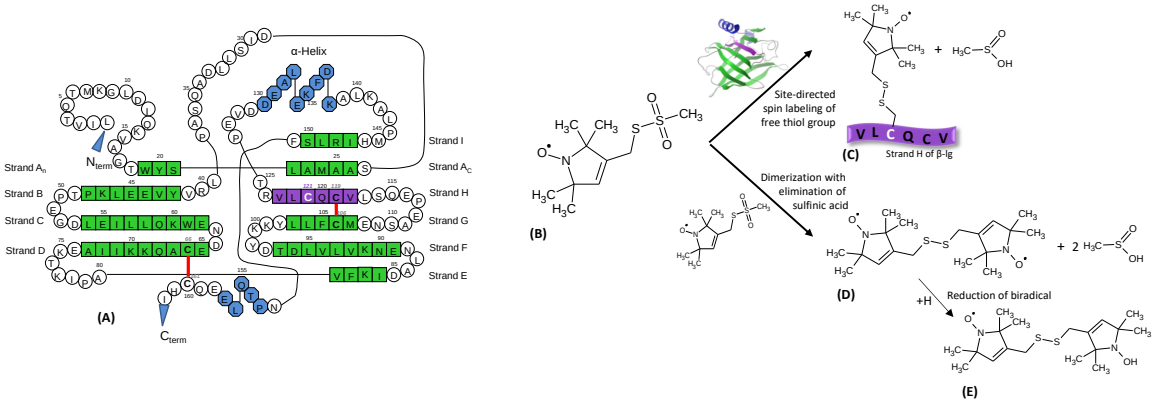

Figure 3-1: Schematic representation of β-lg A, with color-coded protein secondary structure: green β-strands, violet β-strand H with the only free thiol group Cys^{121} (white), blue the α-helix, red lines represent the intramolecular disulfide bridges (modified according to Fogliano et al. (1998) and Keppler et al. (2014) (A). MTSSL monomer (B, 264 m/z). Site-directed spin labeling of MTSSL via the only free thiol group of the native β-lg monomer at position Cys^{121} in the β strand H. Methane sulfinic acid is eliminated (C, 18547 m/z (A') and 18463 m/z (B')). Nitroxide dimer formation by disulfide bonding of two MTSSL monoradicals with elimination of methanesulfinic acid resulting in a biradical according to Markham, Myers, Harris, Volin, & Jaffe, (1993) (D, 370 m/z). Assumed reduction of a biradical into a monoradical dimer (E, 372 m/z odd configuration). Masses and sum formulas are listed in Table 3-3.

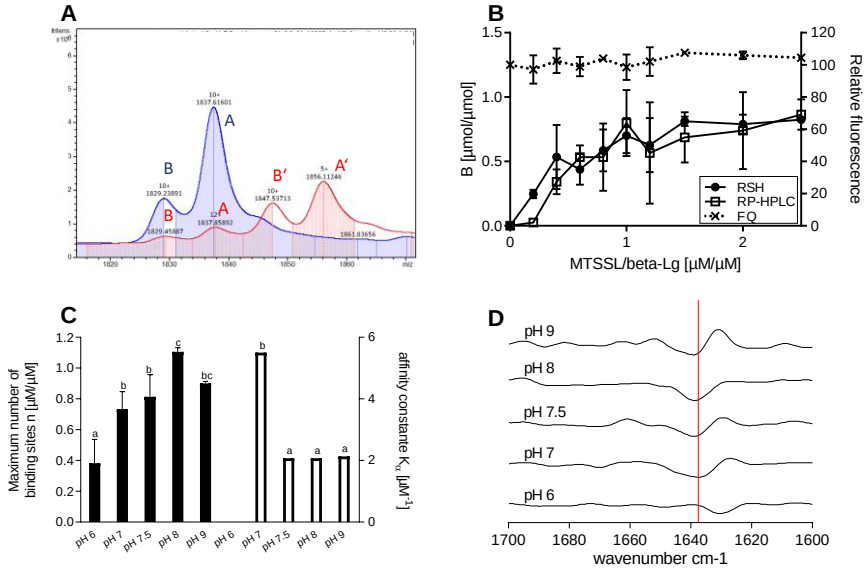

Figure 3-2: Mass spectrometry chromatograms of native β-lg (blue) and labeled with equimolar ratio MTSSL at pH 7.5 (red). The letters in the spectra designate: B – native β-lg B; A – native β-lg A; B' – modified β-lg B; A' – modified β-lg A (A). Molar binding ratio of the ligand MTSSL to β-lg at pH 7.5. The binding sites were calculated by measuring the free thiol groups (RSH – unfilled symbols) and RP-HPLC (filled symbols). The dotted line indicates the relative fluorescence (B). Maximum number of binding sites n [µM/µM] (filled bars) and apparent affinity constant Kα [mM^{-1}] (unfilled bars) of MTSSL to 100 µM native β-lg at different pH values (pH 6-9) measured by RP-HPLC at 205 nm. Different letters indicate significant differences ($p<0.05$, Tuckey), filled and clear columns are considered separately (C). Difference spectra of the second derivative of the amide I region of the ATR-FTIR spectra as a function of pH values. From the spectra of the MTSSL labeled β-lg (equimolar MTSSL:β-lg ratio), comparison spectra with the same amount of solvent DMSO were subtracted (D).

3.4.2 Protein conformation

Conformational changes induced by the spin label are visible in the difference spectra (labeled β-lg minus unlabeled β-lg) (Figure 3-2D), since any difference between the two subtracted spectra would result in a deviation from a horizontal line. In general, conformational changes induced by the spin label increased with increasing pH value. A slight decrease was observed in the β-sheet region (1630-1640 cm^{-1}), with a maximum decrease at pH 7.5. Only at pH 7.5, an increase in the region of β-turns (~1660 cm^{-1}) (Kavanagh, Clark, & Ross-Murphy, 2000) occurred. In contrast, the alpha helix (~1650 cm^{-1}) was not significantly affected when MTSSL was bound to β-lg. In total, most changes were observed in the amide I range (1700-1600 cm^{-1}) at pH 9. For comparison, the 2nd derivative spectra of native and MTSSL labeled β-lg (Figure 3-8) showed a continuous shift of β-sheets to a higher wavenumber between pH 6 and pH 9. This shift was more pronounced for the MTSSL labeled β-lg (pH 6: 1628.2 cm^{-1}; pH 9: 1633.2 cm^{-1}), compared to the control sample (pH 6: 1627.9 cm^{-1}; pH 9: 1632.1 cm^{-1}).

3.4.3 EPR measurements and analysis

When completely dissolved in water at neutral or weak acidic pH values, MTSSL gives a typical three-line isotropic EPR spectrum of a nitroxide that is able to tumble freely (Figure 3-3B, *dashed line*). Increasing the pH from 7 to 9 resulted in additional superposition with five-peak spectra and broader lines (Figure 3-3C-F, *dashed lines*). The higher the pH value, the more pronounced these five-line spectra were. The signal intensities of the entire spectra were reduced with simultaneous broadening of the peaks, however, the double integral indicating the concentration of MTSSL remained constant (Table 3-1). Labeling to β-lg (Figure 3-3, *solid lines*) the superimposed five-line spectra remained, although the intensity of the two intermediate lines became smaller at pH 8 and 9. Simulation of the measured spectrum at pH 7.5 with the EasySpin simulation software showed a total of four MTSSL components that are superimposed (Figure 3-3A). Three three-line spectra were found: unbound MTSSL and two bound components with very different rotational correlation times. For the 4th component, a five-line spectrum was simulated, indicating a paramagnetic dimer of the MTSSL, a biradical (Figure 3-1A).

The concentration of MTSSL, expressed as a double integral of the entire spectrum, remained constant with increasing pH values in water, whereas the peak height (h_0) of the middle field peak decreased (Table 3-1). This also applied to pH 6 in the presence of β-lg. However, increasing pH values led to lower integrals of the spectra and the lowest peak height were measured at pH 8. The width of the total spectrum ($2A_{zz}$) began to broaden significantly in water at pH 8, indicating spin-spin coupling through the formation of biradicals, with nitroxide dynamics still belonging to the fast-motion regime ($\tau_c^{-1} > \Delta\omega$). In the presence

of β-lg, the total spectrum width broadened significantly already at pH 7.5 and the rotational correlation times (τ_c) also increased significantly.

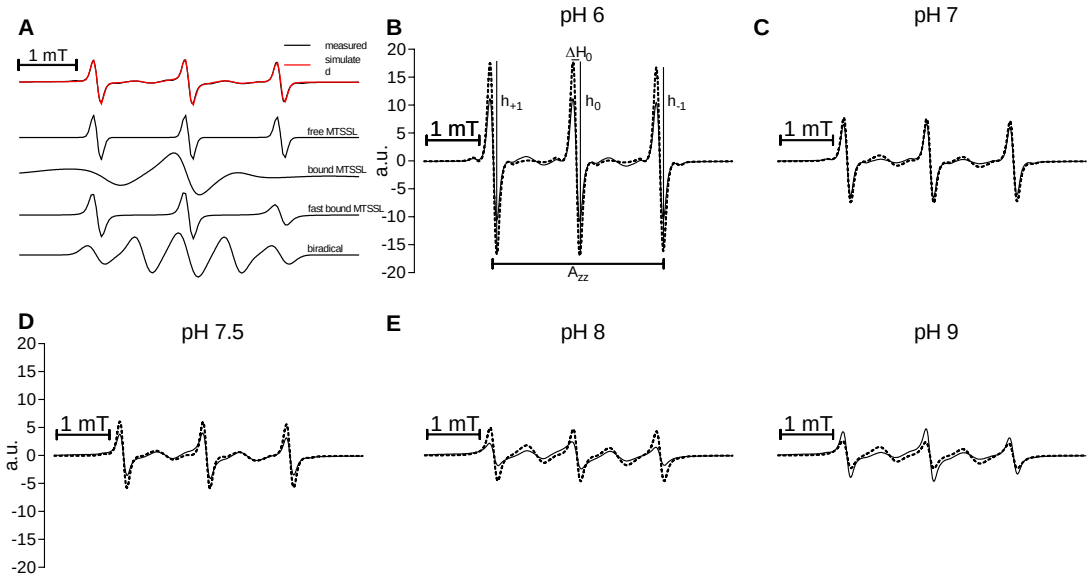

Figure 3-3: Simulation of the EPR spectrum of measured (black) and simulated (red) MTSSL bound to 100 µM native β-lg at pH 7.5. The spectrum is a superposition of a total of four MTSSL components: unbound (32.6%), bound with two different rotational correlation times (slow 47.9%, fast 2.4%), and a paramagnetic dimer (17.1%). Spectra are normalized to the maximal integral (A). EPR spectra of MTSSL (100 µM), in water (dashed lines) or in 100 µM native β-lg solution (solid lines) at pH 6 (B), pH 7 (C), pH 7.5 (D), pH 8 (E), and pH 9 (F).

3.4.4 Mass spectrometry analyses of MTSSL monomers and dimers

The relative abundance of monomers and dimers of the unbound fraction of MTSSL was determined by the mass to charge ratio (m/z) of different adduct types using FT-ICR-MS (Table 3-3). Based on the following assumption, a semi-quantification was conducted: a) the minimum of intensity is at least $1x10^6$ counts; b) the differences in intensity are greater than 30%; c) the signal-to-noise ratio is greater than six. The sum of the m/z intensities for different MTSSL adducts (Figure 3-12) were compared as a dimer-monomer ratio (RDM) (Table 3-1). With a RDM below 1, monomers are the predominant form of the MTSSL, while the RDM above 1 indicates the excess of dimers. The RDM dependents on the pH value and on the concentration of the unbound MTSSL. Both in the absence and in the presence of β-lg, an increase in pH increased the formation of dimers, which is associated with a reduction in MTSSL monomers. A drastic increase in dimer formation associated with a decline in monomers was induced by the increase of the pH from 8 to 9. The extent of dimer formation was considerably higher in pure water, which was adjusted to corresponding pH values than in β-lg solutions with the same pH value.

Table 3-1: Line shape analysis of EPR spectra in water and in β-lg solution as a function of pH value: Peak height (h_0) of the middle field peak, double integral of the entire MTSSL spectrum, total spectrum width ($2A_{zz}$), and the rotational correlation time (τ_c) (n=3). Ratio of MTSSL monomers to dimers (RDM) of unbound MTSSL in water and in β-lg solution as a function of pH value measured by FTICR-MS (n=3).

		*EPR**				*FT-ICR-MS#*
		h_0	double integral	$2A_{ZZ}$ [mT]	τ_C [ns]	RDM
		mean ± sd	mean ± sd	mean ± sd	mean ± sd	mean ± sd
water	pH 6	21.99 ± 5.15^{Aa}	132.99 ± 28.62^{Aa}	3.361 ± 0.0028^{Aa}	0.026 ± 0.000^{Aa}	1.4 ± 0.20
	pH 7	15.15 ± 3.31^{Aab}	123.38 ± 25.54^{Aa}	3.363 ± 0.0000^{Aa}	0.024 ± 0.001^{Aa}	2.2 ± 0.27
	pH 7.5	11.92 ± 2.29^{Abc}	102.23 ± 12.02^{Aa}	3.363 ± 0.0000^{Aa}	0.022 ± 0.001^{Aa}	2.6 ± 0.19
	pH 8	9.36 ± 0.53^{Ac}	156.95 ± 8.10^{Aa}	3.371 ± 0.0028^{Ab}	0.016 ± 0.001^{Aa}	2.4 ± 0.08
	pH 9	4.77 ± 1.46^{Ac}	119.05 ± 38.13^{Aa}	3.385 ± 0.0027^{Ac}	0.014 ± 0.009^{Aa}	4.3 ± 0.04
β-lg solution	pH 6	34.68 ± 5.06^{Ba}	140.86 ± 7.63^{Aa}	3.357 ± 0.0000^{Aa}	0.030 ± 0.000^{Aa}	0.4 ± 0.01
	pH 7	13.21 ± 1.054^{Ab}	67.99 ± 4.69^{Bb}	3.361 ± 0.0028^{Aa}	0.055 ± 0.005^{Aa}	1.3 ± 0.06
	pH 7.5	8.12 ± 0.732^{Abc}	74.01 ± 6.07^{Ab}	3.371 ± 0.0031^{Bb}	0.154 ± 0.010^{Bb}	1.4 ± 0.08
	pH 8	4.88 ± 0.298^{Ac}	74.31 ± 3.84^{Bb}	3.393 ± 0.0048^{Bc}	0.391 ± 0.051^{Bc}	2.6 ± 0.12
	pH 9	9.47 ± 0.615^{Abc}	67.35 ± 11.56	3.381 ± 0.0000^{Ad}	0.260 ± 0.026^{Bd}	9.8 ± 1.19

*Each column was considered separately. Capital letters indicates significant differences between water and β-lg samples, each pH value were considered separately. Small letters indicate significant differences between the pH values, water and β-lg samples were considered separately (p≤0.05).

#Monomers and dimers were analyzed separately as described in 3.3.9 before the monomer-dimer ratio was calculated. Statistical analyses were not performed as this MS technique does not allow for true quantification.

3.4.5 Binding stability at high temperatures and acidic pH values

The strong broadening of the three-line spectrum with simultaneous reduction of intensity (Figure 3-4C-D, *black lines*) compared to water (Figure 3-4A-B, *black lines*) showed the successful binding of the MTSSL to β-lg. The superposition of the spectrum with an additional five-line spectrum indicated the formation of biradicals during the incubation (Figure 3-3A). After adjusting the pH value to 2, the five-line spectrum disappeared in the water samples, while the three-line spectrum showed slightly higher and narrower peaks (Figure 3-4b, *black line*). After heating at 90 °C for five hours, the spectra of the MTSSL in water exhibited the same shape with lower intensity (Figure 3-4A-B, *red lines*). However, the samples with MTSSL bound to β-lg revealed additionally a disappearing of the five-line-spectra, while the three-line spectra exhibited the same shape as before the heating with a slightly lower intensity (Figure 3-4C-D, *red lines*). The midfield peaks of the MTSSL bound to β-lg showed several superimposed MTSSL components. In addition to a decreased proportion of fast rotating MTSSL (narrower top of the signal), there was also a components of bound MTSSL which could rotate less freely (wider base of the signal) in the unheated as well as in the heated sample.

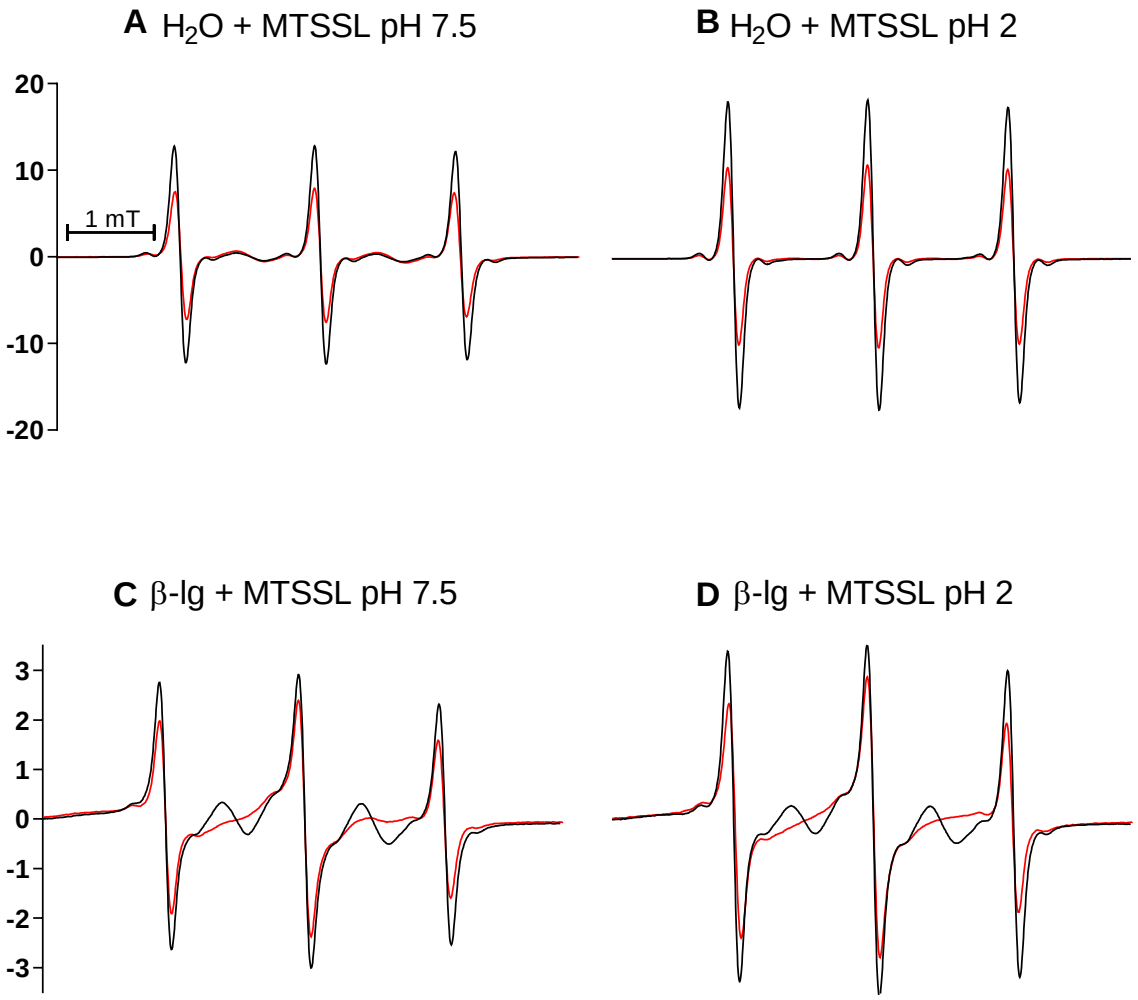

Figure 3-4: EPR spectra of the spin label MTSSL (100 µM) in water (A, B) or in 100 µM native β-lg solution (C, D). Spin labeling was performed for all samples at pH 7.5 at 4 °C over night. The pH values were then adjusted to pH 7.5 (A, C) and pH 2 (B, D) and spectra were recorded before heating (black line) and after five hours incubation at 90°C (red line) (n=3).

During incubation at 90°C, changes in β-lg and MTSSL were monitored at different times by means of rotational correlation time, label concentration and the relationship between monomers and biradicals. The rotational correlation time averaged over all MTSSL components did not change during heat incubation in purely aqueous solutions (Figure 3-5A), before heating ($\tau_{C,pH7.5}$ = 0.024 ± 0.001 ns; $\tau_{C,pH2}$ = 0.026 ± 0.000 ns); after heating ($\tau_{C,pH7,5}$ = 0.054 ± 0.001 ns; $\tau_{C,pH2}$ = 0.033 ± 0.001 ns)). Linked to β-lg, a steadily increasing rotational correlation time of the MTSSL was observed for the acid samples, whereas at pH 7.5 a spontaneous maximum increase of the τ_c was found after 10 min ($\tau_{C,pH7,5}$ = 0.469 ± 0.010 ns) with a subsequent decrease. However, the initial ($\tau_{C,pH7,5}$ = 0.143 ± 0.003 ns; $\tau_{C,pH2}$ = 0.100 ± 0.006 ns) and final rotational correlation times ($\tau_{C,pH7,5}$ = 0.316 ± 0.004 ns; $\tau_{C,pH2}$ = 0.293 ± 0.012 ns) were approximately the same, independent of the pH value after five

hours. Both the integral and the signal intensity of the paramagnetic MTSSL were reduced during heat incubation. The strongest decrease of the respective total radical concentrations, given by the integral, occurred in the first 10 min in the β-lg solution, while a steady decrease was observed in the aqueous solution (Figure 3-5B). The total radical concentration decreased by 40-44% during the five hours heat incubation for the β-lg solutions and the aqueous solution at pH 2, while the radical concentration in the aqueous solution at pH 7.5 showed only a degradation by 17%. When considering the middle field peak (h_0), an increasing height would indicate a degradation of biradicals at a constant total radical concentration (Figure 3-5C). At pH 7.5 there was a strong decrease of h_0 within the first 10 min and an increase during further heating in both aqueous and β-lg solution, whereas at pH 2 there was a steady decrease of h_0. During five hours heating h_0 decreased in β-lg solution by approx. 20%, whereas in aqueous solution a decrease of approx. 40% was observed, independent of the pH value.

Within the first 60 min of heat incubation, at pH 7.5 the amount of labeled β-lg A (β-lg A + MTSSL: 18.548 Da) and β-lg B (β-lg B + MTSSL: 18.463 Da) tended to increase slightly, but over the entire incubation period the intensities of the labeled protein did not change. At pH 2 the signal intensities of both genetic variants were substantially reduced (Figure 3-5D).

The relative abundance of free monomer and dimer adducts formed from the excess of unbound MTSSL after labeling of β-lg was investigated. At pH 2 (Figure 3-5E) the monomers were essentially present as even $[MH_2]^+$ ions, the predominant amount of dimers was found in the odd form of a biradical dimer $[M]^{+\bullet}$ and a monoradical dimer $[MH_2]^{+\bullet}$. During the 5-hour incubation, the relative abundance of the monomers decreased considerably, while that of the dimer species decreased slightly less. At pH value 7.5 (Figure 3-5) the monomers decreased to the same extent, the monoradical dimers, which were clearly the dominant species here, remained on average approximately the same. While virtually no biradicals were found at the more alkaline pH value, the amount of even $[MH_3]^+$ species was higher than at pH value 2. In aqueous controls with the same pH values, more monomer and dimer adducts were found as MTSSL was completely present in its free from (Figure 3-12). At both pH values, the dimer abundance increased at substantially higher MTSSL concentrations, while the monomers also decreased markedly at pH 7.5, but remained stable at pH 2.

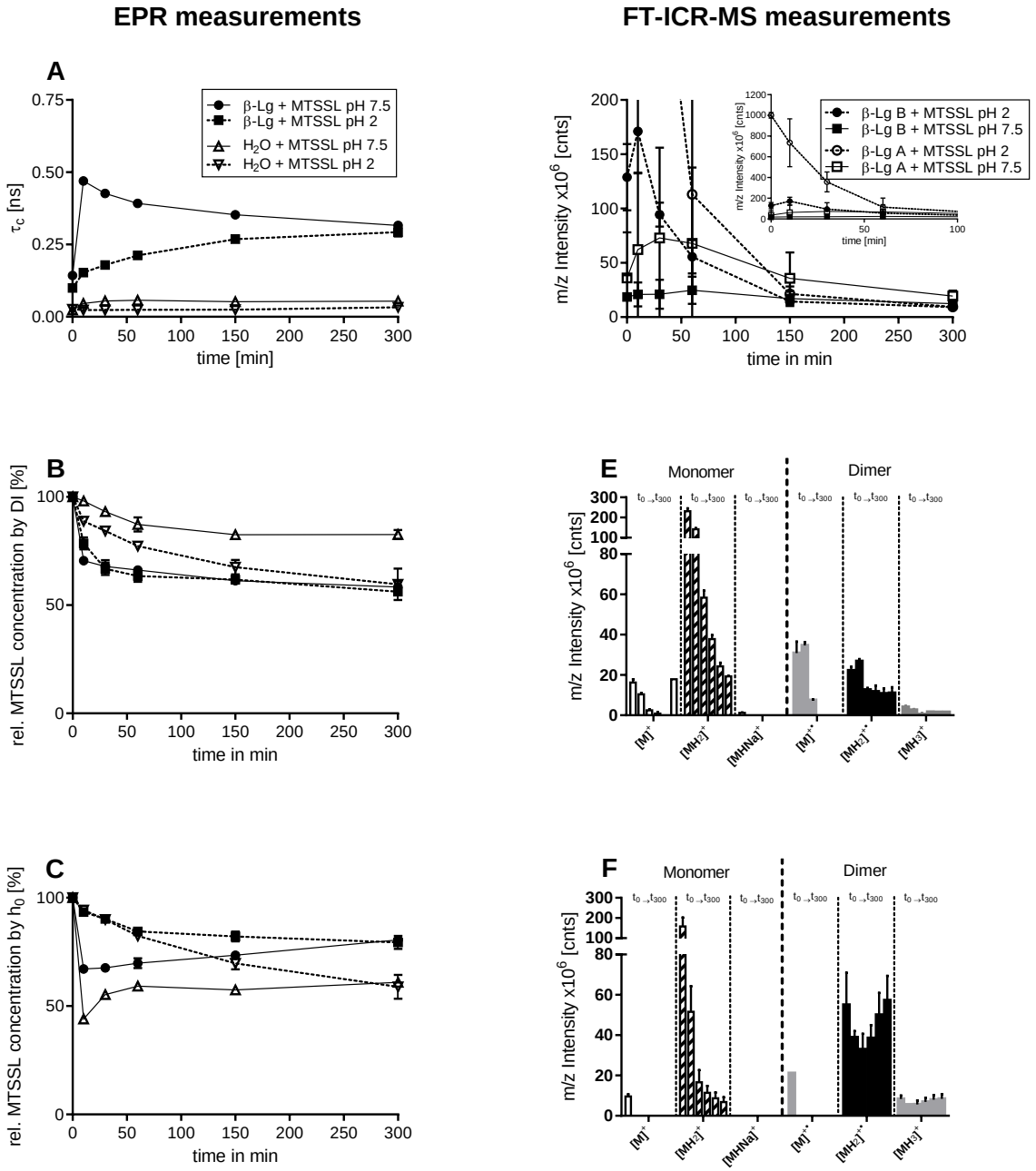

Figure 3-5: Monitoring of the concentration and mobility of the spin label MTSSL as monomers (free and bound to β-lg) and dimers during heat incubation at 90°C for five hours. Labeling of β-lg (100µmol/L) was performed at pH 7.5 (at equimolar ratio of MTSSL and β-lg, incubated at 4°C over night) and then acidified to pH 2. MTSSL dissolved in pH 2 and 7.5 water serves as control. *EPR-measurements only of paramagnetic MTSSL forms*: All measurements were performed at pH 7.5 (solid lines) and pH 2 (dashed lines) (mean ± sd, n=3) Averaged mobility of bound and free MTSSL monomers (rotational correlation time, τ_c) (A). Relative concentration of total MTSSL (including free and bound monomers and dimers) (double integral, DI) of the entire EPR-spectra (B). Relative concentration of MTSSL monomers (including free and bound forms) (intensity of the centerfield peak of MTSSL, h_0) (C). *FT-ICR-MS measurements:* Stability of the two MTSSL-labeled genetic β-lg variants (m/z intensities, positive modus, charge state +10, β-lg B + MTSSL 18.463 Da (filled symbols), β-lg A + MTSSL 18.548 Da (unfilled symbols)) (D). Relative abundance of MTSSL monomer and dimer adducts found at pH 2 (E) and at pH 7.5 (F). Six time points (t_0-t_{300}) were plotted for each adduct: before heating (t_0), after 10, 30, 60, 150 and 300 min (t_{300}). The detailed list of all identified adducts is given in the supplemental (Table 3-3).

3.5 Discussion

3.5.1 Covalent bonding of MTSSL to β-lg

The mass shift of 185 m/z corresponds to the mass of protein-bound MTSSL with elimination of methane sulfinic acid which proves that only one MTSSL was covalently bound to β-lg (Figure 3-2A). The calculated maximum number of binding sites for β-lg as determined by RSH and RP-HPLC with approximately 0.9 mol/mol were always lower than the theoretical maximum number of possible binding sites (Figure 3-2B-C). This is in accordance to other binding studies evaluating the covalent bonding of different ligands to β-lg at Cys^{121}, for example studied in detail for the bioactive food ingredients allicin, diallyl disulfid (Wilde et al., 2016), and allyl-isothiocyanate (Keppler et al., 2014; Rade-Kukic, Schmitt, & Rawel, 2011). The covalent bonding of MTSSL to β-lg has also been confirmed by EPR and FT-ICR-MS. Both, pH-values above 7 and the presence of β-lg resulted in reduced EPR signal intensities (Figure 3-3C-F, Table 3-1) with simultaneous peak broadening. The decrease in peak intensity was due to the signal broadening. Additionally, the three-line spectra of MTSSL was superimposed with a five-line spectra with far broader lines, which was kept in the presence of β-lg, however with lower signal intensities (Figure 3-3). The double integral remained constant (Table 3-1) and indicates the concentration of the nitroxide, whereby the integral depends on the peak width to the square and the peak height (Berliner et al., 1982). The broadening of the signal is induced by hindered tumbling of the nitroxide moiety, which was caused by the successful binding to the protein or the coexistence of paramagnetic dimers (c.f. 3.5.2.3), which is displayed by a quintet spectrum. The exemplary simulation of the β-lg MTSSL spectra at pH 7.5 (Figure 3-3A) proved, among others, the presence of two bound MTSSL components with a common proportion of 50%, which differ strongly in their rotational motion. The cleavage of all disulfide bridges in the presence of DTT confirmed this assumption, as again small peaks with increased intensities arise, which indicates free MTSSL, as already described by Weiner (2012). At the same pH values, lower amounts of free MTSSL monomers are measured in the presence of β-lg than in purely aqueous solutions (Table 3-1), which indicates that MTSSL is bound to β-lg.

3.5.2 Challenges of SDSL as a function of pH value

3.5.2.1 Bonding efficiency

For β-lg, the highest number bound MTSSL molecules and highest affinity constant were observed at pH 8 (Figure 3-2C). The increasing pH-value from 6 to 8 favors the bonding of positive charged reagents through deprotonating of the thiol group ($pK_a = 8.5$) which makes it more reactive (Dunnill & Green, 1966; Qin et al., 1998). These results suggest an optimal pH value for labeling of >8. An increasing binding efficiency depending on the degree of deprotonation of the thiol groups up to a pH value of 8 was also confirmed by EPR data

(Table 3-1). Here, the decreasing signal intensity of the midfield peak and the increasing τ_c with an increasing number of binding sites (Figure 3-2C) corresponded extremely well. For pH values below 9, MTSSL monomers were bound to β-lg without hindrance despite the formation of biradicals (Table 3-1). At pH 9, however, a lower binding rate to the β-lg (Figure 3-2, Table 3-1) and the highest biradical formation (Table 3-1) were observed. This means a reduced binding of MTSSL monomers is accompanied by increasing dimerization at high alkaline pH values (pH 9) (c.f. 3.5.2.3).

3.5.2.2 Conformational changes of β-lg during SDSL

In addition to protein deprotonation, the pH value essentially influences the protein conformation, as shown by RP-HPLC and the FTIR (Figure 3-2D, Figure 3-7A). Because of its five rotatable bonds, MTSSL is known to have a highly flexible linkage to its labeled protein and does not destroy the native state. The FTIR second derivation (Figure 3-8) and difference spectra (Figure 3-2D) confirm that the modified is mostly affected by a signal intensity maximum shift in the β-sheet region with an increase of the 1630 cm^{-1} and a decrease of the 1635 cm^{-1} waveband frequency. Such a shift could indicate an altered monomer-dimer equilibrium. In comparisons, other studies that aimed at changing the protein structure by covalent modification reported strong changes in the β-sheet region, but also altered helix-elements and unordered structures (Keppler et al., 2017; Rade-Kukic et al., 2011). Thus the present changes induced by MTSSL binding to β-lg can be considered as minor.

The overall spectral difference between native and modified β-lg were slightly more pronounced at pH 9 than at lower pH values. It is known that increasing pH value >8.5 leads to irreversible denaturation which results in decreasing β-sheets and increasing random coils while the content of α-helix is unaffected (Casal et al., 1988; Roels, Préaux, & Lontie, 1971). Cooling enhances the effect of alkaline denaturation (incubation at 4 °C, 3.3.2) (Casal et al., 1988; McKenzie & Sawyer, 1967). The changes in signal intensity were due to carboxylate groups in the side chains and reflect deprotonation with increasing pH value (Casal et al., 1988). This effect could also explain the observed slightly stronger difference over the whole amide I band in the pH 9 difference spectra, which is an indication of altered stability against alkaline denaturation in the labeled protein. This minor denaturation was also seen in the RP-HPLC chromatogram (Figure 3-6E), but it affected only a small proportion of the protein, so that the bonding should not be influenced. The additional peaks at shorter and longer retention times indicated the alkaline denaturation. But on the other hand this conformational change did not lead to a changed accessibility of the thiol group at Cys^{121} (Qin et al., 1998).

3.5.2.3 Dimerization of MTSSL under SDSL conditions

The hyperfine structure of the five-line spectrum could be resolved by simulation via the EasySpin software assuming a J-coupling >>100 (Figure 3-3A). It is caused by exchange interaction between two electrons within a biradical (Luckhurst, 1966; Slichter, 1955), which is produced by nitroxide dimer formation by disulfide bonding of two MTSSL monoradicals with elimination of methanesulfinic acid (Khramtsov et al., 1989; Weiner, 2012). This five-line biradical spectrum arises when the average exchange coupling is 10 times stronger than the hyperfine interaction (Berliner et al., 1982), whereas biradicals with short rigid linkers, such as polarized TOTAPOL, have a three line spectrum with a different degree of line broadening (Bordignon, 2007). The presence of biradicals (Figure 3-1D) and other dimers could also be confirmed by FT-ICR-MS (Figure 3-9) due to their mass-to-charge ratio in form of different MTSSL adducts and presented as the monomer to dimers ratio (Table 3-1). Regardless of the presence of protein, the higher the pH value, the more dimers were formed and the fewer MTSSL monomers were observed (Figure 3-3, Table 3-1). Thus, increasing pH values favors not only MTSSL-protein binding, but also the dimerization of MTSSL (Table 3-1), which leads to the loss of reactive labels and to a reduced labeling efficiency (Figure 3-2C, Table 3-1) confirming the observations by Bordignon (2007). In addition, the five-peak spectrum has a disturbing influence on the spectrum analysis. The integral intensity of the spectra remains unchanged by biradical formation, whereas the peak intensity is about 17-fold higher for the monoradical as for the corresponding biradical (Weiner, 2012), which influences the calculation of the rotation correlation time (Equation 5). Bordignon (2007) recommends not to exceed a concentration of more than 200 µmol/L MTSSL to avoid the formation of biradicals. This was confirmed for low pH values, but at pH values above 7, biradicals are also formed at a concentration of 100 µmol/L when dissolved in water. Furthermore, FT-ICR-MS was able to show that even at very low concentrations of less than 1 µmol, which were far below the concentrations detectable with EPR (here 6.6 µmol/L), biradicals were formed as a function of the pH value, although the dominance of biradicals over monomers was clearly recognizable at higher concentrations (Table 3-1, Figure 3-5E/F).

The different monomer and dimer adducts found during mass spectrometric analysis (Figure 3-12) were taken into account as it is known that nitroxides can form various adducts during electrospray ionization (ESI) (Smith, Bartley, Bottle, Micallef, & Reid, 2000). The formation of the even $[MH_2]^+$ ions in the ESI seems quite plausible (Metzger & Griep-Raming, 1999; Smith et al., 2000), since it is a diamagnetic substance, which would not be visible in the EPR, but here the predominant part of the MTSSL is present as monoradical monomer (Figure 3-4). A further biradical formation with the elimination of methane sulfinic acid as well as the reduction of biradicals to monoradical dimers $[MH_2]^+$ during ionization is unlikely, since in the applied positive mode a reduction of a radical by absorbing a proton is not expected (Smith

et al., 2000). Thus, it can be assumed that both reactions occur exclusively during the SDSL process. Control studies at or below the lower limit of detection (LLD) of the ESR at a pH value of 9, at which biradicals should be predominantly present (Table 3-1), clearly showed that in the EPR spectrum there is a significantly higher 3-line spectrum than a typical 5-line spectrum (Figure 3-10), which indicates the distinct presence of a monoradical. However, the presence of monoradical dimers can only be identified by the reduced $[MH_2]^{+\bullet}$ dimer using FT-ICR-MS. In contrast to diamagnetic substances, radicals must be used in higher concentrations in order to be detected in mass spectrometers (Smith et al., 2000). However, for the present FT-ICR-MS, these concentrations are still well below the LLD of the EPR.

All previous protocols recommend the removal of the excess free MTSSL by gel filtration or dialysis (Chen et al., 2007; Kirby et al., 2004; Margittai & Langen, 2004; Török et al., 2002) without further explanation. In order neither to influence the conformation of the protein nor to change the reaction mechanisms of the MTSSL, the removal of the unbound MTSSL was not performed in the present study. For comparison, the MTSSL excess in a sample at pH 7.5 was separated by way of example, so that no five-peak spectrum was detectable in the EPR spectrum. However, free dimers could still be measured with FT-ICR-MS in well detectable concentrations (data not shown). From this it can be deduced that apart from the concentration of MTSSL, the alkaline pH value >8 is the most important factor for the formation of biradicals. During the SDSL a neutral pH range should therefore be chosen, which supports the recommendations of Bordignon (2007).

3.5.2.4 Optimized conditions for SDSL of β-lg with MTSSL

Paramagnetic molecules are generally known as highly reactive compounds. A main difference between the paramagnetic MTSSL and the previously tested diamagnetic ligands was the high affinity of MTSSL to β-lg (Figure 3-2). However, a 4- to 10-fold molar excess with subsequent removal of the excess has also been used for MTSSL so far (Chen et al., 2007; Gu et al., 2016; Kirby et al., 2004; Török et al., 2002). In this study an equimolar ratio of MTSSL and β-lg has been found to be sufficient to label β-lg with MTSSL, regardless of the pH values tested (Figure 3-6). In this way high concentration can be avoided due to the high affinity of the MTSSL. Contrary to the previous studies with β-lg, in which labeling was carried out at pH 8.5 or higher in order to optimize the number of binding sites (Keppler et al., 2014; Wilde et al., 2016), the pH value should be reduced with regard to the labeling conditions for MTSSL in order to limit MTSSL dimerization (c.f. 4.2.3). In summary it can be stated that the optimal conditions for SDSL for β-lg were therefore identified with pH 7.5 at equimolar concentrations of MTSSL and β-lg.

3.5.3 Stability of the disulfide bond under the influence of heat and acids

A prerequisite for tracking aggregations or conformational changes with SDSL is a stable bonding between MTSSL and β-lg that also withstands high temperatures and low pH values during a prolonged time period. Therefore, samples were taken during incubation at 90 °C for five hours and analyzed with EPR and FT-ICR-MS. As expected, the heating at pH 2 and 7.5 led to partial denaturation aggregation of the β-lg as confirmed by the increasing τ_c of bound MTSSL (Figure 3-5A) that steadily increased for the acid samples, but at pH 7.5 a spontaneous maximum τ_c level was found after 10 min. This spontaneous maximum was associated with a sharp decline in the intensity of the midfield peak h_0 in the first 10 min (Figure 3-5C), which is an essential factor in the calculation of τ_c (Figure 3-5A, Equation 5) and could therefore be misleading when calculating the all over averaged τ_c.

The amount of biradicals from excess unbound MTSSL that were formed during labeling at pH 7.5 decreased significantly during subsequent acidification to pH 2, as can be observed from the EPR spectra (Figure 3-4) and the increase in peak intensity of h_0 reflecting the MTSSL monoradical concentration (Figure 3-4A vs Figure 3-4B). After heating, the five-line spectra of the MTSSL biradical also disappeared and only the three-line spectra of bound and free monomers remained (Figure 3-4), which, according to Weiner (2012), might indicate that the disulfide bond of the biradical was cleaved. However, this suggestion conflicts with the results of the FT-ICR-MS measurements. At pH 2 (Figure 3-5E) the monomers were essentially present as even $[MH_2]^+$ ions, the predominant amount of dimers was found in the odd form of a biradical dimer $[M]^{+\bullet}$ and a monoradical dimer $[MH_2]^{+\bullet}$. Although the amount of monomers $[MH_2]^+$ ions decreased during heat incubation and the dimers remained approximately constant (Figure 3-5), no biradicals are visible in the EPR spectrum (Figure 3-4). The strong decrease at pH 7.5 in the signal intensity of the midfield peak in the first 30 min (Figure 3-5C) with a subsequent increase could also be explained by the fact that biradical is reduced during heat incubation and predominantly the monoradical dimer $[MH_2]^{+\bullet}$ is formed. This would also become clear at pH value 2, where the proportion of dimers is significantly lower than that of monomers, but more monoradical dimers are formed by the effect of heat (Figure 3-5E). The formation is even more pronounced in purely aqueous solutions, where the EPR spectra clearly show no presence of biradicals, but the FT-ICR-MS shows an increasing abundance of monoradical dimer (Figure 3-4, Figure 3-12).

The higher abundance for the β-lg A/B-MTSSL adducts at pH 2 compared to pH 7.5 before incubation (Figure 3-5D) probably result from the improved ionization by the pH adjustment (Cañas, Piñeiro, Calvo, López-Ferrer, & Gallardo, 2007). Furthermore, MTSSL is in charge competition with the proteins so that ionization suppression effects may lead to a lower MTSSL abundance in the presence of β-lg. While the labeled β-lg was merely denatured at

pH 7.5 (Figure 3-5D, *squares*), the drastic reduction of the m/z intensities of β-lg A/B-MTSSL at acid pH values indicates the hydrolysis of β-lg into a multitude of peptides (Figure 3-5D, *circles*) (Akkermans et al., 2008), which is also confirmed by RP-HPLC measurements (Figure 3-11). However, the concentration of the paramagnetic MTSSL (Figure 3-5B-C) is only reduced to 60%.

At pH 7.5, the relative abundance of the β-lg-A/B-MTSSL adducts over the incubation time remained approximately the same, it might even be possible that a further binding with MTSSL monomer within the first 30 min, which is also accompanied by a strong reduction of the monomers (Figure 3-5F). However, there was no evidence of the release of previously bound MTSSL during the five hour heat exposure, since neither an increase in the MTSSL monomer (Figure 3-5F) nor a faster τ_c (Figure 3-5A) could be found. The increased dimer formation could also indicate that disulfide bonds within the dimer remains stable, which is contrary to the suggestion of Bordignon (2007) reporting a reversible linkage to the protein backbone for MTSSL. However, due to the significantly longer τ_c of the bound MTSSL compared to those of free MTSSL (Figure 3-5A) and the labeled β-lg (Figure 3-5D), it is clear that the majority of MTSSL are still bound to β-lg.

3.6 Conclusion

The concept of labeling β-lg with MTSSL has proven successful and can be used in thermal and acidic aggregation studies: 1) because MTSSL remains bound to the β-lg under the tested conditions; and 2) the non-covalent protein aggregation can be followed over time by a slower rotation correlation time. A pH value of 7.5 at equimolar concentrations of MTSSL and β-lg were identified as optimal conditions for SDSL of β-lg, although previous studies with β-lg recommend labeling at >pH 8.5 to optimize the number of binding sites of the β-lg. Although MTSSL dimerization can also occur at low pH values and over longer incubation times, the pH value for SDSL should be as low as possible to limit MTSSL dimerization. Based on the FT-ICR-MS results, we have concluded that biradicals were reduced to monoradical dimers $[MH_2]^{+\bullet}$ during the incubation period. Since the monoradical dimers $[MH_2]^{+\bullet}$ could not be distinguished from the monoradical monomers in the EPR spectra, it should be borne in mind that the τ_c calculated from Equation 5 always gives an average value over the τ_c of all MTSSL components, and should therefore be simulated individually for each components. As we could demonstrate, even with chromatographic separation of the excess of unbound MTSSL, monoradical dimers may still be present. For this reason, these monoradical dimers should be considered as an additional MTSSL components when simulating the line shape of MTSSL labeled protein aggregates as performed in our ongoing studies.

Acknowledgement

Authors would like to thank the German Research Foundation (DFG) for financial support of this work within the SPP 1934 priority program DiSPBiotech (project number 315456892).

3.7 Supplementary material for manuscript 1

Table 3-2: Main parameters of the FT-ICR-MS measurements; the method was optimized for small molecules (80-1000 m/z).

	Main parameters	Settings
Source	Capillary	4500 nA
	End Plate Offset	-500 nA
	Nebulizer	1bar
	Dry Gas	4 l/min
	Dry Temp.	200 °C
Source Optics	Capillary Exit	220 V
	Deflector Plate	200 V
Transfer Optics	Time of flight	1.5 ms
	Frequency	4 MHz
	RF Amplitude	350 Vpp
Quadrupole	Q1 Mass	150 m/z
	RF Frequency	2 MHz
Para Cell	Sweep Excitation Power	18%
	Accumulation time	0.5 s
	Size	4 M

Table 3-3: Considered MTSSL adducts for evaluation of FT-ICR-MS data

	Adducts	mass, m/z	e^- configuration	sum formula
Monomer adducts	$[M]^+$	264.07226	even	$C_{10}H_{18}N_1O_3S_2$
	$[MH]^{+\bullet}$	265.080087	odd	$C_{10}H_{19}N_1O_3S_2$
	$[MH_2]^+$	266.08791	even	$C_{10}H_{20}N_1O_3S_2$
	$[MH_3]^{+\bullet}$	267.095737	odd	$C_{10}H_{21}N_1O_3S_2$
	$[MH_4]^+$	268.103562	even	$C_{10}H_{22}N_1O_3S_3$
	$[MH_5]^{+\bullet}$	269.111387	odd	$C_{10}H_{23}N_1O_3S_3$
	$[MH_8]^+$	272.134862	even	$C_{10}H_{26}N_1O_3S_3$
	$[MHNa]^+$	288.0698	even	$C_{10}H_{19}N_1NaO_3S_2$
	$[MH_2Na]^{+\bullet}$	289.077682	odd	$C_{10}H_{20}N_1NaO_3S_2$
	$[MK]^{+\bullet}$	303.035969	odd	$C_{10}H_{18}N_1KO_3S_2$
	$[MHK]^+$	304.043794	even	$C_{10}H_{19}N_1KO_3S_2$
	$[MH_3K]^+$	306.05944	even	$C_{10}H_{21}N_1KO_3S_2$
Dimer adducts	$[M]^{+\bullet}$	370.1743	odd	$C_{18}H_{30}N_2O_2S_2$
	$[MH]^+$	371.1821	even	$C_{18}H_{31}N_2O_2S_2$
	$[MH_2]^{+\bullet}$	372.1899	odd	$C_{18}H_{32}N_2O_2S_2$
	$[MH_3]^+$	373.1978	even	$C_{18}H_{33}N_2O_2S_2$
	$[MNa]^+$	393.164031	even	$C_{18}H_{30}N_2NaO_2S_2$
	$[MHNa]^{+\bullet}$	394.171916	odd	$C_{18}H_{31}N_2NaO_2S_2$
	$[MK]^+$	409.138028	even	$C_{18}H_{30}N_2KO_2S_2$
	$[MHK]^{+\bullet}$	410.1458	odd	$C_{18}H_{31}N_2KO_2S_2$
	$[MH_2K]^+$	411.153679	even	$C_{18}H_{32}N_2KO_2S_2$

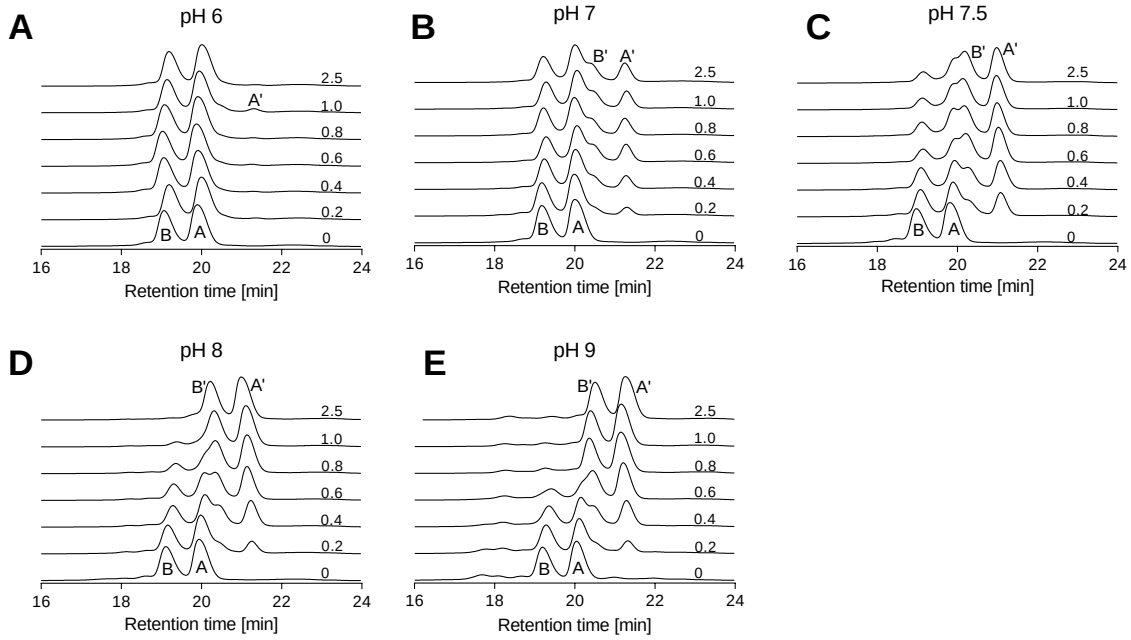

Figure 3-6: RP-HPLC chromatograms of native β-lactoglobulin labelled with MTSSL. Influence of the MTSSL: β-lg ratio (0-2.5 µM/µM) at different pH values after overnight incubation at 4°C. The absorbance was measured at 205 nm. The letters in the spectra designate: B – native β-lg B; A – native β-lg A; B' – modified β-lg B; A' – modified β-lg A.

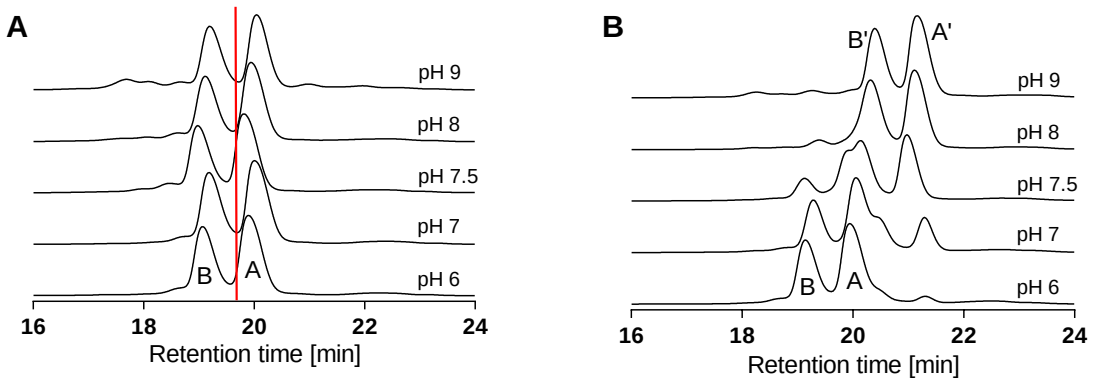

Figure 3-7: RP-HPLC chromatograms of native β-lactoglobulin (100 µmol/l) at increasing pH values (6, 7, 7.5, 8, 9) after overnight incubation at 4°C in the (A) absence and the (B) presence of MTSSL (100 µmol/l). The absorbance was measured at 205 nm. The letters in the spectra designate: B – native β-lg B; A – native β-lg A; B' – modified β-lg B; A' – modified β-lg A.

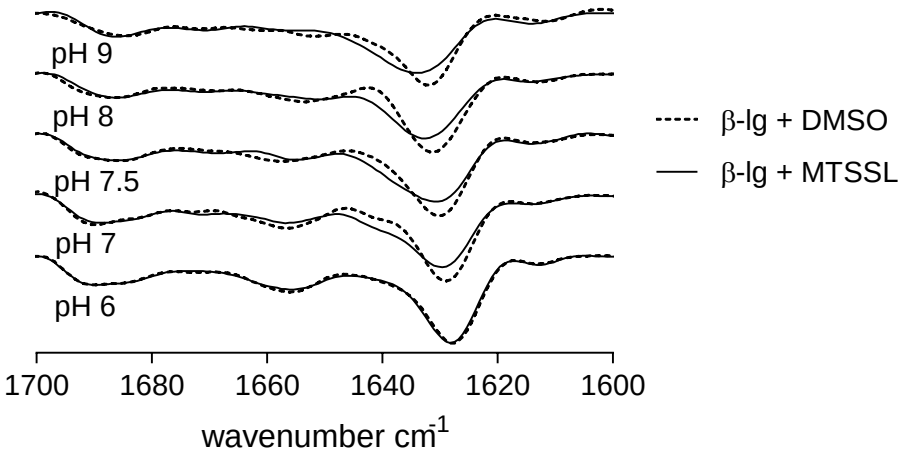

Figure 3-8: Second derivative of the ATR-FTIR spectra of native β-lactoglobulin (100 µmol/l) at increasing pH values (6, 7, 7.5, 8, 9). SDSL was performed during night incubation at 4°C with 100 µmol/l MTSSL pre-dissolved in DMSO (solid line). As control only the corresponding amount of DMSO without MTSSL was added to β-lactoglobulin (dotted line).

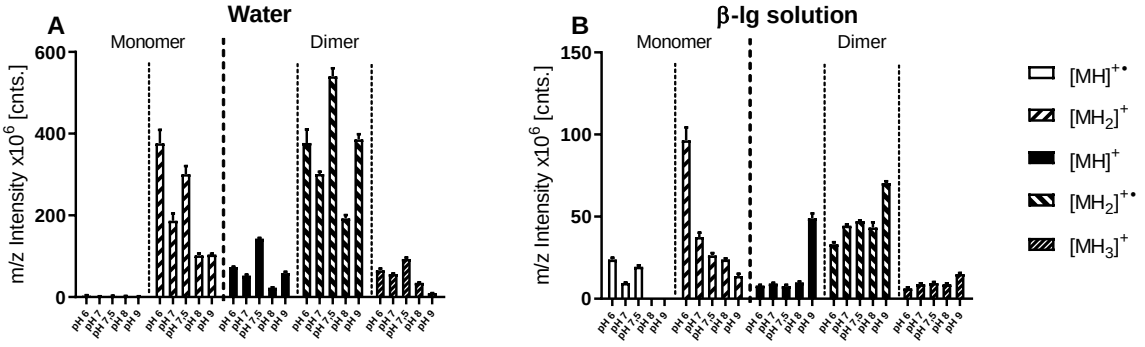

Figure 3-9**:** Relative abundance of MTSSL monomer and dimer adducts in β-lg solution (B) and pH-adjusted water (A) at pH 6, 7, 7.5, 8 and 9. Samples were incubated overnight at 4° C. Masses and sum formulas are listed in Table 3-3.

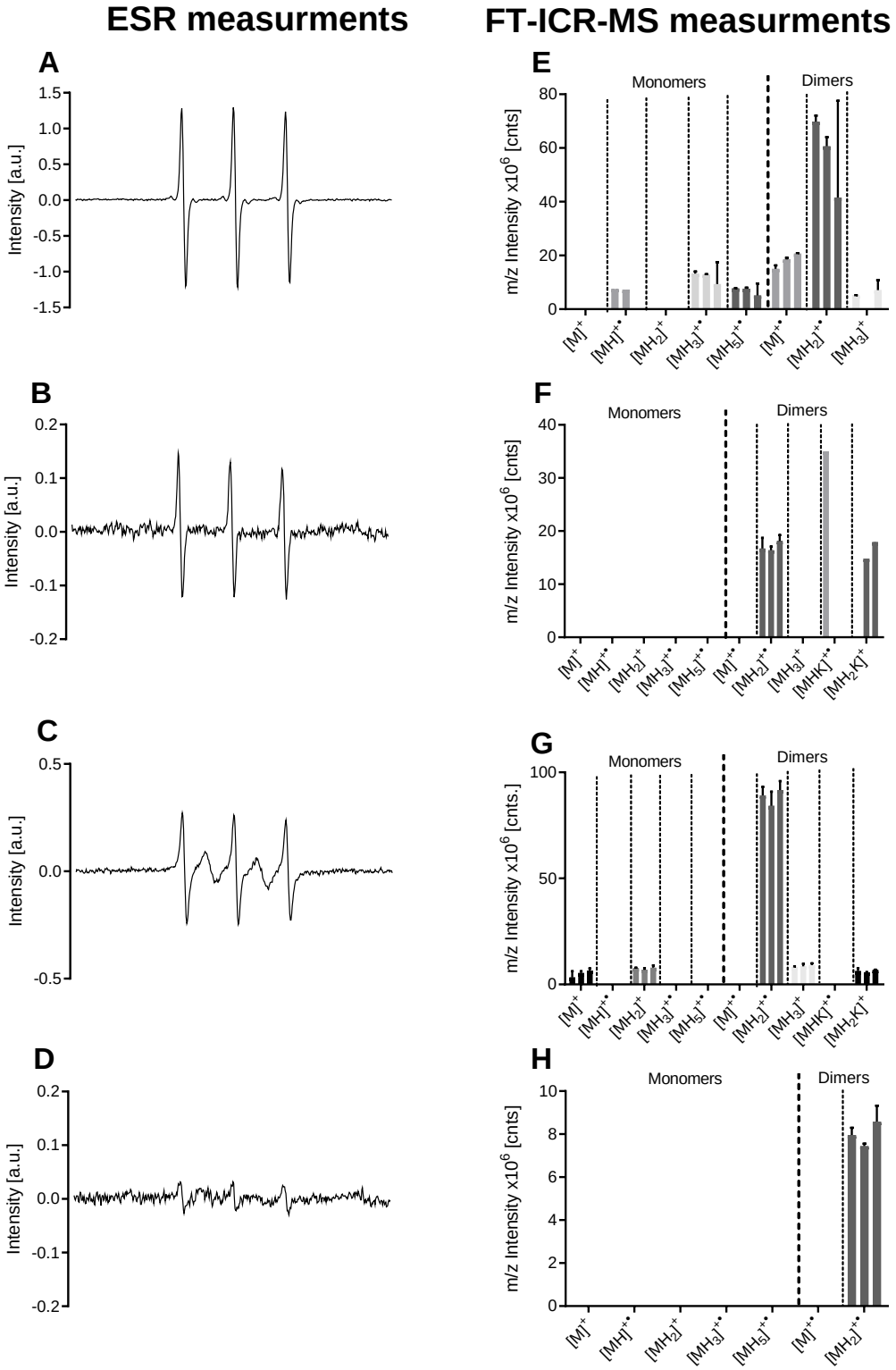

Figure 3-10: EPR spectra (a-d) of MTSSL at the LLD of the EPR (6 µmol/l) (A, C) and in 10-fold dilution (0.6 µmol/l) in aqueous solution at pH 6 (A, B) and pH 9 (C, D). The 3-line spectra show paramagnetic monoradicals and possibly the monoradical dimer, the superimposed 5-line spectrum shows biradicals. Relative abundance (E-H) of MTSSL monomer and dimer adducts with a concentration of 6 µmol/l (E, G) and 0.6 µmol/l (F, H) MTSSL in aqueous solution at pH 6 (E, F) and pH 9 (G, H). The listed adducts result from three measurements of three individual samples each. Masses and sum formulas are listed in Table 3-3.

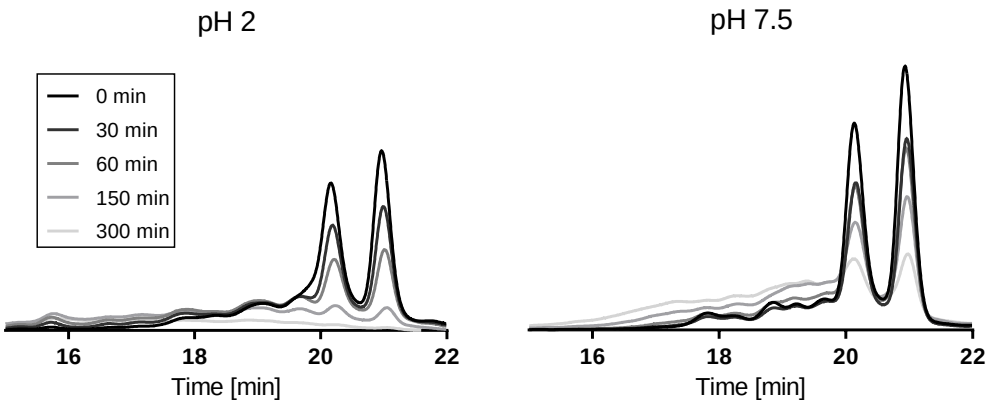

Figure 3-11: RP-HPLC spectra of heated β-lactoglobulin labelled with equimolar MTSSL (at pH 7.5 and incubated at 4°C overnight). The pH was adjusted to 2 and 7.5 after incubation before heat treatment was performed at 90°C for five hours. Samples were taken after 30 min, 60 min, 150 min and 300 min.

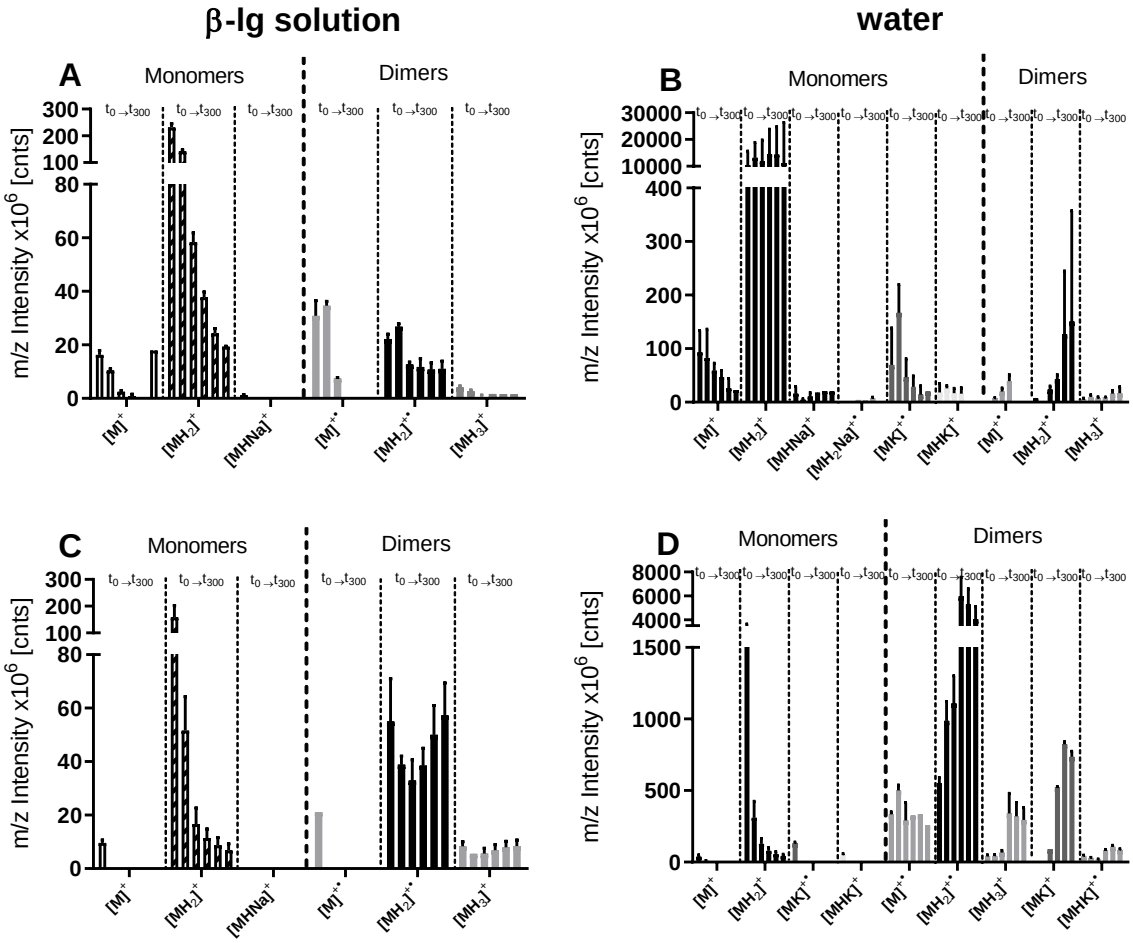

Figure 3-12**:** Relative abundance of MTSSL monomer and dimer adducts in β-lg solution (A and C) and in pH-adjusted water (B and D) at pH 2 (A and B) and pH 7.5 (C and D). The samples were heated for five hours at 90°C. Six time points (t_0-t_{300}) were plotted for each adduct: before heating (t_0), after 10, 30, 60, 150 and 300 min (t_{300}). For masses and molecular formula see Table 3-3. Masses and sum formulas are listed in Table 3-3.

3.8 References

Akkermans, C., Venema, P., van der Goot, A. J., Gruppen, H., Bakx, E. J., Boom, R. M., & van der Linden, E. (2008). Peptides are building blocks of heat-induced fibrillar protein aggregates of beta-lactoglobulin formed at pH 2. *Biomacromolecules*, *9*(5), 1474–1479. https://doi.org/10.1021/bm70|14224

Berliner, L. J., Grunwald, J., Hankovszky, H.O., & Hideg, K. (1982). A novel reversible thiol-specific spin label: Papain active site labeling and inhibition. *Analytical Biochemistry*, *119*(2), 450–455. https://doi.org/10.1016/0003-2697(82)90612-1

Bordignon, E. (2007). EPR Spectroscopy of Nitroxide Spin Probes. *EMagRes*. (6), 235–254. https://doi.org/10.1002/9780470034590.emrstm1513

Cañas, B., Piñeiro, C., Calvo, E., López-Ferrer, D., & Gallardo, J. M. (2007). Trends in sample preparation for classical and second generation proteomics. *Journal of Chromatography a*, *1153*(1-2), 235–258. https://doi.org/10.1016/j.chroma.2007.01.045

Casal, H. L., Köhler, U., & Mantsch, H. H. (1988). Structural and conformational changes of β-lactoglobulin B: An infrared spectroscopic study of the effect of pH and temperature. *Biochimica et Biophysica Acta (BBA) - Protein Structure and Molecular Enzymology*, *957*(1), 11–20. https://doi.org/10.1016/0167-4838(88)90152-5

Chen, M., Margittai, M., Chen, J., & Langen, R. (2007). Investigation of alpha-synuclein fibril structure by site-directed spin labeling. *The Journal of Biological Chemistry*, *282*(34), 24970–24979. https://doi.org/10.1074/jbc.M700368200

Drescher, M. (2012). Elektronenspinresonanz-Spektroskopie: Struktur und Dynamik intrinsisch ungeordneter Proteine. *Chemie in unserer Zeit*. (46), 150–157.

Dunnill, P., & Green, D. W. (1966). Sulphydryl groups and the N⇄R conformational change in β-lactoglobulin. *Journal of Molecular Biology*, *15*(1), 147–151. https://doi.org/10.1016/S0022-2836(66)80216-4

Ellman, G. L. (1959). Tissue Sulfhydryl Groups. *Archnieves of Biochemistry and Biophysics*, *82*, 70–77.

Fang, & Dalgleish (1997). Conformation of beta-Lactoglobulin Studied by FTIR: Effect of pH, Temperature, and Adsorption to the Oil-Water Interface. *Journal of Colloid and Interface Science*, *196*(2), 292–298. https://doi.org/10.1006/jcis.1997.5191

Fogliano, V., Monti, S. M., Visconti, A., Randazzo, G., Facchiano, A. M., Colonna, G., & Ritieni, A. (1998). Identification of a β-lactoglobulin lactosylation site. *Biochimica et Biophysica Acta (BBA) - Protein Structure and Molecular Enzymology*, *1388*(2), 295–304. https://doi.org/10.1016/S0167-4838(98)00177-0

Gu, L., Tran, J., Jiang, L., & Guo, Z. (2016). A new structural model of Alzheimer's Aβ42 fibrils based on electron paramagnetic resonance data and Rosetta modeling. *Journal of Structural Biology*, *194*(1), 61–67. https://doi.org/10.1016/j.jsb.2016.01.013

Hettiarachchi, C. A., Melton, L. D., Gerrard, J. A., & Loveday, S. M. (2012). Formation of β-lactoglobulin nanofibrils by microwave heating gives a peptide composition different from conventional heating. *Biomacromolecules*, *13*(9), 2868–2880. https://doi.org/10.1021/bm300896r

Hubbell, W. L., Gross, A., Langen, R., & Lietzow, M. A. (1998). Recent advances in site-directed spin labeling of proteins. *Current Opinion in Structural Biology*, *8*(5), 649–656. https://doi.org/10.1016/S0959-440X(98)80158-9

Kavanagh, G. M., Clark, A. H., & Ross-Murphy, S. B. (2000). Heat-induced gelation of globular proteins: Part 3. Molecular studies on low pH β-lactoglobulin gels. *International Journal of Biological Macromolecules*, *28*(1), 41–50. https://doi.org/10.1016/S0141-8130(00)00144-6

Keith, A., Bulfield, G., & Snipes, W. (1970). Spin-Labeled Neurospora Mitochondria. *Biophysical Journal*, *10*(7), 618–629. https://doi.org/10.1016/S0006-3495(70)86324-X

Keppler, J. K., Koudelka, T., Palani, K., Stuhldreier, M. C., Temps, F., Tholey, A., & Schwarz, K. (2014). Characterization of the covalent binding of allyl isothiocyanate to β-lactoglobulin by fluorescence quenching, equilibrium measurement, and mass spectrometry. *Journal of Biomolecular Structure & Dynamics*, *32*(7), 1103–1117. https://doi.org/10.1080/07391102.2013.809605

Keppler, J. K., Martin, D., Garamus, V. M., Berton-Carabin, C., Nipoti, E., Coenye, T., & Schwarz, K. (2017). Functionality of whey proteins covalently modified by allyl isothiocyanate. Part 1 physicochemical and antibacterial properties of native and modified whey proteins at pH 2 to 7. *Food Hydrocolloids*, *65*, 130–143. https://doi.org/10.1016/j.foodhyd.2016.11.016

Khramtsov, V. V., Yelinova, V. I., Weiner, L. M., Berezina, T. A., Martin, V. V., & Volodarsky, L. B. (1989). Quantitative determination of SH groups in low- and high-molecular-weight compounds by an electron spin resonance method. *Analytical Biochemistry*, *182*(1), 58–63. https://doi.org/10.1016/0003-2697(89)90718-5

Kirby, T. L., Karim, C. B., & Thomas, D. D. (2004). Electron paramagnetic resonance reveals a large-scale conformational change in the cytoplasmic domain of phospholamban upon binding to the sarcoplasmic reticulum Ca-ATPase. *Biochemistry*, *43*(19), 5842–5852. https://doi.org/10.1021/bi035749b

Levine, R. L. (1977). Fluorescence-quenching studies of the binding of bilirubin to albumin. *Clinical Chemistry*, *23*(12), 2292–2301.

Luckhurst, G. R. (1966). Alternating linewidths. A novel relaxation process in the electron resonance of biradicals. *Molecular Physics*, *10*(6), 543–550. https://doi.org/10.1080/00268976600101481

Margittai, M., & Langen, R. (2004). Template-assisted filament growth by parallel stacking of tau. *Proceedings of the National Academy of Sciences of the United States of America*, *101*(28), 10278–10283. https://doi.org/10.1073/pnas.0401911101

Markham, G. D., Myers, C. B., Harris, K. A., Volin, M., & Jaffe, E. K. (1993). Spatial proximity and sequence localization of the reactive sulfhydryls of porphobilinogen synthase. *Protein Science*, *2*(1), 71–79. https://doi.org/10.1002/pro.5560020107

McKenzie, H. A., & Sawyer, W. H. (1967). Effect of pH on β-Lactoglobulins. *Nature*, *214*(5093), 1101–1104. https://doi.org/10.1038/2141101a0

Metzger, J., & Griep-Raming, J. (1999). Electrospray ionization and atmospheric pressure ionization mass spectrometry of stable organic radicals. *European Journal of Mass Spectrometry*, *5*(1), 157. https://doi.org/10.1255/ejms.263

Qin, B. Y., Bewley, M. C., Creamer, L. K., Baker, H. M., Baker, E. N., & Jameson, G. B. (1998). Structural basis of the Tanford transition of bovine beta-lactoglobulin. *Biochemistry*, *37*(40), 14014–14023. https://doi.org/10.1021/bi981016t

Rade-Kukic, K., Schmitt, C., & Rawel, H. M. (2011). Formation of conjugates between β-lactoglobulin and allyl isothiocyanate: Effect on protein heat aggregation, foaming and emulsifying properties. *Food Hydrocolloids*, *25*(4), 694–706. https://doi.org/10.1016/j.foodhyd.2010.08.018

Roels, H., Préaux, G., & Lontie, R. (1971). Polarimetric and chromatographic investigation of the irreversible transformation of β-lactoglobulin A and B upon alkaline denaturation. *Biochimie*, *53*(10), 1085–1093. https://doi.org/10.1016/S0300-9084(71)80197-9

Schmidt, M. J., Fedoseev, A., Bücker, D., Borbas, J., Peter, C., Drescher, M., & Summerer, D. (2015). EPR Distance Measurements in Native Proteins with Genetically Encoded Spin Labels. *ACS Chemical Biology*, *10*(12), 2764–2771. https://doi.org/10.1021/acschembio.5b00512

Schreier, S., Polnaszek, C. F., & Smith, I. C.P. (1978). Spin labels in membranes problems in practice. *Biochimica et Biophysica Acta - Reviews on Biomembranes*, *515*(4), 395–436. https://doi.org/10.1016/0304-4157(78)90011-4

Sepkhanova, I., Drescher, M., Meeuwenoord, N. J., Limpens, R. W. A. L., Koning, R. I., Filippov, D. V., & Huber, M. (2009). Monitoring Alzheimer Amyloid Peptide Aggregation by EPR. *Applied Magnetic Resonance*, *36*(2-4), 209–222. https://doi.org/10.1007/s00723-009-0019-1

Slichter, C. P. (1955). Spin Resonance of Impurity Atoms in Silicon. *Physical Review*, *99*(2), 479–480. https://doi.org/10.1103/PhysRev.99.479

Smith, C. D., Bartley, J. P., Bottle, S. E., Micallef, A. S., & Reid, D. A. (2000). Electrospray ionization mass spectrometry of stable nitroxide free radicals and two isoindoline nitroxide dimers. *Journal of Mass Spectrometry*, *35*(5), 607–611. https://doi.org/10.1002/(SICI)1096-9888(200005)35:5<607::AID-JMS967>3.0.CO;2-7

Stoll, S., & Schweiger, A. (2006). EasySpin, a comprehensive software package for spectral simulation and analysis in EPR. *Journal of Magnetic Resonance*, *178*(1), 42–55. https://doi.org/10.1016/j.jmr.2005.08.013

Tanford, C., Bunville, L. G., & Nozaki, Y. (1959). The Reversible Transformation of β-Lactoglobulin at pH 7.5 1. *Journal of the American Chemical Society*, *81*(15), 4032–4036. https://doi.org/10.1021/ja01524a054

Török, M., Milton, S., Kayed, R., Wu, P., McIntire, T., Glabe, C. G., & Langen, R. (2002). Structural and dynamic features of Alzheimer's Abeta peptide in amyloid fibrils studied by site-directed spin labeling. *The Journal of Biological Chemistry*, *277*(43), 40810–40815. https://doi.org/10.1074/jbc.M205659200

Weiner, L. (2012). Quantitative Determination of Thiol Status of Proteins and Cells by Nitroxyl Biradical RS-SR. In A. Kokorin (Ed.), *Nitroxides - Theory, Experiment and Applications* (pp. 369–384). InTech. https://doi.org/10.5772/45620

4 Paper 2: Amyloid aggregation of spin-labeled β-lactoglobulin Part I

Influence of spin labeling on amyloid aggregation

Jacqueline Lux[a], Timon R. Heyn[a], Ingo Kampen[b], Karin Schwarz[a], Julia K. Keppler[a,c], Anja Steffen-Heins[a]

[a]Institute of Human Nutrition and Food Science, Food Technology, Kiel University, Germany

[b]Institute for Particle Technology, Technical University Braunschweig, Germany

[c]Food Process Engineering, Wageningen University, P.O. Box 17, 6700 AA, Wageningen, The Netherlands

Published in Food Hydrocolloids (2021), 112, doi: 10.1016/j.foodhyd.2020.106178

Received 28 February 2020, Accepted: 15 July 2020, Available online: 21 July 2020

4.1 Abstract

Site-directed spin labeling (SDSL) of the natural food protein β lactoglobulin (β-lg) was established with the aim of characterizing amyloid aggregation while explicitly avoiding the usual manipulation of primary protein structure. For its successful application, spin labels must not alter secondary protein structure or the formation of β-lg amyloid aggregates. The two spin labels—the MTSSL (flexible S-S binding) and Iodoacetamido-proxyl spin label (IPSL) (more rigid C-S binding)—were used for amyloid aggregation at pH 2 and pH 3.5. At pH 3.5, IPSL caused minor changes in the secondary protein structure, where it reduced intra- and intermolecular β-sheets as determined by ATR-FTIR. Analysis of the extent of amyloid aggregation using thioflavin T fluorescence indicated that the spin probes interfered with the binding of the fluorescent probes to the β sheets. Non-amyloid and amyloid fractions were obtained from the amyloid aggregated system by ultrafiltration (300 kDa), which also proved to be equivalent and independent of the spin labeling process. Atomic force microscopy and size-exclusion chromatography results suggest the same building blocks and morphologies between unlabeled and spin-labeled proteins; therefore, substantial changes in the behavior of β-lg during amyloid aggregation can be excluded. Ultimately, 10-17% of the β-lg molecules were labeled so that the SDSL approach can be used to label the natural food protein at these low concentrations without affecting protein conformation or the formation of amyloid aggregates, which may subsequently provide deep insights into the aggregation mechanism of food proteins under processing conditions.

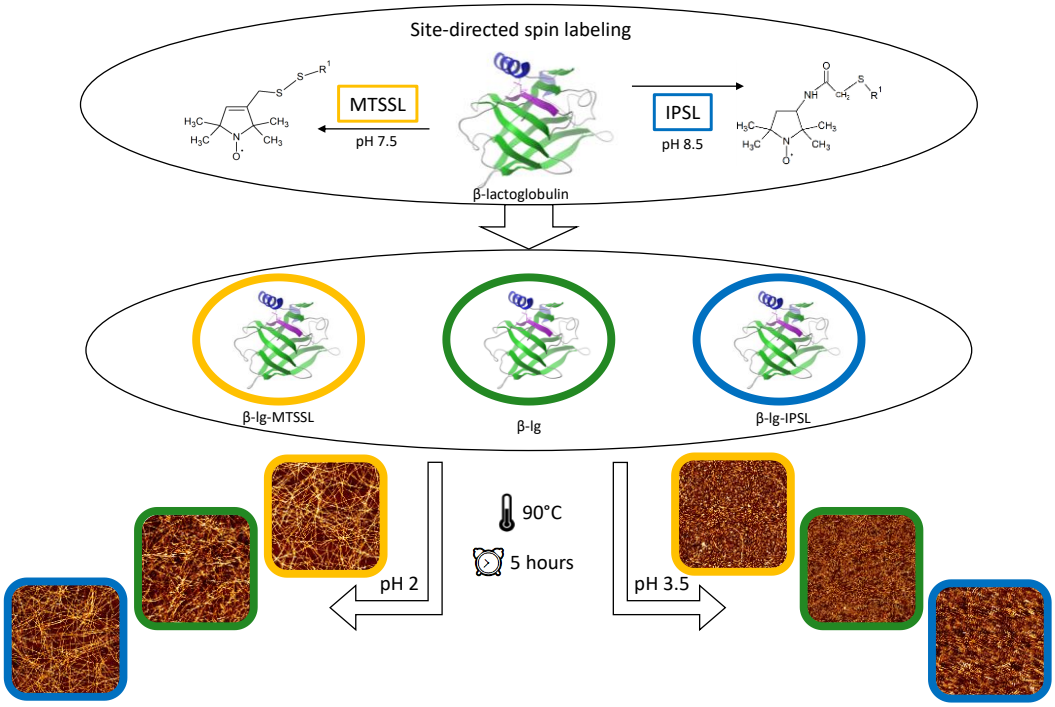

Figure 4-1: Graphical abstract for paper 2

4.2 Introduction

Site-directed spin labeling (SDSL) in combination with electron paramagnetic resonance (EPR) spectroscopy is a common approach in structural biology (Bordignon, 2018). However, this method has never been used in food analysis to date. Important structural information on the protein backbone—such as conformational and dynamic changes during aggregation, accessibility, and the distance of two labels (Klare, 2012)—can be extracted from the mobility parameters of the EPR spectra on the spin-labeled side chains of a protein. To obtain information regarding the protein backbone, a free thiol group within the protein sequence is required to covalently bind a spin label to the protein, if possible, without changing the secondary protein structure. Buried sites are generally not easy to label due to the high probability of interfering with the protein's conformation or folding (Bordignon, 2018). SDSL has previously been used to characterize amyloid aggregates from different proteins, such as α-synuclein (Der-Sarkissian, Jao, Chen, & Langen, 2003), β-amyloid peptide (Gu, Tran, Jiang, & Guo, 2016; Iuraşcu et al., 2009; Török et al., 2002) or pancreatic polypeptide (IAPP) (Jayasinghe & Langen, 2004), without negatively altering the amyloid aggregation. To label these proteins and peptides, their primary structure is typically manipulated by the targeted inclusion of an artificial cysteine residue at a desired position in the amino acid sequence in order to attach the spin label in a site-specific manner (Gu et al., 2016; Sepkhanova et al., 2009; Török et al., 2002). Since the position of the label cannot be predicted in the presence of several cysteine residues, the labeling of these proteins is unusual for SDSL and typically results in additional or unnecessary cysteine residues being removed (Kirby, Karim, & Thomas, 2004; Margittai & Langen, 2004). Such interventions subsequently alter the secondary and tertiary structures of a protein, so that the aggregation behavior differs from that of the natural protein.

Additionally, the label may also interfere with noncovalent protein aggregation as a function of molecular size and the binding site of the label (Dave, Loveday, Anema, Jameson, & Singh, 2014; Di Zhao et al., 2018). The methanethiosulfonate spin label (MTSSL) and Iodoacetamido-proxyl spin label (IPSL) are the most commonly used labels for SDSL in protein aggregation studies. These labels differ in the size, hydrophobicity, binding site, and flexibility of the linked label. MTSSL has a high degree of flexibility due to the five rotatable bonds linking it to the protein (Bordignon 2018) and a smaller molecular weight (MW_{MTSSL} = 264.38 Da) compared to IPSL (MW_{IPSL} = 325.17 Da). Due to its flexibility, MTSSL is able to bind to most thiol groups via a heat-sensitive disulfide bridge without affecting the functionality and native state of the protein (Klare 2012). IPSL forms a C-S bond toward the protein that is not affected by heating (Klare 2012). However, at pH values higher than 8, IPSL can additionally bind to amino groups via C-N bonds that are sensitive to hydrolysis.

Compared to MTSSL, IPSL has a lower selectivity to cysteine, while its lower flexibility may destabilize the protein or alter its conformation. In the case of the whey protein β-lactoglobulin (β-lg), five cysteine residues are naturally present—four of which are linked via two disulfide bridges, with one being free.

Functional amyloid aggregates from β-lg can be formed at high temperatures (70–90°C) and low ionic strength over a period of several hours (Akkermans et al., 2008; Loveday, Wang, Rao, Anema, & Singh, 2012). Notably, amyloid aggregation is a function of many determinants, e.g., the pH value determines the morphologies and building blocks of the aggregates (Keppler, Heyn, Meissner, Schrader, & Schwarz, 2019). During a 5-hour incubation at 90°C, acid hydrolysis cleaves the protein into peptides at pH 2, resulting in the β-sheet-rich peptides sticking together to form long semi-flexible aggregates called fibrils. Under these conditions, the amyloid conversion rate was approximately 30–40% (Heyn et al., 2019; Keppler et al., 2019). In contrast, with the same time and heat treatment at pH 3.5, acid hydrolysis is significantly reduced (Keppler et al., 2019), so that 30–50% worm-like aggregates are formed that consist of the entire protein (Heyn et al., 2019; Keppler et al., 2019). Ultrafiltration techniques (MWCO=300 kDa) were used to determine the conversion rates of amyloid aggregation and also to fractionate the mixed amyloid aggregate systems (AAS). At pH 2, this separation yields in the retentate as the amyloid fraction (AF) containing the long semi-flexible aggregates, and in the permeate as the non-amyloid fraction (n-AF) that most likely consists of non-amyloid aggregates and peptides smaller than the molecular weight cut-off of the UF-membrane (Akkermans et al., 2008; Heyn et al., 2019). This also applies to pH 3.5, but the retentate or amyloid-like fraction (ALF) contains the worm-like aggregates while the permeate is referred to as the non-amyloid-like fraction (n-ALF).

The present study aims to evaluate whether the application of SDSL to natural β-lg is possible without manipulating the primary protein structure. Part I investigates whether a change in the behavior of β-lg during amyloid aggregation can be ruled out, which might possibly result from spin labeling with MTSSL and IPSL at pH 2 and 3.5, respectively. For this reason, ATR-FTIR, intrinsic tryptophan fluorescence, size-exclusion chromatography, and atomic force microscopy were used to study potential changes in hydrophobicity, building blocks, and aggregate morphology caused by SDSL. The extent of amyloid aggregation is monitored by thioflavin T fluorescence, and the non-amyloid and AF are recovered by membrane filtration at a cut-off of 300 kDa. Part II will continue to focus on electron paramagnetic resonance spectroscopy (EPR) and the deconvolution of spectra by the EasySpin tool to determine the exact binding sites of the spin labels at the peptide/protein sequence as well as the incorporation of the labeled protein side chains into the amyloid or non-AF. With this comprehensive characterization of SDSL for β-lg, it will be

possible to gain deep insights into the aggregation mechanism of food proteins under processing conditions.

4.3 Material and methods

4.3.1 Materials

β Lactoglobulin (β lg) was purchased from Davisco Foods International (Eden Prairie, Minnesota, USA) with 97% protein and 96% β-lg in dry matter. The calculated NaCl content was 0.29%. MTSSL (1-oxyl-2,2,5,5-tetramehtylpyrroline-3-methyl) methanethiosulfonate was obtained from Enzo Life Science Inc. (Farmingdale, NY, USA) with a purity of ≥98%. IPSL 3-(2-Iodoacetamido)-PROXYL was purchased from Sigma-Aldrich (St. Louis, USA).

4.3.2 Sample preparation

4.3.2.1 Site-directed spin labeling of β lactoglobulin

β-lg was dissolved in milli-Q water and stirred until complete hydration to a final protein concentration of 5 wt%. For MTSSL, the pH value was adjusted to 7.5 with sodium hydroxide (NaOH), while for IPSL it was adjusted to 8.5, corresponding to their individual labelling optima. The spin labels were then pre-dissolved in DMSO. To prepare a labeled β-lg stock solution, an equimolar ratio of MTSSL (R1) or a 2.5 molar excess of IPSL (R2) in the same amount of DMSO was added and incubated overnight at 4 °C in the dark. As a control, the protein solution was also adjusted to pH 7.5, incubated overnight and treated as the other samples. In the labeled β-lg stock solution ~85% of the protein was labeled with MTSSL and ~50% with IPSL, respectively, which was confirmed by measurements of the free thiol groups. To avoid spin-spin interactions, spin dilution was performed, i.e., the spin-labeled stock solutions were diluted 1:5 with unlabeled, pH-adjusted β-lg solutions. For the further results, the β-lg was labeled with approx. ~17% MTSSL and 10% IPSL, respectively. The unbound spin label was removed by desalting (Sephadex G-25, PD-10 Desalting Column, GE Healthcare, Solingen, Germany). The removal step included a dissolving step with an estimated protein concentration of 2.5%. The exact protein concentration was measured as described in Section 2.3. All samples were prepared in triplicate.

4.3.2.2 Preparation of β-lactoglobulin amyloid aggregates

For fibril formation, the spin-labeled β-lg solution with MTSSL or IPSL—as well as the control sample without a spin label—were adjusted to pH 2 or 3.5, respectively, with hydrochloric acid (HCl). All samples were heated at 90 °C in a water bath for 5 hours and stirred at 350 rpm (2mag AG, Munich, Germany). Samples were taken at different time points: before heating (UH) and after 5 hours (AAS/ALAS).

4.3.2.3 Separation of β lactoglobulin fractions

To separate the amyloid aggregates from the unconverted peptides, the heated samples (AAS/ALAS) were diluted 5-fold (t_{5R}) and filtered with ultrafiltration centrifugal concentrators (Vivaspin 20, 300 kDa, PES, Sartorius, Göttingen, Germany). After washing the concentrators with pH-adjusted water, 10 ml of the diluted sample was centrifuged for 15 min at 1000*g. After refilling the concentrators with pH-adjusted water to the initial weight and resolving the protein (which sticks on the membrane), the procedure was repeated three times. After each filtering step, the filtrate was collected separately, weighed, and the dilution was calculated (F_1–F_4). After the last filtering step, F_1–F_4 were put together as a non-amyloid fraction (n-AF) at pH 2 or non-amyloid-like fraction (n-ALF) at pH 3.5, while the retentate was refilled with pH-adjusted water to the initial volume and further used as AF at pH 2 or ALF at pH 3.5. The n-AF/n-ALF contains mainly small aggregates (<300 kDa), peptides, and unhydrolyzed proteins, whereas the AF/ALF mainly contains aggregates >300 kDa.

4.3.3 ATR-Fourier transformation infrared spectroscopy

ATR-FTIR measurements were performed using a Confocheck^{TM} Tensor 2 spectrometer (Bruker Optics, Ettlingen, Germany) optimized for the analysis of proteins in liquid samples and equipped with a temperature-controlled Attenuated Total Reflection (BIOATR II) crystal. Then, 20 µl of each sample was dried on the crystal at 40°C and subsequently measured. Thereafter, 120 scans with a resolution of 0.7 cm^{-1} were recorded and averaged to generate the spectra from 4000 cm^{-1} to 900 cm^{-1}. Atmospheric correction was performed, which subtracted the absorption of CO_2 and H_2O. Thereafter, the spectra were vector normalized and the amide 1 band (1590 to 1700 cm^{-1}) was excised. The second derivation was performed with nine smoothing points. For the statistical analysis, the minima of the peaks were compared.

4.3.4 Intrinsic tryptophan fluorescence

To measure intrinsic tryptophan fluorescence (ITF), the samples were diluted to a protein concentration of 0.01% and measured in a fluorescence spectrometer (Cary Eclipse, Varian GmbH Darmstadt, Germany) with extinction at the 294 nm wavelength using a quartz cell with four polished sides (Heyn et al., 2019). An emission scan between 300 nm and 500 nm was then taken to follow blue/red and intensity shifts.

4.3.5 Size-exclusion chromatography

Size-exclusion experiments were performed following (Akkermans et al., 2008). Briefly, samples with a protein concentration of ~2.5% were diluted to 0.4% with DGT-buffer (100 mM dithiothreitol and 8 M guanidine hydrochloride in 0.15 M Tris-HCl buffer, pH 8) and shaken for 1 hour at 140 rpm. After shaking, 0.43% 0.15 M Tris-HCl-buffer, pH 8, was added

and the samples were filtered through a 0.20 µm syringe filter (regenerated cellulose, Macherey-Nagel, Düren, Germany). Measurements were performed using an Agilent 1100 Series HPLC with a diode-array detector and size-exclusion chromatography (SEC) column (Superdex^{TM} 200 Increase 10/300 GL, GE Healthcare, Bio-Science AB, Uppsala, Sweden). For the analytical separation, the injection volume was 50 µl, the flow rate 0.3 ml/min and the stop time was 100 min, using 100% 0.15 M Tris-HCl buffer, pH 8, as eluent. The detection wavelength was 215 nm. For samples with lower concentrations, the same ratio of protein and DGT buffer were used as for the higher concentration to ensure complete reduction. Hence, the concentrations are not comparable. For calibration, the Gel Filtration Calibration Kit LMW from GE Healthcare (Solingen, Germany) with a range of 6,500–75,000 da was used.

4.3.6 Atomic force microscopy

Fibril morphology was investigated using atomic force microscopy (NanoWizard 3 BioAFM, JPK Instruments AG, Berlin, Deutschland) using the tapping mode according to Serfert et al. (2014).

4.3.7 Thioflavin-T fluorescent assay

The thioflavin T (ThT) assay was applied to follow fibril formation. ThT binds to β-sheet rich regions in proteins. Since fibrils contain stacked β-sheets, ThT is a useful tool to follow fibril formation (Akkermans et al., 2008). A β-sheet aggregate requires at least five strands to be longer than a molecule of ThT so that ThT can bind and a fluorescence signal can be detected (Krebs, Bromley, & Donald, 2005). The analysis was performed according to Akkermans et al., (2008), Loveday et al., (2012), and Serfert et al., (2014). Briefly, the samples were diluted to a protein concentration of 1%. Then, 48 µl of the diluted sample was mixed with 4 ml ThT solution and measured after a one-minute incubation using a fluorescence spectrometer (Cary Eclipse, Varian GmbH Darmstadt, Germany) with excitation and emission wavelengths set to 440 nm and 482 nm, respectively. In the separation step, the protein concentration was taken undiluted (~0.5%); therefore, these results are not comparable to the fibril formation measurements.

4.3.8 Protein concentration measurement and conversion rate determination

To measure protein concentration, the samples were diluted 20-fold (UH and AAS/ALAS) or 4-fold (R) with pH-adjusted water. The dilution for the filtrate was calculated separately for each replicate. The samples were measured at 278 nm using a UV-Vis spectrometer (Helios Gamma, UV-Vis, Thermo Spectronic, Cambridge, UK) in a quartz cell. Protein concentrations were calculated with calibration functions based on native β-lg, according to DIN 32645 in a range of 0-0.25% β-lg for pH 2 (detection limit = 0.003%, determination

limit = 0.008%, R^2 = 0.9998) and pH 3.5 detection limit = 0.003%, determination limit = 0.010%, R^2 = 0.9998), respectively. The yield was defined as the protein remaining in the retentate (R) after ultrafiltration.

4.3.9 Statistical analysis

All results were presented as means and standard deviations of the replicated analyses. The data were analyzed by two-way ANOVA with Tukey's multiple comparison test at a significance level of α=0.05. All statistics and figures were created using GraphPad Prism (version 6.07, GraphPad Software, San Diego, CA, USA).

4.4 Results

Prior to the amyloid aggregation of β-lg, we demonstrated the successful binding of one molecule MTSSL (Figure 4-7A) or of one molecule IPSL (Figure 4-7B) to only one molecule β-lg, verified by mass spectroscopy. The analysis of the free thiol groups (Figure 4-8) showed a substantially higher affinity constant (K_α) of 2.25 M^{-1} for MTSSL compared to IPSL (K_α = 0.193 M^{-1}) at individual binding optima. Because of these individual binding optima, SDSL of β-lg was performed with MTSSL at pH 7.5 in an equimolar ratio of protein and spin label, while IPSL was bound to the protein at pH 8.5 and with a molar excess of 2.5.

4.4.1 Secondary protein structure measured with ATR-FTIR

After labeling and prior to heating, there were no significant differences in the intensity of the intramolecular β-sheets (~1628-1638 cm^{-1}) (Kavanagh et al. 2000; Keppler et al. 2017) between labeled and unlabeled samples at pH 2 in the unheated samples (UH) (Figure 4-2A). However, at pH 3.5, the intensity of the intramolecular β-sheets of the IPSL-labeled samples was significantly lower compared with MTSSL-labeled and unlabeled samples (Figure 4-2E). After heating for five hours at 90°C, the amyloid aggregate system at pH 2 and pH 3.5 represent an increase of the intermolecular β-sheets at ~1618-1623 cm^{-1} (Baldassarre et al. 2016; Heyn et al. 2019) (Figure 4-2B and F), which reflects the typical change in secondary structures during amyloid aggregation. These observations were very similar for unlabeled, MTSSL-, and IPSL-labeled β-lg aggregates (AAS) at pH 2 (Figure 4-2B). At pH 3.5, the intensity of the intermolecular β-sheets of the MTSSL- and IPSL-labeled samples were comparable, whereas the intensity of the intermolecular β-sheets was slightly increased in the unlabeled samples (Figure 4-2F). The separation of the AF and the n-AF by ultrafiltration resulted in an intensification of the peaks at ~1620 cm^{-1} and ~1637 cm^{-1} in the AF at pH 2 (Figure 4-2C), while signals at 1620 cm^{-1} were completely absent in the n-AF (Figure 4-2D). This indicates that both intra- and intermolecular β sheets were present in AF,

i.e. amyloid structures, whereas no typical secondary structures for amyloids could be identified in n-AF. Also at pH 3.5, the ALF of MTSSL- and IPSL-labeled samples had a slightly lower intensity at ~1621 cm^{-1} when compared to the unlabeled samples (Figure 4-2G), whereas the intensity of the intramolecular β-sheets in the n-ALF was the same for all samples (Figure 4-2H).

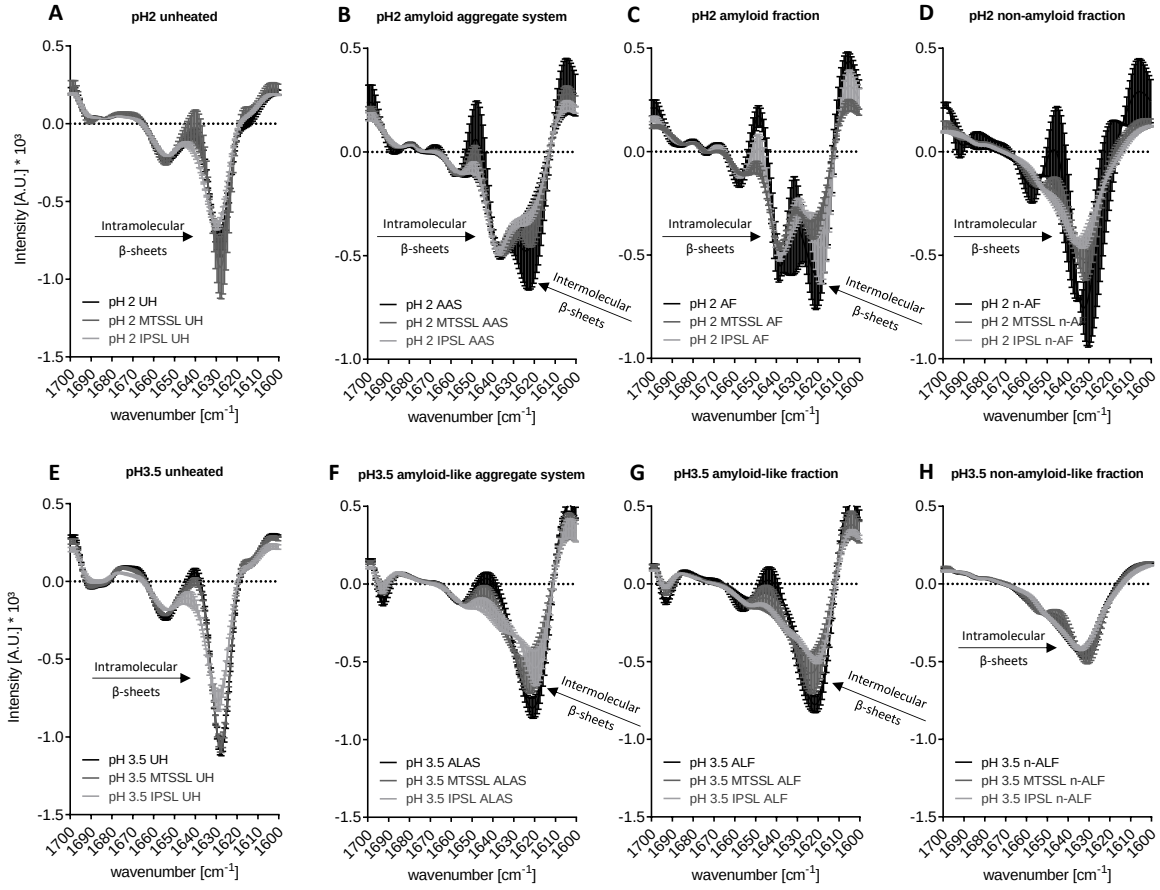

Figure 4-2: Influence of spin labeling on the secondary protein structure of β-lactoglobulin as measured by the second derivation of the amide I band using ATR-FTIR. Samples of β-lactoglobulin solutions with pH values of 2 (A–D) and 3.5 (E–H) were taken before heating (UH) and after 5 hours (AAS; ALAS). The UF-retentate represent the amyloid fraction (AF, pH 2; ALF, pH 3.5) and the filtrate the non-amyloid fraction (n-AF, pH 2; n-ALF, pH 3.5). β-lactoglobulin, in the absence of any spin label (black line), was labeled with MTSSL (dark gray line) or with IPSL (light gray line) (n=3, presented as mean and standard deviation).

4.4.2 Conformational changes measured by intrinsic tryptophan fluorescence

The intrinsic tryptophan (Trp) fluorescence indicates the polarity of the environment surrounding the indole group of the amino acid tryptophan (van Duuren 1961). The wavelength of the maximum emission shifts to a higher wavelength when tryptophan residues are exposed to a more polar environment, which indicates the increasing

accessibility of Trp to the aqueous environment (van Duuren 1961). A redshift (a shift to a higher wavelength) indicates a more polar environment, whereas a blueshift (a shift to a lower wavelength) indicates a nonpolar environment. By changing the polarity, conclusions can be drawn regarding the structure of the protein. During the heating process of five hours at 90°C, there was almost no shift in the wavelength at pH 2, but the fluorescence intensity decreased (Figure 4-3A). At pH 3.5, the intensity increased with a slight redshift, thus indicating a more polar environment of the tryptophan residues (Figure 4-3B). For both pH values and time points (UH and AAS/ALAS), the unlabeled protein always revealed the highest intensity, while labeling with MTSSL or IPSL decreased the fluorescence intensity. At pH 3.5, the MTSSL- and IPSL-labeled samples had similar intensities, whereas the IPSL-labeled sample revealed always the lowest intensity at pH 2 (Figure 4-3A).

After separating the AF from the n-AF by ultrafiltration, the n-AF were red-shifted and the AF were blue-shifted in relation to the AAS samples at pH 2 (Figure 4-3C). The blueshift of the IPSL-labeled protein was less pronounced compared to the blueshift of the unlabeled and MTSSL-labeled samples. At pH 3.5, the n-ALF and the ALF were also red shifted and blue shifted, as previously described for pH 2. However, the red- and blueshift of the n-ALF and ALF was less pronounced at pH 3.5 than at pH 2 (Figure 4-3D).

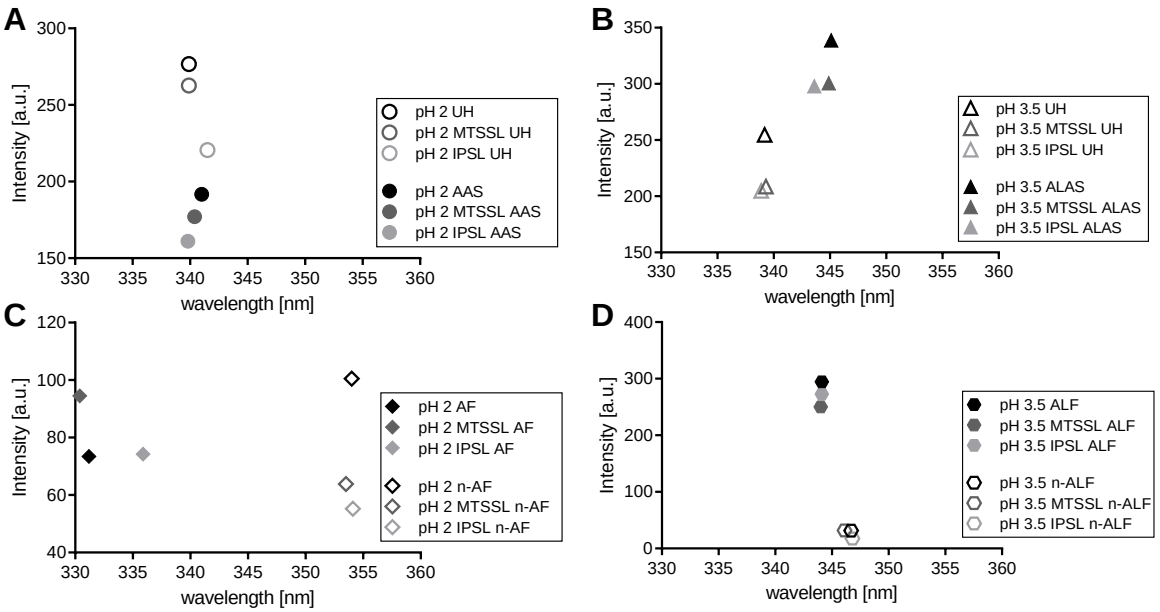

Figure 4-3: Influence of spin labeling on the tertiary protein structure of β-lactoglobulin measured as intrinsic tryptophan fluorescence of the β-lactoglobulin solution in the absence of any spin label (black) or labeling with MTSSL (dark gray) or IPSL (dark gray). Samples were measured before (UH, unfilled symbols) and after heat treatment (amyloid/amyloid-like aggregate system (AAS, ALAS) (filled symbols) at pH 2 (A) and pH 3.5 (B). The UF-retentate represent the amyloid fraction (AF; ALF, – filled symbols) and the filtrate the non-amyloid fraction (n-AF, n-ALF, – unfilled symbols) at pH 2 (C) and pH 3.5 (D). (n=9, the standard derivative is within the symbols).

4.4.3 Building blocks and morphology measured by SEC and AFM

For SEC experiments, the amyloid aggregates were fragmented into their building blocks by reducing potential disulfide bridges with dithiothreitol and disrupting its hydrogen bonds with guanidine hydrochloride. This was performed to check whether labeling with MTSSL or IPSL affects the fibril building blocks. For the UH samples, no differences in the size distribution were observed between the unlabeled, MTSSL and IPSL-labeled protein at pH 2 and 3.5 before heating (Figure 4-4A, B). All UH samples revealed three peaks in the size range of monomers (22.2 kDa), dimers (34.7 kDa) and trimers (54.3 kDa). The AAS at pH 2 consisted of smaller peptides at a size range of 5.2–18.9 kDa; however, the unlabeled, MTSSL- and IPSL-labeled aggregates did not differ in size distribution. Only the intensity of the unlabeled sample was lower than that of the labeled samples (Figure 4-4A). At pH 3.5, most of the protein was still present in the monomeric size range after heating and only a few smaller peptides in the range of 2.5 and 7.0 kDa were formed (Figure 4-4B).

After ultrafiltration, the size distribution in the AF and n-AF was comparable at pH 2, as they only differed in intensity (Figure 4-4C). The size distribution of the ALF at pH 3.5 is comparable to that of the AAS. In n-ALF, fragments of monomeric β-lg and smaller peptides were measured; however, significantly fewer monomers were measured when compared to the ALF (Figure 4-4D). Note that the size distribution in both ALF and n-ALF was the same between the labeled and unlabeled samples.

The AFM images of the AF revealed long fibrils at pH 2 (Figure 4-5A-C) and short, worm-like aggregates at pH 3.5 (Figure 4-5D–F). The aggregate morphology was not affected by spin labeling. No aggregates in n-AF could be found with the method used (data not shown).

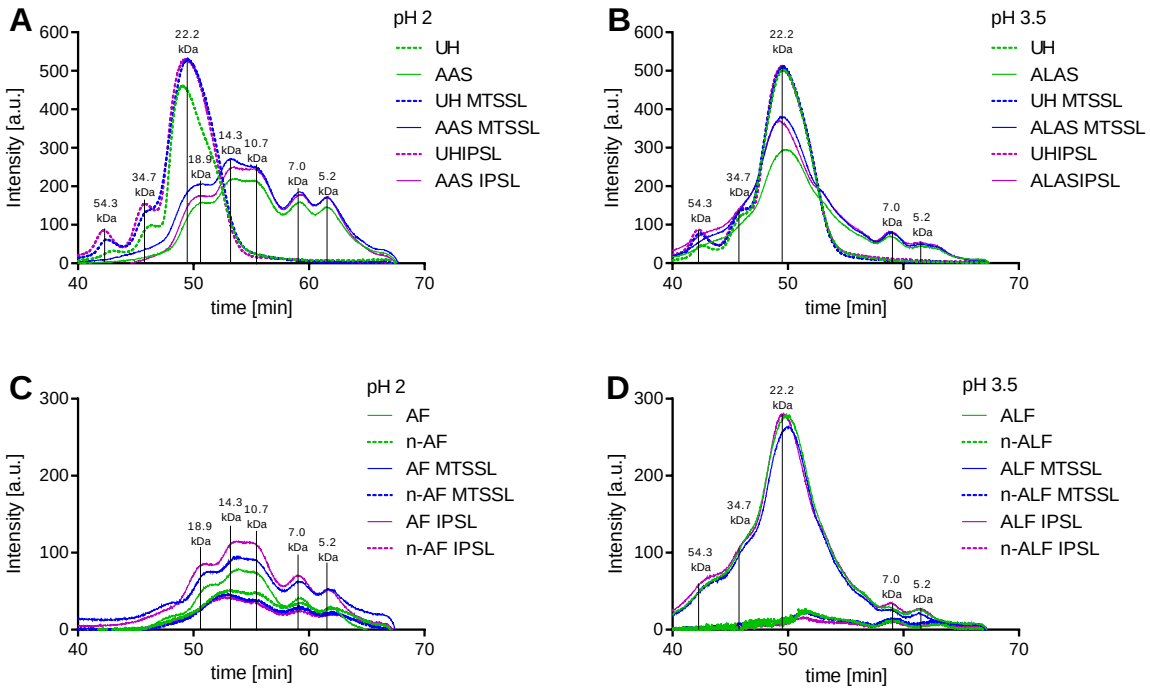

Figure 4-4: Building blocks of β-lactoglobulin solution measured as size-exclusion chromatography in the absence of any spin label (green) or labeling with MTSSL (blue) or IPSL (pink). Samples were measured before (UH, dotted lines) and after heat (solid lines) at pH 2 (A, AAS) and pH 3.5 (B, ALAS). The UF-retentate represent the amyloid fractions (AF, pH 2, C, solid line; ALF, pH 3.5, D, solid line) and the filtrates reflect the non-amyloid fractions (n-AF, pH 2, C, dotted line; n-ALF, pH 3.5, D, dotted line). All samples were dissociated with guanidine and DTT and filtered before the measurement.

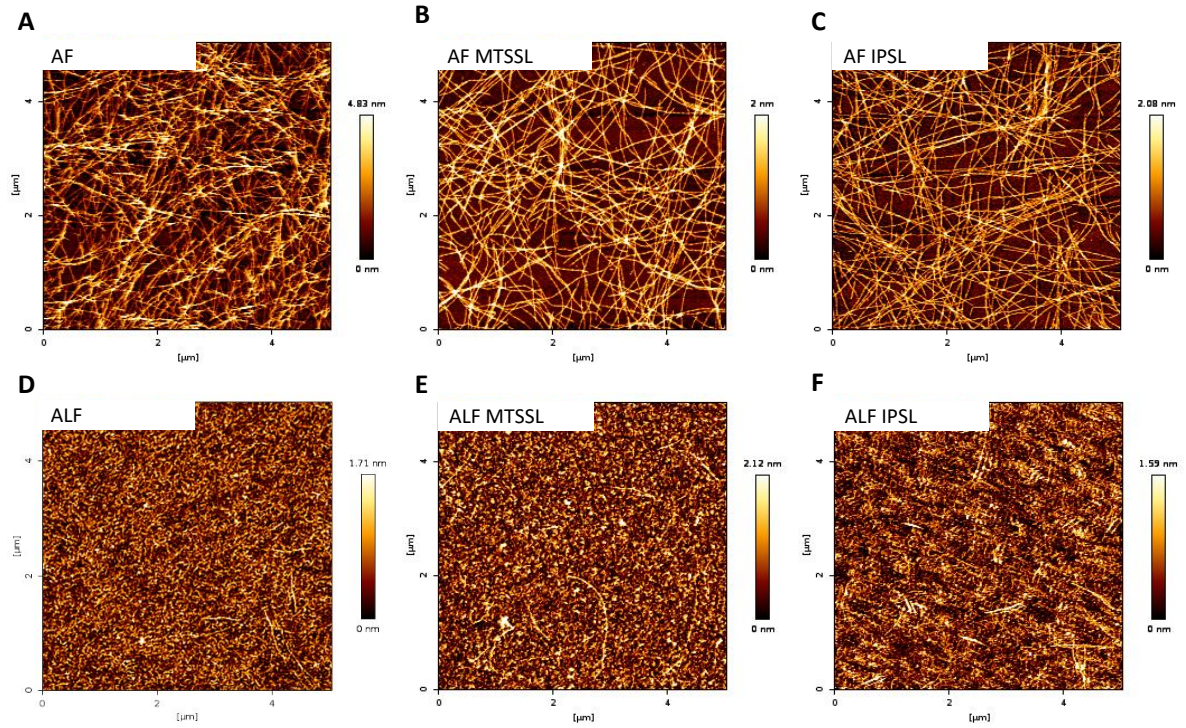

Figure 4-5: AFM images after five hours of heat incubation of unlabeled, MTSSL, or IPSL-labeled β-lg after fractionation in AF (A–C) at pH 2 and ALF (D–F) at pH 3.5. Double images (F) are obtained when a second tip is created by protein material that sticks onto the side of the tip. During scanning, everything is scanned twice: once with the tip and again with the protein particle.

4.4.4 ThT fluorescence and conversion rate measurements of amyloid aggregation

Thioflavin-T (ThT) fluorescence intensity is a measure of amyloid β-sheet formation (Loveday et al. 2012; Serfert et al. 2014; Keppler et al. 2019; Heyn et al. 2019). The UH samples represented neither differences in ThT fluorescence intensity between the labeled and unlabeled protein nor between pH 2 and pH 3.5 (Figure 4-6A). During the heating process, the ThT fluorescence increased for all samples and was significantly higher at pH 3.5 compared to pH 2 (Figure 4-6A). At pH 2, the MTSSL-labeled AAS had a significantly higher ThT fluorescence than the unlabeled and IPSL-labeled AAS. In contrast, for IPSL-labeled ALAS at pH 3.5, significantly lower ThT fluorescence was measured than for unlabeled and MTSSL-labeled ALAS. For the separation of the AF from the n-AF, the AAS (2.5% protein) must be diluted to 0.5% protein concentration (AAS_R). Since the ThT-measurement is dependent on the protein concentration, the AAS_R samples were remeasured to compare these data with the ThT data for the AF. Even so, the diluted samples (AAS_R) demonstrate different intensity ratios compared to the t_5 samples. Notably, a higher protein concentration during measurement (Figure 4-6A, AAS) leads to the unlabeled samples having the highest ThT fluorescence, followed by the MTSSL- and IPSL-labeled samples. Measurement at a

lower protein concentration (Figure 4-6B, AAS_R) resulted in higher ThT fluorescence intensity for the unlabeled protein, followed by the MTSSL- and IPSL-labeled sample. These intensity ratios were also observed in the AF; however, they were more pronounced than in the AAS_R samples (Figure 4-6B). In the AF and ALF, the unlabeled aggregates exhibited the highest ThT fluorescence at pH 2 and pH 3.5, respectively, followed by the MTSSL-labeled aggregates. The IPSL-labeled aggregates represented the significantly lowest ThT fluorescence at pH 2 and pH 3.5 (Figure 4-6B).

The conversion rate indicates what proportion of the protein used has been formed into amyloid aggregates. Protein concentrations before (AAS_R/$ALAS_R$) and after (AF/ALF) ultrafiltration were analyzed using a UV-VIS spectrometer. At pH 2, ~40% of both labeled and unlabeled proteins were converted to amyloid aggregates (Figure 4-6C, filled bars). At pH 3.5, the MTSSL-labeled aggregates exhibited a significantly lower conversion rate than unlabeled and IPSL-labeled aggregates. Additionally, at pH 3.5, the conversion rate was generally significantly higher (~80%) (Figure 4-6C, unfilled bars) when compared to pH 2.

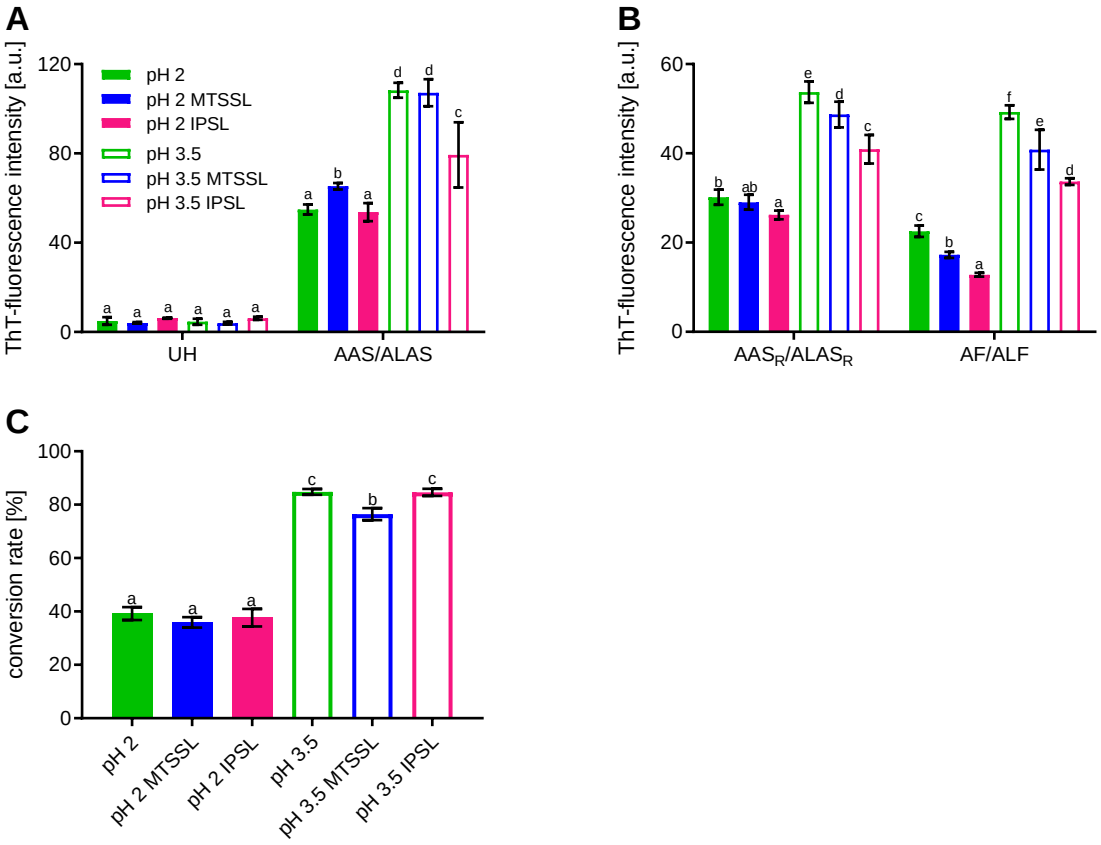

Figure 4-6: Fibrillation of of β-lactoglobulin solution in the absence of any spin label (green), labeled with MTSSL (blue) or IPSL (pink) at pH values of pH 2 (filled bars) and pH 3.5 (unfilled bars) measured by Thioflavin T fluorescence. Samples were taken before (UH) and after heat treatment (AAS/ALAS) (A). Samples were diluted to 0.5% protein concentration ($AAS_R/ALAS_R$). The UF-retentate represent the amyloid fractions (AF/ALF) (B). The conversion rate into amyloid aggregates was related to the protein concentration of the retentate ($AAS_R/ALAS_R$) determined by UV-VIS spectroscopy (C). Different letters indicate significant differences, each time point was considered separately (n = 9, $p < 0.05$, Tukey).

4.5 Discussion

All present results refer to protein solutions in which 10-17% of the total protein content was labeled. Higher concentrations of labeled proteins would most likely have increased the spin label density to such an extent that spin-spin interactions would have occurred and disturbed later EPR measurements of amyloid aggregates. Furthermore, it cannot be excluded that higher concentrations of the labeled protein than those used here could possibly have led to significant changes in the secondary protein structure or morphology of the amyloid aggregates.

4.5.1 Influence of spin labeling on the secondary and tertiary protein structure of β-lactoglobulin

ATR-FTIR measurements were conducted to observe changes in the secondary structure of the protein that might be caused by spin labeling (Figure 4-2). The observed lower β-sheet intensity of the IPSL-labeled samples at pH 3.5, which was not evident at pH 2 (Figure 4-2), may indicate protein destabilization induced by the thiol modification. This was already described by Zimmerman et al. (1970) and by Sakai et al. (2000), who observed dimer dissociation to monomers after thiol modification, likely as a result of interference with the dimer interface. The more flexible bonding of MTSSL compared with IPSL (Bordignon 2018) may explain why the destabilization at pH 3.5 was only visible in the IPSL-labeled samples. Further changes of the secondary protein structure were not observed or were within the range of the standard deviation of the measurement; therefore, no significant influence of the spin labels could be determined. The second derivation of the amide I band (1600–1700 cm^{-1}) was considered because the amid vibration is most commonly used for secondary structure analysis (Barth 2007). Particular attention was paid to the intramolecular β-sheets at ~1628–1638 cm^{-1}—which indicate the remaining native or non-aggregated protein—and to the intermolecular β-sheets at ~1618-1623 cm^{-1}, which are frequently observed in protein associations such as fibril formation (Moran and Zanni 2014; Routledge et al. 2009; Baldassarre et al. 2016; Heyn et al. 2019). The exact wavenumber is dependent on the FTIR method (transmission or ATR), use of liquid or dried samples, and pH value (Keppler et al. 2019). In contrast to the present results, the bonding of allyl isothiocyanate (AITC) to β-lg, which forms C-S or C-N bonds with thiol or amine groups, respectively, resulted in a significant increase in the intramolecular β-sheet content (Keppler et al. 2017). It should be considered that up to five AITC molecules could bind to one molecule β-lg (Keppler et al. 2017), while only one MTSSL molecule was linked to one molecule β-lg (Figure 4-7A). This discrepancy may explain the greater impact on the secondary structure of AITC relative to MTSSL. Likewise, the covalent binding of allicin via S-S bonds also led to a stronger β-sheet signal in β-lg (Wilde et al. 2016); however, the tertiary structure was more affected than the secondary structure. This stresses how differently protein conformation can be affected by the covalent addition of different molecules, depending on the hydrophobicity, charge distribution, number of binding sites and its flexibility (Owenius et al. 1999).

The intensity of the ITF decreased after labeling with both spin labels and at both pH values (Figure 4-3A, B), thus indicating fluorescence quenching. Only a slight decrease in fluorescence intensity was observed between the unlabeled and MTSSL-labeled samples (Figure 4-3A, pH 2: 276.7 → 262.7; Figure 4-3B, pH 3.5: 254.5 → 208.6); however, the decreasing quenching effect was more pronounced at pH 3.5 compared to pH 2. It is well known that the covalent and noncovalent bonding of different compounds to β-lg could

quench the fluorescence (Tayeh et al. 2009; Liang and Subirade 2010). Trp^{61} is involved in the antiparallel interaction of the dimer, though its fluorescence is completely suppressed by the disulfide bridge of Cys^{66}-Cys^{160}, regardless of the pH value or the proportions of monomers and dimers in solution (Sakurai et al. 2009; Croguennec et al. 2004; Albani et al. 2014). In contrast, Trp^{19} is located in the apolar environment in the cavity of the protein, where Cys^{121} is also located (Sakurai et al. 2009). Depending on the size of the bound molecule, the unfolding and destabilization of the protein can be observed and could influence the fluorescence intensity. This effect was more pronounced with increasing pH value and less observable at pH 2, where the protein is already a monomer (Sakai et al. 2000), which was in accordance with the present results. The pH of 7.5 resulted in the local secondary structure of the EF loop being altered by the Tanford transition (Tanford et al. 1959). The open form of the β-barrel seems to change the conformation so that the spin label does not affect tryptophan fluorescence. However, the conformation of the monomeric β-lg seems to be more stable compared to the dimeric form, since the fluorescence intensity was less influenced at pH 2 compared to pH 3.5. ITF results confirm the presence of a tightly bound molecule indicated by the decrease in fluorescence intensity (i.e., quenching effects caused by energy transfer). In addition, a redshift (339.9 nm → 341.5 nm) is evident in the IPSL sample at pH 2, probably caused by the hydrophilic linker of IPSL (Figure 4-3). Furthermore, minor structural changes in the hydrophobic core of the protein can be expected after labeling. Keppler et al. (2014) demonstrated that AITC (99.16 Da) altered the secondary protein conformation; however, in addition to binding to cysteine residues, it is also able to bind to the amino groups, so that up to five AITC molecules can ultimately bind to one β-lg molecule. This implies that apart from the molecular size of the ligand, the number of binding sites, the binding position, and the flexibility of the linker are important complementary factors that are necessary to alter the secondary and tertiary structures.

4.5.2 Interference of the thioflavin-T measurement by the spin labels

ThT fluorescence was reduced by spin labeling with MTSSL and was reduced even more by IPSL (Figure 4-6B). Since the unlabeled samples always exhibited the highest ITF (Figure 4-3), it could be assumed that the spin label quenches the ThT fluorescence as already observed for tryptophan (discussed in Section 0). Another explanation for the reduced ThT fluorescence in labeled samples could be reduced ThT binding. The ThT molecules bind parallel to the long axis of the amyloid aggregates in the channels of the β-sheets (Krebs et al. 2005). The spin labels may influence the migration of the ThT-molecules into these channels. The lower ThT fluorescence in the IPSL-labeled samples compared to the MTSSL-labeled samples may be associated with lower flexibility or the more hydrophilic character of IPSL (Bordignon 2018; Klare 2012), the latter of which may lead to an interruption in ThT binding. Therefore, both effects could reduce the migration of ThT into the channels of the

stacked β-sheet and thus interfere with the accuracy of the measurement. The lower ThT fluorescence of the labeled aggregates was inconsistent with the conversion rate determination (Figure 4-6C) and the intermolecular β-sheet formation (Figure 4-2). At pH 2, the conversion rates of labeled and unlabeled amyloid aggregates were identical, but the conversion of MTSSL-labeled aggregates was lowest at pH 3.5 (Figure 4-6C). In this context, it may be concluded that labeling hardly affects the amyloid aggregation, though interference in ThT-measurements is likely.

4.5.3 Influence of spin labeling on the structure and morphology of the amyloid aggregates

In the samples labeled with MTSSL or IPSL, a less polar environment was observed after five hours heating at pH 3.5 compared to the unheated samples, which was indicated by a clear blueshift of the ITF (Figure 4-3B). However, the shift at pH 2 could be neglected since the shift of the wavelength was very small (Figure 4-3A). The less polar environment of the Trp^{19} indicated a conformational change of the protein. Furthermore, a reduced fluorescence intensity due to spin labeling was observed after heating for five hours, indicating fluorescence quenching, which was already described for the unheated samples (0). Similar to the present findings for the unlabeled protein, Hettiarachchi et al. (2012) also observed a redshift and a decrease in the non-fractionated peak height during the formation of unlabeled amyloid aggregates with β-lg at pH 2. They attributed this effect to unfolding and/or hydrolysis of β-lg during the self-assembly process, resulting in greater exposure of one or both tryptophan residues to the solvent (Hettiarachchi et al. 2012). Our group already observed a strong decrease in tryptophan fluorescence, particularly at pH 2, with AF exhibiting a blueshift and n-AF a redshift (Heyn et al. 2019; Keppler et al. 2019). In the n-AF at pH 2, a fluorescence quenching due to spin labeling was evident (Figure 4-3C); however, the FTIR results indicated no changes in the secondary structure (Figure 4-2G, H). While a higher polarity but identical fluorescence intensities were observed in AF for the IPSL-labeled β-lg compared to the unlabeled sample, the opposite effect was found for the MTSSL-labeled samples (Figure 4-3C). However, these indications of a conformational change caused by spin labeling could not be confirmed by the FTIR results since the proportions of intra- and intermolecular β-sheets in the labeled and unlabeled amyloid aggregates were the same (Figure 4-2C). In contrast, only slight differences in fluorescence intensity and wavelength were observed for ALF and n-ALF at pH 3.5 (Figure 4-3D), thus indicating that the polarity around the tryptophan polarity had hardly changed, which was also validated by FTIR data (Figure 4-2).

As discussed in Section 4.5.2, the conversion rate of labeled and unlabeled samples hardly differed, although it should be noted that the determination of the conversion rate only

describes the number of aggregates larger than 300 kDa, but not their amyloid character. Another effect frequently observed for covalent as well as noncovalent protein-ligand bonding is structure stabilization or destabilization, which would alter the denaturation temperature, acid hydrolysis rate, and conversion rate (Wilde et al. 2016). At pH 2, the label destabilized the protein, while β-lg was stabilized against heat denaturation at pH 3.5. β-lg monomers seem to be more heat resistant compared to their dimers since the quaternary structure is dependent on the pH value. Reversible denaturation could also prevent the formation of high-order aggregates since the SH group is required to form S-S linked protein aggregates (Iametti et al. 1996). This could be evidence of reduced fibril formation measured by ThT fluorescence (Figure 4-4A, B). At pH 2 and >7.5, the repulsion force is strong; therefore, the monomeric form of β-lg is dominant (Yan et al. 2013). In the pH range of 3.7–5.2, β-lg is associated with larger oligomers (Verheul et al. 1999). The dimeric form at pH 3.5 appeared to have been destabilized by the spin label, suggesting that the degree of denaturation might be reduced by the labels. For this reason, we assessed the degree of denaturation as a function of pH value for labeled and unlabeled β-lg during heat incubation at 90°C. The denatured portion was precipitated after an appropriate incubation period and the remaining native protein in the supernatant was measured by RP-HPLC. At pH 2, ~35% of the protein was denatured after 30 min, while at pH 3.5, 55–70% of the protein was already denatured, while no native protein could be detected in any sample after five hours. Although the degree of denaturation did not differ significantly between labeled and unlabeled β-lg, IPSL at pH 3.5 showed a clear tendency to reduce the degree of denaturation. This may also explain the observed decrease in the β-sheets for the IPSL-labeled sample (Figure 4-2). Similar findings were reported for non-covalently interacting molecules and β-lg (Zorilla et al. 2011).

The lower degree of denaturation at pH 2 compared to pH 3.5 may be explained by a reversible and irreversible denaturation. Burova et al. (1998) noted that increasing temperatue up to 110°C at pH 2.05 results in the irreversible denaturation of β-lg; however, the thermal denaturation became reversible if the ligand mercaptopropionic acid was bound to cysteine 121 of β-lg. Iametti et al. (1996) also reported on the effect of iodoacetamide bound to β-lg, which considerably reduces the number of irreversibly denatured molecules (pH 6.8, 70°C). However, these observations could not be clearly confirmed by the present results. Although blocking the free SH group seemed to have an influence on the denaturation, no significant differences were observed in the building blocks (Figure 4-4) and the coarse morphology (Figure 4-5) of MTSSL- or IPSL-labeled β-lg compared to unlabeled protein after five hours of heating at 90°C. Burova et al. (1998) discovered that the secondary structure was not affected by the modification of β-lg with mercaptopropionic acid, though the tertiary structure was altered despite the low molecular weight of 106.14 g/mol. This may

explain why the building blocks (Figure 4-4) were not affected by the labeling, while an influence on the ITF (Figure 4-3) was observed. However, it cannot be excluded that minor structural changes could occur that were below the resolution of the SEC column or only visible through in-depth analysis of the AFM images, which went beyond the scope of the present study. This was in accordance with previous studies. No significant differences were found in the fibril formation of other proteins such as α-synuclein (Der-Sarkissian et al. 2003), while amyloid β (Török et al. 2002) was also not altered by SDSL with MTSSL.

4.6 Conclusion

This part of the study demonstrated that substantial changes in the behavior of β-lg during amyloid aggregation can be excluded when it is labeled with MTSSL and IPSL at pH 2 and 3.5, as evidenced by the same building blocks and morphologies being observed between unlabeled and spin-labeled protein. However, it should be noted that all present results refer to protein solutions in which 10-17% of the total protein content was labeled, since an excessively high spin label density may subsequently cause spin-spin interactions in amyloid aggregates. Thus, it cannot be excluded that higher concentrations of the labeled protein than those used here might possibly lead to significant changes in the secondary protein structure, whereas only minor changes in the secondary protein structure were observed at these low spin label concentrations. This was basically observed at pH 3.5 with IPSL, where it reduced the intra- and intermolecular β-sheets. The comparison of both spin labels, which either bind via S-S bonds and are more flexible like MTSSL or, in contrast, bind more rigidly to the β-lg via C-S bonds (as per IPSL) indicated that the impact of the label on the secondary protein structure is lower for more flexible bonds. The extent of amyloid aggregation in all fractions was monitored by thioflavin-T fluorescence, as is common practice, and it was found that the fluorescence probes and spin probes interfere with each other. As such, this approach should be carefully interpreted when using spin labeling. Non-amyloid and amyloid fractions were recovered from the amyloid aggregated system by membrane filtration at a cut-off of 300 kDa, which were also found to be equivalent and independent of the spin labeling process. From Part I of this study it can be summarized so far that the approach of SDSL can be used to label the natural food protein β-lg without affecting the protein conformation or formation of amyloid aggregates. The second part of this study will further focus on EPR and mass spectroscopy to investigate the exact binding sites of the spin labels at the peptide/protein sequence as well as the incorporation of the labeled protein side chains into the amyloid or non-amyloid fractions.

Acknowledgment

Funding: The authors thank the German Research Foundation (DFG) for financial support of this work within the SPP 1934 DiSPBiotech (project number 273937032).

We are very grateful to Prof. Dr. Arno Kwade (iPAT, TU Braunschweig) for the fruitful cooperation and discussions. We would like to thank Stephanie Michel for the AFM measurements (iPAT, TU Braunschweig) and Sarah Stille (Food Technology, Kiel University) for her competent assistance in the laboratory.

4.7 Supplementary material for paper 2

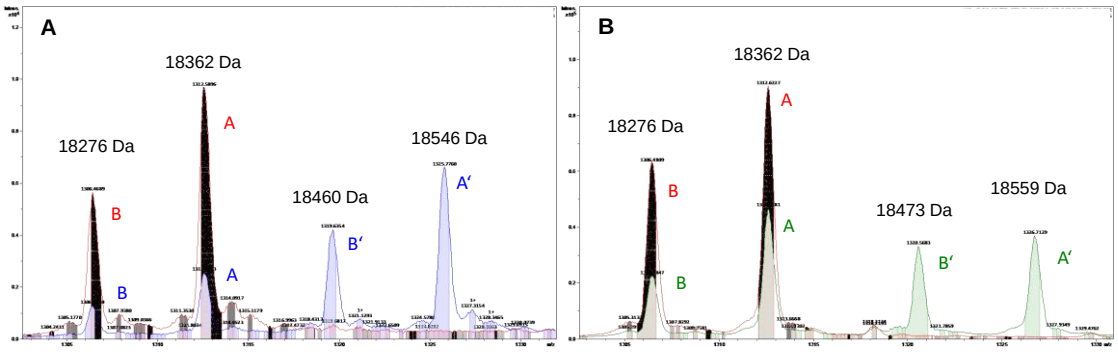

Figure 4-7: Mass spectrometry chromatograms of unlabeled β-lg (red) and labeled with equimolar ratio MTSSL at pH 7.5 (A, blue) or 2.5 molar excess of IPSL at pH 8.5 (B, green). The letters in the spectra designate: B – native β-lg B; A – native β-lg A; B' – spin labeled β-lg B; A' – spin labeled β-lg A.

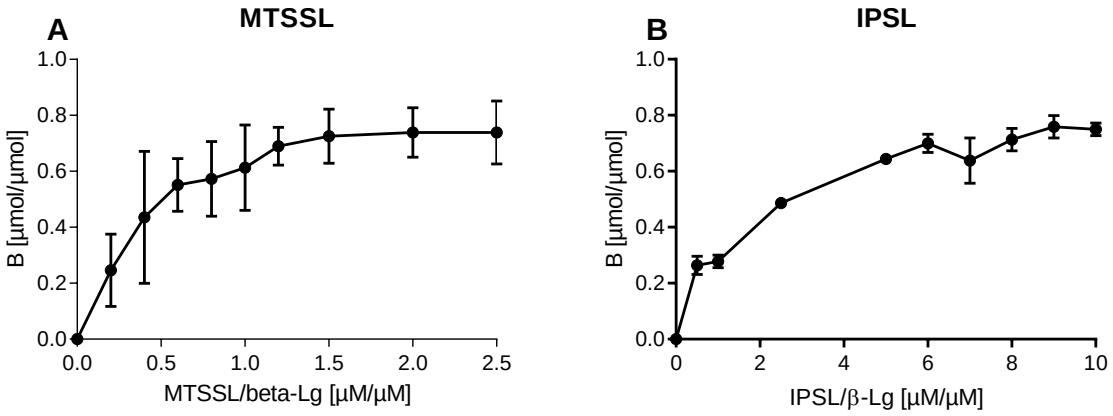

Figure 4-8: Molar binding ratio of MTSSL to β-lg at pH 7.5 (A) and IPSL at pH 8.5 to β-lg (B). The binding sites were calculated by measuring the free thiol groups (RSH).

Methods:

For the LC-MS measurements were conducted at a microTOF-QII mass spectrometer (Bruker Daltonik, Bremen, Germany) via an electrospray ionization source (ESI). Mass spectra over the mass range of 200-3000 m/z were acquired in positive ion mode. Calibration of the instrument and an external recalibration of the acquired mass spectra were performed using ESI TOF Tuning Mix (Agilent Technologies, Waldbronn, Germany). Deconvolution and evaluation of the acquired MS data was conducted using Data Analysis 4.0 (Bruker Daltonics, Bremen, Germany). The prior separation were conduction with a Dionex Ultimate 3000 HPLC system (Thermo Fisher Scientific, Waltham, USA).

Free thiol groups were determined by using the Ellman's assay (Ellman, 1959) using a UV-Vis spectrometer (Helios Gamma, UV-Vis, Thermo Spectronic, Cambridge, UK) and a quartz cell. Each spin label/β-lg ratios were investigated in triplicate. The binding constant was calculated by nonlinear regression of the saturation binding curve using the software Graphpad Prism version 6 (Graphpad Software, La Jolla, USA) according to (Keppler et al., 2014; Wilde et al., 2016). To obtain the binding curves the molar ratio of the MTSSL or IPSL to β-lactoglobulin (B, µM/µM) were plotted against the ligand concentration (µM). B was calculated in the assumption that each thiol group can bind one molecule of MTSSL or IPSL.

4.8 References

Akkermans, Cynthia; Venema, Paul; van der Goot, Atze Jan; Gruppen, Harry; Bakx, Edwin J.; Boom, Remko M.; van der Linden, Erik (2008): Peptides are building blocks of heat-induced fibrillar protein aggregates of beta-lactoglobulin formed at pH 2. In: *Biomacromolecules* 9 (5), S. 1474–1479. DOI: 10.1021/bm7014224.

Albani, Jihad René; Vogelaer, Julie; Bretesche, Loïc; Kmiecik, Daniel (2014): Tryptophan 19 residue is the origin of bovine β-lactoglobulin fluorescence. In: *Journal of pharmaceutical and biomedical analysis* 91, S. 144–150. DOI: 10.1016/j.jpba.2013.12.015.

Baldassarre, Maurizio; Bennett, Matthew; Barth, Andreas (2016): Simultaneous acquisition of infrared, fluorescence and light scattering spectra of proteins. Direct evidence for pre-fibrillar species in amyloid fibril formation. In: *The Analyst* 141 (3), S. 963–973. DOI: 10.1039/c5an02283e.

Barth, Andreas (2007): Infrared spectroscopy of proteins. In: *Biochimica et biophysica acta* 1767 (9), S. 1073–1101. DOI: 10.1016/j.bbabio.2007.06.004.

Bordignon, Erica (2018): EPR Spectroscopy of Nitroxide Spin Probes. In: Daniella Goldfarb und Stefan Stoll (Hg.): EPR Spectroscopy. Fundamentals and Methods. Newark: John Wiley & Sons Incorporated (EMagRes Bks), S. 277–301.

Burova, T. V.; Choiset, Y.; Tran, V.; Haertle, T. (1998): Role of free Cys121 in stabilization of bovine beta-lactoglobulin B. In: *Protein Engineering Design and Selection* 11 (11), S. 1065–1073. DOI: 10.1093/protein/11.11.1065.

Croguennec, Thomas; Mollé, Daniel; Mehra, Raj; Bouhallab, Saïd (2004): Spectroscopic characterization of heat-induced nonnative beta-lactoglobulin monomers. In: *Protein Science* 13 (5), S. 1340–1346. DOI: 10.1110/ps.03513204.

Dave, Anant C.; Loveday, Simon M.; Anema, Skelte G.; Jameson, Geoffrey B.; Singh, Harjinder (2014): Glycation as a Tool To Probe the Mechanism of β-Lactoglobulin Nanofibril Self-Assembly. In: *Journal of agricultural and food chemistry* 62 (14), S. 3269–3278. DOI: 10.1021/jf405441g.

Der-Sarkissian, Ani; Jao, Christine C.; Chen, Jeannie; Langen, Ralf (2003): Structural organization of alpha-synuclein fibrils studied by site-directed spin labeling. In: *The Journal of biological chemistry* 278 (39), S. 37530–37535. DOI: 10.1074/jbc.M305266200.

Di Zhao; Li, Lin; Xu, Dan; Sheng, Bulei; Chen, Juncheng; Li, Bing; Zhang, Xia (2018): Heat-induced amyloid-like aggregation of β-lactoglobulin regulated by glycation. A comparison of five kinds of reducing saccharides. In: *International journal of biological macromolecules* 120 (Pt A), S. 302–309. DOI: 10.1016/j.ijbiomac.2018.08.048.

Gu, Lei; Tran, Joyce; Jiang, Lin; Guo, Zhefeng (2016): A new structural model of Alzheimer's Aβ42 fibrils based on electron paramagnetic resonance data and Rosetta modeling. In: *Journal of structural biology* 194 (1), S. 61–67. DOI: 10.1016/j.jsb.2016.01.013.

Hettiarachchi, Charith A.; Melton, Laurence D.; Gerrard, Juliet A.; Loveday, Simon M. (2012): Formation of β-lactoglobulin nanofibrils by microwave heating gives a peptide composition different from conventional heating. In: *Biomacromolecules* 13 (9), S. 2868–2880. DOI: 10.1021/bm300896r.

Heyn, Timon R.; Garamus, Vasil M.; Neumann, Hendrikje R.; Uttinger, Maximilian J.; Guckeisen, Tobias; Heuer, Monique et al. (2019): Influence of the polydispersity of pH 2 and pH 3.5 beta-lactoglobulin amyloid fibril solutions on analytical methods. In: *European Polymer Journal* 120, S. 109211. DOI: 10.1016/j.eurpolymj.2019.08.038.

Iametti, Stefania; Gregori, Beatrice; Vecchio, Giuseppe; Bonomi, Francesco (1996): Modifications Occur at Different Structural Levels During the Heat Denaturation of beta-Lactoglobulin. In: *Eur J Biochem* 237 (1), S. 106–112. DOI: 10.1111/j.1432-1033.1996.0106n.x.

Iuraşcu, Ionuţ Marius; Cozma, Claudia; Tomczyk, Nick; Rontree, John; Desor, Michael; Drescher, Malte; Przybylski, Michael (2009): Structural characterization of beta-amyloid

oligomer-aggregates by ion mobility mass spectrometry and electron spin resonance spectroscopy. In: *Analytical and bioanalytical chemistry* 395 (8), S. 2509–2519. DOI: 10.1007/s00216-009-3164-3.

Jayasinghe, Sajith A.; Langen, Ralf (2004): Identifying structural features of fibrillar islet amyloid polypeptide using site-directed spin labeling. In: *The Journal of biological chemistry* 279 (46), S. 48420–48425. DOI: 10.1074/jbc.M406853200.

Kavanagh, Gaynor M.; Clark, Allan H.; Ross-Murphy, Simon B. (2000): Heat-induced gelation of globular proteins. Part 3. Molecular studies on low pH β-lactoglobulin gels. In: *International journal of biological macromolecules* 28 (1), S. 41–50. DOI: 10.1016/S0141-8130(00)00144-6.

Keppler, Julia K.; Heyn, Timon R.; Meissner, Philipp M.; Schrader, Katrin; Schwarz, Karin (2019): Protein oxidation during temperature-induced amyloid aggregation of beta-lactoglobulin. In: *Food Chemistry* 289, S. 223–231. DOI: 10.1016/j.foodchem.2019.02.114.

Keppler, Julia Katharina; Koudelka, Tomas; Palani, Kalpana; Stuhldreier, Mayra Christina; Temps, Friedrich; Tholey, Andreas; Schwarz, Karin (2014): Characterization of the covalent binding of allyl isothiocyanate to β-lactoglobulin by fluorescence quenching, equilibrium measurement, and mass spectrometry. In: *Journal of biomolecular structure & dynamics* 32 (7), S. 1103–1117. DOI: 10.1080/07391102.2013.809605.

Keppler, Julia Katharina; Martin, Dierk; Garamus, Vasil M.; Berton-Carabin, Claire; Nipoti, Elia; Coenye, Tom; Schwarz, Karin (2017): Functionality of whey proteins covalently modified by allyl isothiocyanate. Part 1 physicochemical and antibacterial properties of native and modified whey proteins at pH 2 to 7. In: *Food Hydrocolloids* 65, S. 130–143. DOI: 10.1016/j.foodhyd.2016.11.016.

Kirby, Tara L.; Karim, Christine B.; Thomas, David D. (2004): Electron paramagnetic resonance reveals a large-scale conformational change in the cytoplasmic domain of phospholamban upon binding to the sarcoplasmic reticulum Ca-ATPase. In: *Biochemistry* 43 (19), S. 5842–5852. DOI: 10.1021/bi035749b.

Klare, Johann P. (2012): Site-Directed Spin Labeling and Electron Paramagnetic Resonance (EPR) Spectroscopy: A Versatile Tool to Study Protein-Protein Interactions. Rijeka: InTech.

Krebs, M. R. H.; Bromley, E. H. C.; Donald, A. M. (2005): The binding of thioflavin-T to amyloid fibrils. Localisation and implications. In: *Journal of structural biology* 149 (1), S. 30–37. DOI: 10.1016/j.jsb.2004.08.002.

Liang, Li; Subirade, Muriel (2010): Beta-lactoglobulin/folic acid complexes. Formation, characterization, and biological implication. In: *The journal of physical chemistry. B* 114 (19), S. 6707–6712. DOI: 10.1021/jp101096r.

Loveday, S. M.; Wang, X. L.; Rao, M. A.; Anema, S. G.; Singh, H. (2012): β-Lactoglobulin nanofibrils. Effect of temperature on fibril formation kinetics, fibril morphology and the rheological properties of fibril dispersions. In: *Food Hydrocolloids* 27 (1), S. 242–249. DOI: 10.1016/j.foodhyd.2011.07.001.

Margittai, Martin; Langen, Ralf (2004): Template-assisted filament growth by parallel stacking of tau. In: *Proceedings of the National Academy of Sciences of the United States of America* 101 (28), S. 10278–10283. DOI: 10.1073/pnas.0401911101.

Moran, Sean D.; Zanni, Martin T. (2014): How to Get Insight into Amyloid Structure and Formation from Infrared Spectroscopy. In: *The journal of physical chemistry letters* 5 (11), S. 1984–1993. DOI: 10.1021/jz500794d.

Owenius, Rikard; Österlund, Maria; Lindgren, Mikael; Svensson, Magdalena; Olsen, Ole H.; Persson, Egon et al. (1999): Properties of Spin and Fluorescent Labels at a Receptor-Ligand Interface. In: *Biophysical Journal* 77 (4), S. 2237–2250. DOI: 10.1016/S0006-3495(99)77064-5.

Routledge, Katy E.; Tartaglia, Gian Gaetano; Platt, Geoffrey W.; Vendruscolo, Michele; Radford, Sheena E. (2009): Competition between intramolecular and intermolecular interactions in an amyloid-forming protein. In: *Journal of molecular biology* 389 (4), S. 776–786. DOI: 10.1016/j.jmb.2009.04.042.

Sakai, Kazuko; Sakurai, Kazumasa; Sakai, Miyo; Hoshino, Masaru; Goto, Yuiji (2000): Conformation and stability of thiol-modified bovine [beta] lactoglobulin. In: *Camebridge University Press* (9), S. 1719–1729.

Sakurai, Kazumasa; Konuma, Tsuyoshi; Yagi, Masanori; Goto, Yuji (2009): Structural dynamics and folding of beta-lactoglobulin probed by heteronuclear NMR. In: *Biochimica et biophysica acta* 1790 (6), S. 527–537. DOI: 10.1016/j.bbagen.2009.04.003.

Sepkhanova, I.; Drescher, M.; Meeuwenoord, N. J.; Limpens, R. W. A. L.; Koning, R. I.; Filippov, D. V.; Huber, M. (2009): Monitoring Alzheimer Amyloid Peptide Aggregation by EPR. In: *Applied magnetic resonance* 36 (2-4), S. 209–222. DOI: 10.1007/s00723-009-0019-1.

Serfert, Y.; Lamprecht, C.; Tan, C.-P.; Keppler, J. K.; Appel, E.; Rossier-Miranda, F. J. et al. (2014): Characterisation and use of β-lactoglobulin fibrils for microencapsulation of lipophilic ingredients and oxidative stability thereof. In: *Journal of Food Engineering* 143, S. 53–61. DOI: 10.1016/j.jfoodeng.2014.06.026.

Tanford, Charles; Bunville, Lyle G.; Nozaki, Yasuhiko (1959): The Reversible Transformation of β-Lactoglobulin at pH 7.5 1. In: *Journal of the American Chemical Society* 81 (15), S. 4032–4036. DOI: 10.1021/ja01524a054.

Tayeh, Nadim; Rungassamy, Tévamie; Albani, Jihad René (2009): Fluorescence spectral resolution of tryptophan residues in bovine and human serum albumins. In: *Journal of pharmaceutical and biomedical analysis* 50 (2), S. 107–116. DOI: 10.1016/j.jpba.2009.03.015.

Török, Marianna; Milton, Saskia; Kayed, Rakez; Wu, Peng; McIntire, Theresa; Glabe, Charles G.; Langen, Ralf (2002): Structural and dynamic features of Alzheimer's Abeta peptide in amyloid fibrils studied by site-directed spin labeling. In: *The Journal of biological chemistry* 277 (43), S. 40810–40815. DOI: 10.1074/jbc.M205659200.

van DUUREN, BENJAMIN L. (1961): Solvent Effects in the Fluorescence of Indole and Substituted Indoles 1. In: *J. Org. Chem.* 26 (8), S. 2954–2960. DOI: 10.1021/jo01066a079.

Verheul, Marleen; Pedersen, Jan Skov; Roefs, Sebastianus P. F. M.; Kruif, Kees G. de (1999): Association behavior of native β-lactoglobulin. In: *Biopolymers* 49 (1), S. 11–20. DOI: 10.1002/(SICI)1097-0282(199901)49:1<11::AID-BIP2>3.0.CO;2-1.

Wilde, Sandra Catharina; Treitz, Christian; Keppler, Julia Katharina; Koudelka, Tomas; Palani, Kalpana; Tholey, Andreas et al. (2016): β-Lactoglobulin as nanotransporter--Part II. Characterization of the covalent protein modification by allicin and diallyl disulfide. In: *Food Chemistry* 197 (Pt A), S. 1022–1029. DOI: 10.1016/j.foodchem.2015.11.011.

Yan, Yunfeng; Seeman, Daniel; Zheng, Bingqian; Kizilay, Ebru; Xu, Yisheng; Dubin, Paul L. (2013): pH-Dependent aggregation and disaggregation of native β-lactoglobulin in low salt. In: *Langmuir: the ACS journal of surfaces and colloids* 29 (14), S. 4584–4593. DOI: 10.1021/la400258r.

Zimmerman, James K.; Barlow, Grant H.; Klotz, Irving M. (1970): Dissociation of β-lactoglobulin near neutral pH. In: *Archives of Biochemistry and Biophysics* 138 (1), S. 101–109. DOI: 10.1016/0003-9861(70)90289-4.

Zorilla, Raquel; Liang, Li; Remondetto, Gabriel; Subirade, Muriel (2011): Interaction of epigallocatechin-3-gallate with β-lactoglobulin. Molecular characterization and biological implication. In: *Dairy Science & Technol.* 91 (5), S. 629–644. DOI: 10.1007/s13594-011-0036-3.

5 Paper 3: Amyloid aggregation of spin-labeled β-lactoglobulin Part II

Identification of spin-labeled protein and peptide sequences after amyloid aggregation

Jacqueline Lux[a], Mykhailo Azarkh[b], Laura Fitzner[a], Julia K. Keppler[a,c], Karin Schwarz[a], Malte Drescher[b], Anja Steffen-Heins[a]

[a]Institute of Human Nutrition and Food Science, Division of Food Technology, Kiel University, Germany

[b]Department of Chemistry, University of Konstanz, Germany

[c]Food Process Engineering, Wageningen University, P.O. Box 17, 6700 AA, Wageningen, The Netherlands

Published in Food Hydrocolloids (2021), 112, doi: 10.1016/j.foodhyd.2020.106174

Received 28 February 2020, Accepted: 13 July 2020, Available online: 18 July 2020

5.1 Abstract

Site-directed spin labeling (SDSL) of natural β-lactoglobulin (β-lg) was established. Combined electron paramagnetic resonance (EPR) and mass spectrometric analysis following tryptic digestion demonstrated that spin labels bind site-specifically but are not directed to all five cysteine residues to various preferred and reproducible extents. MTSSL and iodoacetamido-proxyl spin label (IPSL) were 80 and 60% reliably bound to the H strand, respectively, and combined in one spectral component and buried in the protein core. After heat incubation at pH 2 and fractionation, all labeled side chains (peptides) were part of the amyloid and non-amyloid fractions, even if they could not detect amyloid structures. It was assumed that the IPSL-labeled side chains of peptides with Cys^{160} from random coil were incorporated into small non-amyloid aggregates in non-polar environments. After heating at pH 3.5, a rearrangement of the previous α-helix was assumed to shift from the autonomous folding domain during partial unfolding, which improved the accessibility of β-sheets to the water/DMSO-environment. β-sheets were likely densely packed by the accumulation of intermolecular β-sheets, which suggests that amyloid-like structures can be formed from building blocks of the entire primary β-lg structure. Double electron-electron resonance (DEER) confirmed that the spatial distribution of labels within the amyloid-like fraction in a one-dimensional arrangement of the entire protein aggregates was similar to a string of pearls. Thus, SDSL of proteins containing several cysteine residues can be used to gain deep insights into the aggregation mechanism of proteins under food processing conditions.

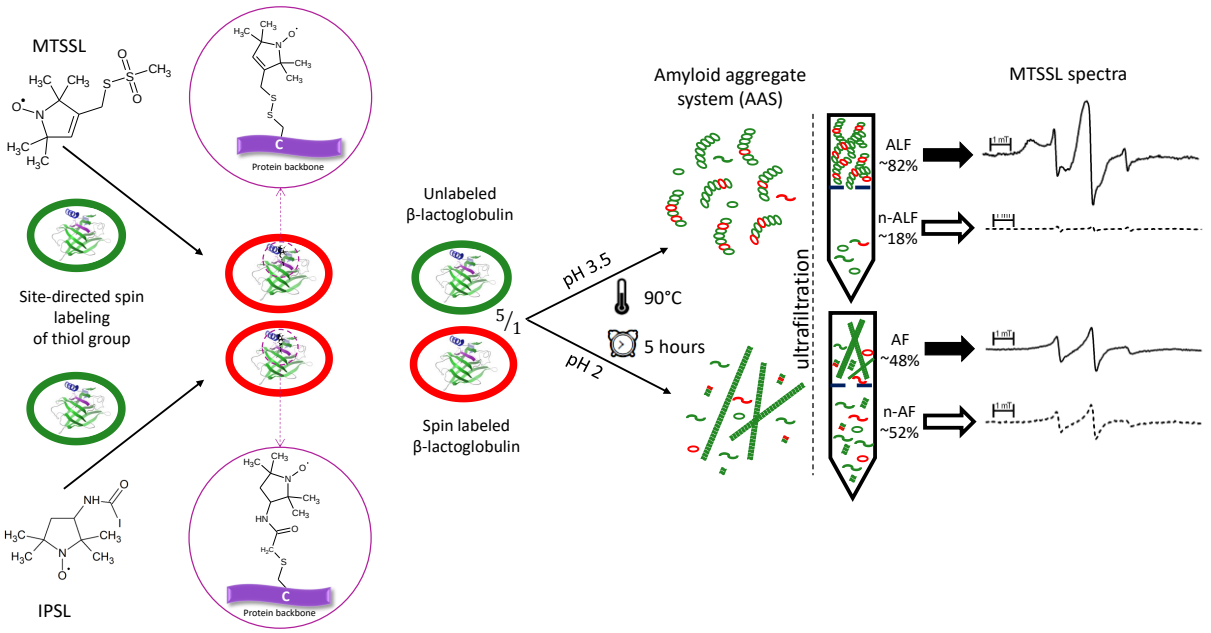

Figure 5-1: Graphical abstract for paper 3

5.2 Introduction

Site-directed spin labeling (SDSL) (Hubbell and Altenbach 1994; Berliner and Reuben 1989) in combination with electron paramagnetic resonance (EPR) spectroscopy is a common method for characterizing the structure and dynamics of proteins, particularly during amyloid aggregation (Drescher 2012a; Török et al. 2002a). SDSL has therefore been used for some time in various areas of structural biology and medicine, e.g. in the Alzheimer's research (Török et al. 2002a; Gu et al. 2016; Sepkhanova et al. 2009; Chen et al. 2007) and other neurodegenerative diseases (Margittai und Langen 2004). Representative examples have been provided by research on amyloid-β aggregates (Sepkhanova et al. 2009; Iuraşcu et al. 2009; Török et al. 2002) and the islet amyloid polypeptide (Jayasinghe and Langen 2004). The line shape in cw EPR spectra of spin-labeled amyloid-β presents several species with different rotational mobilities. Notably, an EPR spectrum typically consists of several superimposed spectra. Spectral simulations provide a quantitative description and allow us to characterize the individual components of the cw EPR spectrum. In the case of amyloid-β, three spectral components with different rotational correlation times (τ_c) were identified and their relative proportions were determined. These spectral components were assigned to large aggregates that are immobilized on the EPR time scale: oligomers with 8–15 molecules (medium rotation, 2.3 ns) and monomeric amyloid-β (fast rotation, 0.12 ns) (Sepkhanova et al. 2009). Utilizing the pulsed EPR technique of double electron-electron resonance (DEER), the frequency of dipolar interaction between paramagnetic centers (i.e., spin labels) can be measured (Milov et al. 1984). This technique provides information regarding the distance between the spin labels and their spatial distribution. This clearly demonstrates that EPR spectroscopy is suitable for studying complex systems where several types of species coexist. However, SDSL has not been applied so far in food chemistry or food biophysics to evaluate the dynamics of non-covalent protein aggregation.

Nitroxides, such as methanothiolsulfonate spin label (MTSSL) and iodoacetamido-proxyl spin label (IPSL), are typically utilized for the SDSL of proteins (Likhtenshtein et al. 2008). One of the common attachment methods involves bonding the label to a cysteine residue. Nitroxides are small in size and thus do not perturb the structure and properties of molecules under study. Given the high sensitivity of continuous-wave (cw) EPR spectra to the rotational mobility of nitroxides in solution (Bordignon 2018), important information regarding the size of spin-labeled proteins and their aggregates can be obtained. The larger the spin-labeled molecule, the slower the rotation of the nitroxide in solution. This effect is most pronounced in nitroxides attached through rigid linkers, while more flexible linkers make nitroxide less responsive to the size of the protein. MTSSL has a high degree of flexibility due to the five rotatable bonds linking it to the protein (Bordignon 2018) and its smaller molecular weight (MW_{MTSSL} = 264.38 Da) compared with IPSL (MW_{IPSL} = 325.17 Da). Due to its flexibility,

MTSSL is able to bind to most thiol groups via a heat-sensitive disulfide bridge without affecting the functionality and native state of the protein (Klare 2012), while IPSL forms a C-S bond toward the protein that is not affected by heating (Klare 2012).

Recently, the combined approach of SDSL and EPR spectroscopy has been successfully utilized to study biomolecules prone to amyloid aggregation. Representative examples have been provided by research on amyloid-β aggregates (Iuraşcu et al., 2009; Sepkhanova et al., 2009a; Török et al., 2002) and the islet amyloid polypeptide (Jayasinghe & Langen, 2004). The line shape in cw EPR spectra of spin-labeled amyloid-β presents several species with different rotational mobilities. Notably, an EPR spectrum typically consists of several superimposed spectra. Spectral simulations provide a quantitative description and allow us to characterize the individual components of the cw EPR spectrum. In the case of amyloid-β, three spectral components with different rotational correlation times (τ_c) were identified and their relative proportions were determined. These spectral components were assigned to large aggregates that are immobilized on the EPR time scale: oligomers with 8–15 molecules (medium rotation, 2.3 ns) and monomeric amyloid-β (fast rotation, 0.12 ns) (Sepkhanova et al., 2009). This clearly demonstrates that EPR spectroscopy is suitable for studying complex systems where several types of species coexist.

Utilizing the pulsed EPR technique of double electron-electron resonance (DEER), the frequency of dipolar interaction between paramagnetic centers (i.e., spin labels) can be measured (Milov, Ponomarev, & Tsvetkov, 1984). This technique provides information regarding the distance between the spin labels and their spatial distribution.

β-lactoglobulin (β-lg), the major whey protein in bovine milk, is of concern for cysteine-specific spin labeling. The natural primary structure of β-lg contains five cysteine residues that could serve as a natural binding site for spin labels. Cys^{121} is postulated as a free cysteine residue with a high propensity to interact with ligands (Burova et al., 1998) such as the bioactive organosulfur compounds allyl isothiocyanate or allicin (Keppler et al., 2014; Rade-Kukic et al., 2011; Wilde, Keppler et al., 2016), while the other four cysteine residues form disulfide bridges (Cys^{66}-Cys^{160} and Cys^{106}-Cys^{119}). Cys^{66}-Cys^{160} is located close to the C-terminus on the surface of the protein, while Cys^{106}-Cys^{119} is located in the core of the protein between two β-sheets. However, it is known that these bioactive compounds can shuffle to other cysteine residues at pH 8.5, and are thus not only located at position 121 (Keppler et al., 2014; Wilde, Keppler et al., 2016), which is close to the pH value used to achieve optimal spin labeling efficiency (Lux et al. 2021). Keppler et al. (2014) discovered that this effect is due to the ability of allyl isothiocyanate to cleave the disulfide bridge Cys^{66}-Cys^{160}. Thus, the spin labels could potentially label different parts of the protein. Additionally, β-lg exists in numerous genetic variants, with the genetic variants A (containing Asp^{64} and Val^{118}) and B (containing Gly^{64} and Ala^{118}) being the most common, with both being present

in bovine milk (Aschaffenburg and Drewry, 1957). In particular, the point mutation at position 118 is very close to the main binding site (Cys^{121}) and may thereby affect the microenvironment of any spin label. To verify the binding position of ligands, Wilde et al. (Wilde, Keppler et al., 2016) used mass spectrometric measurements after tryptic digestion of the modified protein. Since trypsin cleaves the protein after the basic amino acids lysine and arginine, defined peptides are obtained that can then be identified based on their individual masses including the mass shift of one or more ligands.

At high temperatures (>70°C) and low ionic strength over a period of several hours, β-lg forms functional amyloid aggregates (Akkermans, Venema et al., 2008), whereas the conversion rate, building blocks, and morphology are functions of the pH value (Keppler et al., 2019). During a 5-hour incubation at 90°C, 30–40% long semi-flexible fibrils consisting of smaller peptides were formed at pH 2, while short worm-like aggregates comprising the entire protein were produced at pH 3.5 30–45% (Heyn et al., 2019; Keppler et al., 2019). Ultrafiltration techniques (MWCO: 300 kDa) were used to fractionate the mixed amyloid aggregate systems (AAS), yielding the retentate as the amyloid fraction (AF) containing fibrils at pH 2 or the amyloid-like fraction (ALF) consisting of worm-like aggregates at pH 3.5. At both pH values, the permeate is referred to as the non-amyloid fraction (n-AF) or the non-amyloid-like fraction (n-ALF), which likely consists of non-amyloid(-like) aggregates and peptides smaller than the molecular weight cut-off used (Akkermans, Venema et al., 2008; Heyn et al., 2019). In a previous study, we demonstrated that β-lg can be spin labeled with either MTSSL or IPSL without altering the amyloid aggregation at pH 2 and pH 3.5 when compared to unlabeled protein. To understand the amyloid aggregation process and investigate the influence of spin labeling on amyloid aggregation, potential changes in hydrophobicity, building blocks, and aggregate morphology caused by SDSL were studied in detail (Lux et al., 2021). However, to date, it has not been possible to clarify whether spin-labeled peptides, which contain Cys^{121} as the main target labeling position for MTSSL, are included in the amyloid and amyloid-like structures or are rather part of the unincorporated building blocks. According to (Akkermans, Venema et al., 2008), the Cys^{121} residue was found in both AF and n-AF, while (Hettiarachchi et al., 2012) could not find the Cys^{121} containing peptide in the AF.

To gain deep insights into the aggregation mechanism of β-lg under food processing conditions, we used site-specific spin-labeling for the first time in food science. In contrast to common practice, we hypothesize that SDSL is possible at the five intrinsic cysteines of the natural bovine β-lg, without manipulating the positions and number of cysteine residues. We thus evaluate the labelling affinities of two different cysteine binding spin labels such as MTSSL and IPSL. This technique will contribute to the elucidation of individual amyloid and amyloid-like aggregation mechanisms, depending on the β-lg building blocks that are specific

peptides or the entire protein. For this purpose, aggregation of spin-labelled β-lg is performed at pH 2 (amyloid aggregation) and pH 3.5 (amyloid-like aggregation), during 5 hour thermal treatment. Following this, the sample is fractionated by ultrafiltration to separate the amyloid and non-amyloid material. The recorded cw-EPR spectra of the labelled fractions will be simulated with the EasySpin tool for each fraction, to obtain information about the individual components of the superimposed EPR spectra. The exact binding sites of the spin labels to the peptide/protein sequence and the incorporation of the labeled protein side chains into the amyloid or non-amyloid fraction will be evaluated by conducting tryptic digestion and mass spectrometric analysis of the proteins.

5.3 Materials and Methods

5.3.1 Materials

β-lactoglobulin (β-lg) was purchased from Davisco Foods International (Eden Prairie, Minnesota, USA) with 97% protein and 96% β-lg in dry matter. The calculated NaCl content was 0.29%. MTSSL (1-oxyl-2,2,5,5-tetramehtylpyrroline-3-methyl) methanethiosulfonate was purchased from Enzo Life Science Inc. (Farmingdale, NY, USA) with a purity of ≥98%. IPSL 3-(2-Iodoacetamido)-PROXYL, formic acid, iodoacetamide (IAA), and triethylammonium acetate (TEAA) were purchased from Sigma-Aldrich (St. Louis, USA). Ultrapure water, acetonitrile, (ACN) and trypsin were purchased from Carl Roth GmbH & Co. KG (Karlsruhe, Germany).

5.3.2 Sample preparation

5.3.2.1 Spin labeling

The samples were prepared as described by Lux et al. (2021). Unless otherwise stated, β-lg was dissolved in milli-Q water and stirred to a final protein concentration of 5 wt% until complete hydration. For the tryptic digestion, only 1% protein was dissolved and labeled. The pH value was adjusted to 7.5 for MTSSL and to 8.5 for IPSL with sodium hydroxide (NaOH), with a labeling rate of ~50% being achieved for IPSL. The spin labels were pre-dissolved in DMSO and each was incubated with the same amount of DMSO (~0.42% DMSO) with β-lg in an equimolar ratio (MTSSL) or in 2.5-fold molar excess (IPSL) overnight at 4 °C in the dark. To avoid spin-spin interactions, the spin-labeled samples were then diluted 1:5 with unlabeled, pH-adjusted β-lg solutions. The remaining unbound spin label was removed by desalting (Sephadex G-25, PD-10 Desalting Column, GE Healthcare, Solingen, Germany), which includes a dilution step to achieve an estimated protein concentration of 2.5%. The exact protein concentration was measured as described in Lux et al. (2021). All samples were prepared in triplicate.

5.3.2.2 Amyloid aggregation

For amyloid aggregation, the pH value of the labeled samples was set to 2 or 3.5 with HCl. A 5-hour incubation at 90°C was performed using a water proof magnetic stirrer (2mag AG, Munich, Germany). Thereafter, the samples were cooled on ice and stored at 4°C until further use. These samples contain amyloid/amyloid-like aggregates as well as non-amyloid proteins and peptides and were thus named the AAS at pH 2 or the amyloid-like aggregate system (ALAS) at pH 3.5.

5.3.2.3 Fractionation by ultrafiltration

To separate the amyloid aggregates from the unconverted peptides, the heated AAS/ALAS samples were diluted 5-fold and filtered four times with an ultrafiltration centrifugal concentrator (Vivaspin 20, 300,000 Da, PES, Sartorius, Göttingen, Germany) for 15 min at 1000*g. Unless otherwise specified, the retentate was refilled to the initial volume (AF/ALF) after the final filtration step and used without further treatment. The permeate of each filtration step was combined as the total permeate (n-AF/n-ALF).

For DEER measurements, which were only conducted for the ALF, 20% (v/v) of glycerol was added to the ALF and thoroughly mixed. Then, 10 µl of the obtained mixture was transferred into a quartz glass tube (2 mm /3 mm i.d./o.d.), shock-frozen in liquid nitrogen, and kept at -80^{o}C until further use.

5.3.3 Tryptic digestion for LC-MS measurements

To identify the labeled cysteine residues, the labeled protein samples (as described in Section 2.2.1) were subjected to tryptic digestion prior to mass spectrometric measurement. An unlabeled β-lg sample served as the control. Then, 360 µl of the protein solution (1 wt%) was alkylated with 48 µl IAA (400 mM). The mixture was incubated for 30 min at 25°C in the dark. The digestion was then performed using 60 µl of trypsin solution (1.5 mg/ml) at pH 7. To adjust the pH value, 133 µl TEAA (0.25 M, pH 7) was added. The samples were incubated at 37°C for 18 h to ensure complete tryptic digestion.

For the LC-MS measurement, samples were diluted to 0.015 wt% protein with ultrapure water. The measurements were conducted at a microTOF-QII mass spectrometer (Bruker Daltonik, Bremen, Germany) with an electrospray ionization (ESI) source. Mass spectra over the mass range of 200–3000 m/z were acquired in positive ion mode. Ultrapure nitrogen was used as a nebulizer and dry gas (1 bar and 210°C). MS-specific parameters were as follows: capillary voltage 4.5 kV, ion energy 2.0 eV, funnel 1 and 2 RF 300 and 350 Vpp, collision RF 850 Vpp, Hexapole RF 400 Vpp, collision cell filled with nitrogen and a collision energy of 5 eV, transfer time 120 µs, and pre-pulse storage 15 µs. Calibration of the instrument and an

external recalibration of the acquired mass spectra were performed using ESI TOF Tuning Mix (Agilent Technologies, Waldbronn, Germany).

The mass spectrometer was coupled to a Dionex Ultimate 3000 HPLC system (Thermo Fisher Scientific, Waltham, USA) equipped with a Nucleodur C18 Gravity column (100 mm x 2 mm, 1.8 µm particle size, Macherey-Nagel, Berlin, Germany). For the separation, a gradient of ultrapure water with 0.1% formic acid (eluent A) and 80% ACN with 0.1% formic acid (eluent B) was used. The applied gradient was 5% B (0–1 min), 5–15.5% B (1–5 min), 15.5–28% B (5–13.5 min), 28–35% B (13.5–27.5 min), 35–95% B (27.5–28.5 min), 95% B (28.5–32 min), 95–5% B (32–33 min), and 5% B (33–38 min). The injection volume was 5 µl at a flow rate of 0.3 ml/min. The temperature of the column was set at 30°C.

Evaluation of the acquired MS data was conducted using Data Analysis 4.0 (Bruker Daltonics, Bremen, Germany). The presence of MTSSL and IPSL peptides were assigned manually. All five cysteine residues were assumed as possible binding sites. The expected peptides after tryptic digestion with or without IPSL or MTSSL were calculated using the database UniProtKB/SwissProt (PO2754) (“UniProt,” 2019). The respective detected m/z values were matched with theoretical calculated m/z values. Moreover, matching of the measured isotope distribution with the simulated isotope distribution (mSigma value) was used to verify the correct assignment of the peptides.

5.3.4 EPR measurements

5.3.4.1 cw measurements and simulation

The spectra of spin-labeled proteins were recorded using an H-Q-sensitive resonator (Bruker, Rheinstetten, Germany) at room temperature on an Elexsys E500 EPR spectrometer (Bruker, Rheinstetten, Germany) at 9.85 GHz (X-band). The experimental settings were adjusted to avoid saturation and overmodulation. The typical experimental setting included a modulation frequency of 100 kHz, modulation amplitude of 0.1 mT, a time constant of 81.92 ms, conversion time of 81.96 ms, microwave power of 20 mW, center field of 351.19 mT, and a sweep width of 10 mT. Depending on the concentration, 5 to 20 scans were acquired to improve the signal-to-noise ratio.

The cw EPR spectra were simulated using the EasySpin (Stoll & Schweiger, 2006) software package for Matlab. The g-tensor was set to [2.0090 2.0059 2.0025] and the A-tensor was [8 8 100] MHz. The rotational correlation time was fitted, while small variations of the g-tensor and A_{zz} were allowed. A_{zz} values above the standard value of 100 MHz did not result in an improved fit. An intrinsic linewidth was set to 0.15 mT. The mean values and standard deviations were calculated from the fits to the spectra, as measured for three independent sample preparations. To obtain values of micro polarity that can be compared with literature

data, the z-component of the A-tensor (A_{zz}) was further converted from frequency units (ν) in MHz to magnetic field units (B) of mT (Equation 6).

Equation 6: Converting mT in MHz

$$B[mT] = 10^9 \frac{h}{g\mu_B} \nu[MHz] \qquad (6)$$

5.3.4.2 DEER measurements and analysis

DEER measurements were performed at 50 K on an Elexsys E580 spectrometer (Bruker, Rheinstetten, Germany) at 33.88 GHz (Q band). An EN5107D2 Q-band resonator (Bruker, Rheinstetten, Germany) was used. The microwave pulses were amplified with a 10 W solid-state amplifier. Temperature control was realized in a CF935O cryostat equipped with an ITC503 temperature controller (both from Oxford Instruments). A four-pulse dead-time free DEER sequence (Pannier, Veit, Godt, Jeschke, & Spiess, 2000) was applied: $\pi/2_{(obs)} - \tau_1 - \pi_{(obs)} - \tau_1+t - \pi_{(pump)} - \tau_2-t - \pi_{(obs)} - \tau_2 -$ echo. The pump frequency was set to the maximum of the nitroxide absorption spectrum and the observer frequency was shifted 70 MHz lower. The lengths of the microwave pulses were $\pi/2_{(obs)}$ = 22 ns, $\pi_{(obs)}$ = 44 ns, and $\pi_{(pump)}$ = 60 ns. The time delays were τ_1 = 400 ns and τ_2 = 1.5 µs. The typical acquisition time was 16 hours.

DEER data were processed using the DeerAnalysis2018 software package (Jeschke et al., 2006) for Matlab.

5.3.5 Statistical analysis

All results were presented as mean values and standard deviations from nine values. Spectra for three independent sample preparations were recorded and each spectrum was fitted three times, The data were analyzed separately for each spectral component by two-way ANOVA with Tukey's multiple comparison test at a significance level of α=0.05. All statistics and figures were created using GraphPad Prism (version 8.3.0, GraphPad Software, San Diego, CA, USA).

5.4 Results and Discussion

5.4.1 Spin-labeled cysteine residues of natural β-lg

Bovine β-lg naturally contains five cysteine residues and can occur in many different genetic variants. This is in contrast to proteins that are typically used for SDSL since the position of the label cannot be predicted in the presence of several cysteine residues (Kirby et al., 2004; Margittai & Langen, 2004). For this reason, the primary protein structure is usually manipulated prior to SDSL so that only one cysteine residue is present in the desired position

(Gu et al., 2016; Sepkhanova et al., 2009; Török et al., 2002). Such interventions subsequently change the secondary and tertiary structures of a protein so that the aggregation behavior may be different from that of the natural protein. Therefore, the present study focuses on the application of SDSL for food proteins while explicitly avoiding manipulation of the amino acid sequence and using β-lg as a natural protein.

5.4.1.1 Spectral components of spin-labeled β-lactoglobulin obtained by simulation

To achieve a high labeling rate, β-lg was labeled with MTSSL at pH 7.5 and with IPSL at pH 8.5 before the pH was adjusted to pH 2 or 3.5 for aggregation studies (Lux et al. 2021). Prior to the amyloid aggregation, the cw EPR spectra of MTSSL-labeled β-lg indicated an overall slower nitroxide motion at these pH values when compared to β-lg spin labeled with IPSL (Figure 5-2).

Regardless of the pH value, for the same spin label, the experimental spectra appeared very similar. A quantitative description of the experimental spectra was provided by spectral simulations (Table 5-1). Under the assumption of isotropic rotation, all spectra can be described by a superposition of three nitroxide components with different rotational correlation times (τ_c) corresponding to the time the electron-bearing moiety requires to rotate around itself. The lower the τ_c, the faster the mobility of the molecule since it is not restricted by the nearby chemical microenvironment.

The spectral component designated as C(f) (“f” stands for “free”) was identified as the component corresponding to the free nitroxide spin label in solution. The rotational correlation time of 0.03 ns was initially determined from the spectrum of a free nitroxide in solution and used for fitting the spectra of spin-labeled β-lg. The contribution of C(f) did not exceed a few percent (d: ~0.6% for MTSSL and 1.6–3.5% for IPSL) of the total spectrum of labeled β-lg, which indicates an incomplete removal step that can be easily accounted for in the spectral simulation. The z-component of the anisotropic hyperfine coupling tensor A (A_{zz}) is the most sensitive spectral parameter for the polarity of the microenvironment and for interactions with surrounding molecules. This implies that A_{zz} is an indicator of the polarity and proticity of the solvent, with a value of less than 3.69 mT indicating a lower solvent micropolarity than water (Owenius, Engström, Lindgren, & Huber, 2001). As a reference, MTSSL and IPSL were dissolved in DMSO/water (~0.42% DMSO) without protein, for which an A_{ZZ} value of 3.57 mT could be simulated (data not shown) (Owenius et al., 2001; Savitsky, Kühn, Duché, Möbius, & Steinhoff, 2004). The other two spectral components, C(b_1) and C(b_2) represented a slower rotation of the nitroxide and were attributed to the spin label bound to β-lg. The slowest spectral component, C(b_1), was characterized by τ_c values in the range of 6.3–8.7 ns and had the highest contribution to the spectrum, which was significantly higher for MTSSL (d: ~80%) compared to IPSL (d: ~60%) (Table 5-1). The values of A_{zz} were

3.35–3.46 mT and resemble a membrane-like microenvironment (Steinhoff et al., 1999) with a considerably lower polarity compared to water. The second bound component, $C(b_2)$, reported an intermediate rotational motion of a nitroxide and exhibited τ_c values close to 1 ns, which was significantly faster for IPSL (τ_c ~ 0.7 ns) compared to MTSSL (τ_c = 1.6-2.2 ns). The corresponding contributions to the total spectrum differed significantly, with ~18% for MTSSL and ~35% for IPSL—both spin labels being in a DMSO/water environment as determined for the control sample (Table 5-1). Due to the presence of two components in both spin labels and the fact that both spin labels $C(b_1)$ have a higher proportion, lower mobility, and lower polarity compared to $C(b_2)$ indicates that—with both spin labels—the two components reflected the same microenvironment.

Generally, the parameters of the individual components were more dependent on the spin label than on the pH value, which is in agreement with the overall appearance of the EPR spectra. Notably, the MTSSL spectra displayed a slower motion of the spin label than IPSL spectra. This could be due to the tighter interaction between the spin label and the side chain caused by the smaller size and lower flexibility of MTSSL compared to IPSL (Owenius et al., 1999). The spectral component $C(b_1)$ indicated a membrane-like microenvironment for both nitroxides. Taken together, this provides evidence that the IPSL (Hammarström, Owenius, Mårtensson, Carlsson, & Lindgren, 2001) and MTSSL spin labels might be buried in the β-lg interior. The individual components of the MTSSL-labeled sample represented more restricted mobilities, which was significant at pH 3.5 and only significant for $C(b_2)$ at pH 2 (Table 5-1). This could suggest that MTSSL is either more strongly integrated into the protein—or integrated at a higher content—than IPSL since the contribution of MTSSL to $C(b_1)$ was more pronounced. The pH dependency of the side chain mobility could be caused by the dimerization of β-lg at pH 3.5. In the acid pH range (~pH 2), β-lg is present as a monomer, whereas β-lg is mainly present as a dimer between pH 3 and pH 7.5 (Rade-Kukic et al., 2011; Shimizu et al., 1984; Uhrínová et al., 2000), which possibly leads to a lower side-chain mobility at pH 3.5.

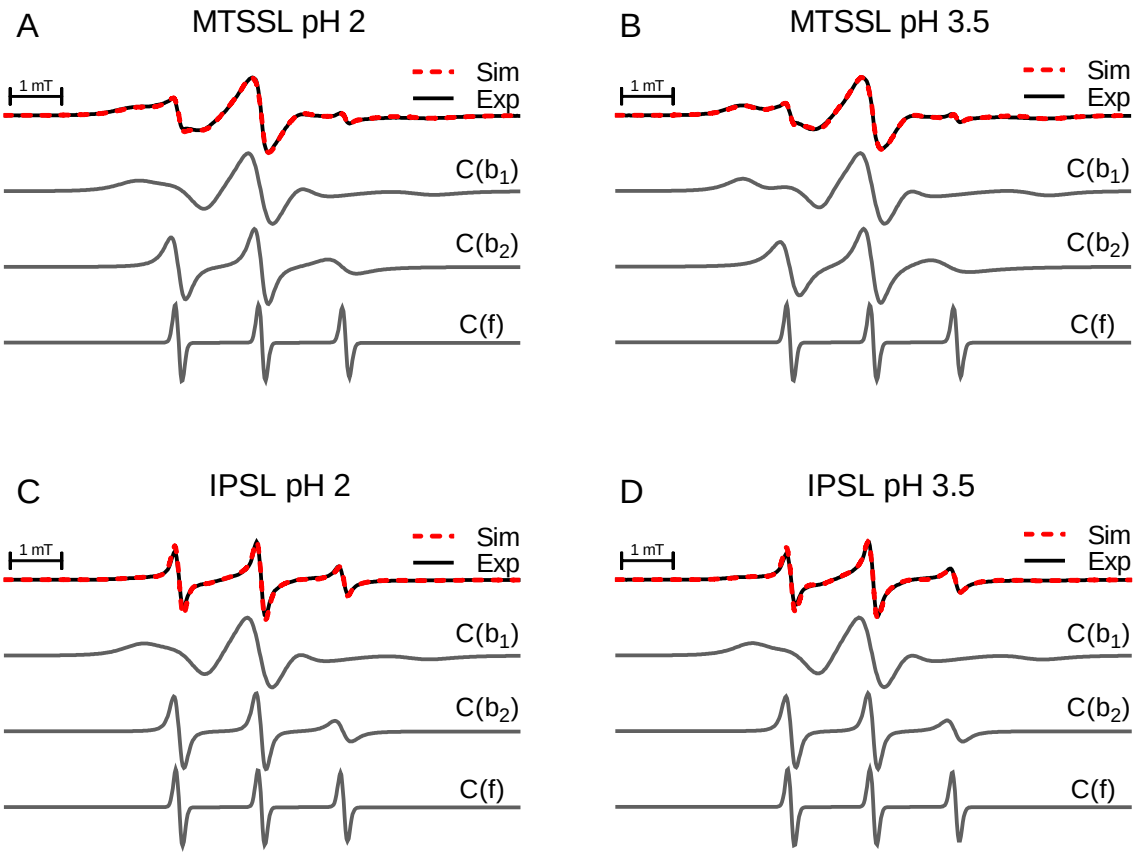

Figure 5-2: cw EPR spectra of β-lg spin labeled with MTSSL (A and B) and IPSL (C and D). The labeling was conducted at pH 7.5 (MTSSL) or pH 8.5 (IPSL). The spin label excess was removed and the pH was set to pH 2 (A and C) or 3.5 (B and D). Spectra were simulated by EasySpin, where the simulation (red) clearly indicates the coexistence of three individual spectral components (gray) attributed to two bound components and one free nitroxide component that differ in rotation correlation times. The corresponding parameters are presented in Table 5-1. All spectra are normalized to the maximum.

Table 5-1: Characteristic parameters of individual components in the EPR spectra by EasySpin simulation of spin labeled β-lg at pH 7.5 (MTSSL) or pH 8.5 (ISPL), the excess spin label was removed and the pH set to pH 2 or 3.5. Spectral components, such as rotational correlation time (τ_c), micro polarity (A_{zz}), and the proportion of the component (d) were assigned to bound nitroxide spin labels, C(b_1), C(b_2), and unbound nitroxides which were freely tumbling in solution C(f). (n=3, ANOVA)

		MTSSL		IPSL	
		pH 2	pH 3.5	pH 2	pH 3.5
		mean ± SD	mean ± SD	mean ± SD	mean ± SD
C(b_1)	τ_c [ns]	6.30 ± 0.12^a	8.71 ± 0.17^b	6.33 ± 0.69^a	6.89 ± 0.02^c
	d [%]	82.3 ± 1.2^a	80.3 ± 0.8^b	60.1 ± 1.5^c	65.3 ± 1.0^d
	A_{zz*} [mT]	3.46	3.43	3.35	3.35
C(b_2)	τ_c [ns]	1.64 ± 0.07^a	2.25 ± 0.03^b	0.74 ± 0.04^c	0.75 ± 0.01^c
	d [%]	17.0 ± 1.1^a	19.1 ± 0.8^b	36.4 ± 1.3^c	33.1 ± 0.8^d
	A_{zz*} [mT]	3.57	3.57	3.57	3.57
C(f)	τ_c [ns]	0.03 ± 0.00^a	0.03 ± 0.00^a	0.03 ± 0.00^a	0.03 ± 0.00^a
	d [%]	0.7 ± 0.0^a	0.6 ± 0.0^a	3.5 ± 0.3^b	1.6 ± 0.2^{ab}
	A_{zz*} [mT]	3.57	3.57	3.57	3.57

Different letters indicate significant differences between the fractions. Each component were considered separately.

*All SDs of A_{zz} were zero, so they are not presented separately for clarity.

5.4.1.2 Assignment of different dynamic modes by identifying the binding position of labels within the β-lg

Two components, C(b_1) and C(b_2), were identified in the EPR spectra (5.4.1.1) of spin-labeled β-lg. These two spectral components were reported on spin labels that displayed different rotational mobilities (τ_c) and were exposed to the environment with different polarities (A_{ZZ}) (Table 5-1). This suggests that these two components are attributed to different microenvironments caused by the protein. Importantly, the EPR spectra of denatured β-lg featured only a single component (Figure 5-7) and were evident for one type of environment for all spin labels in the sample. This implies that two spectral components (5.4.1.1) were linked to the β-lg in the folded state. Regarding the origin of these spectral components and different microenvironments, the role of the two genetic variants of β-lg—A and B—was examined. The purified genetic variants A and B were spin labeled with MTSSL or IPSL and exhibited EPR spectra that resembled those in presented Figure 5-2.

Additionally, the spectral components were identified to be the same (Figure 5-8), which proves that the spin labeling for both genetic variants of β-lg occurred at the same binding sites and was not affected by the minor structural changes of the genetic variances.

Furthermore, the two different mobility states could result from the different binding sites of the spin labels within the protein. This was examined in detail via mass spectrometry. The tryptic digestion of β-lg led to a large number of peptides since trypsin selectively cleaves the peptide sequences according to the basic amino acids arginine and lysine (Fernández & Riera, 2013). Since MTSSL and IPSL bind to the free thiol groups of the cysteine residues, only the cysteine-containing peptides of β-lg were considered. Without reduction of the disulfide bridges, three of the resulting peptides contain cysteine residues. Peptide 61-69 contained Cys^{66} (Figure 5-3A, *blue* symbols), while peptide 102-124 contained Cys^{106}, Cys^{119}, and Cys^{121} (Figure 5-3, *green* symbols), and peptide 149-162 contained Cys^{160} (Figure 5-3, *orange* symbols). As previously described, spin labeling with MTSSL resulted in a mass shift of 184 Da, while binding of IPSL to β-lg exhibited a mass shift of 197 Da (Lux et a. 2021). Moreover, it was observed that both spin labels were bound to all three aforementioned peptides (Table 5-2). Based on the observed signal intensities, MTSSL was found to bind mainly at the peptide 102-124 (Cys^{106}, Cys^{119}, Cys^{121}), whereas IPSL binds predominantly to the peptides 61-69 (Cys^{66}) and 149-162 (Cys^{160}) (Table 5-2). A comparison of the intensity of the spin-labeled peptides 61-69 and 149-162 with peptide 102-124 resulted in a ratio of ~1:22 for MTSSL and ~22:1 for IPSL. However, the mass spectrometry data unambiguously demonstrated that only one spin label was bound to the 102-124 peptide (Figure 5-3A, *green* symbols). Using this method, it was not possible to identify which of the three cysteines in the peptide 102-124 was actually labeled since the intensity of most peptides was too low to conduct MS/MS measurements. In this context, the mSigma value was used to verify the correct assignment of peptides, with lower values indicating a better fit (Table 5-2). The lower the signal intensity, the fewer isotopes can be measured, and thus the mSigma value increases. Since no significant differences in the EPR spectra were expected due to the spatial proximity of the three cysteine residues, which cysteine residue of the 102-124 peptide the spin label was bound was not relevant. The different contributions and polarities of the two spin labels (Table 5-1) were in good agreement with MS measurements. In the case of MTSSL-labeled protein, ~80% of the spectra was attributed to $C(b_1)$, thereby suggesting that ~80% of the spin label was bound to peptide 102-124 (Figure 5-3A, *green* symbols). The MS measurements supported this suggestion since the signal corresponding to the MTSSL-labeled peptide 102-124 had the highest signal intensity of all MTSSL-labeled peptides (Table 5-2). In the case of IPSL-labeled β-lg, $C(b_1)$ contributed to only ~60% of the spectra, thereby suggesting that ~60% of the spin labels were bound to peptide 102-124. The signal of this peptide had the lowest intensity among the MS measurements compared

to other IPSL-labeled peptides (Table 5-2), which suggests that fewer IPSL molecules were bound to the 102-124 peptides compared to MTSSL.

Peptide 102-124 (Figure 5-3A, *green* symbols) was assigned to the component C(b_1) with the highest contribution in the EPR spectrum (Table 5-1), which had the slowest rotational mobility (τ_c: ~6.3-8.7 ns) and the lowest polarity (3.35-3.46 mT). Cys^{106}, Cys^{119}, and Cys^{121} were located in the β-stands G and H, which—together with the β-stand F and the α-helix—form an autonomous folding domain with a high content of hydrophobic amino acids (Kuwata et al., 2001) (Figure 5-3B). All three cysteine residues were located outside of the β-barrel formed by the β-sheets. Hence, it is plausible that they had such similar side chain mobility that they could be grouped under one component in the simulation. In contrast, the cysteine residues Cys^{66} and Cys^{160} were located in one of the outer loops (Figure 5-3A, *blue* and *orange* symbols) on the surface close to the C-terminus (Hoffmann & van Mil, 1997), where they are located in spatial proximity in the tertiary protein structure (Table 5-1 and Figure 5-3B). Accordingly, it could be assumed that C(b_2) represented the spin labels bound at Cys^{66} and Cys^{160}, which had faster rotational mobility (τ_c: ~0.7-2.3 ns) and exposure to a polar microenvironment equivalent to that of a water/DMSO mixture (A_{ZZ}: 3.57 mT) (Table 5-1).

The proven spin labeling of multiple cysteines within β-lg could be caused by differing affinities among the spin labels to different cysteines. For example, a similar C-S bond to that found for IPSL and Cys^{121} or Cys^{66} has been reported between allyl isothiocyanate and cysteine residues (Keppler et al. 2014). However, other molecules that interact via S-S bonding (e.g., allicin) preferred an initial binding with Cys^{121} (Wilde et al. 2016). However, thiol exchange reactions are also possible, which are known to occur in proteins with more than one disulfide bridge at basic pH values (Gilbert, 1995). The exchange rate particularly depends on the concentration of the thiolate anion so that alkaline pH values increase the shuffling effect, whereas this effect does not occur at acidic pH values (Creighton, 1980; McKenzie et al., 1972a; Phelan & Malthouse, 1994). Since a pH value of 7.5 for MTSSL and 8.5 for IPSL is required for efficient binding of the label via the thiol groups (Lux et al. 2021), it is likely that a shuffling of the label to various cysteine residues has occurred during the labeling process. The pH value was acidified to pH 7 after labeling for tryptic digestion to ensure sufficient enzymatic activity. Since the labeling rate of β-lg with MTSSL was already very low at this pH value (Lux et al. 2021) and hardly possible with IPSL (data not shown), it can be assumed that further shuffling during mass spectrometric analysis was unlikely. The higher labeling rate of Cys^{66} and Cys^{160} with IPSL when compared to MTSSL may be caused either by a higher shuffle effect due to the higher pH value or by the fact that it has a higher binding propensity to Cys^{66} based on C-S binding (Rade-Kukic, Schmitt, & Rawel, 2011c). A

previous study used mass spectrometric results to demonstrate that only one MTSSL molecule was bound to one β-lg molecule (Lux et al. 2021). In combination with the results from Table 5-2, it can be concluded that peptide 102-124, which carried the formally free cysteine residue at position 121, is also the main binding position for the spin label MTSSL. Since it could also be proven for IPSL that only one spin label molecule was bound to one β-lg molecule and a stronger shuffling effect must be considered, it is plausible that the labeling of β-sheets and the outer loop can be performed in a similar ratio to each other. By exploiting the different preferences of MTSSL and IPSL toward cysteine positions within β-lg, divergent and complementary information can be obtained from EPR studies of the amyloid aggregation of β-lg.

Table 5-2: Identified peptides after tryptic digestion and mass spectrometry measurements of β-lg spin labeled with MTSSL or IPSL at molar ratios of 1:1 and 1:2.5, respectively, with the subsequent removal of spin label excess. Only the cysteine-containing peptides are presented.

Residues	Peptide	Cysteine residue	Genetic Variant	Charge [z]	Absolute intensity [cts]	m/z	mSigma
	Unlabeled β-lg						
61-69	WENDE**C**^{66}AQK	IAA	A	2	413 ± 31	590.24 ± 0	98.8 ± 45.1
61-69	WENGE**C**^{66}AQK	IAA	B	2	321 ± 20	561.24 ± 0	123.3 ± 2.0
149-162	LSFNPTQLEEQ**C**^{160}HI	IAA	A/B	2	2392 ± 221	858.41 ± 0	20.93 ± 9.6
102-124	YLLF**C**^{106}MENSAEPEQSLV**C**^{119}Q**C**^{121}LVR	Disulfide, IAA	A	3	625 ± 114	910.76 ± 0	105.47 ± 46.6
102-124	YLLF**C**^{106}MENSAEPEQSLa**C**^{119}Q**C**^{121}LVR	Disulfide, IAA	B	3	516 ± 129	901.41 ± 0	74.97 ± 17.9
61-69 + 149-162	WENDE**C**^{66}AQK+LSFNPTQLEEQ**C**^{160}HI	Disulfide	A	4	174,261 ± 3,894	695.31 ± 0.01	5.53 ± 4.6
61-69 + 149-162	WENGE**C**^{66}AQK+LSFNPTQLEEQ**C**^{160}HI	Disulfide	B	4	132,340 ± 3,905	680.81 ± 0	8.73 ± 1.7
	MTSSL labeled β-lg						
61-69	WENDE**C**^{66}AQK	IAA	A	2	260 ± 24	590.23 ± 0.03	135.6 ± 19.2
61-69	WENGE**C**^{66}AQK	IAA	B	2	224 ± 29	561.22 ± 0.02	121.37 ± 14.1
149-162	LSFNPTQLEEQ**C**^{160}HI	IAA	A/B	2	1482 ± 115	858.4 ± 0.02	34.53 ± 14.7
102-124	YLLF**C**^{106}MENSAEPEQSLV**C**^{119}Q**C**^{121}LVR	Disulfide, IAA	A	3	1220 ± 198	910.75 ± 0.01	51 ± 27.4
102-124	YLLF**C**^{106}MENSAEPEQSLa**C**^{119}Q**C**^{121}LVR	Disulfide, IAA	B	3	505 ± 58	901.4 ± 0.01	68.03 ± 15.7
61-69 + 149-162	WENDE**C**^{66}AQK+LSFNPTQLEEQ**C**^{160}HI	Disulfide	A	4	181,953 ± 3,027	695.3 ± 0.02	7.33 ± 2.2
61-69 + 149-162	WENGE**C**^{66}AQK+LSFNPTQLEEQ**C**^{160}HI	Disulfide	B	4	137,248 ± 7,138	680.8 ± 0.02	6.27 ± 1.0
61-69	WENDE**C**^{66}AQK	MTSSL	A	2	585 ± 44	653.76 ± 0.03	136.57 ± 28.4
61-69	WENGE**C**^{66}AQK	MTSSL	B	2	320 ± 46	624.75 ± 0.03	109.9 ± 36.3
149-162	LSFNPTQLEEQ**C**^{160}HI	MTSSL	A/B	2	745 ± 27	921.93 ± 0.01	75.9 ± 15.5
102-124	YLLF**C**^{106}MENSAEPEQSLV**C**^{119}Q**C**^{121}LVR	Disulfide, MTSSL	A	3	25,391 ± 1,300	953.1 ± 0.01	15.87 ± 3.3
102-124	YLLF**C**^{106}MENSAEPEQSLA**C**^{119}Q**C**^{121}LVR	Disulfide, MTSSL	B	3	8,953 ± 1,948	943.76 ± 0.01	35.07 ± 5.2
	IPSL labeled β-lg						
61-69	WENDE**C**^{66}AQK	IAA	A	2	563 ± 179	590.24 ± 0	96.37 ± 44.6
61-69	WENGE**C**^{66}AQK	IAA	B	2	449 ± 130	561.24 ± 0	63.4 ± 43.4
149-162	LSFNPTQLEEQ**C**^{160}HI	IAA	A/B	2	4,002 ± 1579	858.4 ± 0	20.97 ± 7.5
102-124	YLLF**C**^{106}MENSAEPEQSLV**C**^{119}Q**C**^{121}LVR	Disulfide, IAA	A	3	512 ± 110	910.76 ± 0	279.03 ± 103.0
102-124	YLLF**C**^{106}MENSAEPEQSLa**C**^{119}Q**C**^{121}LVR	Disulfide, IAA	B	3	508 ± 92	901.4 ± 0	117.3 ± 19.1
61-69 + 149-162	WENDE**C**^{66}AQK+LSFNPTQLEEQ**C**^{160}HI	Disulfide	A	4	15,6208 ± 3,632	695.31 ± 0	6.57 ± 2.0
61-69 + 149-162	WENGE**C**^{66}AQK+LSFNPTQLEEQ**C**^{160}HI	Disulfide	B	4	114,842 ± 1,597	680.81 ± 0	5.9 ± 1.7
61-69	WENDE**C**^{66}AQK	IPSL	A	2	6,180 ± 500	660.3 ± 0	23 ± 6.3
61-69	WENGE**C**^{66}AQK	IPSL	B	2	4,531 ± 95	631.29 ± 0	21.23 ± 5.3
149-162	LSFNPTQLEEQ**C**^{160}HI	IPSL	A/B	2	9,384 ± 152	928.46 ± 0	17.4 ± 1
102-124	YLLF**C**^{106}MENSAEPEQSLV**C**^{119}Q**C**^{121}LVR	Disulfide, IPSL	A	3	740 ± 145	957.45 ± 0	46.63 ± 11.1
102-124	YLLF**C**^{106}MENSAEPEQSLA**C**^{119}Q**C**^{121}LVR	Disulfide, IPSL	B	3	185 ± 61	948.1 ± 0	321.95 ± 229.46

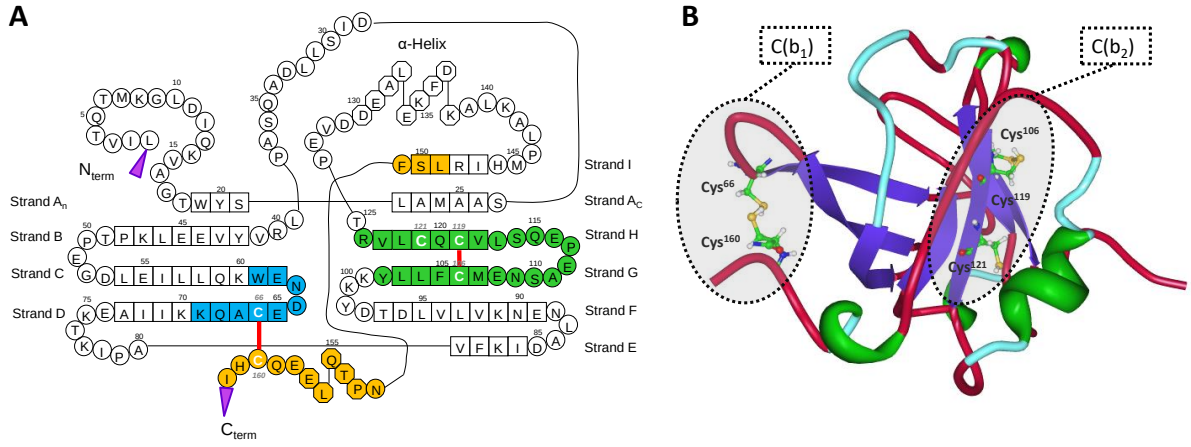

Figure 5-3: Schematic representation of β-lg A with *color*-coded cysteine-containing peptides resulting from the tryptic digestion. *Blue*, peptide 61-69 contains Cys^{66}; *green*, peptide 102-124 contains Cys^{106}, Cys^{119}, and Cys^{121}; and *orange*, peptide 149-162. *White* letters represent the cysteine residues. Symbols represent the secondary structure: *squares*, β-strands; *hexagon*, the α-helix; and *circle*, the random coil. *Red lines* represent the intramolecular disulfide bridges (modified according to Fogliano et al. (1998) and Keppler et al. (2014)) (A). The tertiary structure of β-lg A indicates the plausibility of two spectral components of the spin labels: $C(b_1)$ describes the spectral properties of peptide 102-124, which is part of the β-sheets. The main labeled position, Cys^{121}, is located between the β-barrel and the α-helix. $C(b_2)$ describes the spectral properties of the combination of peptides 61-69 and 149-162, located in the outer loop (RCSB PDB Protein Workshop 4.2.0 (Moreland, Gramada, Buzko, Zhang, & Bourne, 2005)).

5.4.2 Spectral components of spin-labeled β-lg amyloid aggregates at pH 2

Amyloid aggregation at pH 2 during the 5-hour heat incubation of spin-labeled β-lg likewise resulted in superimposed EPR spectra, which were recorded separately for the complete AAS as well as for the AF obtained in the retentate after ultrafiltration and for the non-amyloid fractions (n-AF) in the permeate (Figure 5-4). The AF contains mostly amyloid and other aggregates with molecular weights above 300 kDa, while the n-AF contains smaller aggregates, unfolded protein, and peptides (Lux et al. 2021; (Heyn et al., 2019; Keppler et al., 2019).

The spectral line shapes of the AAS for both cases (i.e., MTSSL and IPSL) reported on the restricted mobility of nitroxides. The rotational mobility of MTSSL appeared to be slower than that of the IPSL (see Section 5.4.1.1). A detailed analysis by spectral simulations revealed that four components with specific τ_c and A_{zz} values were required to satisfactorily describe the experimental EPR line shapes (Table 5-3). One of the spectral components was attributed to a free nitroxide, C(f), and constituted just a few percent of the total spectrum. The other three components reported on nitroxides with varying degrees of motional restriction, which was reflected by different τ_c values. In the case of MTSSL, the dominant

spectral component $C(b_1)$ was characterized by a τ_c of 7.31 ns and a A_{zz} of 3.39 mT (Table 5-3), which was characteristic for a nitroxide buried in the protein (Bordignon & Polyhach, 2013; Savitsky et al., 2004; Steinhoff et al., 1999). The other two components, $C(b_2)$ and $C(b_3)$, with τ_c values of 2.16 and 0.68 ns, respectively, displayed an A_{zz} of 3.57 mT, which was characteristic for a nitroxide exposed to water/DMSO solution (cf. Section 5.4.1). While component $C(b_3)$ could be associated with an MTSSL bound to a free peptide, $C(b_2)$ could represent a peptide-bound MTSSL, which is aggregated with multiple peptides but located on the surface. In the case of IPSL, the dominant spectral component was $C(b_1)$ with a τ_c of 12.62 ns and an A_{zz} of 3.14 mT (Table 5-3). In fact, this was the slowest and most hydrophobic spectral component, indicating that this IPSL bound side chain may be incorporated into the hydrophobic core of a protein aggregate. The other two bound components in the spectra of IPSL-labeled β-lg reported on the nitroxide exposed to water/DMSO solution (A_{zz} = 3.57 mT), which may bind to a single peptide (τ_c = 0.40 ns) or to small peptide aggregates (τ_c = 1.95 ns) analogous to MTSSL. However, it should be noted that—for both spin labels—the $C(b_1)$ spectral component had rotational correlations times τ_c >7 ns, which is too slow for the resolution in the EPR time scale at the microwave frequency used in the X-band. To resolve differences in rotational motion above 7 ns, lower microwave frequencies would have to be used. As a result, this implies that all cases with τ_c >7 ns in this study are classified as very slow spectral components and no statistical discrimination tests can be performed. When compared among the two spin labels, the $C(b_1)$ spectral component was much larger for MTSSL than for IPSL (i.e., 70% vs. 46%). The opposite situation was observed for the $C(b_3)$ spectral component: 2% for MTSSL and 31% for IPSL. This difference in the contribution from different spectral components can explain the general appearance of the spectra (Figure 5-4). The narrow spectral lines, which are typical for fast rotating nitroxides with low τ_c values, were much higher in intensity than the broad spectral lines of slowly rotating nitroxides. Consequently, the higher contribution from the $C(b_3)$ component in the case of IPSL becomes determinative for the overall appearance of the spectrum, thus highlighting the faster rotational motion and hiding the slower rotation motion of the spin label. Although the cysteine-containing peptides after tryptic digestion (Figure 5-2) do not match those formed during acid hydrolysis, it is quite remarkable that the MTSSL-labeled side chain had very similar values for the spectral component $C(b_1)$ (Table 5-1 vs Table 5-3). Since MTSSL was mainly bound in the hydrophobic interior of β-lg, it may be deduced that these respective peptides were not involved in aggregation. In contrast, $C(b_1)$ of the IPSL-labeled side chain was more hydrophobic and restricted in its rotation after amyloid aggregation. Since IPSL was able to bind to Cys^{160} and Cys^{66} to a higher degree than MTSSL, which are part of the outer loops (cf. 5.4.1.2), it may be assumed that these labeled peptides are more likely to be entrapped in the formed aggregates of hydrolyzed peptides.

This conclusion could be made under the assumption that aggregation would be indicated by a lower A_{zz} and a slower τ_c of the spectral components, which did not apply for the side chains labeled by MTSSL.

Notably, as long as one spin label was concerned, spectral line shapes (Figure 5-4) and spectra simulations (Table 5-3) were very similar for AAS and for AF and n-AF obtained by ultrafiltration. Approximately the same protein content of ~50% was measured in both fractions after fractionation at 300 kDa. While the A_{zz} and τ_c of all bound spectral components and the proportion of the C(b_2) component in all fractions changed only marginally, the contribution of the very slow component C(b_1) was significantly reduced for both spin labels of AAS > AF > n-AF, while the opposite ranking was observed for the fastest component C(b_3). These observations were in contrast to our expectations since we assumed that amyloid aggregates would accumulate in AF, which would lead to a considerably higher protein concentration, a broadening of the spectrum, and the corresponding reduced mobility of the spin label (Iuraşcu et al., 2009). The similarity of the spectra (Figure 5-4) and the comparable results of the simulation (Table 5-3) of AF and n-AF for each spin label suggested the same microenvironment of spin labels in both fractions. This indicates that the spin-labeled peptides were not part of the amyloid aggregates, which were greater than 300 kDa (as expected for fibril structures). While only an aggregation of the IPSL-labeled side chain for the C(b_1) component could be observed, which was also present in both fractions, neither intermolecular β-sheets in n-AF could be verified nor could ThT fluorescence be measured (Lux et al. 2021). Furthermore, Akkermans et al. (2008) demonstrated that mostly the peptides 1-32/33 and 1-52/53 were present in the amyloid aggregates. Additionally, they found five other peptides that were present in the AF and n-AF that contained Cys^{106}, Cys^{119}, Cys^{121}, and Cys^{160}. Only Cys^{66} was found exclusively in the n-AF; however, an MWCO of 100 kDa was used to separate the two fractions. Consequently, it is very likely that these aggregates, which are smaller than 300 kDa, do not have an amyloid character. This may support the assumption that they originate from the random coil. Since none of the individual spectral components (Table 5-3) can be clearly assigned to the amyloid aggregates, it can be assumed that the spin labels reflected other aggregates and smaller peptides that were present in both fractions. The retention of some of these small aggregates and peptides in the retentate may be due to its accumulation in the long-fibril filter cake during membrane filtration.

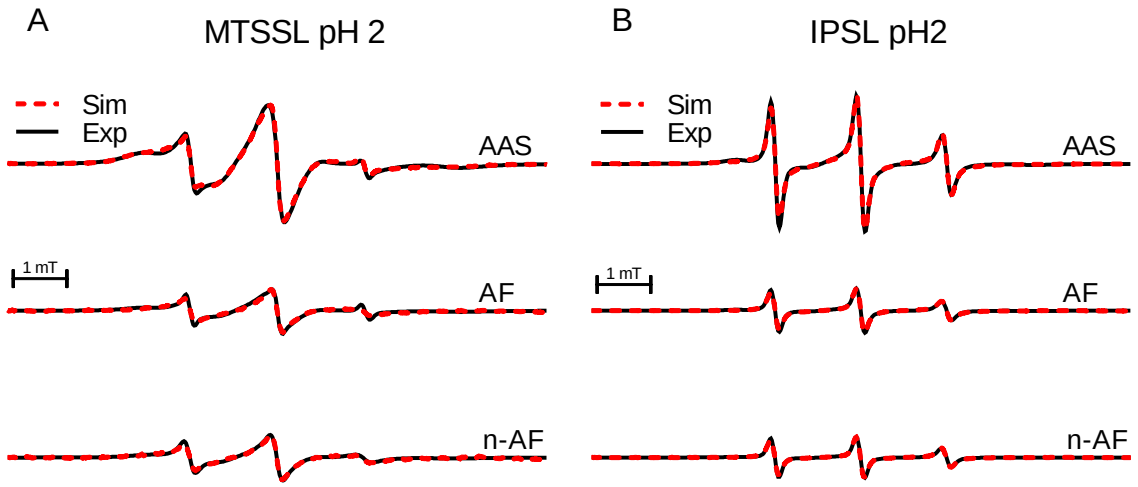

Figure 5-4: cw EPR spectra of β-lg spin labeled with MTSSL (A) and IPSL (B) at pH 2. The spin-labeled samples were heated at 90°C for five hours, resulting in an amyloid aggregate system (AAS) separated by ultrafiltration into an amyloid (AF) and a non-amyloid fraction (n-AF). Experimental (Exp, black line) and simulated (Sim, red dotted line) spectra are demonstrated. All spectra were normalized to the protein concentration. Characteristic parameters obtained from simulations are depicted in Table 5-3.

Table 5-3: Characteristic parameters of individual components in the EPR spectra of the amyloid aggregate system (AAS) at pH 2 from MTSSL or IPSL-labeled β-lg. The AAS was separated into an amyloid fraction (AF) and a non-amyloid fraction (n-AF) by ultrafiltration. Spectral components, such as the rotational correlation time (τ_c), the micro polarity (A_{zz}), and the proportion of the component (d) were assigned to bound nitroxide spin labels ($C(b_3)$, $C(b_2)$, and $C(b_3)$) and a free nitroxide (i.e., component C(f)). (n=3, ANOVA).

Fractions and its protein content at pH 2		Bound components			free component
MTSSL		$C(b_1)$	$C(b_2)$	$C(b_3)$	C(f)
AAS 100%[#]	τ_c [ns]	7.31 ± 0.10[§]	2.16 ± 0.03[a]	0.68 ± 0.03[a]	0.03 ± 0.00[a]
	d [%]	70.9 ± 0.7[a]	25.7 ± 1.0[a]	2.8 ± 0.3[a]	0.6 ± 0.0[a]
	A_{zz} [mT]	3.39	3.57	3.57	3.57
AF 48 ± 3%[#]	τ_c [ns]	6.74 ± 0.38[b]	1.36 ± 0.02[b]	0.59 ± 0.02[a]	0.03 ± 0.00[a]
	d [%]	67.0 ± 0.5[b]	26.9 ± 0.1[b]	6.1 ± 0.4[b]	0.02 ± 0.00[a]
	A_{zz} [mT]	3.39	3.57	3.57	3.57
n-AF 52 ± 3%[#]	τ_c [ns]	7.03 ± 0.28[ab]	1.45 ± 0.04[b]	0.59 ± 0.03[a]	0.03 ± 0.00[a]
	d [%]	65.1 ± 0.9[c]	27.5 ± 0.5[b]	7.4 ± 0.5[c]	0.02 ± 0.00[a]
	A_{zz*} [mT]	3.39	3.57	3.57	3.57
IPSL					
AAS 100%[#]	τ_c [ns]	12.62 ± 0.09[§]	1.95 ± 0.03[a]	0.40 ± 0.00[a]	0.03 ± 0.00[a]
	d [%]	46.1 ± 0.1[a]	18.3 ± 0.9[a]	31.3 ± 0.5[a]	4.2 ± 0.9[a]
	A_{zz*} [mT]	3.14	3.57	3.57	3.57
AF 52 ± 3%[#]	τ_c [ns]	12.73 ± 1.07[§]	1.65 ± 0.09[a]	0.37 ± 0.01[a]	0.03 ± 0.00[a]
	d [%]	38.6 ± 1.7[b]	19.9 ± 1.5[ab]	39.12 ± 0.37[b]	2.4 ± 0.1[a]
	A_{zz*} [mT]	3.14	3.57	3.57	3.57
n-AF 48 ± 3%[#]	τ_c [ns]	13.10 ± 1.13[§]	1.47 ± 0.17[a]	0.31 ± 0.01[a]	0.03 ± 0.00[a]
	d [%]	33.2 ± 1.8[c]	22.1 ± 2.0[b]	42.4 ± 2.2[c]	2.3 ± 0.5[a]
	A_{zz*} [mT]	3.14	3.57	3.57	3.57

[#]Relative protein content of the fractions after ultrafiltration. The sum of the protein content of AF and n-AF was assumed to be 100% (i.e., protein losses during ultrafiltration were not considered).
[§]τ_c >7 ns is below the resolution of the X-band microwave frequency used for the current measurements. All cases with τ_c >7 ns are classified as very slow spectral components and no statistical discrimination tests were performed. *All standard deviations (SDs) of A_{zz} were zero, so they are not presented separately for clarity.
Different letters indicate significant differences between the fractions. Each component and each spin label were considered separately.

5.4.3 Spectral components of spin-labeled β-lg amyloid-like aggregates at pH 3.5

The formation of amyloid-like aggregates during the five-hour heat incubation at pH 3.5 of spin-labeled β-lg also resulted in superimposed EPR spectra, which were recorded separately for the complete ALAS as well as for the ALF obtained in the retentate after ultrafiltration and for the non-amyloid-like fractions (n-ALF) in the permeate (Figure 5-5).

The spectra of ALAS with both MTSSL and IPSL were very similar to those obtained at pH 2 (see Section 3.2). The spectrum with MTSSL reported a slower rotation of the nitroxide spin label when compared to IPSL. When disregarding the type of spin label, spectral simulations for ALAS revealed the presence of four components, one of which was attributed to the free spin label C(f) (Table 5-4). The remaining three spectral components can be interpreted in terms of slow (τ_c >7 ns), intermediate (1< τ_c <7 ns), and fast rotation (τ_c <1 ns) of the nitroxide spin label. The appearance of different superimposed spectral components after (amyloid) aggregation confirms the observation of earlier studies (Iuraşcu et al., 2009; Sepkhanova et al., 2009) that were also based on simulations with different rotation correlation times (Sepkhanova et al., 2009). In the case of MTSSL-labeled β-lg, the spectrum of ALAS was dominated by two components, C(b_1) and C(b_2), with nearly equal contributions of 44 to 48%. However, C(b_2) had a much faster rotation correlation time ($\tau_{c,b2}$ = 4.26 ± 0.03 ns) compared to C(b_1) ($\tau_{c,b1}$ = 21.87 ± 1.08 ns). The fastest bound component C(b_3), with a τ_c of 0.2 ns, contributed only 5% to the total spectrum. In the case of IPSL-labeled β-lg, the slowest component C(b_1) ($\tau_{c,b1}$ = 12.39 ± 0.39 ns) was the dominant one, with a contribution of 53.1%. Additionally, it always displayed the smallest A_{zz} value, thus indicating the environment of spin labels being buried within a protein interior. The other two components had approximately equal contributions of 20–25% and characteristic rotational correlation times of $\tau_{c,\ b2}$ = 2.21 ± 0.06 ns, and $\tau_{c,\ b3}$ = 0.32 ± 0.00 ns. Compared to the labeled β-lg components prior to heat incubation at pH 3.5 (Table 5-1), all components had longer rotational correlation times, which were particularly slow for C(b_1) at τ_c >7 ns and may indicate protein aggregation. As mentioned in Section 3.2, cases with a τ_c of >7 ns were generally regarded as slow components that cannot be distinguished statically on the EPR time scale in the X-band. This result is in agreement with (Iuraşcu et al., 2009), who attributed the reduced mobility of the spin label side group to oligomerization and/or aggregation. In contrast, the components C(b_2) and C(b_3) can be clearly identified because the EPR line shape was very sensitive to the τ_c in the order of several nanoseconds. Since it has been repeatedly demonstrated in previous studies (Heyn et al., 2019; Keppler et al., 2019) that the building blocks of amyloid-like aggregates at pH 3.5 consist of the entire β-lg, it could be assumed that, during aggregation, the three previously assigned binding positions of the spin labels (cf. 5.4.1.2 and Figure 5-3A) can be more clearly distinguished after possible rearrangement when compared with the natural β-lg monomer. Hence, based on the

simulated data, the following assignment of the spectral components would be plausible: $C(b_1)$ still represents the positions Cys^{106}, Cys^{119}, and Cys^{121} outside of the previous hydrophobic β-barrel and thus indicates alterations in the microenvironments of the β-sheets (Figure 5-3A, *green* color code). $C(b_2)$ could represent position Cys^{66}, which was embedded in β-strand D (*blue* color code), while $C(b_3)$ could correspond to Cys^{160}, which was part of the random coil (*yellow* color code). The faster rotational motion of $C(b_3)$ might suggest that the label is extended at the random coil during aggregation, while the labels bound to the β-strands are more restricted in their motion. This assumption would be consistent with the binding positions preferred by MTSSL and IPSL.

To gain deeper insight into the aggregation mechanism, a fractionation of ALAS by membrane filtration was performed. ALF contained approximately 82–90%—while n-ALF contained the remaining 10–18%—of the protein and displayed significantly different signatures in the EPR spectra (Figure 5-5). With both spin labels, the EPR spectra of ALF can still be described by three bound components and one unbound component. In the case of MTSSL, the spectra line shape was clearly determined by slow $C(b_1)$ and intermediate components $C(b_2)$, which contributed 85.9 and 12.2% of the total spectrum (Table 5-4). In the case of IPSL, the contribution of the three components decreased in the following order: $C(b_1)$ with 45.7% > $C(b_2)$ with 33.6% > $C(b_3)$ with 20.6%. Based on these results, we assume that the worm-like structures recognizable in AFM images (Lux et al. 2021; Heyn et al., 2019) are the result of the assembly of monomer-like structures, which is also supported by recently obtained AFM and SAXS results where the height and elliptical cross-section of the worm-like aggregates was that of a monomeric protein (i.e., 3.4 nm) (Heyn et al. 2019). Therefore, we hypothesize that it is likely that the C-terminus $C(b_3)$ will fold outward, as evidenced by higher water/DMSO accessibility (A_{zz} = 3.57) and faster rotational motion ($\tau_{c,b3}$ = 0.33 for MTSSL and $\tau_{c,b3}$ = 0.46 for IPSL) relative to the monomeric β-lg before aggregation (Table 5-1). This rearrangement allows the previous α-helix section to be shifted out of the autonomous folding domain (Belloque & Smith, 1998; Considine, Patel, Anema, Singh, & Creamer, 2007; Keppler et al., 2014; Kuwata et al., 2001) during partial unfolding, which subsequently leads to greater accessibility of the β-sheets to the water/DMSO-environment (A_{zz} $C(b_1)$ = 3.57 mT for MTSSL and A_{zz} $C(b_1)$ = 3.43 mT for IPSL). However, $C(b_1)$ components—with their slow $\tau_{c,b1}$ >7 ns for both spin labels—indicate that the previous intramolecular β-sheets are most likely tightly packed by the accumulation of intermolecular β-sheets. This suggestion is consistent with reports of a partial rearrangement of the β-barrel structure of β-lg after thermal-induced denaturation at neutral pH values (Keppler, Sönnichsen, Lorenzen, & Schwarz, 2014a; Mousavi, Bordbar, & Haertlé, 2008; Song, Chen, Yang, Huang, & Mao, 2005).

An increase of the intermolecular β-sheets is also consistent with results of FTIR and ThT measurements (Lux et al., 2021; Heyn et al., 2019), which in turn support the assumption that amyloid-like structures can be formed from the building blocks of the entire primary β-lg structure.

To verify this model, the spatial distribution of the labeled side chains was determined using the pulsed EPR technique of DEER (Milov et al., 1984). In the case where spin labels are homogeneously distributed, the experimental DEER signal is a decay (Jeschke et al., 2006). Depending on the dimension of the space where the spin labels were distributed, the decay obeys the stretched exponential law of the form:

Equation 7: Exponential stretching of spin label distribution

$$\exp(-kt^{d/3}) \qquad (7)$$

where t is the time axis of the DEER measurement, k quantifies the density of the spins, and d is the dimensionality of the homogeneous distribution. The experimental decay of DEER time traces for ALF at pH 3.5 spin labeled with MTSSL and IPSL was fitted to the stretched exponential and the yielded dimensionality factor d of 1.23 and 1.64 for MTSSL and IPSL, respectively (Figure 5-6).

Two different scenarios are conceivable to explain the fact that the experimentally determined dimension lay between a one-dimensional and a two-dimensional distribution. On the one hand, the bending of the aggregates could cause spin labels to enter the second dimension if they were not strictly rigid rods. The spin labels would not be homogeneously distributed in two dimensions and thus the parameter d would be smaller than two, while still being larger than one. On the other hand, some spin label could stick out of the aggregates. If the spin-labeled β-lg molecules were incorporated in the amyloid-like aggregates in such a way that the spin labels point out of the aggregates in different directions, the strict one-dimensional distribution of spin labels would not be observable. In this case, the distribution will be larger than one, while still being smaller than two. While both explanations are plausible and cannot be excluded, the latter was explicitly supported by the experimental observation that the dimensionality of the distribution was larger for IPSL than for MTSSL. The second scenario would also correspond to the previously derived aggregation model and the assignment of the different spectral components to the different binding positions (Table 5-4 and Figure 5-2). With the observation that IPSL was also preferentially bound in the loop regions C(b_3), this spin label will protrude more from the aggregates than MTSSL, which was predominantly buried in β-lg; therefore, the dimensionality of the spin label distribution will differ more from one. Considering the way spin labels were attached to β-lg, the DEER data

suggest that the proteins were linearly arranged within aggregates like beads on a string. In other words, the worm-like aggregates that can be found by AFM or SAXS after exposure to heat at pH 3.5 (Lux et al., 2021; Heyn et al., 2019; Keppler et al., 2019) are particularly reminiscent of a centipede when IPSL-labeled.

In contrast, the EPR spectra of n-AF can be described by only two spectral components. Based on the A_{zz} values and the difference in rotational motion, the MTSSL-labeled spectral components could be assigned to C(b_1), which was more hydrophobic and buried in a protein interior, as found for the binding positions Cys^{106}, Cys^{119}, and Cys^{121}, and to C(b_3), which tumbled relatively freely and were bound to the protein surface as per the binding position of Cys^{160} (Table 5-4). The dominant component C(b_1) contributed 80% to this fraction, which is similar to C(b_1) before aggregation, even if its rotational motion was between the τ_c values found at pH 2 and pH 3.5 before aggregation (Table 5-1). Similarly, the considerably lower τ_c of C(b_3) may indicate that monomeric structures may be present in the permeate that have different folding due to the effect of pH and heat incubation. This assumption can be confirmed since the unfolding of β-lg was measured after a 5-hour heat incubation at 90°C (Lux et al., 2021), which is also indicated by faster side-chain mobilities and, when fully unfolded in the presence of guanidine-hydrochloride, results in only one fast component (Figure 5-7). On the other hand, it cannot be excluded that n-AF could also contain oligomeric structures with up to 16 monomeric units, which would still have an aggregate size of <300 kDa. However, the presence of small oligomers was recently confirmed by analytical ultracentrifugation (Heyn et al. 2019). The latter assumption suggests that the random coil in the proteins found in n-AF is more pronounced than before heat treatment. This suggestion would also apply for IPSL, for which the EPR spectrum of spectral components in n-ALF can be described with two much faster rotational correlation times of 2.83 and 0.23. These findings may be explained by the more preferred binding positions at the random coil and in strand D, where IPSL could expand during assembly/oligomerization. This could also be confirmed since no amyloid characters in n-AF were found by FTIR or ThT measurements (Lux et al., 2021). Moreover, Iuraşcu et al., (2009) also discovered a bound component in the n-AF and attributed this to the amyloid β-monomer.

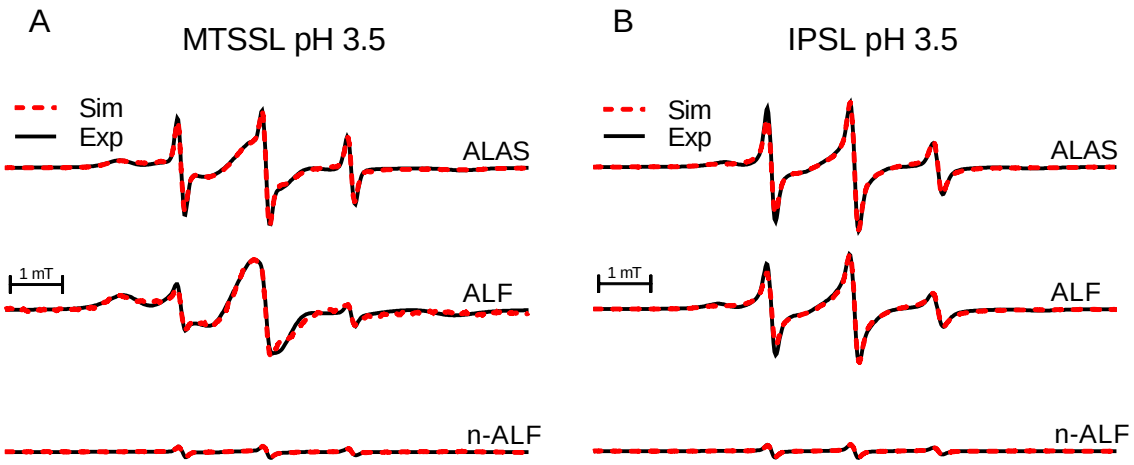

Figure 5-5: cw EPR spectra of β-lg spin labeled with MTSSL (A) and IPSL (B) at pH 3.5. The spin-labeled samples were heated at 90°C for five hours, resulting in an amyloid-like aggregate system (ALAS, containing 100% protein) that was separated by ultrafiltration into an amyloid-like (ALF, containing 90% protein) and a non-amyloid-like fraction (n-ALF, containing 10% protein). Experimental (Exp, black line) and simulated (Sim, red dotted line) spectra are demonstrated. All spectra are normalized to the protein concentration. Characteristic parameters obtained from simulations are depicted in Table 5-4.

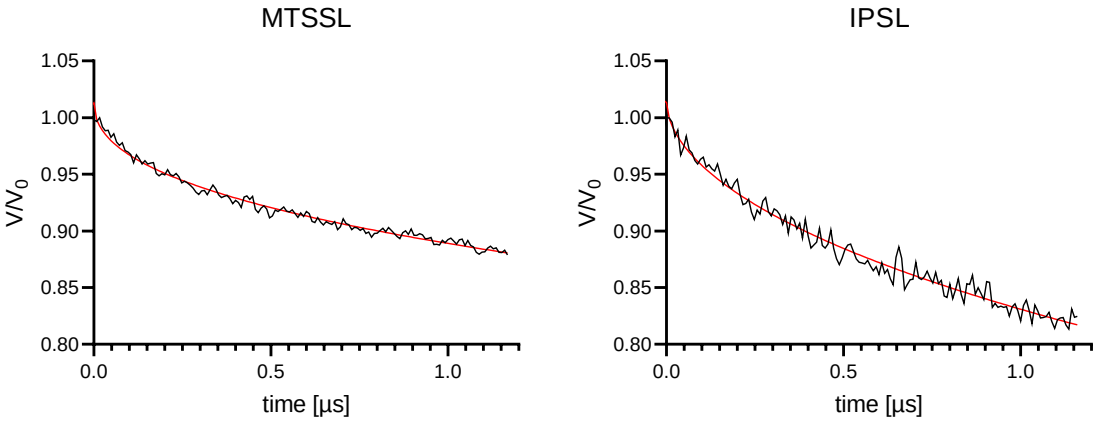

Figure 5-6: Experimental DEER time traces (black) and corresponding stretched exponential fits (red) for spin-labeled ALF with MTSSL and IPSL from amyloid-like aggregates at pH 3.5.

Table 5-4: Characteristic parameters of individual components in the EPR spectra of the amyloid aggregate system (AAS) at pH 3.5 from MTSSL or IPSL-labeled β-lg. The ALAS were separated into an amyloid fraction (ALF) and a non-amyloid fraction (n-ALF) by ultrafiltration. Spectral components, such as rotational correlation time (τ_c), micro polarity (A_{zz}), and the proportion of the component (d) were assigned to bound nitroxide spin labels ($C(b_3)$, $C(b_2)$, $C(b_3)$), and a free nitroxide C(f). (n=3, ANOVA)

Fractions and its protein content at pH 3.5		Bound components			free component
MTSSL		$C(b_1)$	$C(b_2)$	$C(b_3)$	C(f)
ALAS 100%[#]	τ_c [ns]	21.87 ± 1.08[§]	4.26 ± 0.03[a]	0.20 ± 0.01[a]	0.03 ± 0.00[a]
	d [%]	47.8 ± 1.3[a]	43.8 ± 1.6[a]	5.4 ± 0.1[a]	3.1 ± 0.2[a]
	A_{zz^*} [mT]	3.53	3.57	3.57	3.57
ALF 82 ± 3%[#]	τ_c [ns]	10.29 ± 0.1[§]	2.00 ± 0.04[b]	0.33 ± 0.04[a]	0.03 ± 0.00[a]
	d [%]	85.9 ± 0.4[b]	12.2 ± 0.1[b]	1.5 ± 0.7[b]	0.4 ± 0.3[b]
	A_{zz^*} [mT]	3.57	3.57	3.57	3.57
n-ALF 18 ± 3%[#]	τ_c [ns]	7.21 ± 0.49[§]		0.17 ± 0.01[a]	
	d [%]	80.4 ± 1.9[c]		19.6 ± 1.9[c]	
	A_{zz^*} [mT]	3.43		3.57	
IPSL					
ALAS 100%[#]	τ_c [ns]	12.39 ± 0.39[§]	2.21 ± 0.06[a]	0.32 ± 0.00[a]	0.03 ± 0.00[a]
	d [%]	53.1 ± 0.4[a]	25.7 ± 0.3[a]	20.3 ± 0.1[a]	0.9 ± 0.1[a]
	A_{zz^*} [mT]	3.32	3.39	3.57	3.57
ALF 89 ± 0.3%[#]	τ_c [ns]	14.28 ± 0.38[§]	2.64 ± 0.08[b]	0.46 ± 0.01[a]	0.03 ± 0.00[a]
	d [%]	45.7 ± 1.4[b]	33.6 ± 1.2[b]	20.6 ± 0.2[a]	0.01 ± 0.00[a]
	A_{zz^*} [mT]	3.43	3.57	3.57	3.57
n-ALF 11 ± 0.3%[#]	τ_c [ns]		2.83 ± 0.09[b]	0.23 ± 0.00[a]	
	d [%]		60.0 ± 0.6[c]	40.0 ± 0.6[b]	
	A_{zz^*} [mT]		3.57	3.57	

[#]Relative protein content of the fractions after ultrafiltration. The sum of the protein content of AF and n-AF was assumed to be 100% (i.e., protein losses during ultrafiltration were not considered).
[§]τ_c >7 ns is below the resolution of the X-band microwave frequency used for the current measurements.
All cases τ_c >7 ns are classified as very slow spectral components and no statistical discrimination tests were performed. *All SDs of A_{ZZ} were zero, so they are not presented separately for clarity.
Different letters indicate significant differences between the fractions. Each component and each spin label were considered separately.

5.5 Conclusion

The present study demonstrated that the spin labels MTSSL and IPSL can be bound to the free cysteine group of the β-lg without prior manipulation of the primary protein structure of a food protein. Since SDSL requires a pH value of 7.5 for MTSSL and 8.5 for IPSL for efficient labeling, a shuffle effect of the labels or a higher binding propensity of IPSL to Cys^{66} based on C-S binding may occur (i.e., labels bind to all cysteine residues). However, MTSSL and IPSL preferred different but reproducible binding positions, resulting in MTSSL and IPSL being 80 and 60% reliably bound to peptide 102-124, respectively, which carries the formally free Cys^{121}. The combination of mass spectrometric and EPR analyses made it possible to assign the two spectral components of the labels bound to β-lg. One labeled side chain, indicated by a non-polar environment, was located outside of the β-barrel of β-lg (Cys^{106}, Cys^{119}, and Cys^{121}) and thus describes the microenvironment of the β-sheets. The other component was the superposition of labeled Cys^{66} embedded in strand D and Cys^{160} contained in the random coil. Both binding positions were in the DMSO/water environment and were in close proximity to the tertiary protein structure. Combining the results of parts 1 and 2 of the study, it can be concluded that, under given labeling conditions, the behavior of labeled to non-labeled β-lg was the same before and after the heat incubation, independent of the pH values.

Unfortunately, the approach of SDSL for the characterization of fibril formation at pH 2 remains limited since the acid hydrolysis that occurs during heat incubation at this pH value led to different peptides than those obtained by tryptic digestion. However, EPR analysis of amyloid and non-amyloid fractions after ultrafiltration revealed that all labeled side chains were part of both fractions, even if they could not detect amyloid structures. In particular, the IPSL-labeled side chain was incorporated into small non-amyloid aggregates with a very non-polar environment, which appears to be preferentially formed from peptides with Cys^{160} from the random coil structures. In contrast, since the building blocks of the amyloid-like aggregates formed at pH 3.5 consist of the entire protein, it is assumed that the previously assigned three different binding positions of the spin labels during aggregation can be more clearly distinguished after possible rearrangement when compared to the natural β-lg monomer. Therefore, we hypothesize that it is likely that the C-terminus $C(b_3)$ will fold outward, as evidenced by high water/DMSO accessibility and fast rotational motion. This rearrangement allows the α-helix to be shifted out of the autonomous folding domain during partial unfolding, which subsequently leads to greater accessibility of the β-sheets to the water/DMSO-environment. Meanwhile, the β-sheets are most likely compressed by the accumulation of intermolecular β-sheets, which subsequently support the assumption that amyloid-like structures can be formed from the building blocks of the entire primary β-lg

structure. Furthermore, our application of the DEER pulsed EPR technique confirmed the spatial distribution of the labels within the amyloid-like fraction in a one-dimensional arrangement of the entire protein aggregates, which was similar to a string of pearls. It also indicated the extension of the labels bound at the random coil region, which resembles centipede-like structures. Therefore, the SDSL of food proteins containing several cysteine residues can be successfully used to gain deep insights into the aggregation mechanism of food proteins under processing conditions if the binding positions are known.

Acknowledgment

Funding: The authors thank the German Research Foundation (DFG) for financial support of this work within the SPP 1934 DiSPBiotech (project number 273937032).

5.6 Supplementary material for paper 3

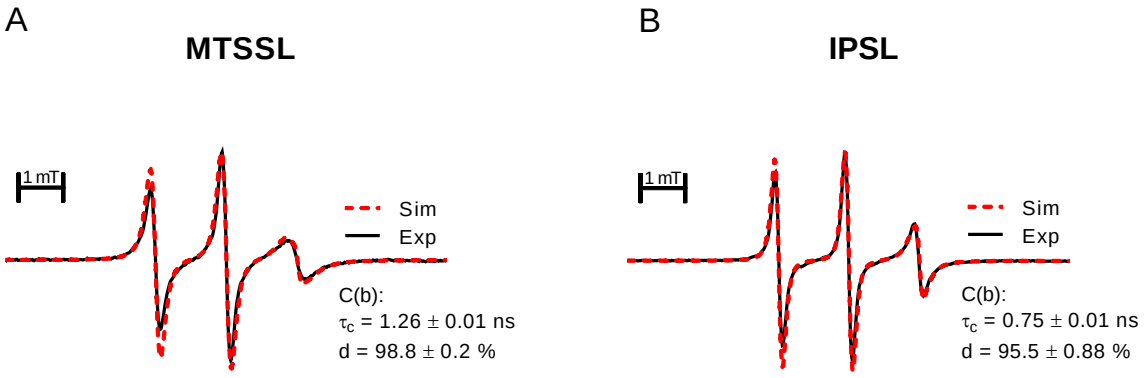

Figure 5-7: EPR spectra of spin labeled β-lactoglobulin with (A) MTSSL and (B) IPSL after denaturation with guanidine. The labeling were conduction at pH 7.5 for MTSSL and pH 8.5 for IPSL and incubated over night. After removing the spin label excess, the protein were denatured with guanidine. The simulation (*red line*) with EasySpin result in only one bound component (C(b)) and one free component with a rotation correlation time (τ_C) of 0.03 ns.

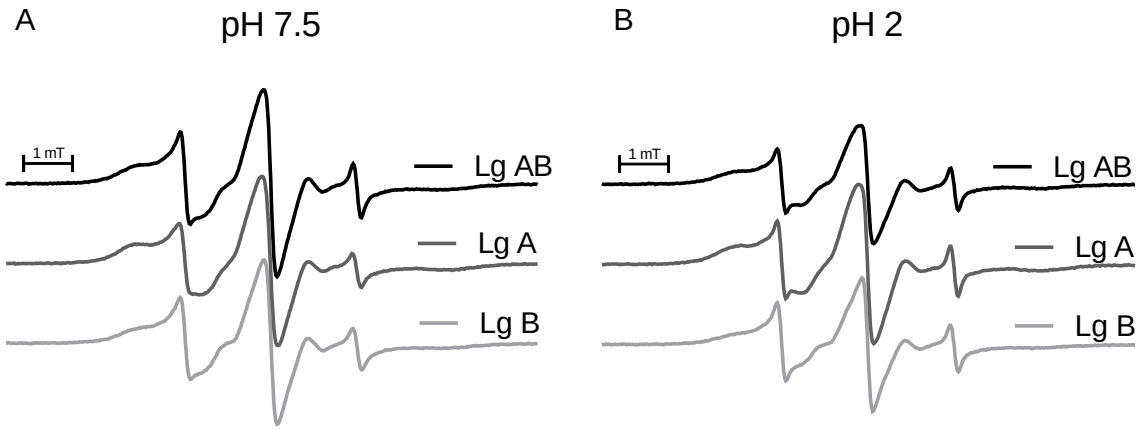

Figure 5-8: Spin labeling of β-lactoglobulin as mixture of the genetic variants A and B (Lg AB), the genetic variant A (Lg A) and the genetic variant B (Lg B) with MTSSL. The spin labeling were conducted at pH 7.5 and the excess removed (A). Afterwards the pH were adjusted to pH 2 (B). All spectra represent superimposed spectra with two bound components.

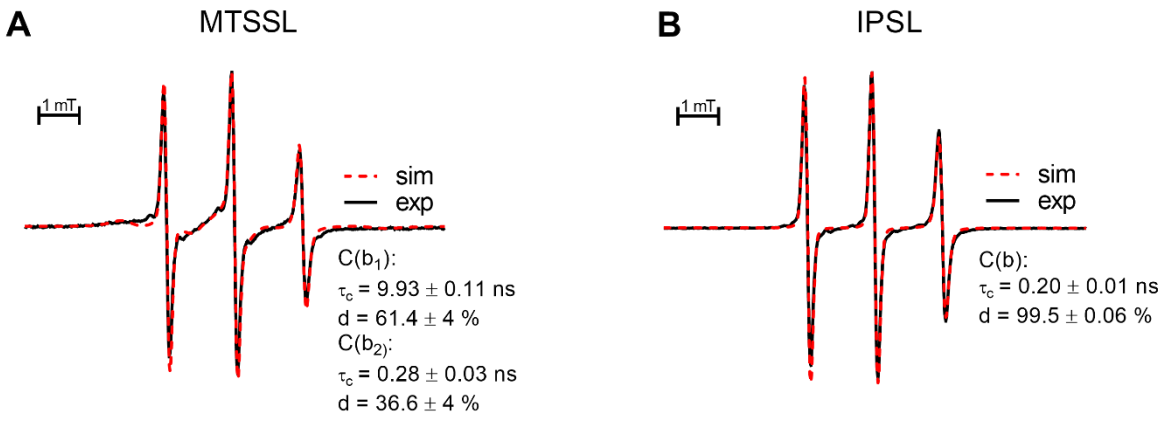

Figure 5-9: EPR spectra of spin labeled β-lactoglobulin with (A) MTSSL and (B) IPSL after tryptic digestion. The labeling were conduction at pH 7.5 for MTSSL and pH 8.5 for IPSL and incubated over night. After removing the spin label excess, the tryptic digestion were conducted as described in 5.3.3. The simulation (*red line*) with EasySpin result in two bound components ($C(b_1)$, $C(b_2)$) for MTSSL and only one bound component (C(b)) for IPSL. For both spin labels also one free component with a rotation correlation time (τ_C) of 0.03 ns were included.

5.7 References

Akkermans, C., Venema, P., van der Goot, A. J., Gruppen, H., Bakx, E. J., Boom, R. M., & van der Linden, E. (2008). Peptides are building blocks of heat-induced fibrillar protein aggregates of beta-lactoglobulin formed at pH 2. *Biomacromolecules*, *9*(5), 1474–1479. https://doi.org/10.1021/bm7014224

Aschaffenburg, R., & Drewry, J. (1957). Improved method for the preparation of crystalline beta-lactoglobulin and alpha-lactalbumin from cow's milk. *The Biochemical Journal*, *65*(2), 273–277. https://doi.org/10.1042/bj0650273

Belloque, J., & Smith, G. M. (1998). Thermal Denaturation of β-Lactoglobulin. A 1 H NMR Study. *Journal of agricultural and food chemistry*, *46*(5), 1805–1813. https://doi.org/10.1021/jf9709313

Berliner, L. J., & Reuben, J. (1989). *Spin Labeling: Theory and Applications* (N). Boston: Springer US.

Bordignon, E., & Polyhach, Y. (2013). EPR techniques to probe insertion and conformation of spin-labeled proteins in lipid bilayers. *Methods in Molecular Biology (Clifton, N.J.)*, *974*, 329–355. https://doi.org/10.1007/978-1-62703-275-9_15

Bordignon, E. (2018). EPR Spectroscopy of Nitroxide Spin Probes. In D. Goldfarb & S. Stoll (Eds.), *EMagRes Bks. EPR Spectroscopy: Fundamentals and Methods* (pp. 277–301). Newark: John Wiley & Sons Incorporated.

Burova, T. V., Choiset, Y., Tran, V., & Haertle, T. (1998). Role of free Cys121 in stabilization of bovine beta-lactoglobulin B. *Protein Engineering Design and Selection*, *11*(11), 1065–1073. https://doi.org/10.1093/protein/11.11.1065

Considine, T., Patel, H. A., Anema, S. G., Singh, H., & Creamer, L. K. (2007). Interactions of milk proteins during heat and high hydrostatic pressure treatments — A Review. *Innovative Food Science & Emerging Technologies*, *8*(1), 1–23. https://doi.org/10.1016/j.ifset.2006.08.003

Creighton, T. E. (1980). Kinetic study of protein unfolding and refolding using urea gradient electrophoresis. *Journal of molecular biology*, *137*(1), 61–80. https://doi.org/10.1016/0022-2836(80)90157-6

Fernández, A., & Riera, F. (2013). β-Lactoglobulin tryptic digestion: A model approach for peptide release. *Biochemical Engineering Journal*, *70*, 88–96. https://doi.org/10.1016/j.bej.2012.10.001

Fogliano, V., Monti, S. M., Visconti, A., Randazzo, G., Facchiano, A. M., Colonna, G., & Ritieni, A. (1998). Identification of a β-lactoglobulin lactosylation site. *Biochimica et Biophysica Acta (BBA) - Protein Structure and Molecular Enzymology*, *1388*(2), 295–304. https://doi.org/10.1016/S0167-4838(98)00177-0

Gilbert, H. F. (1995). [2] Thiol/disulfide exchange equilibria and disulfidebond stability. In H. F. Gilbert (Ed.), *Methods in Enzymology. Thiol/disulfide exchange quilibria and disulphidebond stability* (Vol. 251, pp. 8–28). Elsevier. https://doi.org/10.1016/0076-6879(95)51107-5

Gu, L., Tran, J., Jiang, L., & Guo, Z. (2016). A new structural model of Alzheimer's Aβ42 fibrils based on electron paramagnetic resonance data and Rosetta modeling. *Journal of Structural Biology*, *194*(1), 61–67. https://doi.org/10.1016/j.jsb.2016.01.013

Hammarström, P., Owenius, R., Mårtensson, L.-G., Carlsson, U., & Lindgren, M. (2001). High-Resolution Probing of Local Conformational Changes in Proteins by the Use of Multiple Labeling: Unfolding and Self-Assembly of Human Carbonic Anhydrase II Monitored by Spin, Fluorescent, and Chemical Reactivity Probes. *Biophysical Journal*, *80*(6), 2867–2885. https://doi.org/10.1016/S0006-3495(01)76253-4

Hettiarachchi, C. A., Melton, L. D., Gerrard, J. A., & Loveday, S. M. (2012). Formation of β-lactoglobulin nanofibrils by microwave heating gives a peptide composition different from

conventional heating. *Biomacromolecules*, *13*(9), 2868–2880. https://doi.org/10.1021/bm300896r

Heyn, T. R., Garamus, V. M., Neumann, H. R., Uttinger, M. J., Guckeisen, T., Heuer, M., Keppler, J. K. (2019). Influence of the polydispersity of pH 2 and pH 3.5 beta-lactoglobulin amyloid fibril solutions on analytical methods. *European Polymer Journal*, *120*, 109211. https://doi.org/10.1016/j.eurpolymj.2019.08.038

Hoffmann, M. A. M., & van Mil, P. J. J. M. (1997). Heat-Induced Aggregation of β-Lactoglobulin: Role of the Free Thiol Group and Disulfide Bonds. *Journal of agricultural and food chemistry*, *45*(8), 2942–2948. https://doi.org/10.1021/jf960789q

Hubbell, W. L., & Altenbach, C. (1994). Investigation of structure and dynamics in membrane proteins using site-directed spin labeling. *Current Opinion in Structural Biology*, *4*(4), 566–573. https://doi.org/10.1016/S0959-440X(94)90219-4

Iuraşcu, I. M., Cozma, C., Tomczyk, N., Rontree, J., Desor, M., Drescher, M., & Przybylski, M. (2009). Structural characterization of beta-amyloid oligomer-aggregates by ion mobility mass spectrometry and electron spin resonance spectroscopy. *Analytical and Bioanalytical Chemistry*, *395*(8), 2509–2519. https://doi.org/10.1007/s00216-009-3164-3

Jayasinghe, S. A., & Langen, R. (2004). Identifying structural features of fibrillar islet amyloid polypeptide using site-directed spin labeling. *The Journal of Biological Chemistry*, *279*(46), 48420–48425. https://doi.org/10.1074/jbc.M406853200

Jeschke, G., Chechik, V., Ionita, P., Godt, A., Zimmermann, H., Banham, J., Jung, H. (2006). DeerAnalysis2006—a comprehensive software package for analyzing pulsed ELDOR data. *Applied magnetic resonance*, *30*(3-4), 473–498. https://doi.org/10.1007/BF03166213

Keppler, J. K., Heyn, T. R., Meissner, P. M., Schrader, K., & Schwarz, K. (2019). Protein oxidation during temperature-induced amyloid aggregation of beta-lactoglobulin. *Food Chemistry*, *289*, 223–231. https://doi.org/10.1016/j.foodchem.2019.02.114

Keppler, J. K., Sönnichsen, F. D., Lorenzen, P.-C., & Schwarz, K. (2014). Differences in heat stability and ligand binding among β-lactoglobulin genetic variants A, B and C using (1)H NMR and fluorescence quenching. *Biochimica Et Biophysica Acta*, *1844*(6), 1083–1093. https://doi.org/10.1016/j.bbapap.2014.02.007

Keppler, J. K., Koudelka, T., Palani, K., Stuhldreier, M. C., Temps, F., Tholey, A., & Schwarz, K. (2014). Characterization of the covalent binding of allyl isothiocyanate to β-lactoglobulin by fluorescence quenching, equilibrium measurement, and mass spectrometry. *Journal of Biomolecular Structure & Dynamics*, *32*(7), 1103–1117. https://doi.org/10.1080/07391102.2013.809605

Kirby, T. L., Karim, C. B., & Thomas, D. D. (2004). Electron paramagnetic resonance reveals a large-scale conformational change in the cytoplasmic domain of phospholamban upon binding to the sarcoplasmic reticulum Ca-ATPase. *Biochemistry*, *43*(19), 5842–5852. https://doi.org/10.1021/bi035749b

Kuwata, K., Shastry, R., Cheng, H., Hoshino, M., Batt, C. A., Goto, Y., & Roder, H. (2001). Structural and kinetic characterization of early folding events in beta-lactoglobulin. *Nature Structural Biology*, *8*(2), 151–155. https://doi.org/10.1038/84145

Likhtenshtein, G., Yamauchi, J., Nakatsuji, S.'i., Smirnov, A. I., & Tamura, R. (2008). *Nitroxides: Applications in Chemistry, Biomedicine, and Materials Science*. Hoboken: Wiley-VCH.

Lux, J., Heyn, T.R., Kampen, I., Schwarz, K., Keppler, J.K., Steffen-Heins, A. (2021): Amyloid aggregation of spin-labeled β-lactoglobulin. Part I: Influence of spin labeling on amyloid aggregation. *Food Hydrocolloids*, 112, 106178, https://doi.org/10.1016/j.foodhyd.2020.106178

Margittai, M., & Langen, R. (2004). Template-assisted filament growth by parallel stacking of tau. *Proceedings of the National Academy of Sciences of the United States of America*, *101*(28), 10278–10283. https://doi.org/10.1073/pnas.0401911101

McKenzie, H. A., Ralston, G. B., & Shaw, D. C. (1972). Location of sulfhydryl and disulfide groups in bovine -lactoglobulins and effects of urea. *Biochemistry*, *11*(24), 4539–4547. https://doi.org/10.1021/bi00774a017

Milov, A. D., Ponomarev, A. B., & Tsvetkov, Y.D. (1984). Electron-electron double resonance in electron spin echo: Model biradical systems and the sensitized photolysis of decalin. *Chemical Physics Letters*, *110*(1), 67–72. https://doi.org/10.1016/0009-2614(84)80148-7

Moreland, J. L., Gramada, A., Buzko, O. V., Zhang, Q., & Bourne, P. E. (2005). The Molecular Biology Toolkit (MBT): A modular platform for developing molecular visualization applications. *BMC Bioinformatics*, *6*, 21. https://doi.org/10.1186/1471-2105-6-21

Mousavi, S. H.-A., Bordbar, A.-K., & Haertlé, T. (2008). Changes in structure and in interactions of heat-treated bovine beta-lactoglobulin. *Protein and Peptide Letters*, *15*(8), 818–825. https://doi.org/10.2174/092986608785203700

Owenius, R., Engström, M., Lindgren, M., & Huber, M. (2001). Influence of Solvent Polarity and Hydrogen Bonding on the EPR Parameters of a Nitroxide Spin Label Studied by 9-GHz and 95-GHz EPR Spectroscopy and DFT Calculations. *The Journal of Physical Chemistry A*, *105*(49), 10967–10977. https://doi.org/10.1021/jp0116914

Owenius, R., Österlund, M., Lindgren, M., Svensson, M., Olsen, O. H., Persson, E., Carlsson, U. (1999). Properties of Spin and Fluorescent Labels at a Receptor-Ligand Interface. *Biophysical Journal*, *77*(4), 2237–2250. https://doi.org/10.1016/S0006-3495(99)77064-5

Pannier, M., Veit, S., Godt, A., Jeschke, G., & Spiess, H. W. (2000). Dead-time free measurement of dipole-dipole interactions between electron spins. *Journal of Magnetic Resonance (San Diego, Calif.: 1997)*, *142*(2), 331–340. https://doi.org/10.1006/jmre.1999.1944

Phelan, P., & Malthouse, J. P. (1994). 13C-n.m.r. of the cyanylated beta-lactoglobulins: Evidence that Cys-121 provides the thiol group of beta-lactoglobulins A and B. *The Biochemical Journal*, *302 (Pt 2)*, 511–516. https://doi.org/10.1042/bj3020511

Rade-Kukic, K., Schmitt, C., & Rawel, H. M. (2011). Formation of conjugates between β-lactoglobulin and allyl isothiocyanate: Effect on protein heat aggregation, foaming and emulsifying properties. *Food Hydrocolloids*, *25*(4), 694–706. https://doi.org/10.1016/j.foodhyd.2010.08.018

Savitsky, A., Kühn, M., Duché, D., Möbius, K., & Steinhoff, H.-J. (2004). Spontaneous Refolding of the Pore-Forming Colicin A Toxin upon Membrane Association As Studied by X-Band and W-Band High-Field Electron Paramagnetic Resonance Spectroscopy †. *The Journal of Physical Chemistry B*, *108*(27), 9541–9548. https://doi.org/10.1021/jp036397l

Sepkhanova, I., Drescher, M., Meeuwenoord, N. J., Limpens, R. W. A. L., Koning, R. I., Filippov, D. V., & Huber, M. (2009). Monitoring Alzheimer Amyloid Peptide Aggregation by EPR. *Applied Magnetic Resonance*, *36*(2-4), 209–222. https://doi.org/10.1007/s00723-009-0019-1

Shimizu, M., Saito, M., & Yamauchi, K. (1984). Emulsifying and Structural Properties of β-Lactoglobulin at Different pHs. *Agricultural and Biological Chemistry*, *49*(1), 189–194. https://doi.org/10.1080/00021369.1985.10866680

Song, C. Y., Chen, W. L., Yang, M. C., Huang, J. P., & Mao, S. J. T. (2005). Epitope mapping of a monoclonal antibody specific to bovine dry milk: Involvement of residues 66-76 of strand D in thermal denatured beta-lactoglobulin. *The Journal of Biological Chemistry*, *280*(5), 3574–3582. https://doi.org/10.1074/jbc.M407031200

Steinhoff, H.-J., Pfeiffer, M., Rink, T., Burlon, O., Kurz, M., Riesle, J., Oesterhelt, D. (1999). Azide Reduces the Hydrophobic Barrier of the Bacteriorhodopsin Proton Channel. *Biophysical Journal*, *76*(5), 2702–2710. https://doi.org/10.1016/S0006-3495(99)77422-9

Stoll, S., & Schweiger, A. (2006). EasySpin, a comprehensive software package for spectral simulation and analysis in EPR. *Journal of Magnetic Resonance (San Diego, Calif.: 1997)*, *178*(1), 42–55. https://doi.org/10.1016/j.jmr.2005.08.013

Török, M., Milton, S., Kayed, R., Wu, P., McIntire, T., Glabe, C. G., & Langen, R. (2002). Structural and dynamic features of Alzheimer's Abeta peptide in amyloid fibrils studied by site-directed spin labeling. *The Journal of Biological Chemistry*, *277*(43), 40810–40815. https://doi.org/10.1074/jbc.M205659200

Uhrínová, S., Smith, M. H., Jameson, G. B., Uhrín, D., Sawyer, L., & Barlow, P. N. (2000). Structural changes accompanying pH-induced dissociation of the beta-lactoglobulin dimer. *Biochemistry*, *39*(13), 3565–3574. https://doi.org/10.1021/bi992629o.

UniProt: A worldwide hub of protein knowledge (2019). *Nucleic Acids Research*, *47*(D1), D506-D515. https://doi.org/10.1093/nar/gky1049

Wilde, S. C., Keppler, J. K., Palani, K., & Schwarz, K. (2016). β-Lactoglobulin as nanotransporter--Part I: Binding of organosulfur compounds. *Food Chemistry*, *197*(Pt A), 1015–1021. https://doi.org/10.1016/j.foodchem.2015.11.010

6 Manuscript 4: Surface activity and foaming properties of whey protein isolate amyloid and non-amyloid fractions and their synergistic effects

Jacqueline Lux[a], Helena Schestkowa[b], Jörg Koop[c], Hendrikje R. Neumann[d], Christine Selhuber-Unkel[d], Karin Schwarz[a], Stephan Drusch[b], Julia Keppler[a], Anja Steffen-Heins[a]

[a]Institute of Human Nutrition and Food Science, Divison of Food Technology, Kiel University, Germany

[b]Insitute of Food Technology and Food Chemistry, Department of Food Colloids, Technical University Berlin, Germany

[c]Department of Biochemical and Chemical Engineering, Laboratory of Plant and Process Design, TU Dortmund University, Germany

[d]Institute of Materials Science, Department for Biocompatible Nanomaterials, Kiel University, Germany

6.1 Abstract

Foaming has been used as an exemplary food production process to which amyloid and non-amyloid protein material, including non-amyloid aggregates, peptides and unfolded proteins, from whey protein isolate (WPI) have contributed in different ways. For a better understanding of the foaming properties resulting from the different protein structures, the surface activity at the air-water-interface of fibrils, non-amyloid material <300 kDa and a mixture of both was investigated using drop tensiometry and Langmuir-Schäfer-Blodgett. Non-amyloid material dominated the adsorption behavior in amyloid aggregated systems (AAS), which was not apparent in a faster migration and adsorption rate, but resulted in a better foamability. In this AAS, the non-amyloid material was present in higher quantities, adjusted by lower initial protein concentrations. However, the slower diffusion of the larger fibrils in the foamate could be possibly be compensated by high surface hydrophobicity, possibly based on a faster adsorption and formation of capillary forces between the already adhering fibrils, thus attracting further fibrils. WPI fibrils can probably form a nematic and elastic domain at the air-water interface, in which the small and non-amyloid material present could be embedded. This in turn could increase the density and stiffness of the network and thus the interfacial stability of the WPI. AFM images after foaming indicated that partial mechanical comminution of fibrils occurred, most likely due to the shear stress caused by airflow. As a consequence, fibrils and non-amyloid material acted synergistically at the air-water interface, whereby only small amounts of amyloid aggregates were required to stabilize foams. This in turn demonstrated that when using WPI in the foaming process, all the protein material from the amyloid aggregation at pH 2 should be used.

6.2 Introduction

Whey is a by-product in the dairy industry and as a functional ingredient in a number of food products it is an important protein source for the food industry. It is often used in the form of whey protein isolate (WPI), which consists mainly of β-lactoglobulin (β-lg) (~77%) and proportionally of α-lactalbumin (α-la) (~21%) and bovine serum albumin (~2%) (cf. 2.1). Its increasing demand is due to its properties such as surface activity, gelling, foaming and film formation, which can also be improved by tailor-made structuring of proteins, e.g. by amyloid aggregation. To form functional amyloid aggregates from WPI, it is necessary to heat the proteins at pH values far from the isoelectric point and at low ionic strength where they are highly charged. For pure β-lg, Heyn et al. (2019) recently found that a temperature of >70°C and a pH of <3 is required for fibril formation. However, the most studied conditions for functional β-lg fibrils are heating for at least five hours at ~90°C, pH 2 and low ionic strength (Akkermans, Venema et al., 2008) leading to hydrolyzed β-sheet peptides, which are stacked

to form semi-flexible fibers of several micrometers in length and several nanometers in width. The prerequisite for fibril formation is thus the acid hydrolysis, since the hydrolysates are the building blocks of the fibrils (Akkermans et al., 2008). However, not all peptides are aggregated to fibrils, so that under these conditions 25-30% of pure β-lg were converted into amyloid aggregates (Heyn et al., 2019; Keppler et al., 2019). Various studies have already shown that different protein concentrations during amyloid aggregation lead to different conversion rates (Bolder, Vasbinder et al., 2007; Veerman, Ruis, Sagis, & van der Linden, 2002), which in turn suggests that the ratio between fibrils and non-amyloid protein material can be adjusted by changing initial protein concentrations. To separate fibrils from the non-amyloid protein material, the entire amyloid aggregate system (AAS) is often separated into two fractions by ultrafiltration (Akkermans et al., 2008). While the amyloid fraction (AF) consists primarily of fibrils and other aggregates larger than the selected molecular weight cut off of 300 kDa, the non-amyloid fraction (n-AF) contains mainly non-amyloid aggregates, peptides and remaining unfolded protein <300 kDa (Heyn et al., 2019). However, as currently proved by electron spin resonance spectroscopy, some non-amyloid aggregates and peptides are present in both fractions because they possibly are enclosed in the filter cake and thus remain in the AF (Lux et al., 2021b). In addition, the n-AF may also contain fragments of fibrils destroyed during the filtration step (Akkermans et al., 2008), however, after our ultrafiltration at 300 kDa we can clearly rule out the presence of amyloid material in n-AF (Lux et al., 2021a b).

The interfacial properties of functional amyloid fibrils have attracted much attention in the food industry because of their high foaming and emulsifying capacity. Pure β-lg amyloid fibrils adsorb at oil-water and air-water interfaces, leading to nematic domains and forming highly elastic films (Jordens et al., 2014; Jung et al., 2010). However, Jordens et al. (2014) also described a decrease in interfacial elasticity at higher concentrations of pure amyloid fibrils at the air-water interface, which they attributed to a multilayer adsorption and fibril fracture in the topmost layer. The fibrillar structure reduces the interfacial tension more rapidly than the native monomer system (Jung, Gunes, & Mezzenga, 2010). Apart from this, WPI fibrils have a higher emulsifying capacity, higher microencapsulation efficiency and result in higher oxidative stability than native WPI at pH 2 (Serfert et al., 2014). It is also described for WPI that the fibrillated WPI solution has a higher foam stability compared to untreated WPI due to a higher viscosity and gel-like network in the solution (Mohammadian & Madadlou, 2016). Wan et al. (2016) observed for soy bean fibrils that the fibril system, containing amyloid aggregates and non-amyloid protein and peptides, behave in the same way as pure peptides in reducing the interfacial tension and in foaming behavior, regardless of the pH-value. The pure fibrils reduced the interfacial tension slower and weaker and resulted in a lower foam stability compared with the native protein. However, to determine

consider the main influencing factor of the foamability, the influence of the pure fibrils and the non-amyloid materials on the foaming properties should be investigated separately to determine the driving force and investigate their synergistic effects. Due to the high energetic expenditure necessary for the formation of fibrils, an unheated (UH) and a short-time heated sample (STH) were compared.

With this background, the individual fractions of the WPI AAS obtained by ultrafiltration (MWCO = 300 kDa) after amyloid aggregation at pH 2 and 90°C, was investigated with regard to their surface activity and foaming properties. The individual fractions were investigated separately to determine their impact within AAS. WPI was used instead of pure β-lg due to its relevance for the food industry. During the foaming process, two processes have to be considered: 1. the migration of the surfactants to the surface and 2. its adsorption, including reorientation or rearrangement of the protein. Migration to the surface and the adsorption rate were investigated with the pendant drop tensiometer. The droplet shape depends on the surface tension and can be calculated by optical evaluation. The migration is characterized by the time the surfactant needs to reach the surface and the adsorption rate is the speed of reduction of interfacial tension. Since foam formation is usually a fast process, it is not only important that the interfacial tension (IFT) is greatly reduced, but also that the proteins migrate rapidly to the interface to adsorb there. Furthermore, foamability and foam stability are investigated by foaming amyloid fibril solutions and measuring the foam volume and in relation to the foaming time, as well as by measuring the protein concentration in the foamate and retentate.

6.3 Material and methods

6.3.1 Materials

The whey protein isolate (WPI) (~77% β-lg, ~21% α-la, ~2% bovine serum albumin; analyzed by HPLC) BiPro was purchased from Davisco Foods International (Eden Prairie, Minnesota, USA).

6.3.2 Methods

6.3.2.1 Preparation of WPI amyloid aggregates

Preparation of WPI fibrils was carried out according to Serfert et al. (2014). A WPI solution at a concentration of 2.5% was adjusted to pH 2 with 6 M HCl. For fibril formation the WPI solution was heated at 90°C for five hours under stirring (350 rpm, 2mag MIXdrive 6HT, 2mag AG, Munich, Germany). Sampling was performed at three different times: the unheated samples (UH), short-time heated for 30 min at 90°C (STH) were used as control for

an untreated sample and a partly denatured but non-hydrolyzed and therefore non-fibrillated sample. The five hours heating resulted in the amyloid aggregate system (AAS) consisting of the amyloid fraction (AF) and the non-amyloid fraction (n-AF). Fibril formation was almost completed and all proteins were unfolded after five hour heat incubation (Heyn et al., 2019). Solutions were cooled on ice and stored at 4°C until further use. Additional experiments were carried out by varying the protein concentration from 1% to 5%. For the analysis all dilutions were carried out with MilliQ water adjusted to pH 2 with HCl.

6.3.2.2 Separation of individual fractions by ultrafiltration methods

Although we know that the separation of the two fractions cannot be fully achieved (Lux et al., FOODHYD_2020_529), we assume a sufficient separation to estimate the contribution of the individual fractions. To separate mainly the amyloid aggregates from the non-amyloid aggregates and peptides, the AAS were diluted 5-fold and filtered with ultrafiltration centrifugal concentrators (Vivaspin 20, 300 kDa, PES, Sartorius, Göttingen, Germany). The concentrators were washed with pH-adjusted water. 10 ml of the diluted sample were filled in the washed concentrators, weighted and centrifuged for 15 min at 1000*g at room temperature. After each centrifugation step the retentate were refilling with pH 2 water up to the initial weight and scratching the protein adhering to the membrane with a plastic spatula. The procedure was repeated three times. The retentate of the last centrifugation step was filled up to the initial volume with pH 2 water and hereafter named amyloid fraction (AF). The permeate of each filtering step was combined as a total permeate (n-AF).

The conversion rate from β-lg into amyloid aggregates prepared with initial protein concentrations of 1%, 2.5%, and 5% were determined according to Serfert et al. (2014). The different initial protein concentrations were used to vary the AF/n-AF ratio. The AAS were diluted to 0.1% protein concentration and filtered with ultrafiltration centrifugal concentrators (Vivaspin 2, 300 kDa; Sartorius GmbH, Göttingen, Germany). The samples were washed three times with pH 2-water. The conversion rate was defined as the protein, which remains in the retentate after ultrafiltration.

The protein concentration was measured at 278 nm using a UV-Vis spectrometer (Helios Gamma, UV-Vis, Thermo Spectronic, Cambridge, UK) in a quartz cell and calculated by a calibration curve for WPI at pH 2. For further measurements, all samples were diluted to the same protein concentration.

6.3.2.3 Langmuir-Blodgett measurements

The pressure-area isotherm were recorded with a Langmuir-Blodgett trough (Modell: 611D, NIMA Technology, UK). 50 ml water adjusted to pH 2 was used as sub phase. For the PAI, 50 µl of a 0.01% protein solution was applied dropwise on the surface and equilibrated for 15 min. The area was compressed to 8 cm^2 and expanded to 94 cm^2 with a speed of

0.358 cm^2 s^{-1} and the surface pressure was measured. All measurements were carried out in triplicate.

6.3.2.4 Pendant drop tensiometry

The interfacial tension of AF, n-AF and AAS (1%, 2.5%, 5%) against air was measured with an automated drop tensiometer (OCA20, Dataphysics GmbH, Germany), equipped with a high speed camera (200 frames/second). Therefore, a two-fluid needle system was used as described by Tamm, Sauer, Scampicchio, & Drusch (2012) with slight modifications. Through a large needle (d = 1.65 mm), 14 µL water was dosed manually, whereas 1 µL of 0.15% sample solution was dosed by an automatic injection system through a small needle (d = 0.51 mm) into the initial water droplet. The total protein concentration was 0.01%. Results were evaluated according to Schestkowa et al. (2019), where the migration of the samples through the bulk phase, adsorption, and reduction of the air-water interface were analyzed. The migration through the bulk phase was estimated by the lag time, knowing that the migration is not only diffusion-controlled (Ward & Tordai, 1946). The lag time represents the time period from the beginning of expanding drop volume until the interfacial tension started to decrease. The adsorption rate describe the adsorption process and was calculated by a nonlinear regression using GraphPad Prism (version 6.07, GraphPad Software, San Diego, CA, USA). The span of the nonlinear regression were used as reduction of the interfacial tension.

6.3.2.5 Foaming experiments

The foaming experiments were performed in a glass jacketed column (lower part: 130 mm length, 35 mm inner diameter; upper part: 420 mm length, 20 mm inner diameter), for schematic view see Barackov et al. (2012). The AAS with an initial protein concentration of 1%, 2.5% and 5% were used and diluted to a final concentration of 0.01%. 90 g of the 0.01% AAS solution were used as feed solution. The solution was sparged with gas by a porous glass frit P3 of a pore size 16-40 µm (ROBU, Hattert, Germany), in the bottom of the column. The airflow was set to 7 l/h. The foaming was conducted until the continuous foam flow was interrupted by large holes formed due to lamella rupture and coalescence. The foamate and the retentate were collected, weighted and the protein concentration was measured at 278 nm wavelength using a UV-Vis spectrometer (Spectro 50, Analytik Jena AG, Jena, Germany) in micro UV cuvettes (BRAND, Wertheim, Germany). The foamability was indicated by the volume of the foamate ($V_{Foamate}$) and $V_{Foamate}$/time as surface activity indicator (Halling, 1981). The foam stability was indicated by the protein concentration in the retentate. The decisive factor that changes during foaming is the protein concentration in the liquid phase. This decreases until the foam is no longer stable enough to reach the top of the column. This means that the foam stability at the end of the experiment is the same in all cases. At a lower

retentate concentration, the protein has better foam stabilization properties, as less surfactant is needed to achieve the same effect.

6.3.2.6 AFM measurements

Atomic force microscopy (NanoWizard 3, JPK Instruments AG, Berlin, Germany) was used to visualize fibrillar structures. Foamate samples were diluted to ~0.01% protein with pH 2-water and 2 µl were put on a freshly cleaved mica, dried, and washed with 200 µl ultra-pure water. For tapping mode, ACTA-cantilevers (spring constant 40 N/m, resonance frequency 300 kHz; Applied Nano-Structures, Inc., Mountain View, USA) were used at a scan rate of 0.5 Hz.

6.3.2.7 Statistical analysis

All results were presented as means and standard deviations of the replicated sample preparations and analyses. The data were analyzed by two-way ANOVA with Tukey's multiple comparison test at a significance level of $\alpha=0.05$. All statistics and figures were created using GraphPad Prism (version 6.07, GraphPad Software, San Diego, CA, USA).

6.4 Results

6.4.1 Determination of the conversion rate from WPI to amyloid aggregates

The variation of the initial protein concentration for amyloid aggregation process resulted in different conversion rates (Figure 6-1). The conversion rate was determined by separation of the amyloid aggregates (>300 kDa) from smaller aggregates, peptides and unfolded protein (<300 kDa). The protein concentration of the retentate was measurement in relation the unfiltered samples. The lower the initial protein concentration the lower was the fibril-conversion rate and the higher was the amount of non-amyloid peptides. An initial protein concentration of 1% resulted in 10.6 ± 4%, 2.5% in 18.2 ± 0.03%, and 5% in 27.5 ± 1.1% amyloid aggregates.

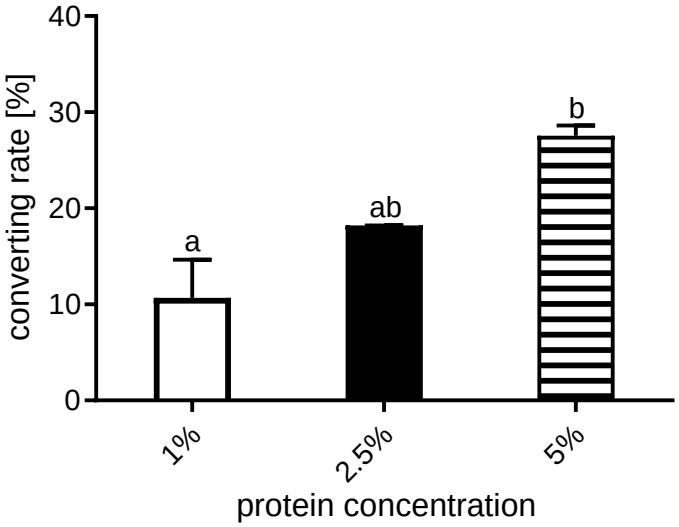

Figure 6-1: Conversion rate of WPI into amyloid aggregates with different initial protein concentration: 1% (unfilled), 2.5% (filled) or 5% (striped), determined by protein concentration measurements in the retentate after ultrafiltration in relation to the protein concentration before ultrafiltration. All initial protein concentrations were diluted to the same protein concentration before separation. Different letters indicate significant differences ($p<0.05$).

6.4.2 Pendant drop measurements

6.4.2.1 Pendant drop measurements of AAS with varying initial protein concentrations

The migration and the adsorption of the amyloid aggregate system (AAS) with different AF/n-AF ratios to the air-water interface, was analyzed using the pendant drop tensiometer (Figure 6-2). By varying the initial protein concentrations (1%, 2.5%, and 5%), different AF/n-AF ratios were achieved. The total reduction of the interfacial tension (ΔIFT, ~72 mN/m → ~59 mN/m) provides information about the ability of a substance to reduce the IFT, whereas a stronger reduction indicates a better surface activity. In the present case, however, the surface activity did not change as a function of the AF/n-AF ratio (Figure 6-2A). The lag time represents the time between sample injection into the droplet and the time point at which the IFT begins to decrease. This in turn describes the migration velocity of the substances to the interface. The migration velocity was also the same for all samples, independent on the protein concentrations during fibril formation (Figure 6-2B). The rate constant or adsorption rate, which indicates how fast a compound can reduce the IFT, was also not significantly affected by a change in the AF/n AF ratio (Figure 6-2C).

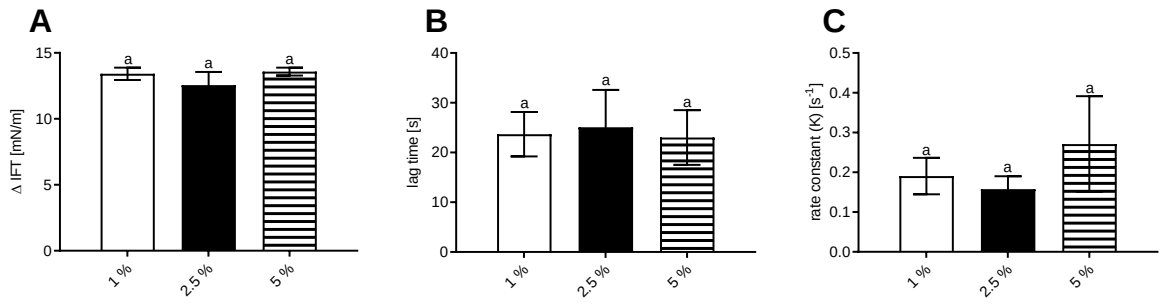

Figure 6-2: Pendant drop measurements of whey protein isolate solution at pH 2, heated for five hours at 90°C (AAS), with different initial protein concentration: 1% (unfilled), 2.5% (filled) or 5% (striped). (A) Total reduction of the IFT, (B) lag time (time between sample injection and reduction of the IFT), and (C) adsorption rate constant ratio (K) measured at pendant drop tensiometer with a droplet volume of 15 µl and a final protein concentration of 0.01%. ($p<0.05$%, ANOVA)

6.4.2.2 Pendant drop analysis of the different fraction

The measurement of the interfacial tension of the pendant drop over time (Figure 6-3A-E) demonstrated that the unheated sample (UH), the short-time heated sample (STH), and the amyloid aggregate system (AAS) displayed a large variance. The separation of the AAS by ultrafiltration resulted in two fractions, which were measured to investigate the surface activity of amyloid aggregates and the non-amyloid fraction separately. The pendant drop measurement of the AF and n-AF resulted in more reproducible results with a much lower variance compared to UH, STH, and AAS (Figure 6-3D-E).

From the pedant drop curves, the lag time, ΔIFT, and the rate constant were extracted (Figure 6-3F-H). AAS, AF, and n-AF exhibited the shortest lag time, which was significantly lower compared with UH and STH WPI (Figure 6-3F). Although a statistically significant difference in the decay of the IFT between STH and AF was found, it is very small and negligible due to the inhomogeneity of the STH measurement (Figure 6-3G). The rate constant (Figure 6-3H) represents the adsorption rate. The n-AF had the significant fastest adsorption rate, followed by the AAS and the AF, having the same rate constant (Figure 6-3H). The UH and STH samples had the slowest adsorption rate.

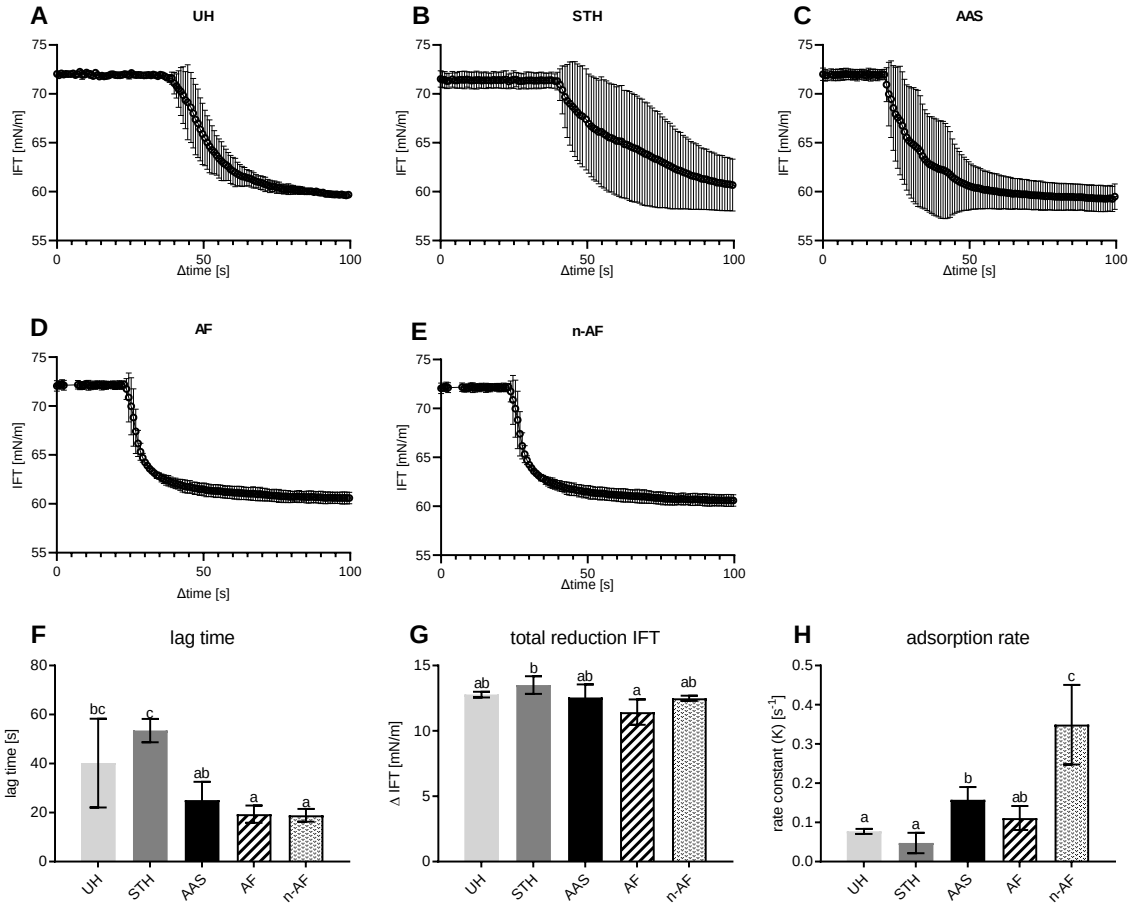

Figure 6-3: Interfacial tension (IFT) measurements (A-E), and the extracted results (F-H) measured at pendant drop tensiometer with a droplet volume of 15 µl and a final protein concentration of 0.01%. 2.5% of unheated (UH) WPI, short time (30 min) heated (STH) or heated for five hours at 90°C, resulting in the amyloid aggregate system (AAS). The AAS were separated by ultrafiltration in the amyloid fraction (AF) and non-amyloid fraction (n-AF). The lag time (F) is the time between the sample injection and the reduction of the IFT, representing the migration rate, ΔIFT (G) represented the total reduction of the interfacial tension, and rate constant (H) represented the adsorption rate. ($p<0.05$, ANOVA)

6.4.3 Pressure-area isotherm recorded with Langmuir-Blodgett trough

The structural characteristics of spread films can be obtained through pressure-area (π–A) isotherms. After equilibrating the samples at the air-water interface, the protein film was compressed and expanded while the interfacial pressure was measured. Summed up, the interfacial tension and the interfacial pressure amount to about -72.8 mN/m. During compression and expansion, the monolayer undergoes several phase transformations. All samples resulted in different π–A isotherms (Figure 6-4A). For all samples, a hysteresis between compression and expansion was observed. However, the expansion curve was similar for all samples. The samples mainly differ in the first phase transition from the gas like phase to a liquid like phase with a lower monolayer compressibility. The AAS sample underwent the phase transition at the largest area (~40 cm^2), followed by the AF and the n-

AF. In contrast, the interfacial pressure of UH and STH only considerably increased at an area <30 cm^2.

To deduce the order of the respective protein molecules and aggregates at the interface, the areas occupied by the proteins at a defined interfacial pressure of 15 mN/m were derived from the compression curves (Figure 6-4B). The larger the surface area when the defined pressure was attained, the faster the proteins reached the first phase transition, i.e., the denser is the protein ordered at the interface. This was the case for AAS followed by AF and n-AF. UH and STH reached 15 mN/m at a significant smaller surface area compared to AAS.

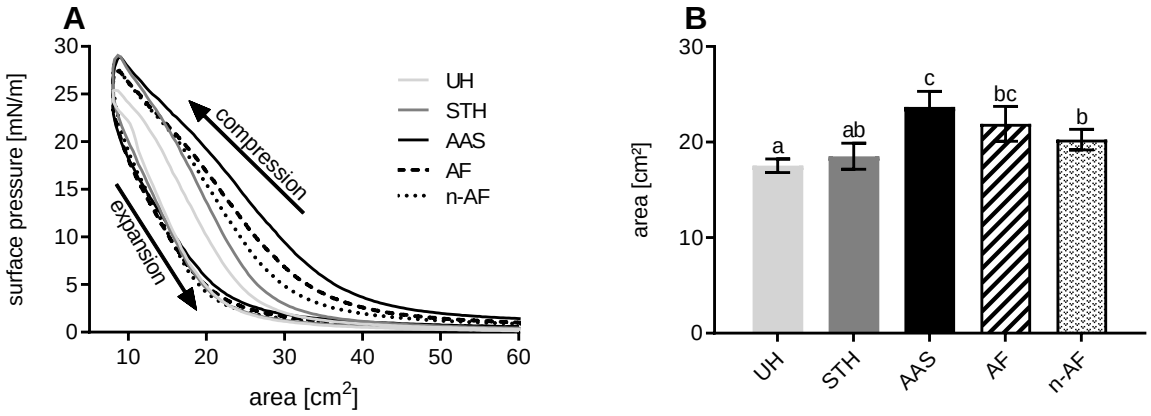

Figure 6-4: Pressure-area isotherm (π–A) of 50 µl sample diluted to 0.01% were compressed and expanded from 94 cm^2 to 8 cm^2 to 94 cm^2 at a Langmuir-Blodgett after equilibration for 15 min (A). Area at a pressure 15 mN/m of the π–A isotherm (B). Different letters indicate significant differences ($p<0.05$, ANOVA).

6.4.4 Foaming measurements of amyloid aggregates with different initial protein concentration

For the measurement of the foamablity and the foam stability a glass jacketed column was used. The foamability describes the capability of a protein to form foam and was measured by the foamate volume ($V_{Foamate}$) (Figure 6-5A) as well as by the mean foamate flow, described by the $V_{Foamate}$ per time ($V_{Foamate}$/time) (Figure 6-5B). The higher the $V_{Foamate}$ and $V_{Foamate}$/time, the better the foamability. A high $V_{Foamate}$, indicates that more water was transported over the whole foaming time, the reason could be that smaller bubbles were formed, or the foam flow was stable for a longer time. Because the protein concentration in the retentate changes only by a small amount and the feed concentration is the same in all experiments, the amount of transferred protein is nearly constant in all experiments. Thus, it can be stated, that less protein is needed to stabilize the interfacial area. On the process

side, that could can either be the result of a lower surface excess needed for stabilization or smaller bubbles leading to a higher foam density (Hofmann, Schembecker, & Merz, 2015).

If $V_{Foamate}$ was calculated relative to foam time, a higher $V_{Foamate}$/time indicates an increased foam density because the airflow is constant in all experiments. Thus, the water content is higher, which affirms the assumption of thicker smaller bubbles (Hofmann et al., 2015). The highest $V_{Foamate}$ (19.13 ml) was measured with an initial protein concentration of 1% during the fibril formation, and decreased with increasing initial protein concentration (Figure 6-5A). The protein concentration in the feed solution were the same for all measurements, independent of initial protein concentration for fibril formation. Similar scheme was seen for $V_{Foamate}$/time (Figure 6-5B). The highest value (0.028 ml/s) was also achieved with an initial protein concentration of 1% but without significant differences to 2.5% (0.022 ml/s) and 5% (0.015 ml/s).

In contrast to the foamability, foam stability indicates how well a protein can stabilize a foam and was given as protein concentration in the retentate (Figure 6-5C). The lower the protein concentration in the retentate, the less protein is required to stabilize the foam (Figure 6-5C). The retentate represents remaining feed solution after foaming. The lowest retentate concentration was measured for an initial protein concentration of 1%, which is significantly lower as the retentate concentration for the samples with an initial protein concentration of 5%.

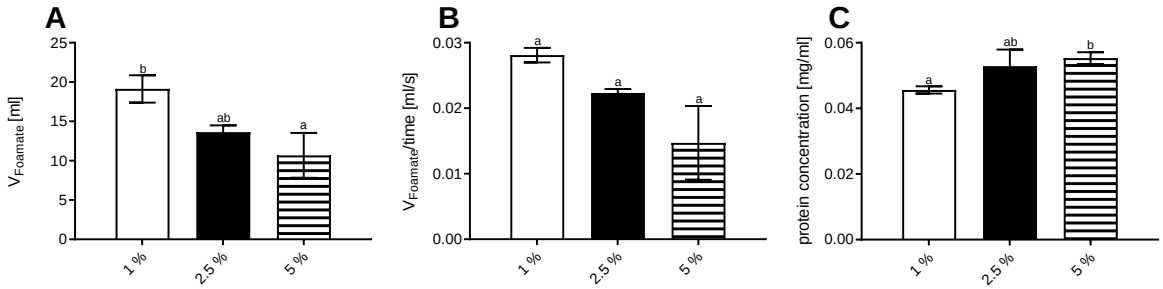

Figure 6-5: Foaming experiments of whey protein isolate solution at pH 2, heated for five hours at 90°C, with different initial protein concentration: 1% (unfilled), 2.5% (filled) or 5% (striped) protein. (A) Foamate volume, foamed until the continuous foam flow was interrupted (B) volume of the foamate per second and (C) retentate concentration. The samples were foamed in a glass jacketed column until the continuous foam flow was interrupted. ($p<0.05$, ANOVA)

6.4.5 AFM images of amyloid aggregates

Regardless of the initial protein concentration, amyloid aggregation at pH 2 resulted in long fibrils, (Figure 6-6A-C) before foaming. After foaming, long intact fibrils as well as smaller fragments were present in the foamate (Figure 6-6D-F), which were likewise independent on the initial protein concentration.

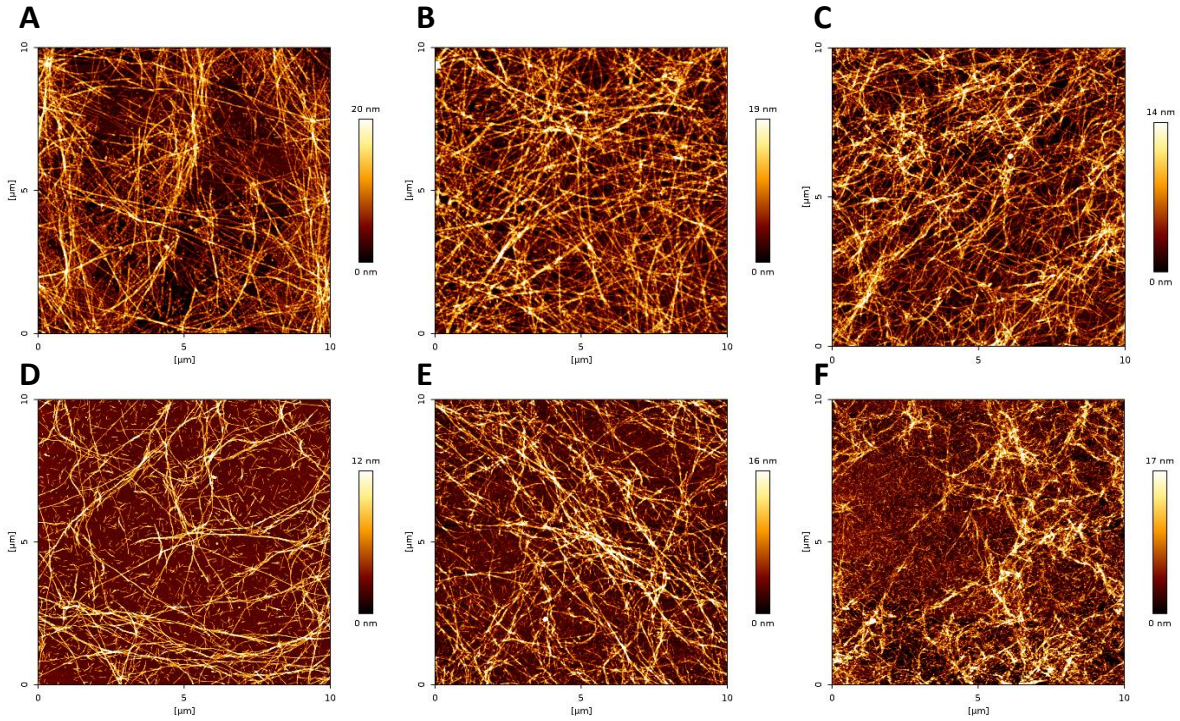

Figure 6-6: AFM images of amyloid aggregate solutions with initial protein concentrations of (A) 1%, (B) 2.5%, and (C) 5% and foamed amyloid aggregate solutions (D-F). The solutions were foamed in a glass jacketed column until the continuous foam flow was interrupted. The foamate were resuspended and prepared on a mica for recording of AFM images.

6.5 Discussion

6.5.1 Adsorption kinetic of AAS, AF, and n-AF

The change in the dynamic interfacial tension at the air-water interface after addition of UH (untreated proteins), STH (partly denatured proteins), or AAS (mixture of~18% fibrils and non-amyloid aggregates, peptides and partially unfolded proteins) revealed remarkable variances, which confirms the described molecular variety (Figure 6-3A-C). The diverse protein material migrated and adsorbed at different rates to the interface dependent on molecular weight, surface hydrophobicity, charge anisotropy and molecular flexibility of the individual particles (Atkinson, Dickinson, Horne, & Richardson, 1995; Bolder, Vasbinder et al., 2007; Unterhaslberger, Schmitt, Sanchez, Appolonia-Nouzille, & Raemy, 2006; Veerman et al., 2002) and resulted in high standard deviations. However, n-AF and AF had lower

standard deviations than AAS resulting from a more homogeneous peptide and aggregate size distribution after ultrafiltration (Figure 6-3D-E). The analysis of the dynamic surface tension demonstraded that the reduction of the IFT was comparable for all investigated samples (Figure 6-3G). The small difference between STH and AF in their ability to reduce the IFT is rather due to the variability of the protein material and therefore negligible.

The equally fast migration of the AAS, AF, and n-AF to the surface were contrary to the expectations that smaller peptides migrate faster to the interface than long rigid aggregates. It was also unexpected that no significant differences in the migration velocity of AAS or AF compared with n-AF could be observed (Figure 6-3F), since AAS and AF definitely contain larger aggregates than 300 kDa. For denatured and aggregated β-lg a more slowly migration to the interface and a slower adsorption rate were already described (Rullier, Novales, & Axelos, 2008; Unterhaslberger et al., 2006). It should also be taken into account that Schestkowa et al. (2019) assumed that the convection is similar for all samples at the same dosing rate and drop volume in all measurements and is therefore not responsible for any variations in the observed lag time. Nevertheless, the lag time of the AF were as short as for the n-AF, however, both were not significant shorter comparted to AAS (Figure 6-3F). From this observation, it may be concluded that some smaller aggregates <300 kDa and peptides may have remained in the AF, the retentate, because they may have accumulated in the long fibrillar filter cake during membrane filtration. This assumption has already been made for amyloid aggregates of pure β-lg, for which EPR measurements confirmed that spin labeled peptides and non-amyloid aggregates thereof smaller than 300 kDa were present in both fractions (AF and n-AF) after separation of the AAS by ultrafiltration (Lux et al., FOODHYD_2020_529). In addition, the low surface hydrophobicity of the n-AF (Heyn et al. 2019) could prevent rapid adsorption to the interface. The diffusion of the larger fibrils, which may be slowed down by the high aspect ratio and charge anisotropy, could be possibly be compensated by high surface hydrophobicity. This compensation may be based on a faster adsorption and formation of capillary forces between the already adhered fibrils, which may attract further fibrils.

The slower adsorption rate of proteins at the interface in the UH and STH samples compared to the AAS, AF and n-AF samples, which mostly consist of unfolded and hydrolyzed protein (Figure 6-3H), may be explained by the low conformational flexibility of the globular protein at pH 2. This leads to the fact that during its adsorption at the interface conformational changes and a rearrangement of the tertiary structure is needed (Atkinson et al., 1995), while simultaneously at pH 2 repulsion effects of the highly charged protein occurs, which may be probably less pronounced in the anisotropic distribution in the long fibrils. As expected, due to the smaller peptides and aggregates in n-AF and higher molecular flexibility compared to

those of AF, the former were able to adsorb much faster at the interface. Similarly, the comparable adsorption rates of AAS and AF are plausible, since the AAS contained ~20% WPI amyloid aggregates larger than 300 kDa (Figure 6-1). The AAS showed a slight trend towards a slightly faster adsorption than the pure fibrils, possibly indicating a steric hindrance of the smaller aggregates and peptides by the fibrillar structures. In addition, the n-AF peptides are more hydrophilic than the AF, because more hydrophobic amino acids were present in the amyloid aggregates (Akkermans et al., 2008; Heyn et al., 2019). Although the higher hydrophobicity of the AAS is associated with improved adsorption at the interface, the large size and rigidity of the aggregates and the associated reduced migration rates of the AAS could resulted in the slower adsorption rate compared to the n-AF. In addition, for freeze dried β-lg amyloid aggregates it was demonstrated that the n-AF had a higher zeta potential as well as lower nil red activity, as a direct measure for surface hydrophobicity, than the AF and AAS (Heyn et al., 2019) which in turn could have led to slower adsorption of the peptides due to the higher electrostatic repulsion of n-AF (Keppler, Steffen-Heins, Berton-Carabin, Ropers, & Schwarz, 2018). The slower aggregation may have favored rapid adsorption at the interface, since the peptides, if not aggregated, do not need to be rearranged for adsorption at the interface. Contrary to the study of Heyn et al. (2019), the present study used WPI, so the fractions contained also α-la and bovine serum albumin, which also could adsorb at the interface (Keppler et al., 2017; Keppler et al., 2018; Medrano et al., 2012). At pH 2 as much α-la adsorbs to the interface as at pH 7.5, while at pH 2 significantly less β-lg is adsorbed than at pH 2 (Dickinson & Matsumura, 1994; Keppler et al., 2018). The change in the conformation to a molten global state of α-la thus improves the adsorption at acidic pH values.

6.5.2 Structural characteristics of amyloid and non-amyloid films at the interface

The structural characteristics of the protein films at the air-water interface were determined by the π–A isotherms, whereby all investigated fractions demonstrated hysteresis (Figure 6-4A). While the absence of a hysteresis would have indicated a stable and reversible film (Glomm, Volden, Halskau, & Ese, 2009), the hysteresis loops indicated a slow adjustment of the molecular structure during expansion or a desorption from the film at high surface pressure (Glomm et al., 2009; Wang & Narsimhan, 2005). The higher decayed of the interfacial pressure during compression of the UH and STH samples compared with AAS (Figure 6-4B) could be explained by the smaller surface of proteins in UH and STH samples, and the associated smaller area that a protein can occupy at the air-water interface. Heating for five hours at 90°C resulted in a mixture of semi-flexible fibrils, peptides, non-amyloid aggregates, and monomeric sized protein, which in turn implies that the degradation of the protein into peptides and smaller aggregates leads to an increased surface requirement for the same protein content. Likewise, the low flexibility of the amyloid aggregates could result

in an increase of the surface pressure even with a larger area. Jordens et al. (2014) reported that at pH 2 the purified β-lg fibrils (MWCO = 100 kDa) aligned at the air-water interface into a 2D nematic domain with a strong network formation creating a very elastic interface. In this case, 70% of the interface was occupied by aligned fibrils, while the remaining area was covered by disordered filaments. Considering these findings, it may be assumed for WPI AAS that the present fibrils (~11-28%, Figure 6-1) also form a network at the interface, while the smaller aggregates, peptides and unfolded proteins may be incorporated into the fibrillar network interspaces. This suggestion might explain the early increase of the interfacial pressure of the AAS (Figure 6-4A), since the embedded smaller protein material may stiffen the fibrillar network. In contrast, the later rise in interfacial pressure of AF relative to AAS (Figure 6-4A) may be due to the reduced availability of smaller protein material. This would imply that if no or few peptides are embedded in the interspaces of the fibrillar network, the latter might be more compressible before the interfacial pressure increases. Because there were no amyloids and aggregates >300 kDa present in the n-AF, which would have formed a fibrillar network, the interfacial network of peptides and small non-amyloid aggregates may be compressed even more compared with AF and AAS.

6.5.3 Foaming behavior of the AAS with different initial protein concentrations

The amyloid aggregates with an initial protein concentration of 1% demonstrated the highest foamability and foam stability and the lowest ones at 5% (Figure 6-5). The lower the initial protein concentration, the lower was the fibril-conversion rate and the higher was the amount of peptides and non-amyloid aggregates, which applied for 1% protein (Figure 6-1). This effect was already described by Bolder et al. (2007), who heated WPI at 80°C for 34 h, which likewise resulted in a lower conversion rates for 1%, 2%, and 3% protein concentration but higher conversion rate (~45%) for 5% protein after 10 hours. Veerman et al. (2002) on the other hand, reported higher conversion rates in their study compared to the present results (1% → 45%; 2% → 60%; 4% → 70%). However, they used pure β-lg and a different method to determine the conversion rate; i.e. they separated the AF by removing all aggregates, which are insoluble at pH 4.8, regardless of the particle size, so that they include also non-fibrillar aggregates. Under the same conditions of amyloid aggregation and using ultrafiltration with the same MWCO, Keppler et al. (2019) measured a conversion rate of ~30% and Heyn et al. (2019) one of ~25% for pure β-lg with a protein concentration of 2.5%. Since the WPI used here had only a β-lg content of about 77%, a measured conversion rate of ~18% at a protein concentration of 2.5% (Figure 6-1) was consistent with the results of Heyn et al. (2019) and supported the observation that only β-lg from the WPI contribute to fibril formation (Bolder et al., 2006).

A higher content of peptides and small non-amyloid aggregates were favorable for foamability and foam stability (Figure 6-5), which could be explained by the high adsorption rate of the small molecular weight peptides (Figure 6-3H), as discussed in 6.4.1 In the case of transient foams, i.e. foams with a lifetime in the range of a few minutes, the foamability and foam stability cannot be considered separately because they are interdependent (Wang et al., 2016). The foaming behavior of AAS seems to be dominated by these peptides and peptide aggregates, whose content was higher at lower initial protein concentrations (Figure 6-1). This was in line with the observations of (Wan, Yang, & Sagis, 2016) who demonstrated for soy glycine fibril systems that the peptides are responsible for the foaming properties because they moved faster to the interface than the fibrils.

Also in a WPI bead system, the smaller constitutes were likely to play the major role on the rheological properties at the air-water interface (Yang, Thielen, Berton-Carabin, van der Linden, & Sagis, 2020). Apart from that, the strong electrostatic repulsion and the slower adsorption at the interface of the amyloid aggregates formed at pH 2 (Peng et al., 2017) might cause the involvement of the fibrils in the foaming process to be very low. This assumption could be further supported by the observations of Oboroceanu et al. (2014) since they could prove that foam stability and foamability were independent of the length of the amyloid fibrils and consequently of the migration rate. The dominant influence of peptides and peptide aggregates in AAS with different initial protein concentrations was found only in the foaming experiments (Figure 6-5), whereas the measurements with the pendant drop tensiometer showed no significant differences in surface activity as a function of the initial protein concentration (Figure 6-2). On the one hand, the flow forces generated in the foaming process used here may overlap the migration of the protein material, so that the particle size-related migration may be less relevant. On the other hand, the foaming process is much more complex and cannot be characterized solely by investigations of the interfacial tension, i.e., that other factors apart from the adsorption rate also determine the foaming properties (Rullier et al., 2008). Davis and Foegeding (2004) investigated the impact of polymerized WPI on the reduction of the IFT. The more polymerized protein was present, the slower were the reduction of the IFT. Also Rullier et al. (2008) found that the amount of aggregates in a mixture of monomeric β-lg and bigger aggregates has a strong influence on the foam formation and stability. Only 2% non-aggregated protein needed to be present to reach a foam formation as without any aggregates. For the foam stability, at least 10% monomeric protein was necessary. Only a low amount of non-aggregated protein was sufficient to dominate the foaming properties. The foaming experiments (Figure 6-5) confirmed that the more amyloid aggregates were present, the lower the foam formation and stability.

6.5.4 Physical stability of the AAS at the air-water interface during foaming

In the AFM images of the AAS with different protein concentrations after foaming (Figure 6-6D-F) compared with the samples before foaming (Figure 6-6A-C), not only the long fibrils but also smaller fibrillar structures were visible. Two different scenarios are plausible which may explain this observation. On the one hand, the adsorption at the interface may cause mechanical comminution, which may occur either by the adsorption process itself or by the adsorption at a curved interface. It is known that native β-lg undergoes a rearrangement of the tertiary structure by adsorption at the interface (Atkinson et al., 1995). This effect may also play a role in the adsorption of the fibrillar structure and, due to the low flexibility of the fibrils, consequently leading to their rupture. The assumption that rather curvature of the surface is likely to be responsible for the rupture might be confirmed by the study of Jordens et al. (2014; 2013) who could demonstrate no or only a minor mechanical comminution of the fibrils by adsorption at the planar air-water interface measured by the Langmuir-Schäfer-Blodgett method. On the other hand, it is very likely that the air flow used for foaming in the glass jacketed column generated sufficient shearing to result in the comminution of the fibrillar structures. Recently, Uttinger et al. (2020) observed that the comminution of amyloid aggregates is related to energy input, even though they describe a complete disintegration of the aggregates. However, this would suggest that the foaming process only locally led to a sufficient energy input that was strong enough to break up the amyloid aggregates which in turn suggests that the second scenario is more likely.

6.5.5 Synergistic effects of AF and n-AF

The larger surface area of the n-AF than that of the unheated protein (Figure 6-4A) may be explained by the extreme inflexibility and by a tight folding of native β-lg at pH 2 (Keppler et al., 2017), which also resulted in a low surface adsorption capacity at low pH values (Keppler et al., 2018). Contrary to that, the acid hydrolyzed peptides of the n-AF revealed an open conformation (Heyn et al., 2019) and may probably freely spread on the surface. The foamability and the foam stability were significantly enhanced at a lower initial protein concentration (Figure 6-5), which is related to a higher content of hydrolyzed peptides and non-amyloid aggregates relative to fibrils (Figure 6-1). This observation was consistent with the study of Wan et al. (2016), who investigated that the adsorption behavior of a soy bean fibril system was mainly dominated by the non-amyloid peptides, particularly in the initial adsorption due to the faster migration and adsorption rate. In summary, it can be deduced from these results and the literature data that when considering short periods of time, e.g. the adsorption behavior or the foaming via glass jacketed column, the smaller aggregates and particularly the peptides were more surface active than the fibrillar structures. However, the π–A isotherm of the mixture of the AF and n-AF demonstrated an early increase in interfacial

pressure at a large relative surface area, indicating an early phase transition from the gas phase to the liquid-like phase (Figure 6-4A). This would imply the synergistic effect of fibrils and small non-fibrillar material, because aligned long fibrils at the air-water interface and smaller aggregates and peptides embedded therein may form a denser network (cf. 6.4.2). However, it should be noted that formation of this synergistic network is on a larger time scale than the measurement of adsorption behavior or foaming. From this it may be concluded that amyloid aggregates supported a good foamability in the long term, but the small aggregates and peptides indicated better surface activity in the short term measurements.

6.6 Conclusion

The present study investigated the contribution of the individual fractions of an amyloid aggregate system from WPI to surface activity and foaming behavior. The fractions used were obtained by ultrafiltration. The non-amyloid fraction consisted of non-amyloid aggregates <300 kDa, peptides, and unfolded protein (β-lg, α-la, bovine serum albumin), while the amyloid fraction contained fibrillar structures with some residues of small non-amyloid material. Considering different time scales, the contribution to surface activity switched between both fractions. In short-term measurements, the peptides and small non-amyloid aggregates were more surface active, because they exhibited a faster migration and adsorption rate than the fibrillar structures. This was also confirmed by a better foamability of AAS in which the smaller non-amyloid aggregates, peptides and unfolded protein were present in higher quantities, adjusted by lower initial protein concentrations. However, it was not possible to determine exactly which of these smaller materials –whether peptides or aggregates– improve foamability the most. The diffusion of the larger fibrils, which may be slowed down by the high aspect ratio and charge anisotropy, could be possibly be compensated by high surface hydrophobicity. This compensation may be based on a faster adsorption and formation of capillary forces between the already adhered fibrils, which may attract further fibrils. After a period longer than a few minutes, the WPI fibrils may align at the air-water interface and probably form a nematic and elastic domain as described for pure β-lg fibrils (Jordens et al., 2014). The existing small and non-amyloid material could be embedded in this fibrillar network, which in turn could increase the density and stiffness of the network and thus the interfacial stability of the WPI. However, the AFM images after foaming indicate that partial mechanical comminution of fibrils occurred, most likely due to the shear stress caused by air injection. As a consequence, the amyloid aggregates had a supporting effect on the non-amyloid fraction, which is crucial for a rapid reduction of the interfacial pressure, so that the entire aggregated system may be useful when using WPI for foaming. Therefore it

can be recommended for food purposes to preferably use WPI as fibrillated protein, since the synergisms of few fibrils and more non-amyloid aggregates can improve the foaming properties compared to pure β-amyloid aggregates.

Acknowledgment

Funding: The authors thank the German Research Foundation (DFG) for financial support of this work within the SPP 1934 DiSPBiotech (project number 273937032).

We would like to thank Judith Kolodziej (Food Technology, Kiel University) for her competent assistance in the laboratory.

6.7 References

Akkermans, C., Venema, P., van der Goot, A. J., Gruppen, H., Bakx, E. J., Boom, R. M., & van der Linden, E. (2008). Peptides are building blocks of heat-induced fibrillar protein aggregates of beta-lactoglobulin formed at pH 2. *Biomacromolecules*, *9*(5), 1474–1479. https://doi.org/10.1021/bm7014224

Atkinson, P. J., Dickinson, E., Horne, D. S., & Richardson, R. M. (1995). Neutron reflectivity of adsorbed β-casein and β-lactoglobulin at the air/water interface. *J. Chem. Soc., Faraday Trans.*, *91*(17), 2847–2854. https://doi.org/10.1039/FT9959102847

Barackov, I., Mause, A., Kapoor, S., Winter, R., Schembecker, G., & Burghoff, B. (2012). Investigation of structural changes of β-casein and lysozyme at the gas-liquid interface during foam fractionation. *Journal of Biotechnology*, *161*(2), 138–146. https://doi.org/10.1016/j.jbiotec.2012.01.030

Bolder, S. G., Hendrickx, H., Sagis, L. M. C., & van der Linden, E. (2006). Fibril assemblies in aqueous whey protein mixtures. *Journal of Agricultural and Food Chemistry*, *54*(12), 4229–4234. https://doi.org/10.1021/jf060606s

Bolder, S. G., Vasbinder, A. J., Sagis, L. M.C., & van der Linden, E. (2007). Heat-induced whey protein isolate fibrils: Conversion, hydrolysis, and disulphide bond formation. *International Dairy Journal*, *17*(7), 846–853. https://doi.org/10.1016/j.idairyj.2006.10.002

Davis, J. P., & Foegeding, E. A. (2004). Foaming and Interfacial Properties of Polymerized Whey Protein Isolate. *Journal of Food Science*, *69*(5), C404-C410. https://doi.org/10.1111/j.1365-2621.2004.tb10706.x

Dickinson, E., & Matsumura, Y. (1994). Proteins at liquid interfaces: Role of the molten globule state. *Colloids and Surfaces B: Biointerfaces*, *3*(1-2), 1–17. https://doi.org/10.1016/0927-7765(93)01116-9

Glomm, W. R., Volden, S., Halskau, & Ese, M.-H. G. (2009). Same system-different results: The importance of protein-introduction protocols in Langmuir-monolayer studies of lipid-protein interactions. *Analytical Chemistry*, *81*(8), 3042–3050. https://doi.org/10.1021/ac8027257

Halling, P. J. (1981). Protein-stabilized foams and emulsions. *Critical Reviews in Food Science and Nutrition*, *15*(2), 155–203. https://doi.org/10.1080/10408398109527315

Heyn, T. R., Garamus, V. M., Neumann, H. R., Uttinger, M. J., Guckeisen, T., Heuer, M., Keppler, J. K. (2019). Influence of the polydispersity of pH 2 and pH 3.5 beta-lactoglobulin amyloid fibril solutions on analytical methods. *European Polymer Journal.* Advance online publication. https://doi.org/10.1016/j.eurpolymj.2019.08.038

Hofmann, A., Schembecker, G., & Merz, J. (2015). Role of bubble size for the performance of continuous foam fractionation in stripping mode. *Colloids and Surfaces A: Physicochemical and Engineering Aspects*, *473*, 85–94. https://doi.org/10.1016/j.colsurfa.2014.12.042

Jordens, S., Isa, L., Usov, I., & Mezzenga, R. (2013). Non-equilibrium nature of two-dimensional isotropic and nematic coexistence in amyloid fibrils at liquid interfaces. *Nature Communications*, *4*, 1917. https://doi.org/10.1038/ncomms2911

Jordens, S., Rühs, P. A., Sieber, C., Isa, L., Fischer, P., & Mezzenga, R. (2014). Bridging the gap between the nanostructural organization and macroscopic interfacial rheology of amyloid fibrils at liquid interfaces. *Langmuir: the ACS Journal of Surfaces and Colloids*, *30*(33), 10090–10097. https://doi.org/10.1021/la5020658

Jung, J.-M., Gunes, D. Z., & Mezzenga, R. (2010). Interfacial activity and interfacial shear rheology of native β-lactoglobulin monomers and their heat-induced fibers. *Langmuir: the ACS Journal of Surfaces and Colloids*, *26*(19), 15366–15375. https://doi.org/10.1021/la102721m

Keppler, J. K., Heyn, T. R., Meissner, P. M., Schrader, K., & Schwarz, K. (2019). Protein oxidation during temperature-induced amyloid aggregation of beta-lactoglobulin. *Food Chemistry*, *289*, 223–231. https://doi.org/10.1016/j.foodchem.2019.02.114

Keppler, J. K., Steffen-Heins, A., Berton-Carabin, C. C., Ropers, M.-H., & Schwarz, K. (2018). Functionality of whey proteins covalently modified by allyl isothiocyanate. Part 2: Influence of the protein modification on the surface activity in an O/W system. *Food Hydrocolloids*, *81*, 286–299. https://doi.org/10.1016/j.foodhyd.2018.03.003

Keppler, J. K., Martin, D., Garamus, V. M., Berton-Carabin, C., Nipoti, E., Coenye, T., & Schwarz, K. (2017). Functionality of whey proteins covalently modified by allyl isothiocyanate. Part 1 physicochemical and antibacterial properties of native and modified whey proteins at pH 2 to 7. *Food Hydrocolloids*, *65*, 130–143. https://doi.org/10.1016/j.foodhyd.2016.11.016

Lux, J., Heyn, T.R., Kampen, I., Schwarz, K., Keppler, J.K., Steffen-Heins, A. (2021a). Amyloid aggregation of spin-labeled β-lactoglobulin. Part I: Influence of spin labeling on amyloid aggregation. *Food Hydrocolloids*, 112, 106178, https://doi.org/10.1016/j.foodhyd.2020.106178

Lux, J., Azarkh, M., Fitzner, L., Keppler, J.K., Schwarz, K., Drescher, M., Steffen-Heins, A. (2021b). Amyloid aggregation of spin-labeled β-lactoglobulin. Part II: Identification of spin labeled protein and peptide sequences after amyloid aggregation. *Food Hydrocolloids*, 112, 106174, https://doi.org/10.1016/j.foodhyd.2020.106174

Medrano, A., Abirached, C., Araujo, A. C., Panizzolo, L. A., Moyna, P., & Añón, M. C. (2012). Correlation of average hydrophobicity, water/air interface surface rheological properties and foaming properties of proteins. *Food Science and Technology International = Ciencia Y Tecnologia De Los Alimentos Internacional*, *18*(2), 187–193. https://doi.org/10.1177/1082013211415137

Mohammadian, M., & Madadlou, A. (2016). Characterization of fibrillated antioxidant whey protein hydrolysate and comparison with fibrillated protein solution. *Food Hydrocolloids*, *52*, 221–230. https://doi.org/10.1016/j.foodhyd.2015.06.022

Oboroceanu, D., Wang, L., Magner, E., & Auty, M. A.E. (2014). Fibrillization of whey proteins improves foaming capacity and foam stability at low protein concentrations. *Journal of Food Engineering*, *121*, 102–111. https://doi.org/10.1016/j.jfoodeng.2013.08.023

Peng, D., Yang, J., Li, J., Tang, C., & Li, B. (2017). Foams Stabilized by β-Lactoglobulin Amyloid Fibrils: Effect of pH. *Journal of Agricultural and Food Chemistry*, *65*(48), 10658–10665. https://doi.org/10.1021/acs.jafc.7b03669

Rullier, B., Novales, B., & Axelos, M. A.V. (2008). Effect of protein aggregates on foaming properties of β-lactoglobulin. *Colloids and Surfaces A: Physicochemical and Engineering Aspects*, *330*(2-3), 96–102. https://doi.org/10.1016/j.colsurfa.2008.07.040

Schestkowa, H., Wollborn, T., Westphal, A., Maria Wagemans, A., Fritsching, U., & Drusch, S. (2019). Conformational state and charge determine the interfacial stabilization process of beta-lactoglobulin at preoccupied interfaces. *Journal of Colloid and Interface Science*, *536*, 300–309. https://doi.org/10.1016/j.jcis.2018.10.043

Serfert, Y., Lamprecht, C., Tan, C.-P., Keppler, J. K., Appel, E., Rossier-Miranda, F. J., Schwarz, K. (2014). Characterisation and use of β-lactoglobulin fibrils for microencapsulation of lipophilic ingredients and oxidative stability thereof. *Journal of Food Engineering*, *143*, 53–61. https://doi.org/10.1016/j.jfoodeng.2014.06.026

Tamm, F., Sauer, G., Scampicchio, M., & Drusch, S. (2012). Pendant drop tensiometry for the evaluation of the foaming properties of milk-derived proteins. *Food Hydrocolloids*, *27*(2), 371–377. https://doi.org/10.1016/j.foodhyd.2011.10.013

Unterhaslberger, G., Schmitt, C., Sanchez, C., Appolonia-Nouzille, C., & Raemy, A. (2006). Heat denaturation and aggregation of β-lactoglobulin enriched WPI in the presence of arginine HCl, NaCl and guanidinium HCl at pH 4.0 and 7.0. *Food Hydrocolloids*, *20*(7), 1006–1019. https://doi.org/10.1016/j.foodhyd.2005.10.017

Uttinger, M. J., Heyn, T. R., Jandt, U., Wawra, S. E., Winzer, B., Keppler, J. K., & Peukert, W. (2020). Measurement of length distribution of beta-lactoglobulin fibrils by multiwavelength analytical ultracentrifugation. *European Biophysics Journal: EBJ.* Advance online publication. https://doi.org/10.1007/s00249-020-01421-4

Veerman, C., Ruis, H., Sagis, L.M.C., & van der Linden, E. (2002). Effect of Electrostatic Interactions on the Percolation Concentration of Fibrillar β-Lactoglobulin Gels. *Biomacromolecules*. (3), 869–873.

Wan, Z., Yang, X., & Sagis, L. M. C. (2016). Contribution of Long Fibrils and Peptides to Surface and Foaming Behavior of Soy Protein Fibril System. *Langmuir: the ACS Journal of Surfaces and Colloids*, *32*(32), 8092–8101. https://doi.org/10.1021/acs.langmuir.6b01511

Wang, J., Nguyen, A. V., & Farrokhpay, S. (2016). A critical review of the growth, drainage and collapse of foams. *Advances in Colloid and Interface Science*, *228*, 55–70. https://doi.org/10.1016/j.cis.2015.11.009

Wang, Z., & Narsimhan, G. (2005). Interfacial dilatational elasticity and viscosity of beta-lactoglobulin at air-water interface using pulsating bubble tensiometry. *Langmuir: the ACS Journal of Surfaces and Colloids*, *21*(10), 4482–4489. https://doi.org/10.1021/la047374g

Ward, A. F. H., & Tordai, L. (1946). Time- Dependence of Boundary Tensions of Solutions I. The Role of Diffusion in Time- Effects. *The Journal of Chemical Physics*, *14*(7), 453–461. https://doi.org/10.1063/1.1724167

Yang, J., Thielen, I., Berton-Carabin, C. C., van der Linden, E., & Sagis, L. M.C. (2020). Nonlinear interfacial rheology and atomic force microscopy of air-water interfaces stabilized by whey protein beads and their constituents. Food Hydrocolloids, 101, 105466. https://doi.org/10.1016/j.foodhyd.2019.105466

7 General discussion

The central aim of this thesis was to evaluate if a deeper insight into the mechanism of amyloid aggregation of β-lactoglobulin (β-lg) can be obtained by the approach of site-directed spin labeling (SDSL) in combination with electron paramagnetic resonance spectroscopy (EPR). Functional amyloid aggregates are mainly dependent on pH value, temperature, and shearing, which determine the protein building blocks, morphology, and the amount of amyloid and amyloid-like aggregates formed, i.e., at pH 2 peptides form fibrils (amyloid aggregate system, AAS). At pH 3.5 the entire protein is part of worm-like aggregates (amyloid-like aggregate systems, ALAS). In this thesis, both, the resulting amyloid aggregates (AF)/amyloid-like aggregates (ALF) and the non-amyloid/non-amyloid-like protein material (n-AF/n-ALF) separated by membrane filtration (MWCO = 300 kDa), were evaluated. To systematically work on and achieve the aim of the present thesis, the SDSL approach was first established for the natural β-lg (**7.1** and **manuscript 1**, **3**; **manuscript 2**, **4**), followed by the verification whether SDSL of β-lg can elucidate the structure and dynamics of different amyloid and non-amyloid materials (**7.2** and **manuscript 3**, **5**). To evaluate the contribution of the different protein materials during foaming, as an exemplary food production process, the foaming properties and surface activity at the air-water interface for fibrils and non-amyloid peptides were investigated exemplarily for pH 2 systems (**7.3** and **manuscript 4**, 6). The structure of the thesis and the context of the working hypotheses (**1.2**) are schematically outlined in **Figure 7-1**.

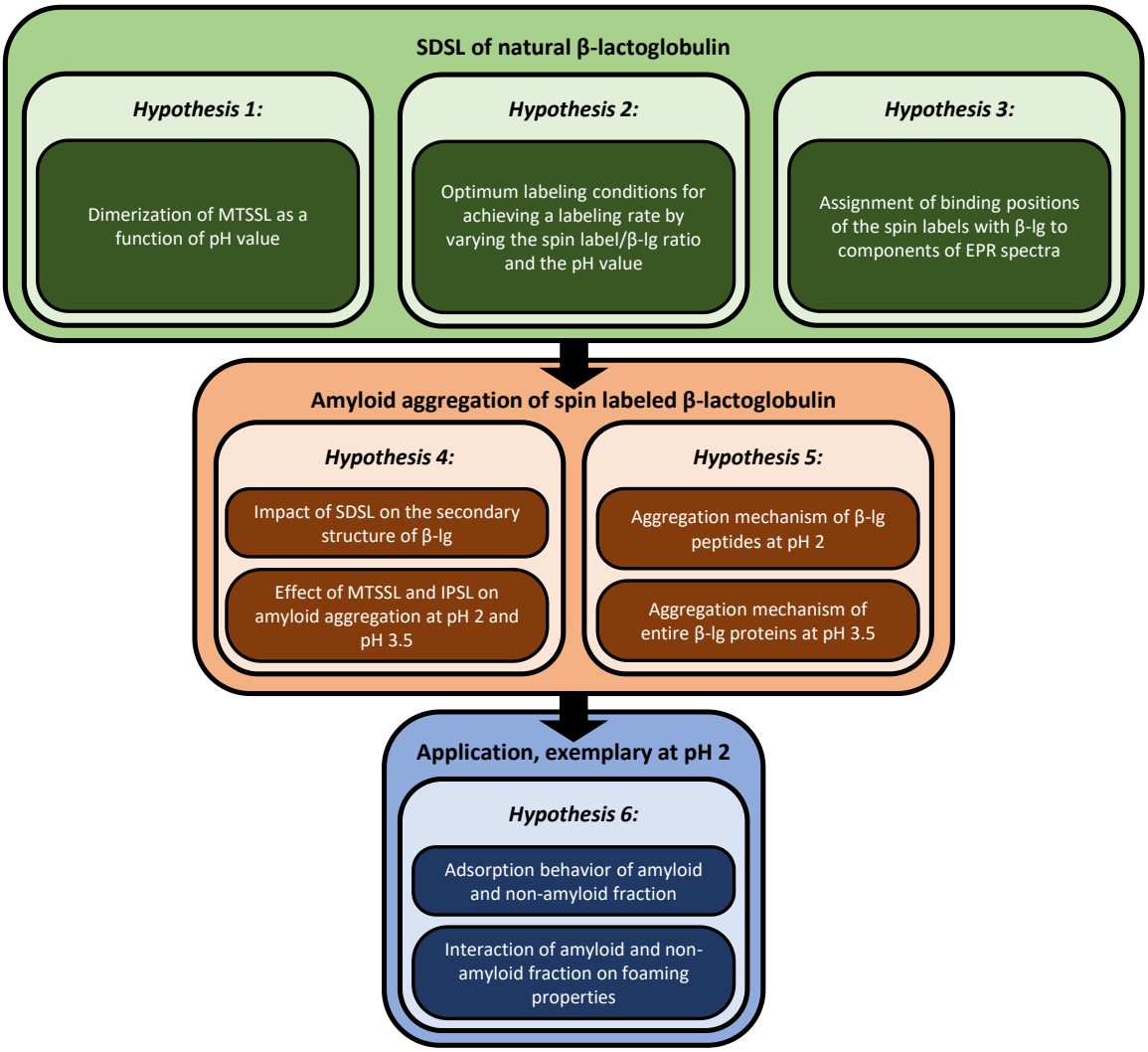

Figure 7-1: Outline of the structure of the thesis and the context of the working hypotheses.

7.1 Site-directed spin labeling of natural β-lactoglobulin

Since SDSL has not been used to date to study aggregation of food proteins, the binding conditions first had to be evaluated in order to determine possible spin label interferences (***hypotheses 1***, **manuscript 1**, **3**) and to minimize possible changes in secondary protein structure (***hypotheses 4***, **manuscript 2**, **4**). In addition, it had to be excluded that the conditions of amyloid aggregation such as high temperature and low pH values would break the binding between spin label and β-lg (***hypotheses 2***, **manuscript 1**, **3**). Because of the naturally occurring five cysteine residues in one β-lg monomer, it is crucial to be able to assign the binding positions of the spin labels in β-lg to the individual spectral components (***hypotheses 3***, **manuscript 3**, 5), which in turn are needed later to interpret the mechanistic changes during aggregation.

7.1.1 Dimerization and binding properties of the spin labels MTSSL and IPSL as a function of pH value

The methanethiosulfonate spin label (MTSSL) and the iodoacetamido-proxyl spin label (IPSL) are mostly used spin labels for SDSL (Bordignon, 2018; Drescher et al., 2008; Hammarström et al., 2001; Ionuţ et al., 2009; Margittai & Langen, 2006; Owenius et al., 1999) and was therefore used for the first labeling experiments in this thesis. These labels differ in their molecular weight (MW_{MTSSL} = 264.38 Da; MW_{IPSL} = 325.17 Da) and in their bonding (MTSSL: S-S bond; IPSL: C-S bond) (**2.3.1.1**). For a successful application of SDSL, it was necessary that the chemical structure and the binding properties of the spin labels were not changed by the conditions during the labeling in a way that could lead to misinterpretation of the EPR spectra (***hypothesis 1*****, manuscript 1**). The spectrum of an unbound nitroxide radical is characterized by its typical three-peak spectrum. All three peaks were very narrow and had the same width (**Figure 3-4A**). The three narrow peaks represented a free tumbling electron with a fast rotation correlation time (τ_c) (**Figure 3-5**). For the calculation of the rotation correlation time, the peak height and the peak width were used (**3.3.6**, **Equation 5**). The bonding of the spin labels to the protein resulted in the broadening of the peaks (**Figure 3-4B**), which is accompanied by a decreased peak height and τ_c increased, indicating a lower mobility of the spin labeled side chain and the tumbling of the free electron were hindered.

The labeling was conducted under different pH values. In the case of MTSSL, the increased pH value resulted in two additional peaks in the EPR spectra (**Figure 3-4**). This five-peak spectrum was characteristic for the formation of biradicals. Biradicals were formed when two MTSSL monomers were linked via a disulphide bridge and sulfinic acid was released (**Figure 2-4**, **Figure 3-1**). This dimerization was already described (Bordignon, 2018) and the typical five-peak spectrum was caused by the exchange reaction of the two electrons when the average exchange coupling was 10 times stronger than the hyperfine interaction (Berliner et al., 1982; Luckhurst, 1966; Slichter, 1955). However, this was described for concentrations >200 µmol/L (Bordignon, 2018) but the biradical formation was observed even at a concentration of 100 µmol/L and were increased with increasing pH values, regardless of the presence of protein (**Table 3-1**, **Figure 3-3**). In the case of IPSL, the higher pH values did not change the spectra shape. Higher pH values could be applied because IPSL does not dimerize. However, also for IPSL the pH value should not exceed pH 8.5, because at higher pH values the iodacetamide group in IPSL can interact with lysine, histidine, and methionine (Goldfarb & Stoll, 2018).

The presence of the biradicals had a disturbing influence on the spectrum analysis, since the peak height of the biradicals were much lower compared to the peak height of same

concentration of monoradicals. However, the integral intensity remained unchanged (**Figure 3-5**). The integral intensity is also a measure for the radical concentration and depends on the peak width to the square and the peak height (Berliner et al., 1982; Weiner, 2012). Therefore, the analysis of the MTSSL spectra was impaired and a removal of the unbound spin label was recommended. However, not only biradical dimers were formed during the labeling, also MTSSL monoradical dimers were detected (**Figure 3-5**), which could not be distinguished from MTSSL monomers using EPR. The identification of monomers, biradicals, and monoradical dimers were confirmed by FT-ICR-MS due to their m/z ratio (**Table 3-2**, **Table 3-3**). Furthermore, FT-ICR-MS was able to measure biradicals and monoradical dimers even at very low concentrations of less than 1 µmol/L, which were far below the concentrations detectable with EPR (here 6.6 µmol/L) (**Figure 3-10**). Biradicals were formed as a function of the pH value, although the dominance of biradicals over monomers was clearly recognizable at higher concentrations (**Table 3-1**, **Figure 3-5E, F**, **Figure 3-10**).

The five-line spectra of the MTSSL biradical disappeared after heating and only the three-line spectra of bound and free monomers remained (**Figure 3-4**), which, according to Weiner (2012), might indicate that the disulfide bond of the biradical was cleaved. However, this suggestion conflicts with the results of the FT-ICR-MS measurements. At pH 2 (**Figure 3-5E**) the monomers were essentially present and a predominant amount of dimers were found in the odd configuration of a biradical dimer $[M]^{+\bullet}$ and a monoradical dimer $[MH_2]^{+\bullet}$. Although the amount of monomers $[MH_2]^{+}$ decreased during heat incubation and the dimers remained approximately constant (**Figure 3-5**), no biradicals were visible in the EPR spectrum (**Figure 3-4**). This suggested, that the heating did not destroy the biradicals, but led to the formation of monoradical dimers and therefore to a reduction of the total radical concentration, visible by EPR (**Figure 3-5**).

The increased biradical formation of MTSSL at increasing pH values effect the spectra analysis. Not only the binding to β-lg was favored at higher alkaline pH values, but also the dimerization of two MTSSL. ***Hypothesis 1*** has to be rejected because the formation of biradicals, which occur, both, at low pH values and concentrations <200 µM. The increasing biradical formation could decrease the binding rate because of the reduced availability of MTSSL monomers. Although IPSL cannot dimerize under the tested conditions, a pH value under 8.5 was recommended, because other binding positions via amino groups can occur that might lead to misinterpretation of the EPR spectra.

7.1.2 Identification of optimum labeling conditions for achieving a high labeling rate with low biradical formation

The conditions for binding spin labels to β-lg were optimized to achieve the highest possible binding rate while minimizing biradical formation to reduce negative effects on binding

efficiency and spectra analysis (**7.1.1**). For that reason, pH value and spin label/β-lg ratio were varied (***hypothesis 2*****, manuscript 1**). The successful bonding was seen in broadening of the EPR spectrum (**Figure 3-4**) and the faster rotation correlation time (τ_C) compared to the unbound spin label (**Figure 3-5**). The spin labeling of β-lg resulted in a superimposed EPR spectrum (**Figure 3-1**). The spectrum of MTSSL bound to β-lg, without removing the excess, consisted of four components (**Figure 3-4**): one free tumbling component, which reflected the unbound MTSSL; one five-peak spectrum, reflecting the biradicals; and two bound components. The two bound components differed in their rotation correlation time (**Table 5-1**). For the bonding of IPSL to β-lg, the increased pH value also increased the maximum number of binding sites (**Figure 10-2**). The Verification by mass spectrometry measurements (**Figure 3-1**) could be performed due to the mass shift of 185 m/z, which corresponded to the mass of protein-bound MTSSL with eliminated methane sulfinic acid (**Figure 2-3**). The labeling of IPSL resulted in a mass shift of 197 m/z due to the elimination of –IH (**Figure 2-3**). The shift of 185 m/z and 197 m/z confirmed that only one MTSSL or one IPSL molecule were covalently bound to one β-lg molecule (**Figure 3-2**, Fehler! Verweisquelle konnte nicht gefunden werden.). To enhance the labeling efficiency, the pH value and the protein/spin label ratio were varied. The highest number of bound MTSSL molecules and the highest affinity constant were observed at pH 8 (**Figure 3-2**). The increasing pH value from 6 to 8 favors the binding of positive charged reagents by deprotonating of the thiol group (pKa = 8.5) and thus the thiol group became more reactive (Dunnill & Green, 1966; Qin, Bewley et al., 1998). A further increased pH value resulted in a decreased labeling rate (**Figure 3-2**), due to the increased formation of biradicals (**7.1.1**). The calculated maximum number of binding sites for MTSSL bound to β-lg of 0.9 mol/mol (**Figure 3-2**), determined by RSH and RP-HPLC, were below the theoretical maximum number of possible binding sites. Because of the high affinity of MTSSL (K_α = 2.1 μM^{-1}) an equimolar ration of MTSSL/β-lg was sufficient to reach a saturation in binding (**Figure 3-1**). Whereas for the labeling with IPSL, a pH value of 8.5 and a 10-fold molar excess were necessary for labeling ~80% of the protein (**Figure 10-2**). The lower affinity constant (K_α = 0.193 μM^{-1}) (**Figure 10-2**) compared to MTSSL caused the higher pH value and the higher amount of spin label (Hammarström et al., 2001). This was in accordance to other binding studies evaluating the covalent bonding of different molecules to β-lg at Cys^{121}, for example studied in detail for the bioactive food ingredients allicin, diallyl disulfid (Wilde, Treitz et al., 2016), and allyl-isothiocyanate (Keppler et al., 2014; Rade-Kukic et al., 2011). The best binding conditions for MTSSL and IPSL were determined by varying the pH-value and the β-lg/spin label ratio (***hypothesis 2***). However, for MTSSL also at pH 7.5 biradicals are formed and influenced the spectra analysis, since a superimposed spectrum was created. The EPR spectra display all radical components present in the sample at the same time. The

overlay of different EPR spectra, representing various microenvironments, and the optical interpretation of the spectra was affected. Therefore, a removal of the excess and the simulation (**2.3.2**) of the superimposed spectra is recommended for the successful analysis of the EPR spectra. The removal of the excess resulted in a three line spectrum with three components, one unbound and two bound components (**Figure 5-2**, **Table 5-1**). In the case of IPSL, a 10-fold molar excess resulted in the highest labeling rate (**Figure 10-2**), but higher concentrations were not investigated in this work. Furthermore, only 2.5-fold molar excess was used for further investigation, as the higher binding rate using a 10-fold molar excess was disproportionate to the higher costs. **Hypothesis 2** can be partly accepted. The labeling rate can be achieved by varying the spin label/β-lg ratio and the pH value. However, the reduced availability of MTSSL monomers due to biradical formation limited the labeling rate.

7.1.3 Assignment of the spectral components to binding positions of the spin labels in the β-lg monomer

The EPR spectra of both spin labels were superpositions of different spectral components, form which of one was a free spin label component and two components were attributed to bonding spin labels, which differed in their mobility and polarity (**Table 5-1**). To assign the spectral components to possible binding sites (***hypothesis 3,* manuscript 3**), the spin labeled protein was digested with trypsin and the peptides were measured by mass spectrometry. β-lg has five cysteine residues (Cys^{66}-Cys^{160} and Cys^{106}-Cys^{119}/Cys^{121}), whereby four are incorporated in two disulfide bridge (McKenzie et al., 1972). The tryptic digestion of β-lg led to a large number of peptides, since trypsin selectively cleaves the peptide sequences after the basic amino acids arginine and lysine (Fernández & Riera, 2013). Three of the peptides resulting from the tryptic digestion contained cysteine residues. The peptide 61-69 contains Cys^{66} (**Figure 5-3A–*blue* symbols**), the peptide 102-124 contains Cys^{106}, Cys^{119}, and Cys^{121} (**Figure 5-3A–*green* symbols**), and the peptide 149-162 contains Cys^{160} (**Figure 5-3A–*orange* symbols**). Both spin labels were bound to all three peptides (**Table 5-2**). The spin label MTSSL was mainly bound to the peptide 102-124 and to a lesser proportion to the peptides 61-69 and 149-162, whereas IPSL were mainly bound to the peptide 61-69 and 149-162 and less to 102-124. This was in accordance with the components of the EPR measurements (**Table 5-1**). The two bound components differed in their contribution, rotation correlation, time and polarity. The component with the slower rotation correlation time and the lower polarity (**Table 5-1**) were assigned to the peptide 102-124. The three cysteine residues of this peptide (Cys^{121}, Cys^{119}, and Cys^{106}) were located between the β-sheets, outside of the β-barrel and the α-helix (Kuwata et al., 2001) (**Figure 5-3B**). The location buried in the protein explained both, the slow τ_c and the polarity lower compared to water/DMSO. The other bound component from the EPR spectra with a lower contribution, a higher rotation correlation time, and a polarity comparable to water/DMSO

(**Table 5-1**) was assigned to the peptides 61-69 and 149-162. These two peptides contain the cysteine residues Cys^{66} and Cys^{160}, which are located close to the C-terminus on the surface of the protein exposed to the water (McKenzie et al., 1972) (**Figure 5-3B**). The location on the surface of the protein explained both, the faster τ_c, since the electron could tumble more freely compared to the buried spin label, and the higher micropolarity of the spin label, which was comparable to water/DMSO. However, MTSSL were mainly bound to the cysteine residues buried within the protein (~81%) and less were bound at the surface of the protein (~18%), whereas IPSL were bound to a lower proportion to the β-strands buried within the protein (~63%) and to a higher ratio on the surface (~35%) (**Table 5-1**). The different contributions of the two binding sites (**Table 5-2**) could be explained by the higher shuffling rate of IPSL due to higher labeling pH value, which favors the thiol shuffling (Creighton, 1980; McKenzie et al., 1972; Phelan & Malthouse, 1994), or by the fact that IPSL has a higher binding propensity to Cys^{66} based on C-S binding (Rade-Kukic, Schmitt, & Rawel, 2011). ***Hypothesis 3*** can therefore be accepted. It was possible to label all five cysteine residues of β-lg, without prior genetic or chemical modification of the protein. Cys^{121} was the main binding site for both spin labels. But IPSL was bound to a significant higher amount to Cys^{66} and Cys^{160} compared to MTSSL. It was not possible to determine to which cysteine, from peptide 102-124, the spin labels were bound. Nevertheless, it was possible to assign the different components of the ESR spectrum to the binding sites in the protein.

7.1.4 Stability of the bonding between spin labels and β-lg at high temperatures and acidic pH values

A stable bonding of the spin label to β-lg at high temperatures and low pH value is the prerequisite to follow the amyloid aggregation of β-lg by EPR. Both EPR and FT-ICR-MS measurements confirmed the stability of the bonding at 90°C for five hours (**Figure 3-5**). A release of the spin label from β-lg would have resulted in a faster rotation correlation time, narrower peaks, and a mass shift to the mass of unlabeled β-lg. After five hours at 90°C, the rotation correlation time were slightly increased (**Figure 3-5A**), the peak width were not altered (**Figure 3-4**), and the m/z ratio of the mass spectrometry measurements were unchanged (**Figure 3-5D**). This indicated no release of the spin label MTSSL from β-lg. The increased τ_c of the bound MTSSL (**Figure 3-5A**) was explained by the denaturation and aggregation of β-lg after heating at pH 2 and 7.5. At pH 7.5, labeled β-lg was merely denatured (**Figure 3-11**) but the bonding stayed intact as it was observed by the τ_C. (**Figure 3-5D**). Over the entire period of heating, the mass of the labeled protein could be measured with nearly constant m/z intensities at pH 7.5 (**Figure 3-5D**), confirming the stability of the bonding. The drastic reduction of the m/z intensities of MTSSL-labeled β-lg at pH 2 (**Figure 3-5D**) indicated the acidic hydrolysis of β-lg into a multitude of peptides (Akkermans et al., 2008; Hettiarachchi et al., 2012; Heyn et al., 2019; Keppler et al., 2019). The acidic

hydrolysis were revealed by RP-HPLC measurements (**Figure 3-11**). Furthermore, the rotation correlation time was increased also at pH 2 over five hours of heating (**Figure 3-5A**), indicating a stable bonding. The stability of the bond at 90°C for five hours at pH 2 and pH 7.5 was given.

7.1.5 Impact of SDSL on the secondary structure of β-lg

In order to draw conclusions about the unlabeled protein, it was of great importance that the spin label did not affect the conformation of the protein (***hypothesis 4,*** **manuscript 1 and 2**). Only small changes in the protein secondary structure were caused by the labeling with MTSSL or IPSL observed by FTIR (**Figure 3-8**, **Figure 3-2D**, **Figure 4-2**) or ITF (**Figure 4-3**). The ATR-FTIR measurements were conducted to observe changes in the secondary structure of the protein that might be caused by spin labeling. Particular attention was paid on the intra- and intermolecular β-sheets, which are frequently observed in protein associations such as fibril formation (Baldassarre et al., 2016; Heyn et al., 2019; Kayser et al., 2020). The labeling mostly affected the signal intensity of the β-sheet region (**Figure 4-2A**). The observed lower β-sheet intensity of the IPSL-labeled samples at pH 3.5 but not at pH 2 (**Figure 4-2A**) may indicate protein destabilization induced by the labeling (Sakai et al., 2000; Zimmerman et al., 1970). However, it must be considered that only one fifth of the protein was labeled, to avoid spin-spin interactions. At pH 2, the protein was already monomeric, whereas at pH 3.5 the protein was also associated as a dimer (Rade-Kukic et al., 2011; Shimizu et al., 1984; Uhrínová et al., 2000; Yan et al., 2013). The more flexible bonding of MTSSL compared with IPSL (Bordignon, 2018) explained why the destabilization at pH 3.5 was only visible in the IPSL-labeled samples. In comparisons, other studies, aimed at the changing of the protein structure by covalent modification reported strong changes in the β-sheet region, but also altered helix-elements and unordered structures (Keppler et al., 2017; Rade-Kukic et al., 2011). The intrinsic tryptophan fluorescence (ITF) intensity were decreased after labeling with both spin labels (**Figure 4-3A, B**) indicating fluorescence quenching (Liang & Subirade, 2010; Tayeh et al., 2009). A shift in the emission wavelength indicated changes in the local polarity of tryptophan residue. This were only detected for the IPSL-labeled samples at pH 2 (**Figure 4-3B**). Because of its five rotatable bonds, MTSSL is known to have a highly flexible linkage to its labeled protein and does not destroy the native state (Klare, 2012). The influence of the bonding was more dependent on the flexibility or the length of the linker than on the size of the bound molecule. This was demonstrated, for an example, by the small reactive plant compound allyl-isothiocyanat (AITC) (99.16 Da), which significantly influenced the protein secondary structure (Keppler et al., 2014), although the molecule was smaller compared to MTSSL and IPSL. Only minor structural changes in the hydrophobic core of the protein were measured and the current changes induced by SDSL of

β-lg induced changes in the secondary structure measured by ATR-FTIR can be considered negligible (***hypothesis 4***).

The site-directed spin labeling of β-lg with MTSSL and IPSL were successful. The best labeling conditions and the binding position were achieved, the bonding was stable against heating and at acetic conditions, and the spin labels did not alter the secondary structure of β-lg (**manuscript 1 and manuscript 2**).

7.2 Verification of the contribution of SDSL to the elucidation of the structure of amyloid and non-amyloid material depending on the β-lg building blocks

It was of particular importance to demonstrate that spin labeled and unlabeled β-lg have the same aggregation behavior (***hypothesis 4,*** **manuscript 2**, **7.2.1**). SDSL of β-lg was then used to describe the structure of aggregates and non-aggregated proteins and peptides. For that reason, different building blocks of β-lg were investigated that form either amyloid aggregates from peptides at pH 2 (**7.2.2**) or amyloid-like aggregates from the entire protein at pH 3.5 (**7.2.3**) and their respective non-amyloid fractions (***hypothesis 5*****, manuscript 3**).

7.2.1 Effect of MTSSL and IPSL on amyloid aggregation at pH 2 and pH 3.5

The spin labeling had only minor influence on the protein structure (**7.1.5**) and the bond were stable for at least five hours at 90°C (**7.1.4**). To characterize the amyloid aggregates by SDSL, the spin labels MTSSL and IPSL should not influence the amyloid aggregation (***hypothesis 4*****, manuscript 2**). Minor differences in the amyloid aggregation were observed by ATR-FTIR (**Figure 4-2**) and ITF (**Figure 4-3**), but no influence on the building blocks (**Figure 4-4A-D**), the conversion rate (**Figure 4-5C**), and on the morphology, measured by AFM, (**Figure 4-4E-J**) were determined. Only the thioflavin-T (ThT) fluorescence, which is an indicator for parallel β-sheets (Krebs et al., 2005), were significantly reduced due to the spin labeling (Figure 4-5). There were two ways to explain the reduction of ThT fluorescence, even there were only minor influence on the secondary structure and no influence on the conversion rate: On the one hand, the spin label could quench the fluorescence, as it was already described for the ITF of the native protein (**Figure 4-3A, B**, **7.1.5**), or on the other hand, the spin labels may influence the migration of the ThT-molecules into the channels of the β-sheets (**10.1.2.2**). The fluorescence quenching was already described for the covalent and non-covalent bonding of various compounds to β-lg (Liang & Subirade, 2010; Tayeh et al., 2009). The lower ThT-fluorescence of IPSL-labeled compared to MTSSL-labeled samples may be associated with a lower flexibility or a more hydrophilic character of IPSL (Bordignon, 2018; Klare, 2012). However, the influence on the ThT-fluorescence were not confirmed by the conversion rate or the morphology measurements (**Figure 4-5**, **Figure 4-6**). Therefore, it can be concluded, that not the amyloid aggregation was affected, but the ThT-

fluorescence measurements. Since the fluorescence quenching was already described for the ITF (**7.1.5**), it was likely that also the ThT-fluorescence were quenched due to the spin labeling with MTSSL and IPSL. Taking into consideration of section **7.1.5**, ***hypothesis 4*** can be accepted under the given condition, SDSL did not influence neither the secondary structure of the unheated protein significantly nor the amyloid aggregation and therefore the approach can be used to analyze the amyloid aggregation.

7.2.2 Aggregation mechanism of β-lg peptides at pH 2

For characterization of the aggregation mechanism, the EPR spectra of the amyloid aggregate system (AAS) and the individual fractions were simulated (***hypothesis 5*****, manuscript 3**). The formation of amyloid aggregates at pH 2 resulted in superimposed spectra, which were recorded separately for the complete AAS as well as for the amyloid fractions (AF) obtained in the retentate after ultrafiltration and for the non-amyloid fractions (n-AF) in the permeate (**Figure 5-4**). During the amyloid aggregation process at pH 2 only 40% of the protein were converted into amyloid aggregates (**Figure 4-6**) and the building blocks of both fractions were peptides and rearranged protein (**Figure 4-4**). Therefore, it was unknown where the spin labeled side chains were located. The detailed analysis by spectra simulation of the superimposed EPR spectra revealed that four components were required to describe the experimental line shapes with similar parameters for AAS, AF, and n-AF (**Table 5-3**). The line shape for all three samples were comparable (**Table 5-3**). All spectra consisted of three bound and one unbound component (**Table 5-3**). The three bound components differed in their degree of motional restriction. The dominant spectral component ($C(b_{1:MTSSL})$, ~67%; $C(b_{1:IPSL})$, ~39%), was characterized by the slowest rotation correlation time (>7 ns) and a polarity lower of water/DMSO ($A_{ZZ(MTSSL)}$ = 3.39 mT; $A_{ZZ(IPSL)}$ = 3.14 mT; $A_{ZZ(water/DMSO)}$ = 3.57 mT) (**Table 5-3**), which was characteristic for a spin label buried in the protein (Bordignon & Polyhach, 2013; Savitsky et al., 2004; Steinhoff et al., 1999). Rotational correlation times τ_c >7 ns were too slow for the resolution in the EPR time scale at the microwave frequency used in the X-band, therefore all τ_c >7 ns were classified as very slow spectral components. The other two bound components demonstrated faster rotation correlations times and the polarity of the water/DMSO environment (**Table 5-3**). While component $C(b_3)$ could be associated with a spin label bound to a free peptide, $C(b_2)$ could represent a peptide, which is aggregated with multiple peptides, but the spin label was located on the surface. The fact that $C(b_1)$ represented the slowest and most hydrophobic spectral component, indicated that the IPSL bound side chain may be incorporated into a hydrophobic core of a protein aggregate, while MTSSL was mainly bound in the hydrophobic interior of β-lg, it may be deduced that these respective peptides were not involved in aggregation. Whereas, IPSL was able to bind to Cys^{160} and Cys^{66} to a higher degree than

MTSSL, which are part of the outer loops (**7.1.3**), it may be assumed that these labeled peptides are more likely to be entrapped in the formed aggregates of hydrolyzed peptides.

Since the same components were present in the AF and in the n-AF (**Table 5-3**) and no amyloid aggregates were found in the n-AF (**Figure 4-5**, **Figure 4-2**), it can be concluded that the spin labels were not incorporated into the amyloid aggregates formed at pH 2. Peptides of the N-term are mainly incorporated in the stucked β-sheet, which build the long semi-flexible fibrils (Akkermans et al., 2008). The N-terminal peptides were the only one that were exclusively in the AF, all others were found in both fractions by Akkermans et al. (2008). According to (Hettiarachchi et al., 2012) only two peptides containing Cys^{66} were found in the AF. Furthermore, the appearance of the spin labels in both fraction indicated an incomplete separation of the two fractions. The ATR-FTIR measurements demonstrate that no intermolecular β-sheets were found in the n-AF (**Figure 4-2**) and the intrinsic tryptophan fluorescence indicated different polarities of the tryptophan environment suggesting a successful separation of the two fractions (**Figure 4-3**). However, ATR-FTIR based on measuring the protein structure and intrinsic tryptophan fluorescence was an indicator for tertiary structure, whereas the EPR measuring demonstrate the spin labeled side chains. Therefore ***hypothesis 5*** must be rejected in the case of amyloid aggregation at pH 2. Both spin labels were not incorporated into the amyloid aggregates and therefore no aggregation mechanism could be derived from the EPR spectra. However, other hydrophobic aggregates were found in both fractions and should be investigated in more detail.

7.2.3 Aggregation mechanism of entire β-lg proteins at pH 3.5

For characterization of the aggregation mechanism at pH 3.5, the EPR spectra of the amyloid-like aggregate system (ALAS) and the individual fractions were simulated and spin label distribution in the ALF measured (***hypothesis 5*****, manuscript 3**). The formation of amyloid-like aggregates at pH 3.5 resulted in superimposed spectra which were recorded separately for the complete ALAS as well as for the amyloid-like fractions (ALF) obtained in the retentate after ultrafiltration and for the non-amyloid-like fractions (n-ALF) in the permeate (**Figure 5-5**). During the amyloid aggregation process at pH 3.5, only 80% of the protein were converted into amyloid-like aggregates (**Figure 4-6**) and the building blocks of both fractions were rearranged protein (**Figure 4-4**).

The spectrum of the ALAS and the ALF were superimposed with four components, three bound components and one free component (**Table 5-4**). The three bound components were interpreted in terms of slow (τ_c >7 ns), intermediate (1< τ_c <7 ns), and fast rotation (τ_c <1 ns) of the nitroxide for both spin labels. But the contribution of the three components differed between the two spin labels. While for the MTSSL-labeled sample C(b_1) and C(b_2) had almost equal contributions of 44% and 48%, for the IPSL-labeled sample C(b_1) were

dominant with 53.1%, whereas C(b_2) and C(b_3) had equal contributions with ~20% and ~25%. In addition, C(b_1) displayed for both spin labels the lowest A_{ZZ} value. The appearance of different superimposed spectral components after (amyloid) aggregation confirms the observation of earlier studies (Iuraşcu et al., 2009; Sepkhanova et al., 2009), which were also based on simulations with different rotation correlation times (Sepkhanova et al., 2009).

The order to obtain detailed information about the aggregation mechanism, the ALAS was separated by ultrafiltration into the ALF and the n-ALF. Clear differences in the spectral line shape were observed (**Figure 5-5**). The ALF contained about 82–90% and the n-ALF 10–18% of the protein (**Table 5-4**, **Figure 4-6**). For both spin labels, the ALF were described by three bound components, whereas n-ALF were only described by two components. Since the contribution of the two bound components of the n-ALF were similar to those before heating and the rotation correlation times were slightly faster in the n-ALF, it can be assumed, that the n-ALF consists of monomeric protein structures with a different folding compared to the unheated β-lg (**Table 5-1**, **Table 5-4**). This was verified by the size exclusion chromatography. However, both fractions contained mainly structures with the size of monomeric protein (**Figure 4-4**). Based on these results, the worm-like structures recognizable in AFM images (**Figure 4-5**) were assumed to result of the assembly of monomer-like structures, which was also supported by recently obtained AFM and SAXS results, where the height and elliptical cross-section of the worm-like aggregates was that of a monomeric protein (i.e., 3.4 nm) (Heyn et al., 2019).

Therefore, it was likely that the C-terminus C(b_3) is fold outwards the aggregates, as evidenced by high water/DMSO accessibility (A_{zz} = 3.57) and faster rotational motion ($\tau_{c,b3}$ = 0.33 for MTSSL and $\tau_{c,b3}$ = 0.46 for IPSL) relative to the monomeric β-lg before aggregation (Table 5-1). This rearrangement allowed the α-helix to be shifted out of the autonomous folding domain (Kuwata et al., 2001) during partly unfolding, which in turn leads to greater accessibility of the β-sheets to the water/DMSO-environment (A_{zz} C(b_1) = 3.57 mT for MTSSL and A_{zz} C(b_1) = 3.43 mT for IPSL). Meanwhile, however, C(b_1) components with their slow $\tau_{c,b1}$ >7 ns for both spin labels indicate that the β-sheets are most likely tightly packed by the accumulation of intermolecular β-sheets. The suggestion that amyloid-like structures can be formed from building blocks of the entire primary β-lg structure were supported by FTIR and ThT measurements (**Figure 4-2**, **Figure 4-6**) and confirmed by the results of Heyn et al. (2019).

To verify this model, the spatial distribution of the spin labeled side chains was determined using pulsed EPR technique of double electron-electron resonance (DEER) (Milov et al., 1984). The experimental decay of DEER time traces for ALF at pH 3.5 spin labeled with

MTSSL and IPSL was fitted to the stretched exponential and the yielded dimensionality factor d of 1.23 and 1.64 for MTSSL and IPSL, respectively (**Figure 5-6**).

The explanation for the fact, that the spin label distribution was not exactly one-dimensional, was that some spin labels were sticked out of the aggregates, while the other spin labels were within the amyloid-like aggregates. Therefore, the strict one-dimensional distribution of spin labels was not observable. In this case, the distribution will be larger than one, but still smaller than two. This suggestion was supported by the experimental observation that the dimensionality of the distribution was larger for IPSL than for MTSSL and also corresponded to the assignment of the different spectral components to the different binding positions (**Table 5-4**, **Figure 5-2**). Since IPSL was preferentially bound in the loop regions C(b_3) (**7.1.3**), this spin label will stick out from the aggregates more than MTSSL, which was predominantly buried in β-lg, and thus the dimensionality of the spin label distribution will differ more from one. Taking into account the way spin labels were attached to β-lg, the DEER data suggest that β-lg proteins were linearly arranged within aggregates, like beads on a string. Or in other words, the worm-like aggregates that can be found by AFM (**Figure 4-5**) or SAXS (Heyn et al., 2019) after exposure to heat at pH 3.5 were particularly reminiscent of a centipede. Therefore, ***hypothesis 5*** can be accepted. It was possible to gain deeper knowledge about the aggregation mechanism of β-lg at pH 3.5.

7.3 Contribution of amyloid and non-amyloid protein material during foaming

Foaming was used as an exemplary food production process, to which amyloid and non-amyloid protein material contributed in different ways. For a better understanding of the foaming properties resulting from the different amyloid and non-amyloid structures (**7.3.2**), the surface activity at the air-water- interface for fibrils and non-amyloid peptides were investigated exemplarily for pH 2 systems (**7.3.1** – ***hypothesis 6*****, manuscript 4**).

7.3.1 Adsorption behavior of amyloid and non-amyloid fractions at the air-water-interface

For the surface activity and foaming experiments, whey protein isolate (WPI) were used, since WPI has a higher relevance for application compared to pure β-lg. It should be noted that WPI contains only ~77% β-lg, which results in a conversion rate of ~18% amyloid aggregates using an initial protein concentration of 2.5% (**Figure 6-1**). The other components of the WPI (α-lactalbulin (α-la) and bovine serum albumin) are expected in the n-AF, since at least α-la does not form fibrils in the WPI (Bolder et al., 2006). Unheated (UH) and short-time heated (STH) samples were used as control for the AAS. The pendant drop measurements demonstrate high standard deviation for STH samples and the amyloid aggregate system

compared to the individual fractions of AAS (AF and n-AF) (**Figure 6-3A-E**). These variations resulted from the inhomogeneous samples. The STH sample consist of native, denatured and partly denatured protein and therefore of particles with very different sizes. The individual fraction was considered to evaluate which part of the AAS determines the surface activity of the AAS. As the AF consist of amyloid aggregates >300 kDa and the n-AF of smaller aggregates, peptides, and monomeric sized protein, different adsorption behaviors of the two fractions were expected. Contrary to the expectations, there were no significant difference in the diffusion rate between the AAS, AF, and n-AF (**Figure 6-3F**). Whereas the adsorption rate of the n-AF was significant faster compared to the AAS and AF (**Figure 6-3H**). These results suggest an incomplete separation of the two fractions as also already mentioned in **7.2.2**. Bigger aggregates, as contained in the AF, are known to diffuse slower to interface and have a slower adsorption rate (Rullier et al., 2008; Unterhaslberger et al., 2006). Nevertheless, the AF migrated to the interface as fast as the AAS and n-AF, confirming the presence of smaller aggregates or peptides in the AF. However, the significant lower adsorption rate of the AF compared to the n-AF (**Figure 6-3H)** indicated that amyloid aggregates adsorb slower to the interface and reduce interfacial tension more slowly than n-AF. On the one hand, the rearrangement of bigger aggregates at the interface leads to a slower adsorption (Atkinson et al., 1995), and on the other hand, the AF was more hydrophobic, what was associated with an improved adsorption (Akkermans et al., 2008).

7.3.2 Interaction of amyloid and non-amyloid material improves foaming properties

The characterization of the monolayer suggest a synergistic effect of the AF and n-AF (**Figure 6-3A**). To investigate the foaming properties, ASS were produced with different AF/n-AF ratios. The π–A isotherm of the mixture of the AF and n-AF demonstrated an early increase in interfacial pressure at a large relative surface area, indicating an early phase transition from the gas-like phase to the liquid-like phase (**Figure 6-4A**). This would imply the synergistic effect of fibrils and small non-fibrillar material, because aligned long fibrils at the air-water interface and smaller aggregates and peptides embedded therein may form a denser network.

By varying the initial protein concentration during the amyloid aggregation process, the conversion rate was altered. A higher initial protein concentration resulted in a higher conversion rate (**Figure 6-1**), which was already described before (Bolder et al., 2007; Veerman et al., 2002). The foamability and also the foam stability were significantly better using a lower initial protein concentration (**Figure 6-5**). The better foamability was due to the higher amount of non-aggregated peptides and smaller aggregates. The resulting faster diffusion of these aggregates is decisive for the improved foamability of AAS (Peng et al., 2017; Wan et al., 2016). However, Rullier et al. (2008) pointed out, that the adsorption rate

does not only determine the foaming properties, but demonstrated that a mixture of aggregates and the smaller native protein were necessary for foaming. Furthermore, because of the air flow used for foaming in the glass jacketed column, the migration (**Figure 6-3F**) has less relevance in the foaming in the column.

The AFM images of the foamed AAS demonstrate small fragments, which were not visible before foaming (**Figure 6-6**). Parts of the amyloid aggregates were destroyed by adsorption at the interface. However, it was not clear whether the degradation of the fibrils were conducted by the adsorption or the energy input generated by the airflow. The morphology of amyloid aggregates adsorbed at a planar air-water interface represent no degradation of the aggregates (Jordens et al., 2014; Jordens et al., 2013). Since the degree of disruption amyloid aggregates is dependent on the energy input (Uttinger et al., 2020), it could be concluded, that the locally energy input during the foaming process led to the partly comminution of the aggregates.

For better understanding of the foaming properties and the best ratio of AF and n-AF, a method has to be investigated for a complete separation of the AF and n-AF first, followed by foaming experiments with the individual fractions and different AF/n-AF ratios. Under consideration of **7.3.1 *Hypothesis 6*** can be accepted, since it was demonstrated, that the individual fraction has a different foaming behavior. As the migration becomes less relevant during the foaming because of the air flow, the critical factor was the faster adsorption rate of the n-AF. However, the role of the amyloid aggregates is still unclear.

7.4 Outlook

The results of the present work demonstrated that the amyloid aggregates and the non-aggregated material had a synergistic effect on the surface activity. For further investigation, the separation method should be improved to reach a complete separation and to analyze the fraction separately. The used dead-end filtration resulted in the appearance of unconverted peptides in the AF, which was probably due to the fact that the amyloid aggregates were pressed onto the membrane during centrifugation, thus holding the smaller peptides between them. Nevertheless, this method was used because it is a very fast method but with a greater cut-off compared to previous studies in order to achieve more efficient filtration. Other ways to separate the two fractions are the cross-flow filtration, dialysis, or precipitation. However, dialysis is, compared to ultrafiltration, a very time-consuming method, whereas shear forces of the cross-flow filtration could destroy the amyloid aggregates. The precipitation has two disadvantages. First, the change of the pH-value, which leads to a change of the aggregate morphology. Second, the different proteins

and peptides probably precipitate at different pH-values. Another possibility could be a preparative SEC, provided that the column does not destroy the aggregates.

The spin labeling was successful, even if the spin labeling was not site directed. Both spin labels were bound to all five cysteine residues and therefore the EPR spectra do not represent a specific side chain. Nevertheless, the components resulted from spectra simulation could be assigned to the different binding sites. To avoid the shuffling, it could be investigated, how it was done for the tryptic digestion, if the labeling at lower pH values resulted in only one binding side. The labeling rate will be decreased at lower pH values, but since the labeled protein has to be diluted with unlabeled protein, the lower labeling rate could be sufficient.

Even if the spin labels were not incorporated in the amyloid aggregates at pH 2, the method of SDSL could be used to investigate the interfacial behavior and conformation of the unheated protein as well as the interfacial behavior of the peptides. This approach SDSL can also be used to investigate the adsorption of peptides and smaller aggregates formed at pH 2 and the amyloid-like aggregates formed at pH 3.5 to the air-water and to the oil-water interface. Furthermore, SDSL can be used to investigate dry and solid materials from β-lg, like films or spray-dried emulsions.

The investigation of the hydrophobic aggregates found in the AF and n-AF would be interesting. For example, a multi-stage filtration could give information about the size of the aggregates. The hydrophobicity of these aggregates could indicate a high surface activity and could be the reason for the high foaming behavior of the AAS. In this context, the surface activity of the amyloid-like aggregates formed at pH 3.5 shall be investigated.

Further investigations are necessary for the application of amyloid aggregates in food. The amyloid aggregates are neither process nor pH stable. The effects of the process conditions are the subject of Timon Heyn's dissertation and can be read there. Stabilization against pH is of particular importance for aggregates produced at pH 2, as they change their morphology when the pH is increased to a food-relevant range. But also here the method of SDSL could be used to get more detailed information about the change of the structure and to find a suitable stabilizer.

7.5 References

Akkermans, C., Venema, P., van der Goot, A. J., Gruppen, H., Bakx, E. J., Boom, R. M., & van der Linden, E. (2008). Peptides are building blocks of heat-induced fibrillar protein aggregates of beta-lactoglobulin formed at pH 2. *Biomacromolecules*, *9*(5), 1474–1479. https://doi.org/10.1021/bm7014224

Atkinson, P. J., Dickinson, E., Horne, D. S., & Richardson, R. M. (1995). Neutron reflectivity of adsorbed β-casein and β-lactoglobulin at the air/water interface. *J. Chem. Soc., Faraday Trans.*, *91*(17), 2847–2854. https://doi.org/10.1039/FT9959102847

Baldassarre, M., Bennett, M., & Barth, A. (2016). Simultaneous acquisition of infrared, fluorescence and light scattering spectra of proteins: Direct evidence for pre-fibrillar species in amyloid fibril formation. *The Analyst*, *141*(3), 963–973. https://doi.org/10.1039/c5an02283e.

Berliner, L. J., Grunwald, J., Hankovszky, H.O., & Hideg, K. (1982). A novel reversible thiol-specific spin label: Papain active site labeling and inhibition. *Analytical Biochemistry*, *119*(2), 450–455. https://doi.org/10.1016/0003-2697(82)90612-1

Bolder, S. G., Hendrickx, H., Sagis, L. M. C., & van der Linden, E. (2006). Fibril assemblies in aqueous whey protein mixtures. *Journal of Agricultural and Food Chemistry*, *54*(12), 4229–4234. https://doi.org/10.1021/jf060606s

Bolder, S. G., Vasbinder, A. J., Sagis, L. M.C., & van der Linden, E. (2007). Heat-induced whey protein isolate fibrils: Conversion, hydrolysis, and disulphide bond formation. *International Dairy Journal*, *17*(7), 846–853. https://doi.org/10.1016/j.idairyj.2006.10.002

Bordignon, E., & Polyhach, Y. (2013). EPR techniques to probe insertion and conformation of spin-labeled proteins in lipid bilayers. *Methods in Molecular Biology (Clifton, N.J.)*, *974*, 329–355. https://doi.org/10.1007/978-1-62703-275-9_15

Bordignon, E. (2018). EPR Spectroscopy of Nitroxide Spin Probes. In D. Goldfarb & S. Stoll (Eds.), *EMagRes Bks. EPR Spectroscopy: Fundamentals and Methods* (pp. 277–301). Newark: John Wiley & Sons Incorporated.

Creighton, T. E. (1980). Kinetic study of protein unfolding and refolding using urea gradient electrophoresis. *Journal of Molecular Biology*, *137*(1), 61–80. https://doi.org/10.1016/0022-2836(80)90157-6

Drescher, M., Godschalk, F., Veldhuis, G., van Rooijen, B. D., Subramaniam, V., & Huber, M. (2008). Spin-label EPR on alpha-synuclein reveals differences in the membrane binding affinity of the two antiparallel helices. *Chembiochem: a European Journal of Chemical Biology*, *9*(15), 2411–2416. https://doi.org/10.1002/cbic.200800238

Dunnill, P., & Green, D. W. (1966). Sulphydryl groups and the N⇄R conformational change in β-lactoglobulin. *Journal of Molecular Biology*, *15*(1), 147–151. https://doi.org/10.1016/S0022-2836(66)80216-4

Fernández, A., & Riera, F. (2013). β-Lactoglobulin tryptic digestion: A model approach for peptide release. *Biochemical Engineering Journal*, *70*, 88–96. https://doi.org/10.1016/j.bej.2012.10.001

Goldfarb, D., & Stoll, S. (Eds.) (2018). *EPR Spectroscopy: Fundamentals and Methods*. *EMagRes Bks*. Newark: John Wiley & Sons Incorporated. Retrieved from https://ebookcentral.proquest.com/lib/gbv/detail.action?docID=5317477

Hammarström, P., Owenius, R., Mårtensson, L.-G., Carlsson, U., & Lindgren, M. (2001). High-Resolution Probing of Local Conformational Changes in Proteins by the Use of Multiple Labeling: Unfolding and Self-Assembly of Human Carbonic Anhydrase II Monitored by Spin, Fluorescent, and Chemical Reactivity Probes. *Biophysical Journal*, *80*(6), 2867–2885. https://doi.org/10.1016/S0006-3495(01)76253-4

Hettiarachchi, C. A., Melton, L. D., Gerrard, J. A., & Loveday, S. M. (2012). Formation of β-lactoglobulin nanofibrils by microwave heating gives a peptide composition different from

conventional heating. *Biomacromolecules*, *13*(9), 2868–2880. https://doi.org/10.1021/bm300896r

Heyn, T. R., Garamus, V. M., Neumann, H. R., Uttinger, M. J., Guckeisen, T., Heuer, M., . . . Keppler, J. K. (2019). Influence of the polydispersity of pH 2 and pH 3.5 beta-lactoglobulin amyloid fibril solutions on analytical methods. *European Polymer Journal*, *120*, 109211. https://doi.org/10.1016/j.eurpolymj.2019.08.038

Ionuţ, I. M., Cozma, C., Tomczyk, N., Rontree, J., Desor, M., Drescher, M., & Przybylski, M. (2009). Structural characterization of beta-amyloid oligomer-aggregates by ion mobility mass spectrometry and electron spin resonance spectroscopy. *Analytical and Bioanalytical Chemistry*, *395*(8), 2509–2519. https://doi.org/10.1007/s00216-009-3164-3.

Iuraşcu, I. M., Cozma, C., Tomczyk, N., Rontree, J., Desor, M., Drescher, M., & Przybylski, M. (2009). Structural characterization of beta-amyloid oligomer-aggregates by ion mobility mass spectrometry and electron spin resonance spectroscopy. *Analytical and Bioanalytical Chemistry*, *395*(8), 2509–2519. https://doi.org/10.1007/s00216-009-3164-3

Jordens, S., Isa, L., Usov, I., & Mezzenga, R. (2013). Non-equilibrium nature of two-dimensional isotropic and nematic coexistence in amyloid fibrils at liquid interfaces. *Nature Communications*, *4*, 1917. https://doi.org/10.1038/ncomms2911

Jordens, S., Rühs, P. A., Sieber, C., Isa, L., Fischer, P., & Mezzenga, R. (2014). Bridging the gap between the nanostructural organization and macroscopic interfacial rheology of amyloid fibrils at liquid interfaces. *Langmuir: the ACS Journal of Surfaces and Colloids*, *30*(33), 10090–10097. https://doi.org/10.1021/la5020658

Kayser, J. J., Arnold, P., Steffen-Heins, A., Schwarz, K., & Keppler, J. K. (2020). Functional ethanol-induced fibrils: Influence of solvents and temperature on amyloid-like aggregation of beta-lactoglobulin. *Journal of Food Engineering*, *270*, 109764. https://doi.org/10.1016/j.jfoodeng.2019.109764

Keppler, J. K., Heyn, T. R., Meissner, P. M., Schrader, K., & Schwarz, K. (2019). Protein oxidation during temperature-induced amyloid aggregation of beta-lactoglobulin. *Food Chemistry*, *289*, 223–231. https://doi.org/10.1016/j.foodchem.2019.02.114

Keppler, J. K., Koudelka, T., Palani, K., Stuhldreier, M. C., Temps, F., Tholey, A., & Schwarz, K. (2014). Characterization of the covalent binding of allyl isothiocyanate to β-lactoglobulin by fluorescence quenching, equilibrium measurement, and mass spectrometry. *Journal of Biomolecular Structure & Dynamics*, *32*(7), 1103–1117. https://doi.org/10.1080/07391102.2013.809605

Klare, J. P. (2012). *Site-Directed Spin Labeling and Electron Paramagnetic Resonance (EPR) Spectroscopy: A Versatile Tool to Study Protein-Protein Interactions*. Rijeka: InTech.

Krebs, M. R. H., Bromley, E. H. C., & Donald, A. M. (2005). The binding of thioflavin-T to amyloid fibrils: Localisation and implications. *Journal of Structural Biology*, *149*(1), 30–37. https://doi.org/10.1016/j.jsb.2004.08.002

Kuwata, K., Shastry, R., Cheng, H., Hoshino, M., Batt, C. A., Goto, Y., & Roder, H. (2001). Structural and kinetic characterization of early folding events in beta-lactoglobulin. *Nature Structural Biology*, *8*(2), 151–155. https://doi.org/10.1038/84145

Liang, L., & Subirade, M. (2010). Beta-lactoglobulin/folic acid complexes: Formation, characterization, and biological implication. *The Journal of Physical Chemistry. B*, *114*(19), 6707–6712. https://doi.org/10.1021/jp101096r

Luckhurst, G. R. (1966). Alternating linewidths. A novel relaxation process in the electron resonance of biradicals. *Molecular Physics*, *10*(6), 543–550. https://doi.org/10.1080/00268976600101481

Margittai, M., & Langen, R. (2006). Spin Labeling Analysis of Amyloids and Other Protein Aggregates. In M. Margittai & R. Langen (Eds.), *Methods in Enzymology. Spin labeling Analysis of Amyloids and Other Protein Aggregates* (Vol. 413, pp. 122–139). Elsevier. https://doi.org/10.1016/s0076-6879(06)13007-4

McKenzie, H. A., Ralston, G. B., & Shaw, D. C. (1972). Location of sulfhydryl and disulfide groups in bovine -lactoglobulins and effects of urea. *Biochemistry*, *11*(24), 4539–4547. https://doi.org/10.1021/bi00774a017

Milov, A. D., Ponomarev, A. B., & Tsvetkov, Y.D. (1984). Electron-electron double resonance in electron spin echo: Model biradical systems and the sensitized photolysis of decalin. *Chemical Physics Letters*, *110*(1), 67–72. https://doi.org/10.1016/0009-2614(84)80148-7

Owenius, R., Österlund, M., Lindgren, M., Svensson, M., Olsen, O. H., Persson, E., Carlsson, U. (1999). Properties of Spin and Fluorescent Labels at a Receptor-Ligand Interface. *Biophysical Journal*, *77*(4), 2237–2250. https://doi.org/10.1016/S0006-3495(99)77064-5

Peng, D., Yang, J., Li, J., Tang, C., & Li, B. (2017). Foams Stabilized by β-Lactoglobulin Amyloid Fibrils: Effect of pH. *Journal of Agricultural and Food Chemistry*, *65*(48), 10658–10665. https://doi.org/10.1021/acs.jafc.7b03669

Phelan, P., & Malthouse, J. P. (1994). 13C-n.m.r. of the cyanylated beta-lactoglobulins: Evidence that Cys-121 provides the thiol group of beta-lactoglobulins A and B. *The Biochemical Journal*, *302 (Pt 2)*, 511–516. https://doi.org/10.1042/bj3020511

Qin, B. Y., Bewley, M. C., Creamer, L. K., Baker, H. M., Baker, E. N., & Jameson, G. B. (1998). Structural basis of the Tanford transition of bovine beta-lactoglobulin. *Biochemistry*, *37*(40), 14014–14023. https://doi.org/10.1021/bi981016t

Rade-Kukic, K., Schmitt, C., & Rawel, H. M. (2011). Formation of conjugates between β-lactoglobulin and allyl isothiocyanate: Effect on protein heat aggregation, foaming and emulsifying properties. *Food Hydrocolloids*, *25*(4), 694–706. https://doi.org/10.1016/j.foodhyd.2010.08.018

Rullier, B., Novales, B., & Axelos, M. A.V. (2008). Effect of protein aggregates on foaming properties of β-lactoglobulin. *Colloids and Surfaces A: Physicochemical and Engineering Aspects*, *330*(2-3), 96–102. https://doi.org/10.1016/j.colsurfa.2008.07.040

Sakai, K., Sakurai, K., Sakai, M., Hoshino, M., & Goto, Y. (2000). Conformation and stability of thiol-modified bovine [beta] lactoglobulin. *Camebridge University Press*. (9), 1719–1729.

Savitsky, A., Kühn, M., Duché, D., Möbius, K., & Steinhoff, H.-J. (2004). Spontaneous Refolding of the Pore-Forming Colicin A Toxin upon Membrane Association As Studied by X-Band and W-Band High-Field Electron Paramagnetic Resonance Spectroscopy †. *The Journal of Physical Chemistry B*, *108*(27), 9541–9548. https://doi.org/10.1021/jp036397l

Sepkhanova, I., Drescher, M., Meeuwenoord, N. J., Limpens, R. W. A. L., Koning, R. I., Filippov, D. V., & Huber, M. (2009). Monitoring Alzheimer Amyloid Peptide Aggregation by EPR. *Applied Magnetic Resonance*, *36*(2-4), 209–222. https://doi.org/10.1007/s00723-009-0019-1

Shimizu, M., Saito, M., & Yamauchi, K. (1984). Emulsifying and Structural Properties of β-Lactoglobulin at Different pHs. *Agricultural and Biological Chemistry*, *49*(1), 189–194. https://doi.org/10.1080/00021369.1985.10866680

Slichter, C. P. (1955). Spin Resonance of Impurity Atoms in Silicon. *Physical Review*, *99*(2), 479–480. https://doi.org/10.1103/PhysRev.99.479

Steinhoff, H.-J., Pfeiffer, M., Rink, T., Burlon, O., Kurz, M., Riesle, J., Oesterhelt, D. (1999). Azide Reduces the Hydrophobic Barrier of the Bacteriorhodopsin Proton Channel. *Biophysical Journal*, *76*(5), 2702–2710. https://doi.org/10.1016/S0006-3495(99)77422-9

Tayeh, N., Rungassamy, T., & Albani, J. R. (2009). Fluorescence spectral resolution of tryptophan residues in bovine and human serum albumins. *Journal of Pharmaceutical and Biomedical Analysis*, *50*(2), 107–116. https://doi.org/10.1016/j.jpba.2009.03.015

Uhrínová, S., Smith, M. H., Jameson, G. B., Uhrín, D., Sawyer, L., & Barlow, P. N. (2000). Structural changes accompanying pH-induced dissociation of the beta-lactoglobulin dimer. *Biochemistry*, *39*(13), 3565–3574. https://doi.org/10.1021/bi992629o.

Unterhaslberger, G., Schmitt, C., Sanchez, C., Appolonia-Nouzille, C., & Raemy, A. (2006). Heat denaturation and aggregation of β-lactoglobulin enriched WPI in the presence of arginine HCl, NaCl and guanidinium HCl at pH 4.0 and 7.0. *Food Hydrocolloids*, *20*(7), 1006–1019. https://doi.org/10.1016/j.foodhyd.2005.10.017

Uttinger, M. J., Heyn, T. R., Jandt, U., Wawra, S. E., Winzer, B., Keppler, J. K., & Peukert, W. (2020). Measurement of length distribution of beta-lactoglobulin fibrils by multiwavelength analytical ultracentrifugation. *European Biophysics Journal: EBJ.* Advance online publication. https://doi.org/10.1007/s00249-020-01421-4

Veerman, C., Ruis, H., Sagis, L.M.C., & van der Linden, E. (2002). Effect of Electrostatic Interactions on the Percolation Concentration of Fibrillar β-Lactoglobulin Gels. *Biomacromolecules*. (3), 869–873.

Wan, Z., Yang, X., & Sagis, L. M. C. (2016). Contribution of Long Fibrils and Peptides to Surface and Foaming Behavior of Soy Protein Fibril System. *Langmuir: the ACS Journal of Surfaces and Colloids*, *32*(32), 8092–8101. https://doi.org/10.1021/acs.langmuir.6b01511

Weiner, L. (2012). Quantitative Determination of Thiol Status of Proteins and Cells by Nitroxyl Biradical RS-SR. In A. Kokorin (Ed.), *Nitroxides - Theory, Experiment and Applications* (pp. 369–384). InTech. https://doi.org/10.5772/45620

Wilde, S. C., Treitz, C., Keppler, J. K., Koudelka, T., Palani, K., Tholey, A., Schwarz, K. (2016). β-Lactoglobulin as nanotransporter--Part II: Characterization of the covalent protein modification by allicin and diallyl disulfide. *Food Chemistry*, *197*(Pt A), 1022–1029. https://doi.org/10.1016/j.foodchem.2015.11.011

Yan, Y., Seeman, D., Zheng, B., Kizilay, E., Xu, Y., & Dubin, P. L. (2013). pH-Dependent aggregation and disaggregation of native β-lactoglobulin in low salt. *Langmuir: the ACS Journal of Surfaces and Colloids*, *29*(14), 4584–4593. https://doi.org/10.1021/la400258r.

Zimmerman, J. K., Barlow, G. H., & Klotz, I. M. (1970). Dissociation of β-lactoglobulin near neutral pH. *Archives of Biochemistry and Biophysics*, *138*(1), 101–109. https://doi.org/10.1016/0003-9861(70)90289-4

8 Summary

To gain a deeper insight into the mechanism of amyloid aggregation of the natural β-lactoglobulin (β-lg), the suitability of site-directed spin labeling (SDSL) in combination with electron paramagnetic spectroscopy (EPR) was verified. To make this possible, SDSL was established for the first time for food proteins. The formation of functional amyloid aggregates are mainly dependent of pH value, temperature, and shearing. These parameters determine the protein building blocks, morphology, and the amount of amyloid and amyloid-like aggregates formed, i.e., at pH 2 peptides form fibrils, at pH 3.5 the entire protein molecule is part of worm-like aggregates. Amyloid aggregate systems were separated into the amyloid and non-amyloid fraction using ultrafiltration.

Two spin labels (MTSSL and IPSL) were used for SDSL. The best labeling conditions for MTSSL were at a pH value >7 and an equimolar MTTSL/β-lg ratio, whereas for IPSL molar excess was required at pH 2.5 to achieve a saturation in binding. However, not only the binding to β-lg was favored at higher alkaline pH values, but also the dimerization of two MTSSL molecules, whereas IPSL did not form any dimers. These MTSSL biradicals reduced the binding efficiency and had an interfering effect on the spectra analysis. With FT-ICR-MS, biradicals and monoradical dimers were detected far below the concentrations detectable with EPR.

Both MTSSL and IPSL bound to all five cysteine residues present in β-lg, but with varying degree, as demonstrated by mass spectroscopy after tryptic digestion. These five binding sides could be assigned to two spectral components, which superimposed each other in the EPR spectrum. One spectral domain included Cys^{106}, Cys^{119}, and Cys^{121} being located outside of the β-barrel between the β-sheets and the α-helix. This domain was characterized by a rotation correlation time of ~6-8 ns and a membrane-like polarity, which is associated with a spin label buried in the protein. The second domain represented the binding with Cys^{66} and Cys^{160}, which are located close to the C-terminus on the surface of the protein characterized by rotational correlation times of ~2 ns for MTSSL and ~0.7 ns for IPSL. The faster rotation and a polarity like the unbound spin label in water/DMSO revealed the location of these spin labeled side chains on the surface of the protein.

Since neither the secondary structure of β-lg nor the amyloid aggregation were changed by spin labeling compared with unlabeled β-lg, this approach was used to characterize the mechanism of amyloid aggregation at pH 2 or pH 3.5. For amyloid aggregates formed at pH 2, EPR spectra shapes were similar in the amyloid and the non-amyloid fraction. This points to the fact that the spin labels were not incorporated into the amyloid aggregates, which was confirmed by spectra simulation. However, small (<300 kDa) hydrophobic

aggregates were found in both fractions. The simulation of the EPR spectra indicated that these aggregates are formed by the C-terminal peptides, which were obtained from acid hydrolysis. For amyloid aggregates formed at pH 3.5, different EPR spectra shapes were found for the amyloid-like and the non-amyloid-like fraction, suggesting that the spin labels were incorporated into the amyloid aggregates. This allows the characterization of the aggregation mechanism as follows. It was suspected that the α-helix may be pushed out of the autonomous folding domain during partly unfolding, which in turn led to greater accessibility of the β-sheets to water. The β-sheets were most likely densely packed by the accumulation of intermolecular β-sheets, which support the assumption that amyloid-like structures can be formed from partially unfolded proteins with monomeric size. The simulation of the EPR spectra and the supporting results of the pulsed EPR measurements, confirmed the assumption that monomeric β-lg were partly unfolded and arranged like beads on a string, while the other parts of the protein protruded out of the aggregates, which were particularly reminiscent of a centipede.

Foaming has been used as an exemplary food production process to which amyloid and non-amyloid protein material from whey protein isolate (WPI) have contributed in different ways. The amyloid aggregation of whey protein isolate at pH 2 resulted in ~18% amyloid aggregates and ~82% smaller aggregates, peptides, and mostly unfolded proteins of monomeric size. Because of the high degree of the n-AF, it was of major interest to determine the impact of the n-AF on the surface activity and the interaction of the two fractions. The fractions had a synergistic effect on the stabilization of interfaces as WPI fibrils can probably form a nematic and elastic domain at the a/w interface, in which the small and non-amyloid material present could be embedded. This in turn could increase the density and stiffness of the network and thus the interfacial stability of the WPI. The film of the amyloid aggregates system was more flexible, measured at a Langmuir-Blodgett trough, compared to the individual fraction. However, the lower the amount of amyloid aggregates in the amyloid aggregate system, the higher were the foamability and the foam stability of the foam produced in a foaming column.

In conclusion, the approach of SDSL was successfully established for natural β-lg and it was verified that the structure and dynamics of different amyloid and non-amyloid material can be elucidated by means of SDSL. Furthermore, the contribution of the different protein materials was exemplarily demonstrated for the food production process foaming as well as the surface activity at the air-water interface for amyloid aggregates formed at pH 2.

The approach of SDSL can be applied for food proteins, which naturally contains cysteine residues where spin labels can bind. The simulation of the spectral components can be used

to describe the mechanism of structural alternations and aggregation for food proteins during processing.

9 Zusammenfassung

Um einen tieferen Einblick in den Mechanismus der amyloiden Aggregation von natürlichem β-Lactoglobulin (β-lg) zu erhalten, wurde die Methode der ortsspezifischen Spinmarkierung (SDSL) in Kombination mit der paramagnetischen Elektronenspektroskopie (EPR) etabliert. Die Bildung von funktionellen amyloiden Aggregaten ist hauptsächlich von dem pH-Wert, der Temperatur und Scherung abhängig. Diese Faktoren bestimmen die Bausteine, die Morphologie und die Menge der gebildeten amyloiden und amyloid-ähnlichen Aggregate. Bei pH 2 stellen Peptide die Bausteine da, während bei pH 3,5 das gesamte Protein als Baustein fungiert. Amyloide Aggregat-Systeme wurden mittels Ultrafiltration in die amyloide und nicht-amyloide Fraktion getrennt.

Für SDSL wurden zwei Spin-Labels (MTSSL und IPSL) verwendet und Bindungsbedingungen dahingehend angepasst, dass eine möglichst hohe Bindungsrate und eine geringe Biradikalbildung erreicht wurden. Dazu wurden der pH-Wert und das Spin-Label/β-lg-Verhältnis variiert. Alkalische pH-Werte begünstigten nicht nur die Bindung, sondern auch die Dimerisierung zweier MTSSL-Moleküle, während IPSL keine Dimere bildete. Diese MTSSL-Biradikale reduzierten die Bindungseffizienz und hatten einen störenden Effekt auf die Spektrenanalyse.

Sowohl MTSSL als auch IPSL waren an allen fünf in β-lg vorhandenen Cysteinresten gebunden, welches durch Massenspektroskopie nach tryptischen Verdau nachgewiesen wurde. Diese fünf Bindungsstellen konnten zwei Spektralkomponenten zugeordnet werden, die sich im EPR-Spektrum überlagerten. Eine Spektraldomäne befand sich zwischen den β-Faltblättern und der α-Helix. Die andere Domäne befand sich in der Nähe des C-Terminus auf der Oberfläche des Proteins. Während MTSSL zu ~80 % im Inneren des Proteins gebunden war und nur zu ~20 % an der Oberfläche, war IPSL zu 40 % an der Oberfläche gebunden und nur zu 60 % im Inneren des Proteins.

Da weder die Sekundärstruktur von β-lg noch die amyloide Aggregation durch die Spinmarkierung im Vergleich zu unmarkiertem β-lg verändert wurden, konnte dieser Ansatz zur Charakterisierung des Mechanismus der amyloiden Aggregation bei pH 2 und pH 3,5 verwendet werden. Bei pH 2 wurden die Spin-Label jedoch nicht in die amyloiden Aggregate eingebaut, jedoch konnte mit diesem Ansatz nachgewiesen werden, dass sich sowohl in der amyloiden als auch in der nicht-amyloiden Fraktion kleine (<300 kDa) hydrophobe Aggregate befanden. Bei pH 3,5 wurden die Spin-Label in die amyloid-ähnlichen Aggregate eingebaut. Dieses erlaubte die Charakterisierung des Aggregationsmechanismus. Es wurde vermutet, dass die β-Faltblätter durch die Akkumulation von intermolekularen β-Faltblättern dicht gepackt waren und die α-Helix durch die Neuausrichtung der Tertiärstruktur des Proteins

nach außen ragte. Die Simulation der EPR-Spektren und die Übereinstimmung mit den Ergebnissen der gepulsten EPR-Messungen bestätigten die Annahme, dass monomeres β-lg teilweise entfaltet und wie Perlen auf einer Schnur bei pH 3,5 angeordnet waren, während die anderen Teile des Proteins aus den Aggregaten herausragten, was an die Form eines Tausendfüßlers erinnerte.

Das amyloide Aggregat-System aus Molkenproteinisolat bei pH 2 bestand zu ~18 % aus amyloiden Aggregaten und ~82 % aus kleineren Aggregaten, Peptiden und überwiegend entfalteten Proteinen von monomerer Größe. Das Verschäumen wurde als exemplarisches Verfahren der Lebensmittelproduktion verwendet. Aufgrund des hohen Anteils der n-AF war es von großem Interesse, den Einfluss der n-AF auf die Oberflächenaktivität des amyloiden Aggregat-Systems und die Interaktion der beiden Fraktionen zu bestimmen. Die Fraktionen hatten einen synergistischen Effekt auf die Stabilisierung von Grenzflächen, da WPI-Fibrillen wahrscheinlich eine nematische und elastische Domäne an der Wasser-Luft-Grenzfläche bildeten, in der das vorhandene kleine und nicht-amyloide Material eingebettet wurde. Je geringer jedoch die Menge an amyloiden Aggregaten im amyloiden Aggregat-System war, desto höher waren die Verschäumbarkeit und die Schaumstabilität des in einer Schaumkolonne erzeugten Schaums.

Der Ansatz von SDSL wurde erfolgreich für natürliches β-lg etabliert. Es wurde verifiziert, dass mit SDSL die Struktur und Dynamik verschiedener amyloider und nicht-amyloider Materialien aufgeklärt werden kann. Darüber hinaus konnte der Beitrag der verschiedenen Proteinmaterialien während des Verschäumens als exemplarischer Prozess der Lebensmittelproduktion und die Oberflächenaktivität an der Luft-Wasser-Grenzfläche exemplarisch für amyloide Aggregate bei pH 2 bestimmt werden.

Der Ansatz von SDSL kann für Lebensmittelproteine angewendet werden, die von Natur aus Cysteinreste enthalten, an die sich Spin-Label binden können. Die Simulation der spektralen Komponenten kann zur Beschreibung des Mechanismus von Strukturänderungen und der Aggregation von Proteinen in Lebensmittelprozessen verwendet werden.

10 Supplemental

10.1 Experimental and analytical approach

10.1.1 Analysis of binding properties

10.1.1.1 Reversed-phase high performance liquid chromatography (RP-HPLC)

Solved molecules can be separated, identified and quantified using HPLC. A pressurized liquid (mobile phase) and the sample are injected in a chromatographic column (stationary phase). The separation of the molecules results from the relative affinity of the sample to the stationary phase of the column. This results in a separation of the different molecules in the sample due to different elution times. In this thesis, a diode array detector, a UV-Vis absorbance detector, was used to detect the molecules. The reversed-phase indicates a nonpolar stationary phase, so that the separation is on basis of hydrophobic interactions. The area under the curve indicates the concentration of the molecule and a calibration curve enables its quantification.

For the calculation of binding sites, it is necessary that the unlabeled and the labeled proteins have different hydrophilicities, so that they appear at different retention times. The hydrophobic MTSSL makes the β-lg molecule more hydrophobic, so that labeled genetic variants appear at a later retention time compared to the unlabeled β-lg. Due to the labeling with different molar ratios of MTSSL to β-lg, the binding kinetic and the maximum number of binding sites can be calculated by using the fraction quench method of (Levin, 1977).

10.1.1.2 Free thiol group determination

Free thiol groups were determined by using the Ellman's assay (Ellman, 1959). The Ellman's reagent 5,5'-Dithio-bis (2-nitrobenzoic acid) (DTNB) reacts with –SH groups under release of 2-Nitro-5-thiobenzoat (TNB^-), which is deprotonated to the yellow dye TNB^{2-} in neutral or basic solutions. The yellow dye can be photometrically quantified at a wavelength of 412 nm.

The binding constant was calculated by nonlinear regression of the saturation binding curve using the software Graphpad Prism version 6 (Graphpad Software, La Jolla, USA). To obtain the binding curves the molar ratio of MTSSL to β-lg (B, µM/µM) was plotted against the ligand concentration (µM). B was calculated in the assumption that each thiol group can bind one molecule of MTSSL.

10.1.2 Analysis of amyloid aggregates

10.1.2.1 Conversion rate determination by UV-Vis spectroscopy

UV-Vis spectroscopy is frequently used in analytical chemistry to determine and quantify different molecules. Organic compounds can absorb light in the visible spectral region, which

raised the molecule from its ground state to an electronically excited state. This absorption can be measured and used for the quantification of the molecules. At 278 nm, the aromatic amino acids tyrosine, tryptophan, and phenylalanine absorb the light and therefore the protein concentration can be determined. For quantification, a calibration curve or an absorption coefficient are necessary to calculate the concentration. Is this work, the quantification was conducted with a calibration curve of native β-lg.

To determine the conversion rate of β-lg in amyloid aggregate formation, the amyloid aggregates were separated from the unconverted material by ultrafiltration. The amyloid aggregates remain in the retentate, whereas the unconverted material went through the filter is collected in the filtrate. The protein concentration was measured with an UV-Vis spectrometer at 278 nm (Akkermans, Venema et al., 2008).

10.1.2.2 Thioflavin-T measurement using a fluorescence spectrometer

Thioflavin-T (ThT) is a specific dye to identify amyloid fibrils. ThT binds in the ‘channels’ (Figure 10-1) that run along the length of the stacked β-sheets (Krebs et al., 2005). The channel is 6.5-6.95 Å wide, which is the width between every second residue (Salemme, 1983), but the free space is likely to be less. However, ThT is 6.1 Å along its short axis and only 4.3 Å thick, so that ThT could bind into this channel with its short axis perpendicular to the fibril axis. Also native proteins contain binding channels without being in an amyloid state. However, the binding channels in the native β-sheets are more likely to be disordered and irregular. At least five β-strands with a total length of 18.8 Å are necessary to bind ThT.

The dye ThT, as well as other dyes and biomolecules are used in analytical chemistry. In contrast to the absorption (10.1.2.1) in fluorescence spectroscopy, the reemitting light is measured. The excitation needs more energy, therefore the fluorescence spectra are shifted to longer wavelengths (Stokes-Shift). The excitation wavelength for ThT is 440 nm and the emission wavelength 482 nm.

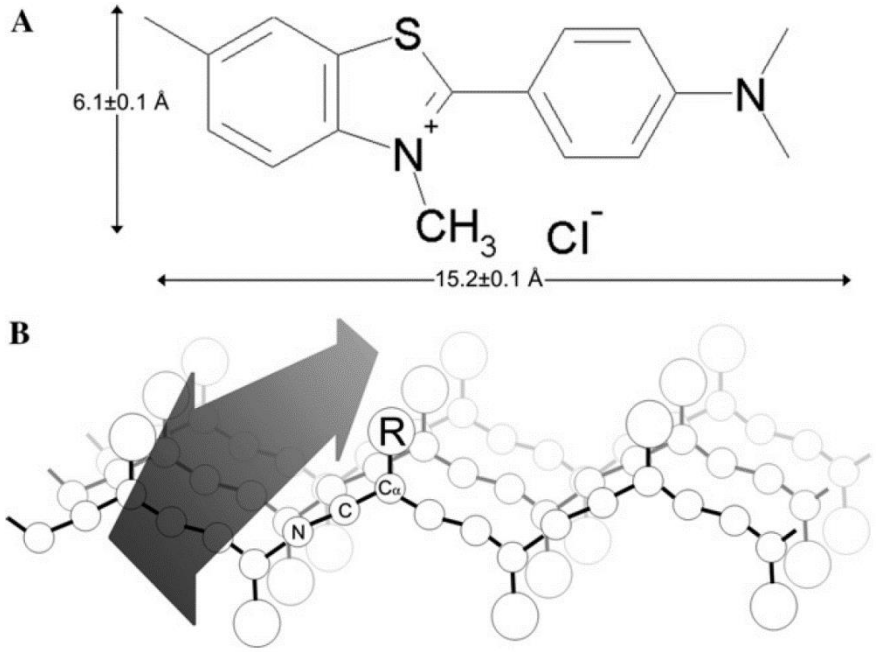

Figure 10-1: (A) Structure of thioflavin-T (ThT) molecule, which is ~4.3 Å thick. (B) Schematic illustration of a β-sheet with the arrow indicating a binding channel for ThT (Krebs et al., 2005).

10.1.2.3 Intrinsic tryptophan fluorescence (ITF)

ITF is based on the natural fluorescence of the amino acid tryptophan and measured with a fluorescence spectrometer as described in 10.1.2.2. It indicates the polarity of the environment of the indole group of the amino acid tryptophan (van DUUREN, 1961). The excitation wavelength for tryptophan is 294 nm and the emission is scanned in the range of 300 - 500 nm. The wavelength of the maximum emission shifts to a higher wavelength when tryptophan residues are exposed to a more polar environment (van DUUREN, 1961). A red shift, the shift to a higher wavelength, indicates a more polar environment, whereas a blue shift, the shift to a lower wavelength, indicates a nonpolar environment. By changing the polarity, conclusions can be drawn about the structure of the protein. In this work, ITF was used to follow the amyloid aggregation and to analyze difference in amyloid aggregation due to spin labeling.

10.1.2.4 Size exclusion chromatography (SEC) for fibril building blocks determination

The principle of SEC is similar to that of RP-HPLC, but the molecules are separated because of their size and not because of their hydrophobicity. This method is usually used to analyze macromolecular complexes such as proteins and other polymers. For the stationary phase, a porous polymer is used and the columns are filled with a hydrophilic, porous and cross-linked material which are composed of dextran polymers (Sephadex), agarose (Sepharose), or polyacrylamide (Sephacryl). Small molecules penetrate deeper in the column material and

have, therefore, a later retention time. Lager particles cannot enter into the pores and simply pass through the column. The larger the particles the faster is the elution.

The SEC was used to measure the building blocks of the amyloid aggregates. The measurement was conducted under reducing conditions, to measure the proteins and peptides and not the aggregates. This was done to verify whether the amyloid aggregation leads to the same fragments after labeling with MTSSL or IPSL as without spin labeling and whether the amyloid aggregates consist of the same building blocks.

10.1.2.5 Atomic force microscopy (AFM) for fibrils imaging

The AFM is widely used in surface science. Here the tapping mode was used for imaging of the amyloid aggregates. The AFM consists of a small measuring arm, which is called cantilever. At the end of the cantilever is a sharp tip with a radius in the order of nanometer, which is used to scan the surface. The imaging is conducted in the tapping mode. In the tapping mode, the cantilever oscillates, which is achieved with a small piezo element in cantilever holder. The frequency is close to the resonance frequency of the cantilever. The interaction between the cantilever and the surface results in changes in the frequency, which can be measured.

10.2 Additional results

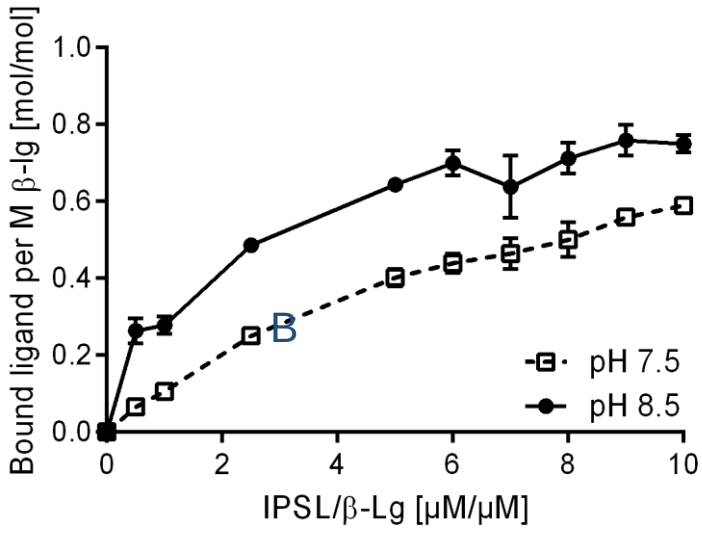

Figure 10-2: Molar binding ratio of the ligand IPSL to β-lg at pH 7.5 (unfilled symbols) and pH 8.5 (filled symbols). The binding sites were calculated by measuring the free thiol groups RSH at different IPSL concentrations. The affinity constant were calculated by a nonlinear fit Kα.pH7.5 = 0.082 µM-1, Kα.pH8.5 = 0.193 µM-1.

10.3 References

Akkermans, Cynthia; Venema, Paul; van der Goot, Atze Jan; Gruppen, Harry; Bakx, Edwin J.; Boom, Remko M.; van der Linden, Erik (2008): Peptides are building blocks of heat-induced fibrillar protein aggregates of beta-lactoglobulin formed at pH 2. In: *Biomacromolecules* 9 (5), S. 1474–1479. DOI: 10.1021/bm7014224.

Ellman, George L. (1959): Tissue Sulfhydryl Groups. In: *Archnieves of Biochemistry and Biophysics* 82, S. 70–77.

Krebs, M. R. H.; Bromley, E. H. C.; Donald, A. M. (2005): The binding of thioflavin-T to amyloid fibrils. Localisation and implications. In: *Journal of structural biology* 149 (1), S. 30–37. DOI: 10.1016/j.jsb.2004.08.002.

Levin, Rodney L. (1977): Fluorescence-Quenching Studies of the Binding of Bilirubin to Albumin. In: *Clinical Chemistry* (23), S. 2292–2301.

Salemme, F. R. (1983): Structural properties of protein β-sheets. In: *Progress in Biophysics and Molecular Biology* 42, S. 95–133. DOI: 10.1016/0079-6107(83)90005-6.

van DUUREN, BENJAMIN L. (1961): Solvent Effects in the Fluorescence of Indole and Substituted Indoles 1. In: *J. Org. Chem.* 26 (8), S. 2954–2960. DOI: 10.1021/jo01066a079.